The Thesis Committee for Vikram Chandrasekar
Certifies that this is the approved version of the following thesis:

An Experimental and Simulation Study of the Effect of Geochemical Reactions on Chemical Flooding

APPROVED BY
SUPERVISING COMMITTEE:

Gary A. Pope, Supervisor

Mojdeh Delshad, Co-Supervisor

An Experimental and Simulation Study of the Effect of Geochemical Reactions on Chemical Flooding

by

Vikram Chandrasekar, B. Tech

Thesis

Presented to the Faculty of the Graduate School of

The University of Texas at Austin

in Partial Fulfillment

of the Requirements

for the Degree of

Master of Science in Engineering

The University of Texas at Austin

December 2010

Dedication

To God and my family

Acknowledgements

Woochan Lee, Devender Mohan and James Lau. I also appreciate the support of the other members of the Chemical EOR research group - Abhinav Sharma, Nitish Koduru, Hourshad Mohammadi, Hyuntae Yang, Ahra Lee, Heesong Koh, Seungjun Lee, Oluwaseun Magbagbeola and Mohammed Ali Farhadinia to name a few.

Finally, I would like to thank my parents, D. Chandrasekaran and Radhika Chandrasekar, and my sister Vandana Chandrasekar for their love and support, without which, this would not have been possible.

<div align="center">December 2010</div>

Abstract

An Experimental and Simulation Study of the Effect of Geochemical Reactions on Chemical Flooding

Vikram Chandrasekar, M. S. E

The University of Texas at Austin, 2010

Supervisor: Gary A. Pope

Co-Supervisor: Mojdeh Delshad

The overall objective of this research was to gain an insight into the challenges encountered during chemical flooding under high hardness conditions. Different aspects of this problem were studied using a combination of laboratory experiments and simulation studies.

Chemical Flooding is an important Enhanced Oil Recovery process. One of the major components of the operational expenses of any chemical flooding project, especially Alkali Surfactant Polymer (ASP) flooding is the cost of softening the injection brine to prevent the precipitation of the carbonates of the calcium and magnesium ions which are invariably present in the formation brine. Novel hardness tolerant alkalis like sodium metaborate have been shown to perform well with brines of high salinity and

hardness, thereby eliminating the need to soften the injection brine. The first part of this research was aimed at designing an optimal chemical flooding formulation for a reservoir having hard formation brine. Sodium metaborate was used as the alkali in the formulation with the hard brine. Under the experimental conditions, sodium metaborate was found to be inadequate in preventing precipitation in the ASP slug. Factors affecting the ability of sodium metaborate to sequester divalent ions, including its potential limitations under the experimental conditions were studied.

The second part of this research studied the factors affecting the ability of novel alkali and chelating agents like sodium metaborate and tetrasodium EDTA to sequester divalent ions. Recent studies have shown that both these chemicals showed good performance in sequestering divalent ions under high hardness conditions. A study of the geochemical species in solution under different conditions was done using the computer program PHREEQC. Sensitivity studies about the effect of the presence of different solution species on the performance of these alkalis were done.

The third part of this research focused on field scale mechanistic simulation studies of geochemical scaling during ASP flooding. This is one of the major challenges faced by the oil and gas industry and has been found to occur when sodium carbonate is used as the alkali and the formation brine present in situ has a sufficiently high hardness content. The multicomponent and multiphase compositional chemical flooding simulator, UTCHEM was used to determine the quantity and composition of the scales formed in the reservoir as well as the injection and production wells. Reactions occurring between the injected fluids, in situ fluids and the reservoir rocks were taken into consideration for this study. Sensitivity studies of the effect of key reservoir and process parameters like the physical dispersion and the alkali concentration on the extent of scaling were also done as a part of this study.

Table of Contents

List of Tables

List of Figures

xxiv

Chapter 1: Introduction

The overall objective of this research is to have an understanding of the challenges faced during chemical flooding in the presence of large concentrations of hardness causing divalent ions. This research is a continuation of the ongoing research in the area of Chemical Enhanced Oil Recovery at the University of Texas at Austin.

1.1 MOTIVATION AND RESEARCH OBJECTIVES

Enhanced Oil Recovery is of increasing importance in the oil and gas industry as more and more reservoirs approach their economic limits through primary and secondary recovery. Many of these reservoirs have a substantial portion of their oil unrecovered and trapped as residual oil. Many of these reservoirs are candidates for chemical enhanced oil recovery using surfactants to reduce the interfacial tension (IFT) and polymers for mobility control and to improve the sweep efficiency. Research has shown that chemical costs can often be substantially reduced by injecting surfactants and polymers at high pH in the form of an Alkali-Surfactant-Polymer (ASP) slug since the high pH reduces the surfactant adsorption.

ASP flooding using conventional alkali such as sodium carbonate requires soft water to prevent the precipitation of the carbonates by calcium and magnesium ions. This limits the potential application of the ASP flooding to situations where the brines can be softened economically. Flaaten et al. (2008) described a laboratory and modeling approach to ASP flooding without the need for softening the brine. They showed that sodium metaborate used as an alkali provided good divalent ion tolerance. The first part of this research was to identify the factors affecting its performance including its limitations. The second part of this research involved geochemical modeling to

understand novel alkali and chelating agents such as tetrasodium EDTA. The computer program PHREEQC was used as the geochemical model.

The last part of this research deals with the problem of geochemical scaling faced by the oil and gas industry, specifically with regards to ASP flooding. When conventional alkalis are injected with the ASP slug in reservoirs containing hard formation brines, scaling results due to the precipitation of calcium and magnesium carbonate scales. This has several undesirable consequences (Moghadesi, 2003, Moghadesi, 2004).

The three-dimensional multicomponent and multiphase chemical simulator, UTCHEM, has been used to mechanistically simulate scaling on a field scale. The chemical reactions between the in situ brine, injected fluids and the reservoir rock have been taken into account while simulating this process. Simulations have been performed to determine the sensitivity to dispersion and the alkali concentration to determine the quantity of precipitates in the reservoir and in the well bore.

1.2 SUMMARY OF CHAPTERS

Chapter 2 discusses the relevant literature and concepts involved in this research. Chapter 3 presents a discussion of the experimental methodology as well as the equipments and data analysis techniques used for performing the phase behavior and core flooding experiments. Chapter 4 discusses the experimental results aimed at designing an optimal chemical flooding formulation for a reservoir under high hardness conditions. Chapter 5 presents a study of geochemical species in the presence of novel alkali like sodium metaborate and tetrasodium EDTA. Chapter 6 discusses the results of field scale mechanistic simulation studies of geochemical scaling during ASP flooding. Chapter 7 presents a summary of this research and discusses the conclusions made from the results.

Chapter 2: Review of Literature and Concepts

2.1 INTRODUCTION

This chapter presents a review of previous literature and the relevant concepts pertaining to the subject of this research, thereby providing a theoretical background for this research. Recent advances in the development of EOR chemicals are reviewed, along with the development and theory of phase behavior and core flooding experiments to screen and design optimal EOR formulations.

2.2 BACKGROUND AND KEY CONCEPTS INVOLVED

The use of surfactants in enhanced oil recovery has been a subject of research for the past 50 years. Reisberg and Doscher (1956) and Gogarty (1967) presented some of the earliest attempts to using surfactants in enhanced oil recovery processes. The key phenomenon controlling the tertiary recovery of oil by means of chemical flooding with surfactants is the reduction of the interfacial tension (IFT), and hence the capillary forces through the addition of surfactants. The typical interfacial tension between the brine and the oil, which is of the order of 10-30 dynes/cm, is reduced to about 10^{-3} dynes/cm by the addition of surfactants (Green and Willhite, 1998; Austad and Miller, 1998). This process can be modeled by a capillary desaturation curve as a function of the trapping number (Jin, 1995; Delshad, 1996; Pope et al., 2000). CDC curves are plots of the residual phase saturations versus the trapping number, where the trapping number is defined as the ratio of the magnitude of the vector sum of the viscous forces and the buoyancy forces to that of the capillary forces as follows:

$$N_{T_1} = \frac{\left| \overline{\overline{k}}.(\overline{\nabla}\Phi_{1'} + g(\rho_{1'} - \rho_1)\overline{\nabla}D) \right|}{\sigma_{ll'}}$$

where,

N_{T_1} = Capillary Number

$\overline{\overline{k}}$ = Permeability Tensor

$\overline{\nabla}\phi_{1'}$ = Flow Potential Gradient

g = Acceleration due to gravity

$\rho_{1'}$ = Density of the displacing phase

ρ_1 = Density of the displaced phase

$\sigma_{ll'}$ = Interfacial Tension between the displacing and displaced phases

2.2.1 Microemulsions

When the surfactant, oil and brine phases are mixed together, they form distinct and thermodynamically stable phases called microemulsions (Windsor, 1954; Bourrel and Schechter, 1988). Healy et al. (1974) defined a microemulsion to be a stable, translucent micellar solution of oil, water that may contain electrolytes, and one or more amphiphilic compounds (surfactants, alcohols etc). Such phases are fundamentally different from emulsions, which are thermodynamically unstable. Windsor classified the microemulsions into three types. A Type I microemulsion is an oil-in-water microemulsion in which a portion of the oil is solubilized by the surfactant. A Type II microemulsion is a water-in-oil microemulsion in which a portion of the water is solubilized by the surfactant. A Type III microemulsion is a microemulsion in which a portion of both the oil and the water are solubilized by the surfactant and is in equilibrium with the excess oil and water phases as a bicontinous phase. The salinity at which equal

4

amounts of oil and water are solubilized by the surfactant is termed the optimum salinity and the corresponding solubilization ratio is termed the optimum solubilization ratio.

2.2.2 Phase behavior of microemulsions

Several factors are known to affect the phase behavior of microemulsions. Some of these are the types and concentration of surfactants, co-surfactants, hydrocarbons and brine; temperature and pressure (Green and Willhite, 1998; Aoudia and Wade, 1995). Increase in the brine salinity, alkyl chain length of the surfactant, oil aromaticity and the number of propylene oxide groups in the surfactant molecule are some factors that cause a transition from a lower to upper phase microemulsion. On the other hand, a decrease in the Equivalent Alkane Carbon Number (EACN) of the oil causes an upper to lower phase transition (Aoudia and Wade, 1995; Green and Willhite, 1998).

2.2.3 Microemulsions and IFT

Healy et al. (1974) developed empirical correlations between the solubilization ratios and the interfacial tension. Huh (1979) derived a theoretical relation between the solubilization ratio and the IFT. A simplified form of this relation is given by

$$\gamma = \frac{C}{\sigma^2}$$

where the constant, C has a value of approximately 0.3 dynes/cm and γ is the solubilization ratio defined as the volume of oil/water solubilized per unit volume of the surfactant. This expression thus gives an easy and accurate measure of the IFT.

2.3 CHEMICALS USED IN EOR

A typical chemical EOR solution consists of a mixture of (primary) surfactants, co-surfactants, co-solvents, polymer, alkali and brine (electrolyte). This section describes these chemicals.

2.3.1 Surfactants and co-surfactants

Surfactants are surface active agents that adsorb or concentrate at a surface or a fluid-fluid interface when present in low concentrations (Rosen, 2004). They significantly alter the interfacial properties of a pair of fluids like the interfacial tension (Bourrel and Schechter, 1988). This is the property of surfactants that makes them useful in chemical enhanced oil recovery. Surfactant molecules consist of a lypophilic 'tail' and a hydrophilic 'head' group. A balance between the hydrophilic and lypophilic parts of the surfactant molecule (characterized by a number called HLB) gives it the characteristics of a surface acting agent (Green and Willhite, 1998). Co-surfactants improve the behavior of the primary surfactant (Nelson, 1984).

The best surfactants used for EOR applications typically have a branched hydrophobe. Hydrophobe branching is a desirable trait for EOR surfactants. Linear surfactants have a tendency to form highly viscous gels (Levitt et al. 2006). The chain length of the hydrophobe has a good correlation with the Equivalent Alkane Carbon Number (EACN) of the crude of interest (Aoudia et al., 1995).

Surfactants are classified based on the ionic nature of the head group as anionic, cationic, non-ionic and zwitterionic. Anionic and non-ionic surfactants have been widely used in EOR applications. Anionic surfactants are the most widely used because of their relatively low adsorption on negatively charged surfaces such as usual for sandstone at

reservoir pH. Non-ionic surfactants are usually used as hydrophilic co-surfactants to improve the aqueous phase behavior.

Anionic surfactants

The most widely used anionic surfactants for Chemical Enhanced Oil Recovery applications include Alkyl Benzene Sulfonates (ABS), Aryl Alkyl Sulfonates (AAS), Internal Olefin Sulfonates (IOS), Alpha Olefin Sulfonates and Alcohol Alkoxy (usually Ethoxy (EO) or Propoxy (PO)) Sulfates.

Alkyl Benzene Sulfonates and Alkyl Aryl Sulfonates are some of the oldest surfactants used for Enhanced Oil Recovery applications. Such molecules have been observed to show high solubilization ratios with crudes. However, they suffer from low aqueous stability limits and have a low tolerance for divalent ions (Jackson, 2006). More often than not, they are used in combination with a different type of surfactant.

Internal Olefins have a carbon-carbon double bond at an internal position of the aliphatic carbon chain. After sulfonation of the olefin, due to the presence of the double bond at an internal position, the resulting IOS surfactants have twin hydrophobic tails that vary in lengths. This inherent branching in the hydrophobe helps the surfactant perform well in a wide variety of conditions. IOS surfactants have shown excellent performance in both sandstone and dolomite rocks/cores (Falls et. al, 1992; Sanz and Pope 1995; Levitt et al. 2006; Jackson, 2006; Zhao et al. 2006; Flatten et al. 2008; Barnes et al. 2008; Yang et al. 2010; Barnes et al., 2010). These surfactants have also been shown to have low retention in both sandstone and dolomite cores (Levitt et al., 2006; Yang et al. 2010; Yang 2010).

Alcohol Propoxy and Ethoxy Sulfates are made from commercially available branched alcohols. They contain ethoxy (EO) and propoxy (PO) groups respectively.

Ethoxylated groups increase the hydrophilicity of the surfactant and hence improve its aqueous stability and calcium tolerance. On the other hand, the presence of propoxy groups improves the hydrophobicity of the surfactant and reduces the optimum salinity as well as the required alcohol chain length for a given EACN (Aoudia et al. 1995). Addition of these groups also improves the tolerance towards divalent ions (Bourrel and Schechter, 1988; Austad and Milter, 1998). Ethoxy and propoxy sulfates have been studied extensively and have been found to perform well under different conditions. (Wellington et al., 1997; Jayanti et al. 2001; Salager et al., 2005; Levitt et al., 2006; Zhao et al. 2008; Flatten et al. 2008; Adkins et al. 2010).

Non-ionic surfactants

Non-ionic surfactants have been used in chemical flooding for a long time (Hayes et al., 1979; Falls et al., 1994). Currently, they are typically used as co-surfactants to increase the hydrophilicity of the surfactant mixture, thereby improving the aqueous stability. The additional benefit of using them is to reduce or even eliminate the requirement of co-solvents. Alcohol ethoxylates are the most commonly used non-ionic surfactants. They have been shown to perform better than conventional co-solvents such as alcohols and glycol ethers under some circumstances (Sahni et al., 2010). A small amount of alcohol ethoxylate has been shown to perform equally well or better than a large amount of co-solvent in some cases. This gives a significant advantage towards the economics of chemical flooding.

2.3.2 Co-solvents

Co-solvents serve to improve the solubility of surfactants and to reduce the oil-water microemulsion viscosity, thereby reducing the tendency to from viscous gels and

emulsions. They partition between the surfactant hydrophobes at the oil-water interfaces in the microemulsion (Bourrel and Schechter, 1988; Sanz and Pope, 1995). They also promote rapid equilibration of the microemulsion and improve its coalescence. On the flip side, they reduce the solubilization ratios of the oil and water phases in the microemulsion phase i.e they increase the IFT.

Low molecular weight alcohols (C3-C5) have been the most common types of co-solvents used for Chemical EOR applications (Jones and Dreher, 1976; Wade et al., 1978; Levitt et al. 2006; Flaaten et al. 2008). The hydrophilicity of the co-solvent has been found to increase with an increase in branching of the alcohol for the same molecular weight (Hsieh and Shah, 1977).

Glycol Ethers like EGBE, DGBE and TEGBE have also been used as co-solvents. They have advantages over alcohols such as a higher flash point (Jackson, 2006; Sahni et al., 2010). Recently, butanol ethoxylates have been tested as co-solvents (Sahni et al., 2010).

2.3.3 Alkali

Addition of alkali to an SP slug serves two main purposes. The first is to raise the solution pH so as to reduce surfactant adsorption by increasing the negative charge on the rock surface (Nelson et al., 1984; Zhang et al., 2006). The second is to generate soap in situ by reacting with the naphthenic acids present in reactive crude oils (Johnson, 1976; Zhang et al., 2006). This reduces the amount of surfactant required for the chemical flood and has the potential to have significant cost benefits (Surkalo, 1990).

Conventional Alkali

Sodium carbonate and to a lesser extent sodium hydroxide are the most common alkali used for EOR applications. Sodium carbonate has the advantages of smaller alkali consumption and lesser surfactant adsorption compared to sodium hydroxide (Zhang et al. 2006). In addition, sodium carbonate has other desirable properties such as its tendency to increase the solubilization ratio and decrease the equilibration time of the microemulsion (Jackson, 2006).

In spite of these advantages, sodium carbonate suffers from certain limitations as an alkali under certain conditions, thereby restricting its applicability. Sodium Carbonate precipitates as calcite in the presence of gypsum and anhydrite in the rock, and as calcite and magnesite in the presence of significant concentrations of divalent ions (namely $Ca++$ and $Mg++$) (Labrid, 1991). One of the main objectives of this research is to understand this phenomenon of geochemical scaling in the presence of hard formation brines through mechanistic simulation studies on a field scale.

Novel Alkali and Chelating Agents

Recent studies have indicated that under high hardness conditions, novel alkali sodium metaborate and chelating agents like tetrasodium Ethylenediamine Tetraacetate (Na_4EDTA) have been found to have high tolerance for divalent cations in solution while at the same time producing high pH in solution (Flaaten et al., 2008; Zhang et al. 2008; Hirasaki et al., 2008; Yang et al., 2010).

Sodium metaborate, present in the borate form ($[B(OH)_4]^-$) under high pH conditions, forms soluble metal borate complexes with divalent ions present in the solution (Ingri, 1963; Farmer, 1982). The formation of soluble borate complexes prevents

the precipitation of divalent ions as carbonates. The corresponding complexation reactions are given by,

$$Ca^{2+} + [B(OH)_4]^- \rightleftharpoons Ca[B(OH)_4]^+$$

$$Mg^{2+} + [B(OH)_4]^- \rightleftharpoons Mg[B(OH)_4]^+$$
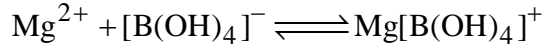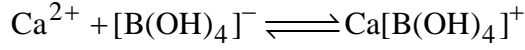
Tetrasodium EDTA is a powerful chelating agent due to the presence of two amine and four carboxylate groups in the molecule by forming soluble metal chelates with the calcium and magnesium ions present in the solution, thereby preventing their precipitation as calcium and magnesium carbonates. Moreover, it also increases the pH of the solution high enough to generate in-situ soap with the naphthenic acids present in the crude oil as well as reduce adsorption (Adkins et al. 2010, Yang et al. 2010).

2.3.4 Polymers

The main function of the addition of polymer to the chemical EOR solution is to increase the viscosity of the chemical slug, thereby achieving improved mobility control and increasing the sweep efficiency. In the absence of sufficient mobility control, the surfactant slug will finger into the oil/water bank causing early breakthrough and poor sweep efficiency (Green and Willhite, 1998). Hydrolyzed polyacrylamides (HPAM) is the most common polymer used for EOR applications (Sorbie, 1991; Lake, 1989). Sorbie (1991) gives a comprehensive overview of polymers used in chemical EOR. Levitt et al. (2008) describes the process of selection and screening of polymers for Enhanced Oil Recovery.

2.4 PHASE BEHAVIOR EXPERIMENTATION

Phase behavior experiments are used to screen chemicals for EOR by characterizing microemulsions. These experiments provide a quick and inexpensive method for screening and selecting EOR chemicals. These techniques were first developed by Stegemeier and co-workers at Shell Development Co. in the 1960s (Nelson, 1984). These are static experiments in which the chemicals are mixed and allowed to equilibrate with the oil for several days and observations were made to determine the transition of the microemulsion from type I to type II (Nelson and Pope, 1978). Levitt et al (2006) describes a systematic procedure to screen EOR chemicals through phase behavior experiments. This method has been found to be highly effective in selecting the best surfactant for use with different crude oils under widely varying conditions (Jackson 2006; Zhao et al., 2008; Flaaten et al., 2008; Yang et al., 2010; Adkins et al., 2010; Sahni et al., 2010).

2.5 CORE FLOODING EXPERIMENTS

Core flooding experiments are used to validate the effectiveness of promising SP/ASP formulations identified through phase behavior screening experiments to recover oil. Here, the actual oil displacement behavior is studied by flow experiments with the SP/ASP slug on outcrop/reservoir cores that are usually already at water flood residual oil saturation.

Salinity Gradient

The most important concept involved in designing SP/ASP core floods is the concept of a negative salinity gradient described by Nelson and Pope (1978) and Pope

and Nelson (1978) and further investigated in detail by Pope et al. (1979), Nelson (1982) and Hirasaki et al. (1983) among others. A negative salinity gradient design means the salinity decreases going from the initial salinity (formation brine) to the SP slug to the polymer drive so that under initial conditions the phase behavior is Type II and at the salinity of the polymer drive it is Type I. Such a design increases the chances of having a Type III salinity region, which has an ultra low IFT, somewhere in the mixing zone. This also reduces the chances of high surfactant retention caused by phase trapping in the Type II region (Hirasaki et al., 1983).

Chapter 3: Experimental Description

3.1 INTRODUCTION

This chapter describes the experimental apparatus, methodology and methods for data analysis used in the current research. The first section gives an overview of the various EOR fluids used in the experiments. The next section describes the experimental apparatus and methodology used for phase behavior experimentation, which is used to screen high performance EOR formulations. The last section describes the experimental equipment, setup and the methodology of the core flooding experiments, which tested the high performance EOR formulations identified through phase behavior experimentation for oil recovery from cores.

3.2 CHEMICAL EOR FLUIDS

This section gives an overview of the different EOR fluids tested in the phase behavior and core flooding experiments as a part of this research. These include surfactants, co-solvents, polymers, brines and crude oils.

Surfactants and Co-surfactants

Several different types of surfactants and co-surfactants that have historically proven to be successful for use in Chemical EOR were tested as a part of this research. Most of them were anionic surfactants like alkyl benzene sulfonates, internal olefin sulfonates, ethoxy and propoxy sulfates as well as carboxylates. They had either branched or linear carbon chains with a chain length ranging from 15 to 24 carbon atoms. A few non-ionic co-surfactants were also tested. However, these served the function of co-solvents and are discussed under that heading below.

Co-solvents

Several different co-solvents were tested in the phase behavior experiments. These included alcohols like Iso Butyl Alcohol (IBA) and Secondary Butyl Alcohol (SBA) as well as glycol ethers like Diethylene Glycol Monobutyl Ether (DGBE) and Triethylene Glycol Monobutyl Ether (TEGBE). In addition to these, several non-ionic co-surfactants like Neodol 25-12 (C_{12-15} 12EO), Tridecyl Alcohol 6EO (C_{13} 6EO) and Tridecyl Alcohol 18EO (C_{13} 18 EO), which served the function of co-solvents were also used in a few experiments.

Alkali

Two different alkali were used in the experiments, namely sodium carbonate and sodium metaborate. Sodium metaborate was used for cases where the injection slug contained significant amounts of hardness causing ions like calcium and magnesium.

Polymers

A hydrolyzed polyacrylamide (HPAM), Floppam 3330S was used for the experiments. This polymer is about 30% hydrolyzed and has a molecular weight of about 8 million Daltons.

3.3 PHASE BEHAVIOR EXPERIMENTATION

This section describes the microemulsion phase behavior and aqueous stability experiments used to characterize microemulsions for Chemical EOR. These experiments offer a quick, economical and efficient method to test different EOR chemicals and screen them with respect to their ability to from microemulsions with low IFT. The best

formulations identified through these experiments were then tested through core flood experiments wherein the actual displacement behavior in porous media was studied.

The first part of this section describes the apparatus and analytical equipments used for the phase behavior experimentation. The second part describes the experimental procedure. The last part discusses the characterization of microemulsions by analyzing the data obtained through these experiments.

3.3.1 Experimental Equipment

Several types of experimental and analytical equipments were used for performing phase behavior experiments. These are described below.

Borosilicate pipettes

Fischer brand standard 5ml borosil pipettes were used for performing the phase behavior experiments. These are graduated with 0.1ml markings. The open ends of the pipettes were flame sealed after dispensing the fluids into the pipettes.

Fluid repeater/dispenser

Eppendorf Repeater Plus brand fluid repeater/dispenser was used for dispensing fluids into the pipettes. Disposable plastic syringes of different volumes were attached to the ends of the repeater to deliver accurate quantities of fluids into the pipettes.

Pipette sealing apparatus

A Benzomatic TS4000 torch was used to flame seal the pipette ends in order to prevent the contents from evaporating.

Convection ovens

The pipettes were stored in convection ovens which maintained the contents at constant temperatures. This temperature was set to be at the reservoir temperature so that the reservoir temperature conditions were simulated as closely as possible.

3.3.2 Experimental Procedure

Preparation of brines and stock solutions

The initial step for performing the phase behavior experiments is the preparation of the synthetic brines (electrolytes) and the surfactant and polymer stock solutions required for the experiments.

The synthetic brines and injection waters required for the phase behavior experiments were prepared by adding accurately weighed quantities of salts like sodium chloride, calcium chloride, magnesium chloride, sodium sulfate, sodium carbonate/bicarbonate, barium chloride etc to deionized water. The concentration of these salts replicated the actual concentrations of various ions like Na^+, Ca^{2+}, Mg^{2+}, Cl^-, $SO4^{2-}$ and $CO3^{2-}$ in the solution. In many cases, softened synthetic brines were used in which case no calcium and magnesium chloride was added. These were replaced by an equivalent amount of sodium chloride so as to maintain the total TDS content of the softened brines the same as that of the original synthetic brines.

The surfactant stock solutions were prepared by mixing the required quantity of the surfactants, co-surfactants, co-solvents and brines. The concentrations of the stock solutions were typically several times as much as that of the final solutions (usually 4 or 8 times as concentrated). These solutions were diluted by mixing with other components during the process of preparing the phase behavior pipettes to yield final solutions of the

desired concentrations. The contents were stirred with magnetic stir bars for about 30 minutes to ensure uniform mixing.

The polymer stock solutions were prepared in 500ml batches. A concentration stock solution was initially prepared (typically 5000ppm) in the injection brine which was then diluted to the desired polymer concentration. The injection brine was initially taken in a container and slowly stirred with the help of magnetic stir bars, thereby creating a vortex. The polymer powder was then sprinkled slowly into the shoulder of the vortex, while ensuring that the polymer particles do not clump together. After adding the polymer powder, the solution was mixed at a slower rate for a period of at least 24 hours. The prepared polymer solution was then filtered through a 1.2 micron filter paper under a constant pressure of 15 psi. The quality of the prepared polymer stock solution was determined through the filtration ratio, which is the ratio of the time taken for equal volumes of the solutions to be filtered at the beginning and the end of the filtration process. For a 120ml volume of the filtering solution, it is given by

$$F.R = \frac{\Delta t_{80-100}}{\Delta t_{40-60}} \dots\dots\dots\dots\dots\dots\dots\dots\dots\dots\dots\dots\dots\dots\dots\dots\dots (3.1)$$

where,

Δt_{80-100} = Time taken for the filtration of polymer from the 80th to the 100th ml

Δt_{40-60} = Time taken for the filtration of polymer from the 20th to the 40th ml

For a well mixed polymer stock solution, the filtration ratio is less than or equal to 1.2. A higher value of the filtration ratio indicates that sufficient hydration of the polymer has not taken place.

18

Pipette preparation

      Phase behavior experiments involve mixing a continuously varying proportion of the surfactant stock solution, injection brine, alkali stock solution (for ASP) and injection brine in an array of pipettes. Two kinds of experiments were performed depending on the substance whose concentration is varied, namely salinity scan and oil scan experiments.

      In a salinity scan, the concentrations of the alkali stock solution and/or injection brine added to the pipettes were varied from one pipette to the next one. Such a series of pipettes show a classical transition in microemulsion phase behavior from Type I through Type III to Type II.

      An oil scan on the other hand is used to determine the effect of water oil ratios on the phase behavior to determine the activity map for the oil in case of reactive crudes. Oil scans typically involve salinity scans at each value of the water oil ratio for which the oil scan is done. Varying the water oil ratio varies the proportion of in situ soap generated in the case of reactive crudes and hence affects the optimum salinity.

      Another very important aspect of phase behavior experimentation is the order in which the different substances are added. Since the stock solutions used are several times as concentrated as that of the final solution, there is the risk of precipitation due to super saturation. To minimize this risk, the typical order of addition followed was the addition of the electrolyte solution followed by the injection water. This was followed by the surfactant stock solution, thereby completing the aqueous phase. The aqueous fluid level was then noted (This is required for the solubilization ratio calculations) and crude oil was the last component added.

Sealing and mixing of the pipettes

After all the required components were added to the pipettes, the ends of the pipettes were sealed using the pipette sealing apparatus described above. The contents were allowed to mix well by inverting and reverting back a few times and then allowed to equilibrate at the reservoir temperature in a convection oven. This increases the contact area between the oleic and aqueous phases and aids in faster equilibration of the samples. The greater contact area between the phases is also a better representation of the porous medium than with the original contact area in the pipettes.

Aqueous stability experiments

The principle objective of performing aqueous stability experiments is to determine the compatibility of the surfactants and polymers with the electrolytes. Aqueous stability experiments were performed for each of the formulations for which microemulsion phase behavior experiments were done. The idea is to ensure that any potential formulation that is to be injected in the reservoir is a clear single phase solution without any precipitates. This is a necessary condition for any formulation to be deemed successful in phase behavior experiments and being considered for core flood experiments. The aqueous phase components were added in the same order as that of the microemulsion phase behavior experiments into vials with the exception of the additional component, the polymer solution, which is added as the first component. These vials were then capped and visually inspected after a few hours for the salinity level up to which a clear and stable single phase solution results without the presence of precipitates.

3.3.3 Measurement, Observation and Calculations

Both qualitative as well as quantitative observations were used to characterize microemulsions. These are described in the section below, along with the associated calculations.

Visual assessment

A qualitative, visual assessment of the pipettes was used to assess the presence of gels or highly viscous macroemulsion phases. Such phases may cause the plugging of the rock as well as increase the surfactant retention. Formulations that form such phases during the microemulsion phase behavior experiments were not considered for core flooding experiments.

Quantitative measurements

After an initial screening by visual inspection described above, the levels of the pipettes were noted after different equilibration times. From these level readings, the volumes of the oleic, aqueous and the microemulsion phases can be calculated, as also the oil and water solubilization ratios described below. Readings were taken till the levels of these phases remained stable for an extended period of time, after which the sample is said to have been fully equilibrated. These readings were then used for the calculations described below. The time taken for achieving complete equilibration of the samples is an important parameter for characterizing microemulsions.

Calculations

The most important parameters calculated by reading the pipette levels are the oil and water solubilization ratios. From these, the interfacial tension between the different phases may be estimated. These are discussed below.

Oil solubilization ratio

Oil solubilization ratio is defined as the volume of oil solubilized in the microemulsion phase to that of the surfactant added and is given by,

$$\sigma_0 = \frac{V_o}{V_s} \quad \text{……………………………………………} \quad (3.2)$$

where,

σ_0 = Oil solubilization ratio

V_o = Volume of oil solubilized (i.e. in the microemulsion phase)

V_s = Volume of surfactant added

In this calculation, all the surfactant is presumed to be in the microemulsion phase. Hence, the volume of surfactant added is equal to that present in the microemulsion phase. The volume of oil solubilized is calculated as the difference between the initial aqueous level (before adding the oil) and the oil -microemulsion interface level.

Water solubilization ratio

Water solubilization ratio is defined as the volume of water solubilized into the microemulsion phase to that of the surfactant added and is given by,

$$\sigma_w = \frac{V_w}{V_s} \quad\text{...} \quad (3.3)$$

where,

σ_w = Water solubilization ratio

V_w = Volume of water solubilized (i.e. in the microemulsion phase)

V_s = Volume of surfactant added

Here too, all the surfactant is assumed to be in the microemulsion phase. Hence, the volume of surfactant added is equal to that present in the microemulsion phase. The volume of water solubilized is calculated as the difference between the initial aqueous level (before adding the oil) and the microemulsion - water interface level.

Optimum solubilization ratio and optimal salinity

The optimum solubilization ratio is defined as the solubilization ratio at the point where the oil and water solubilization ratios are equal. The corresponding salinity is defined as the optimal salinity. They are usually determined from the lab data by plotting the oil and water solubilization ratios on the same plot versus the salinity for a series of pipettes. The optimum solubilization ratio is defined as the ordinate of the point of intersection of the two curves, while the optimal salinity is the corresponding abcissa. The optimal solubilization ratio is given by,

$$\sigma^* = \sigma_0 = \sigma_w \quad\text{.....................................} \quad (3.4)$$

where,

σ^* = Optimum solubilization ratio.

At the optimal salinity (and hence the optimal solubilization ratio), all the microemulsion is of the bicontinuous Windsor Type III type.

Interfacial tension

The interfacial tension is calculated from the optimum solubilization ratio using the Chun Huh equation (Huh, 1979) and is given by,

$$\gamma = \frac{0.3}{(\sigma^*)^2} \quad \ldots\ldots\ldots\ldots\ldots\ldots\ldots\ldots\ldots\ldots\ldots\ldots\ldots\ldots\ldots\ldots\ldots (3.5)$$

where,

γ = Interfacial tension

σ^* = Optimum solubilization ratio.

3.3.4 Scan Refinement and Optimization

Criteria for screening

The phase behavior mixtures were screened based on the qualitative and quantitative parameters discussed above. Qualitative screening criteria include absence of viscous gels and formation of free flowing low viscous microemulsions. Quantitative screening criteria included a solubilization ratio of more than 10 and a reasonably low equilibration time (typically less than 7 days).

Scan Refinement

Initial screening tests usually cover a larger salinity range to identify roughly the salinity range at which the type III microemulsion phase occurs. Once the mixtures which

pass the screening criteria has been identified through these initial scans, further salinity scans with smaller salinity increments between the adjacent pipettes were done. From these, the best mixture is selected, provided it also passes the aqueous stability tests.

Optimization of the formulation

After the best formulation has been identified by means of phase behavior experiments, it is optimized so as to minimize the chemical costs. One of the main steps in this regard is the reduction of the co-solvent concentration. The optimal formulation identified here was then tested by means of core flooding experiments for fluid displacement behavior in porous media.

3.4 CORE FLOODING EXPERIMENTS

Core flooding experiments were performed to test the formulations identified through phase behavior experiments for fluid displacement behavior in porous media through flow experiments. A detailed description of the core flood experimental equipment, the experimental setup, design and the analysis of the experimental data are discussed in this section.

3.4.1 Experimental Setup

Figure 3.1 shows the experimental setup used for the core flooding experiments. In these experiments, mineral oil acts as the displacing medium for the brine/ASP slug/ Polymer drive solutions which are placed in glass columns and is driven by a pump. The fluids were injected into the core, which was maintained at the reservoir temperature in a convection oven. The effluent solutions were collected in calibrated burettes or test tubes.

Experimental Equipment

This section describes the experimental equipment used for performing the core flood experiments.

Cores

Cores are essentially cylindrical sections of rocks, both outcrop and reservoir rocks obtained by the coring process. Cores used for the core flooding experiments were usually about one foot in length and about 1.5-2" in diameter. In the case of outcrop cores, a single core of about 1 ft in diameter was used. In the case of the reservoir cores, multiple short (about 0.25 ft) core plugs were stacked in a core holder and held in place under high pressure (upto 1000-1500 psi). The outcrop cores used for the experiments described here were of Berea sandstone, while the reservoir cores tested were also sandstone cores, which were obtained from the site of the reservoir.

Core Holders

Stainless steel core holders were used for holding the reservoir core plugs which were stacked one over the other to obtain a nearly foot long core. To prevent the core plugs from getting displaced during the experiments, the core holder was maintained under high pressure conditions (upto 1000-1500 psi). Pressure drops across different sections of the core were measured through three pressure taps located in the core holder.

In the case of outcrop cores like Berea sandstone, Lexan tubes were used as core holders. The core preparation procedure for Berea cores is described in the next section.

Glass Columns

Glass columns were used to store fluids for injection into the core. Smaller columns (capacity about 200 ml) were used for storing the SP/ASP slug. Larger columns (capacity about 700ml) were used for storing the brine (for the brine and the water floods) and the polymer drive. These columns were capped at the ends using end pieces and sealed with Teflon tape to prevent any leakage of the fluid.

Stainless steel columns

Stainless steel columns were used to store fluids at high pressure for injection into the core. This is used to store the crude oil which was injected into the core during the oil flood under high pressure (~100psi).

Pumps

Instrument Speciality Company's ISCO LC-5000 syringe pump was used for injecting fluids into the core. Synthetic mineral oil was used as the pumping fluid.

Pressure Transducers

The pressure drops across different sections of the core were measured using differential pressure transducers. The transducers used were of the piezoelectric type which has an internal diaphragm whose deflection was converted to electric voltage. The output voltage is fed to a data acquisition card which converts it to a calibrated pressure reading. Figure 3.1 shows the locations of the different pressure transducers in the core flood experimental setup.

Data Acquisition Recorder

The real time pressure data from core flood experiments was gathered using National Instruments USB 6008 multifunctional data acquisition card with the Labview 7.0 software providing the interface.

Fractional collector

An Instrument Speciality Company (ISCO) Retriever II fractional collector was used for collecting the effluent samples from the outlet of the core and was programmed to collect effluent samples at fixed intervals of time. This timer was adjusted depending on the flow rate used in the experiment in such a way that a reasonable (2-3 ml) of the effluent was collected in each test tube.

Filter Press Apparatus

Filtration of solutions like the polymer, SP/ASP slug, polymer drive, crude oil etc was done using a stainless steel OFITE filter press apparatus. The samples were forced through the filter paper at a pressure of about 15 psi using compressed air. Crude Oil was filtered using 0.45 micron Millipore hydrophilic cellulose filter. Polymer solutions were filtered using a 1.2 micron sized filter.

Viscometer

The viscosity of solutions like the polymer solution, SP/ASP slug, polymer drive, crude oil and the effluent samples were measured using a Contraves LS-30 (Low Shear) Couette type viscometer. This instrument is designed to measure viscosities for shear rates ranging from 0.0174 to 128.5 s^{-1}.

TA Instruments' Advanced Rheometric Expansion System (ARES) LS-1 viscometer was used to measure the viscosities for some of the solutions used in the core flooding experiments. The Force Rebalance Transducer (FRT) and the Low Shear (LS) motor measure the torque generated in response to a shear strain applied to a sample. This torque is converted to a time varying or steady state quantities which are displayed on the data acquisition software for the viscometer known as the TA Orchestrator.

3.4.3 Experimental Procedure

Preliminary measurements and calculations

Some of the preliminary measurements and calculations to determine the bulk volume, pore volume and porosity of the core are described below.

The Bulk volume of the core is calculated by measuring the dimensions of the core and is given by,

$$V_b = \frac{\pi}{4} D^2 L \dots\dots\dots\dots\dots\dots\dots\dots\dots\dots\dots\dots\dots\dots\dots\dots\dots\dots\dots \text{(3.6)}$$

where,

V_b = Bulk volume of the core

D = Diameter of the core

L = Length of the core

The Pore Volume of the core is calculated by the difference in the mass of the core before and after saturating the core with water/brine and is given by,

29

$$V_p = \frac{W_{sat} - W_{dry}}{\rho_{brine}} \quad \text{..} \quad (3.7)$$

where,

V_p = Pore volume of the core

W_{sat} = Weight of the core saturated with brine

W_{dry} = Weight of the dry core

ρ_{brine} = Density of the brine

Porosity of the core is given by the ratio between the pore volume of the core to its bulk volume, i.e

$$\phi = \frac{V_p}{V_b} \quad \text{..} \quad (3.8)$$

where,

ϕ = Porosity of the core

V_p = Pore volume of the core

V_b = Bulk volume of the core

It should be noted that the above described methods of calculating the pore volume and porosity of the core were used only for the case of Berea sandstone cores. For the case reservoir cores which were made by stacking the individual core plugs and subjecting them to a confining pressure to hold them in place, tracer tests were used to determine the pore volume. These are described in the following section on the preliminary flooding experiments on the core.

Preliminary flooding experiments

The cores were subjected to a series of preliminary flooding experiments to replicate the conditions existing in the reservoir prior to the chemical flood. These experiments are described below.

Brine Flooding

The core was initially saturated with synthetic reservoir formation brine at the reservoir temperature. About 3-4 PV of the brine was injected into the core at a high flow rate (~5 ml/min) using synthetic mineral oil as the displacing fluid. The effluent was collected in burettes. The flow rates were measured by measuring the time required for a particular volume of the effluent to be collected in the burette (usually 5-10 ml). The flooding was continued till a constant pressure profile, as measured by the pressure transducers was obtained in all sections of the core. The pressure drop values obtained during the brine flood were used to calculate the brine permeability using Darcy's law.

Tracer Flooding

This particular step was done only for the case of reservoir cores to determine the pore volume of the core. A mixture of 1000 ppm Iso propyl Alcohol (IPA) and 1000 ppm n-Pentanol was used as tracers. Of these, IPA is a non-partitioning tracer while n-Pentanol partitions into the oil phase. The use of a mixture of a partitioning and a non-partitioning tracer for the tracer test enabled us to confirm the presence of any residual oil in the core plugs. About 0.5 PV of the tracer was injected followed by about 2.5 PV of the synthetic formation brine. The tracer concentration in the effluent was analyzed using a gas chromatograph and from the analysis of the normalized tracer concentration plot, the pore volume of the core was calculated.

Oil Flooding

The brine saturated core after the brine flood was injected with filtered crude oil. Crude oil was kept in a stainless steel column and was displaced by brine kept in another stainless steel column which in turn was displaced with mineral oil. The crude oil was injected from the top of the core to ensure gravity stability. The effluent was collected in burettes and the volume of the brine so collected was measured to determine the oil saturation in the core by material balance. The oil flood was continued till a water cut of less than 1% was obtained. The pressure drop values measured during the oil flood were used to calculate the oil permeability and hence the oil relative permeability.

Aging the core

This step was done only for the case of reservoir core floods. The core was aged for a week at the reservoir temperature to allow for a change in wettability to more realistically mimic field scale wettability conditions. After aging, the core was oil flooded again and the new oil saturation was determined by the same procedure as outlined above.

Water Flooding

The oil saturated core was then flooded with synthetic formation brine. A low injection rate was used (~4ft/day) which corresponds to typical pressure drops of less than 5 psi/ft which is close to the actual field values. The effluent was collected in burettes. From the measured volume of oil collected in the burette, the residual oil saturation was calculated through a simple material balance. The experiment was continued till an oil cut of less than 1% was obtained. The pressure drop values measured

during the water flood were used to calculate the water permeability and hence the relative permeability.

Calculations Related to the Preliminary Flooding Experiments

Permeability calculations

Pressure and flow data from the individual flooding experiments were used to calculate the corresponding permeabilities using Darcy's law. These calculations assume a steady state flow regime. This is assumed to be nearly true when the pressure data vary by less than 5% over a 0.2 PV period. Hence, all the flow experiments were continued till these conditions were met to enable the accurate determination of the permeabilities.

Brine permeability

Brine permeability was calculated from the brine flood pressure drop and flow rate data using Darcy's law. For single phase flow of brine at a water saturation of 1, the permeability is given by: ,

$$k = \frac{q\mu L}{A\Delta P}$$ …………………………………………………..……… (3.9)

where,

k = Brine permeability

q = Flow rate during the brine flood (at steady state)

μ = Viscosity of the brine

L = Length of the core

A = Area of the core

ΔP = Pressure drop across the core (at steady state)

End Point Oil Permeability

End point oil permeability at connate water saturation was calculated using the oil flood pressure drop and the flow rate data using Darcy's law. The oil permeability is given by,

$$k_0 = \frac{q_0 \mu_0 L}{A\Delta P}$$ …………………………………………………… (3.10)

where,

k_o = Oil permeability at connate water saturation

q_o = Flow rate during the oil flood (at steady state)

μ_o = Viscosity of the oil

End Point Oil Relative Permeability

The End point oil relative permeability is given by the ratio of the oil permeability at connate water saturation to the brine permeability at a water saturation of 1. permeability of the core, i.e.

$$k_{ro} = \frac{k_o}{k}$$ ……………………………………………….………… (3.11)

where,

k_{ro} = Oil relative permeability

k_o = Oil permeability

k = Brine permeability

End Point Water Permeability

The End point water permeability was calculated from the steady state single phase flow water flood pressure drop at residual oil saturation using Darcy's law:

$$k_w = \frac{q_w \mu_w L}{A \Delta P} \ldots\ldots\ldots\ldots\ldots\ldots\ldots\ldots\ldots\ldots\ldots\ldots\ldots\ldots..\ldots\ldots.. \text{ (3.12)}$$

where,

k_w = Water permeability

q_w = Flow rate at steady state

μ_w = Viscosity of water

End Point Water Relative Permeability

The End point water relative permeability is given by the ratio of the water permeability at residual oil saturation to the brine permeability at a brine saturation of 1.

$$k_{rw} = \frac{k_w}{k} \ldots\ldots\ldots\ldots\ldots\ldots\ldots\ldots\ldots\ldots\ldots\ldots.\ldots\ldots\ldots.. \text{ (3.13)}$$

where,

k_{rw} = Water relative permeability

k_w = Water permeability

k = Brine permeability

Phase Saturation Calculations

As described in the section on the preliminary flooding experiments, the saturations were calculated from a material balance based on the volumes of the effluent samples generated during the corresponding floods. These calculations are described below.

Initial Oil Saturation

The initial oil saturation is determined from the volume of water collected in the burette during the oil flooding experiment as,

$$S_{oi} = \frac{V_w}{V_p} \qquad\qquad\qquad\qquad\qquad\qquad\qquad\qquad (3.14)$$

where,

S_{oi} = Initial Oil Saturation

V_w = Volume of water in the effluent (during the oil flood)

V_p = Pore Volume of the core

Residual Oil Saturation

The Residual oil saturation is determined from the volume of oil recovered in the effluent during the water flood and is given by,

$$S_{or} = \frac{V_o}{V_p} \qquad\qquad\qquad\qquad\qquad\qquad\qquad (3.15)$$

where,

S_{or} = Residual Oil Saturation

V_o = Volume of oil in the effluent (during the water flood)

V_p = Pore Volume of the core

3.4.5 Chemical Flooding

After the preliminary flooding experiments, the core is ready to be flooded with the SP/ASP slug. This section describes the calculations involved in the design of the chemical flood, followed by the chemical flooding procedure and finally by the methods and calculations involved in the analysis of the chemical flood experimental data.

Design calculations

The formulation of the SP/ASP slug is determined by the phase behavior experiments described in the previous section. However, for the design of a chemical flood, concepts like salinity gradient and mobility control are important. The calculation and estimation of these are described in this section.

Mobility and Mobility Ratio

Mobility of a fluid is defined as the ratio between the permeability of the fluid to its viscosity and describes the ability of a fluid to flow under a pressure gradient. Mathematically,

$$\lambda = \frac{k}{\mu} \quad \text{...} \quad (3.16)$$

where,

λ = Mobility of the fluid

k = Permeability of the medium towards the fluid

37

μ = Viscosity of the fluid

Mobility Ratio is defined as the ratio between the mobility of the displacing fluid to that of the displaced fluid. Mathematically,

$$M = \frac{\lambda_{\text{displacing}}}{\lambda_{\text{displaced}}} = \frac{k_{\text{displacing}} / \mu_{\text{displacing}}}{k_{\text{displaced}} / \mu_{\text{displaced}}} \quad \text{.....................} \quad (3.17)$$

where,

M = Mobility Ratio

$\lambda_{\text{displacing}}$ = Mobility of the displacing fluid

$\lambda_{\text{displaced}}$ = Mobility of the displaced fluid

$k_{\text{displacing}}$ = Permeability of the displacing fluid

$k_{\text{displaced}}$ = Permeability of the displaced fluid

$\mu_{\text{displacing}}$ = Viscosity of the displacing fluid

$\mu_{\text{displaced}}$ = Viscosity of the displaced fluid

For a stable displacement front, a mobility ratio of less than one is desirable.

Apparent Viscosity

Apparent viscosity is defined as the inverse of the total relative mobility of the flood. Mathematically,

$$\mu_{\text{app}} = \frac{1}{\dfrac{k_{\text{rw}}}{\mu_{\text{w}}} + \dfrac{k_{\text{ro}}}{\mu_{\text{o}}}} \quad \text{..} \quad (3.18)$$

where,

μ_{app} = Apparent viscosity

k_{rw} = Relative permeability to water

k_{ro} = Relative permeability to water

μ_w = Brine/Water viscosity

μ_o = Oil viscosity

The chemical flood is so designed that the apparent viscosity of the SP/ASP slug is greater than or equal to the apparent viscosity of the oil bank. This ensures a favorable mobility ratio and hence a stable displacement front.

Chemical Flooding Procedure

The core at residual oil saturation after the water flood was flooded with about 0.3 PV of the SP/ASP slug and is then followed by about 2 PV of the polymer drive. To maintain optimal salinity gradient, the SP/ASP slug was injected at or near the optimal salinity of the formulation while the polymer drive was injected at a salinity of about 50-60% of the salinity of the SP/ASP slug. An injection rate of about 1 ft/day was used to mimic field scale interstitial velocities. The effluent was collected in tubes at regular intervals using a fractionating collector.

Post Flood Effluent Analysis

Oil recovery was determined by measuring the cumulative volume of crude oil collected in the tubes. The oil recovery history was plotted as the fraction of the residual oil recovered with respect to dimensionless time.

The pH, viscosity and electrical conductivity of the effluent were measured and plotted as the respective histories against dimensionless time. Measurement of the

electrical conductivity of the effluent enables the determination of the salinity history of the flood which helps to verify whether sufficient salinity gradient was being maintained during the flood. The pH history of the case of ASP floods enabled us to determine whether sufficient amount of alkali was present throughout the length of the flood (after allowing for the consumption of the alkali through various mechanisms) to maintain sufficiently alkaline conditions throughout the flood. The viscosity histories enabled us to determine whether sufficient mobility control was being maintained throughout the length of the flood.

The surfactant retention in the core was determined by measuring the the produced surfactant concentrations in the effluent samples using a High Performance Liquid Chromatograph (HPLC) and doing a simple material balance with the injected surfactant.

Chemical Flooding Calculations

Some of the important parameters calculated from the chemical flood data are the cumulative oil recovery, the polymer permeability reduction factor and the resistance factor. These are described below.

Cumulative Oil Recovery

The cumulative oil fraction recovered in the chemical flood is calculated by adding up the volumes of the free oil recovered in the different tubes. Mathematically, it is given by,

$$f = \sum_{i=1}^{n} \frac{V_{o,i}}{S_{or} V_p}$$ …………………………………………….. (3.19)

where,

f = Fraction of the cumulative residual oil recovered

$V_{o,i}$ = Volume of free oil recovered in the ith tube

S_{or} = Residual Oil Saturation of the core

V_p = Pore volume of the Core

Polymer Permeability Reduction factor

Polymer permeability reduction factor is the ratio between the effective brine permeability to that of the effective polymer permeability and is given by,

$$R_k = \frac{k_w}{k_p} \dots\dots\dots\dots (3.20)$$

where,

R_k = Permeability Reduction Factor

k_w = Effective brine permeability

k_p = Effective polymer permeability

Polymer Resistance Factor

Polymer Resistance factor is defined as the ratio of the mobility of the brine to that of the polymer. This ratio is equivalent to the inverse of the ratios of the corresponding pressure drops and is given by,

$$R_f = \frac{\lambda_w}{\lambda_p} = \frac{k_w \mu_p}{k_p \mu_w} \dots\dots\dots\dots (3.21)$$

where,

41

R_f = Resistance Factor

λ_w = Mobility of water

λ_p = Mobility of the polymer
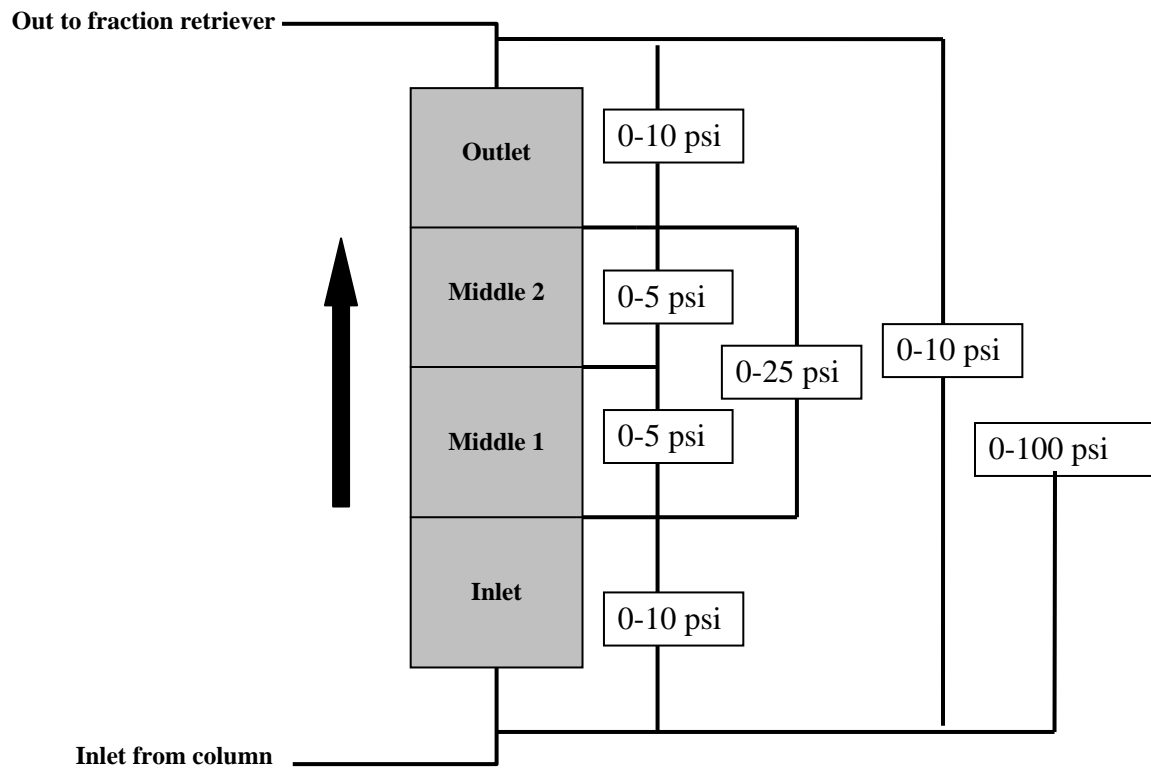
Figure 3.1: Core Flood Experimental setup showing the different sections of the core and the positions of the corresponding differential pressure transducers

Chapter 4: Design and Optimization of an EOR Formulation under High Hardness Conditions

This chapter describes and analyzes the experimental results of the current research which were aimed at designing an optimal chemical formulation for a reservoir with a hard formation brine. The first section describes the results of phase behavior experiments performed to identify an optimal Surfactant Polymer formulation for the crude. The next section describes the results of core flooding experiments performed to validate the SP formulation and optimize the design. The third section describes phase behavior and core flooding experiments to design and optimize an Alkali Surfactant Polymer formulation for the same reservoir. These experiments used the novel alkali, sodium metaborate with the hard brine so as to obtain high pH necessary to reduce the surfactant adsorption, while at the same time minimizing the costs associated with softening the brine before injection. Finally, the results are summarized and the conclusions drawn from these results are discussed.

4.1 CRUDE OIL AND FORMATION BRINE DESCRIPTION

The crude oil is from a low temperature (25°C) sandstone reservoir having a moderate average permeability (~150 md). The crude oil is light (API gravity of 37 degrees) and has a low viscosity of 6.5 cp. The oil is non-reactive with an acid number of about 0.1 mg KOH/ gm oil. The reservoir formation brine has a salinity of 65000 ppm TDS with about 2000 ppm of Ca^{2+} and 800 ppm of Mg^{2+}. The make up injection water used was a fresh lake water (218 ppm TDS). Table 4.1 lists the ionic composition of the synthetic formation brine (53019 ppm TDS) used for the phase behavior and core flooding experiments in the laboratory, along with that of the synthetic injection water.

4.2 PHASE BEHAVIOR EXPERIMENTS

Chemical components of SP/ASP formulations include surfactants, co-surfactants, co-solvents, polymer, brine and alkali. Optimization of the formulation involves the screening of high performance chemicals as well as optimizing their concentrations. This section describes the microemulsion phase behavior experiments performed to identify a suitable SP/ASP formulation. Screening criteria included a high solubilization ratio of at least 10 at the optimal salinity, a wide three phase (type 3) region, smooth free flowing interfaces having low viscosity, the absence of gels or other viscous phases and a short coalescence time for the microemulsion. In addition, the aqueous SP solution at the optimal salinity must be a clear, single phase, stable solution.

A systematic procedure was followed for screening high performance EOR chemicals through phase behavior experiments. As a first step, a general surfactant screening was done. This step identified potential EOR surfactants that could be used with the crude. This was followed by co-solvent screening experiments, wherein different co-solvents and non-ionic co-surfactants were screened in an attempt to improve the aqueous stability of the formulation. This was finally followed by experiments that optimized the formulation. The optimization parameters included the surfactant concentration, the co-solvent concentration and the surfactant to co-surfactant ratio. The following sections describe these experiments in detail.

4.2.1 Initial surfactant and co-surfactant screening

The initial set of experiments was used to screen potential surfactants and co-surfactants. The objective of these experiments was to try and obtain a surfactant/co-surfactant combination that would provide a high solubilization ratio (more than 10 cc/cc), which corresponds to an ultralow interfacial tension (IFT) (less than 10^{-3}

dynes/cm). Additional screening criteria included a sufficiently wide three phase region and a fluid middle phase with low viscosity and the absence of gels.

The chemical compositions of the surfactants selected for the initial screening experiments were based on previous research with similar crudes and a basic knowledge of the crude oil composition. Previous studies with two light crude oils having similar properties have shown that a mixture of a propoxylated sulfate containing a branched C_{16-17} carbon chain (C_{16-17} 7PO SO_4) and a branched C_{15-18} Internal Olefin Sulfonate (C_{15-18} IOS) performed well with respect to the different phase behavior screening parameters (Levitt, 2006; Jackson, 2006). Moreover, they have also been shown to perform well under conditions of high salinity and hardness (Flaaten, 2008). These surfactants, both individually as well as in combination, were among the formulations tested in the initial screening experiments.

For the first set of initial screening experiments, sodium carbonate was used as the alkali as well as for providing salinity. Scans were done by adding increasing amounts of sodium carbonate to the injection water. Secondary Butyl Alcohol (SBA) was used as the co-solvent. Table 4.2 lists the formulations tested in the initial set of surfactant screening experiments. From among the formulations tested, a mixture of 1.5% C_{16-17} 7PO SO_4 and 0.25% of C_{20-24} IOS showed the best performance. However, the aqueous phase was not clear at the optimal salinity. Figures 4.1 and 4.2 show the solubilization plots for the experiments that showed a good performance in the phase behavior experiments.

Oil scan

Once an initial formulation was identified, an oil scan was done by varying the oil concentration to check for any signs of soap generation in the presence of alkali. Figures 4.3 to 4.7 show the corresponding solubilization plots. From the oil scan results, the

activity map for the oil was constructed. This is shown in Figure 4.8. The small slope of the optimum salinity indicates that crude oil is non-reactive with optimum salinities in the narrow range of 3.65% to 3.85% when the oil concentration changed from 10% oil to 50% oil..

4.2.2 Experiments to improve the Aqueous Stability

The next set of experiments sought to improve the aqueous stability limit of the formulation identified as the best performing through the initial screening experiments.

Scans with the Synthetic Formation Brine and sodium chloride

As discussed in the previous section, the oil scan showed the oil to be non-reactive. Hence, the next set of surfactant screening experiments used a mixture of the synthetic formation brine (SFB) and the injection water (IW) for varying the salinity rather than using sodium carbonate. The synthetic formation brine had a salinity of about 53019 ppm TDS (which included a divalent ion content of about 2800 ppm) while the injection water had a salinity of about 218 ppm TDS. Salinity was varied by mixing different proportions of the synthetic formation brine and injection water. A few experiments also used sodium chloride for varying the salinity in place of the brines in order to compare the aqueous stability. These experiments are described in this section.

The formulation showing good phase behavior identified above, namely a mixture of 1.5% C_{16-17} 7PO SO_4 and 0.25% of C_{20-24} IOS, was tested for aqueous stability using sodium chloride instead of sodium carbonate to vary the salinity. Isobutyl Alcohol (IBA) was used as the co-solvent in this case. This has been shown to give a comparable performance to that of Secondary Butyl Alcohol (SBA) used in the initial screening

experiments, while at the same time having a lower cost. The aqueous stability limit was found to be 20000 ppm, the same as that for the sodium carbonate scan.

Co-surfactant screening

Previous experiments using C_{20-24} IOS as the co-surfactant did not satisfy the aqueous stability criterion. In order to improve the aqueous stability, co-surfactant screening experiments were performed using more hydrophilic co-surfactants in combination with the C_{16-17} 7PO SO_4 as the primary surfactant. For the purposes of general screening, aqueous stability tests were initially done with different co-surfactants in combination with C_{16-17} 7PO SO_4 as the primary surfactant. Once co-surfactants with significantly higher aqueous stability limits as compared to the experiments with C_{20-24} IOS as the co-surfactant were identified, phase behavior experiments were performed to determine the optimal salinity.

Table 4.3 lists the results of these experiments. Co-surfactants tested included EO/PO carboxylates, alkyl benzene sulfonates (ABS) and a lower molecular weight internal olefin sulfonate (C_{15-18} IOS). Of the co-surfactants tested, only the C_{15-18} IOS showed a significantly higher aqueous stability limit of 39764 ppm TDS. A phase behavior experiment was then done with the crude oil. Figure 4.9 shows the corresponding solubilization plot. The formulation showed an optimum salinity of 38500 ppm TDS which was within the aqueous stability limit, along with a sufficiently high solubilization ratio of 13 and a low viscosity microemulsion phase.

4.2.3 Optimization of the Formulation

Once the formulation showing the best performance was identified, the next step was to optimize the formulation. A series of experiments, both microemulsion phase

behavior experiments as well as aqueous stability experiments were performed. These included experiments which sought to reduce the co-solvent concentration, experiments with non-ionic co-surfactants as co-solvents, experiments for optimizing the surfactant concentration and experiments with sodium metaborate as alkali. These are discussed in the following sections.

Reducing the surfactant / co-surfactant concentration

Next experiments were done with progressively decreasing total surfactant concentrations. The main objective was to obtain sufficiently high solubilization ratios using a lower surfactant concentration. The total surfactant concentration was systematically reduced in steps from 2% to 0.5%, keeping the surfactant to co-surfactant ratio as well as the co-solvent concentration constant. The results of these experiments are summarized in Table 4.4. Figures 4.9 to 4.11 show the corresponding solubilization ratio plots.

The results indicate that it is possible to obtain high solubilization ratios at a total surfactant concentration as low as 0.5%.The optimal salinity goes down slightly from 38500 ppm TDS at 2% total surfactant concentration to 35000 ppm TDS at 0.5% total surfactant concentration. The aqueous stability limit goes up from 39764 ppm TDS at 2% total surfactant concentration to 45066 ppm TDS at 0.5% total surfactant concentration.

Co-solvent optimization

Optimization of the co-solvent in the formulation involved experiments which tested different co-solvents for their performance through aqueous stability experiments. Co-solvents tested included both alcohol and glycol ether co-solvents as well as non-ionic hydrophilic co-surfactants. Microemulsion phase behavior experiments were also

performed for promising co-solvents. The best performing co-solvents were then further optimized by testing at lower concentrations so as to minimize the costs associated with their use. The current section describes the results of these experiments.

Co-solvent screening

Co-solvent screening experiments included experiments in which different co-solvents were systematically tested for their performance with respect to the aqueous stability of the formulation and the microemulsion phase behavior.

The initial set of experiments described in the previous sections used two of the butyl alcohols, namely sec-butyl alcohol (SBA) and iso-butyl alcohol as co-solvents. In addition to this, glycol ethers like Diethylene Glycol Butyl Ether (DGBE) and Triethylene Glycol Butyl Ether (TEGBE) were also tested. All these co-solvents were tested at different total surfactant and co-solvent concentrations. The results of these experiments are listed in Tables 4.5 to 4.7. The results indicate that IBA was the best performing co-solvent at higher surfactant concentrations (2% total surfactant), while DGBE showed good performance at lower surfactant concentrations (0.3% total surfactant).

The next set of experiments tested several non-ionic hydrophilic co-surfactants as co-solvents. Non-ionics tested included Neodol 25-12 (C_{12-15} Alcohol Ethoxylate), Tridecyl Alcohol 18EO (TDA 18EO) and Tridecyl Alcohol 6EO (TDA 6EO). The results of these experiments tabulated in Table 4.8 show that Neodol 25-12 and TDA 18 EO show high aqueous stability limits. However, in all three cases, the phase behavior showed very high optimal salinities (greater than 53019 ppm, the salinity of the formation brine). In the salinity range tested, all samples were in the type I region.

In an effort to reduce the optimal salinity, a mixture of co-solvents like IBA and DGBE with non-ionic co-surfactants was tested in the next set of experiments. Table 4.9 lists the results of these experiments. These formulations showed an aqueous stability limit comparable to that with the alcohol and glycol ether co-solvents like IBA and DGBE. However, the optimal salinities were still greater than the salinity of the formation brine due to which all the samples tested were in the Type 1 region for the entire salinity range.

From the co-solvent screening experiments described above, Isobutyl Alcohol (IBA) turned out to be the best performing co-solvent. The next step is to optimize the concentration of IBA so as to minimize the chemical cost. This is described in the next section.

Optimization of the Co-solvent concentration

A series of aqueous stability experiments as well as microemulsion phase behavior experiments were performed to optimize the co-solvent concentration. These scans used successively lesser concentrations of IBA from the initial 2% to 0.5%. They were performed at two different total surfactant concentrations (1% and 0.5%). Table 4.10 and 4.11 list the results of these experiments. Figures 4.10, 4.12 and 4.13 show the corresponding solubilization plots for the best performing formulations.

Experiment S-24 which used a 1% co-solvent concentration with a 1% total surfactant concentration gave a good solubilization ratio of 23 at an optimum salinity of 39800 ppm TDS. The aqueous phase was clear up to 42415 ppm TDS. When a co-solvent concentration of less than 1% was used, viscous gels were seen in the pipettes. Hence, the formulation for the experiment S-24, namely a mixture of 0.75% C_{16-17} 7PO SO_4, 0.25%

of C_{15-18} IOS and 1% IBA at an optimal salinity of 39800 ppm TDS was selected as the final formulation.

4.2.4 Final SP formulation for the core flooding experiments

For the core flooding experiments, it was decided to replace the synthetic formation brine with an equivalent brine (designated as the synthetic produced brine) having a TDS of 65000 ppm and containing about 2700 ppm of Ca^{2+} ions (equivalent to the amount of total divalent ions present in the formation brine) added to the synthetic injection water. The ionic composition of the synthetic produced brine is listed in table 4.12. The experiment with the best performing formulation identified above (S-24) was repeated using the synthetic produced brine instead of synthetic formation water. Figure 4.14 shows the solubilization plot for this experiment (S-100). The optimal salinity of about 25,000 ppm TDS was found to be lower as compared to the earlier experiment (S-24).

There was also a change in the batch of the surfactants supplied by the manufacturer, which had a different manufacturing process compared to the samples used for the phase behavior experiments. This necessitated fresh experiments with the new batch of surfactants. The solubilization plot of the experiment S-131 which was used to design the core flood experiments are shown in figure 4.15. The optimal salinity in this case was 25500 ppm TDS with an optimal solubilization ratio of 20. The aqueous stability limit was about 32700 ppm TDS.

4.3 SURFACTANT-POLYMER CORE FLOOD EXPERIMENTS

The purpose of performing core flood experiments is to test the performance of the SP formulation identified through phase behavior experiments by injecting it into

cores. In addition to the ability to recover oil, core floods also help us to obtain important parameters like the effective permeability, the phase saturations of the different phases, expected pressure drops, surfactant retention and the pH and viscosity histories of the effluent.

This section describes two surfactant polymer (SP) core flooding experiments performed with the formulation identified in the phase behavior experiments described in the previous section for crude 'S'.

4.3.1 Core Flood S-5

The purpose of this experiment was to test the formulation identified in the phase behavior experiments above (Expt. S-131) using a Berea sandstone core.

Core Preparation and Properties

The core used for the experiment was a Berea sandstone core of length 28.5 cm and a diameter of 2 inch. Five minute epoxy was used to affix the end pieces. The core was then placed in a Lexan tube of 7.5" diameter and was cast in a slow setting epoxy with a hardener to epoxy ratio of 1:2. Table 4.13 lists the properties of the core. The setup of the core flood experiment is shown in figure 3.1.

Brine flood

The core was saturated with the synthetic produced brine to measure the brine permeability. The composition of the synthetic produced brine is listed in Table 4.12. About 12 PV of the brine was injected at a flow rate of 8 ml/min which corresponds to a frontal advance rate of about 89 ft/day, until steady state was reached. Figure 4.16 shows

the plot of the pressure drop along different sections of the core during the flood. From the pressure drop data, the corresponding brine permeabilities were calculated using Eq. 3.8. Table 4.14 lists the permeabilities of the different sections of the core. The overall brine permeability was determined to be 433 md.

Oil flood

The core, which was fully saturated with brine, was then flooded with the filtered crude. The filtration was done through a 0.45 micron filter paper. The oil flood was done at a constant pressure of about 88 psi at the reservoir temperature of 25°C. The viscosity of the filtered oil was measured to be 7.9 cp. Figure 4.17 shows the pressure drop across the core during the oil flood. After the oil flood, it was seen that a substantial amount of water was getting produced after getting displaced by the oil. Hence, a second oil flood was performed at the same pressure. Figure 4.18 shows the pressure drop across the core during the second oil flood. From the pressure drop and flow rate data, the oil permeability and oil relative permeability were calculated using Equations 3.10 and 3.11 respectively. The initial oil saturation was calculated from the volume of water collected in the burette at the effluent using Equation 3.14. Table 4.15 lists the different properties of the core calculated from the oil flood data.

Water flood

The oil saturated core at the initial oil saturation was flooded with the synthetic produced brine at a flow rate of about 0.34 ml/min (~4 ft/day). The pressure drops along different sections of the core during the water flood are shown in Figure 4.19. From the pressure drop data, the water permeability and relative permeability were calculated using

54

Equations 3.12 and 3.13 respectively. From the volume of oil collected in the burette at the effluent, the residual oil saturation was calculated using Equation 3.15. Table 4.16 lists the properties of the core calculated from the water flood data.

Chemical flood

Design of the chemical flood

The key parameters in the design of the chemical flood are the salinity of the polymer drive in order to ensure a sufficient salinity gradient and the concentrations of the polymer used in the SP slug and the polymer drive to maintain a favorable mobility ratio.

The formulation used for the surfactant polymer slug was the formulation identified in the phase behavior experiment S-131 described in the previous section and consisted of a mixture of 0.75% C_{16-17} 7PO SO_4, 0.25% of C_{15-18} IOS and 1% IBA at a salinity of 22000 ppm TDS, which is close to the optimal salinity of 25500 ppm TDS. The polymer drive was injected at a salinity of 8000 ppm TDS to ensure sufficient salinity gradient.

The polymer used in the formulation was Flopam 3330S. Figure 4.20 shows the viscosities of the polymer at the salinities of the SP slug and the polymer drive at different polymer concentrations plotted against the polymer concentration.

The concentration of the polymer used in the SP slug and the polymer drive was determined using the apparent viscosity concept described in Section 3.4.5. A polymer concentration of 3000 ppm TDS was used for the SP slug while the polymer drive used a polymer concentration of 2500 ppm TDS. The corresponding viscosities were measured to be 17.3 cp and 20 cp, respectively. Figures 4.21 and 4.22 show the viscosity vs shear rate plots for the SP slug and the polymer drive, respectively.

Chemical flooding

The core at residual oil saturation was injected with 0.3 PV of the surfactant polymer slug followed by about 2 PV of the polymer drive. The injection was done at a rate of 0.10 ml/min, which corresponds to a frontal advance rate of 1 ft/day. Effluent samples were collected in graduated tubes every 30 minutes giving a sample size of nearly 3 ml. Figure 4.23 shows the pressure drop across different sections of the core during the chemical flood plotted against the pore volumes injected.

Oil Recovery

Figure 4.24 shows the cumulative oil recovered during the chemical flood plotted against the pore volumes injected, along with the corresponding oil cut and the residual oil saturation. An oil bank was seen between 0.3 PV and 0.83 PV when the emulsion breakthrough occurs. Microemulsion was produced between 0.83 PV and 1.47 PV. The cumulative oil recovered during the chemical flood was 70%. About 58% of the residual oil was produced in the oil bank as free oil while about 12.6% was recovered during the microemulsion and emulsion production. The residual oil saturation after the chemical flood was 0.11.

Chemical Flood Effluent Analysis and Calculations

The pH of the effluent samples was measured and is shown in Figure 4.25 plotted against the pore volumes injected. Since no alkali was used in this flood, the pH remains at or near 7 at all times.

The ionic conductivities of the effluents were also measured using an ionic conductivity probe. The TDS is assumed to be proportional to the ionic conductivity and

is calculated using calibration curves with standard samples of known salinity. The calculated TDS is shown in Figure 4.26 plotted against the pore volumes injected. An HPLC analysis of the effluent was done and no surfactant was detected. The calculated adsorption on the core was 0.31 mg surfactant/gm rock.

Chemical flooding parameters like the permeability reduction factor and the polymer resistance factor were calculated using Equations 3.20 and 3.21 respectively and are summarized in Table 4.17, along with other flooding parameters.

Summary of the flood and conclusions

Table 4.18 summarizes the results of the core flood experiment S-5. One possible reason for the relatively low oil recovery is the low pH of the crude oil equilibrated with the brine (about 6.5). A fresh crude oil sample was received and used for the subsequent core floods. This fresh crude oil sample had a higher pH when equilibrated with the brine. The next section describes the next core flood experiment using the same formulation with the new crude oil sample.

4.3.2 Core Flood S-7

The purpose of this core flood experiment was to test the formulation identified in the phase behavior experiments, namely a mixture of 0.75% C_{16-17} 7PO SO_4, 0.25% C_{15-18} IOS and 1% IBA in a Berea sandstone core using the new oil sample.

Phase Behavior Experiments with the new oil sample

A phase behavior experiment was initially done with the new oil sample with the same formulation. Figure 4.27 shows the solubilization plot for the same. The optimal

salinity was about 33000 ppm TDS with an optimal solubilization ratio of about 42 after an equilibration time of 7 days. The high solubilization ratio can be attributed to the equilibration time not being long enough to ensure complete equilibration of the samples. The aqueous phase was clear up to a salinity of 42450 ppm TDS.

Core Properties

The core used for the experiment was a Berea sandstone core of length 11.2" (28.45 cm) and a diameter of 2". Five minute epoxy was used to affix the end pieces. The core was then placed in a Lexan tube of 7.5" diameter and was cast in a slow setting epoxy with a hardener to epoxy ratio of 1:2. Table 4.19 lists the properties of the core.

Brine flood

The core was saturated with the synthetic produced brine to measure the brine permeability. The composition of the synthetic produced brine is listed in Table 4.12. Several pore volumes of the brine was injected at a flow rate of 12 ml/min which corresponds to a frontal advance rate of about 140 ft/day, until steady state was reached. Figure 4.28 shows the plot of the pressure drops along different sections of the core. From the pressure drop data, the corresponding brine permeabilities were calculated using Equation 3.9. Table 4.20 lists the permeabilities of the different sections of the core. The overall brine permeability was calculated to be 429 md.

Oil flood

The core, which was fully saturated with brine was then flooded with the filtered crude 'S'. The filtration was done through a 0.45 micron cellulose filter paper under a

constant pressure of about 50 psi at the reservoir temperature of 25°C. The oil flood was done at a constant pressure of about 83psi at the reservoir temperature of 25°C. The viscosity of the filtered oil was measured to be 7.9 cp. Figure 4.29 shows the pressure drop across the core during the oil flood. From the pressure drop and flow rate data, the oil permeability and oil relative permeability were calculated using Equations 3.10 and 3.11 respectively. The initial oil saturation was calculated from the volume of water collected in the burette at the effluent. Table 4.21 lists the different properties of the core calculated from the oil flood data.

Water flood

The oil saturated core at the initial oil saturation was flooded with the synthetic produced brine at a flow rate of about 0.88 ml/min (~10 ft/day). The pressure drops along different sections of the core during the water flood is shown in Figure 4.30. From the pressure drop data, the water permeability and relative permeability were calculated using Equations 3.12 and 3.13 respectively. From the volume of oil collected in the burette at the effluent, the residual oil saturation was calculated. Table 4.22 lists the properties of the core calculated from the water flood data.

Chemical Flood

Design of the chemical flood

The formulation used for the surfactant polymer slug was the formulation identified in the phase behavior experiment S-200 described earlier in this section. The solubilization plot for the formulation is shown in Figure 4.27. The formulation consisted of a mixture of 0.75% C_{16-17} 7PO SO_4, 0.25% of C_{15-18} IOS and 1% IBA at a salinity of

33000 ppm TDS which is the optimum salinity of the formulation. The polymer drive was injected at a salinity of 22000 ppm TDS to ensure sufficient salinity gradient.

Figure 4.31 shows the viscosities of the polymer Floppam 3330S used in the SP slug and the polymer drive at the salinities of the SP slug and the polymer drive at different polymer concentrations plotted against the polymer concentration.

The concentration of the polymer used in the SP slug and the polymer drive was determined using the apparent viscosity concept described in Section 3.4.5. A polymer concentration of 3000 ppm TDS was used for both the SP slug and the polymer drive. The corresponding viscosities were measured to be 17.7 cp and 17.1 cp respectively. Figures 4.32 and 4.33 show the viscosity vs shear rate plots for the SP slug and the polymer drive respectively.

Chemical flooding

The core at residual oil saturation was injected with 0.3 PV of the surfactant-polymer slug followed by about 2 PV of the polymer drive. The formulation used for the surfactant polymer slug consisted of a mixture of 0.75% C_{16-17} 7PO SO_4, 0.25% of C_{15-18} IOS 1% IBA and 3000 ppm of FP3330S at a salinity of 33000 ppm TDS. The polymer drive consisted of a solution of 3000ppm FP 3330S and was injected at a salinity of 20000 ppm TDS to ensure sufficient salinity gradient. The ionic composition of the SP slug and the polymer drive are listed in Tables 4.23.

The injection was done at a rate of 0.18ml/min which corresponds to a frontal advance rate of 2 ft/day. Effluent samples were collected in graduated tubes every 17 minutes giving a sample size of nearly 3 ml. Figure 4.34 shows the pressure drops across different sections of the core during the chemical flood plotted against the pore volumes injected.

Oil Recovery

The cumulative oil recovered during the chemical flood is shown in Figure 4.35 plotted against the pore volumes injected, along with the corresponding oil cut and the residual oil saturation. An oil bank was seen between 0.28 PV and 0.71 PV, when the emulsion breakthrough occurs. Microemulsion was produced between 0.71 PV and 1.39 PV. The cumulative oil recovered during the chemical flood was 97.7%. About 72% of the residual oil was produced in the oil bank as free oil while about 25.7% was recovered during the microemulsion production. The residual oil saturation after the chemical flood was about 0.007.

Chemical Flood Effluent Analysis and Calculations

The pH and viscosities of the effluent samples were measured. The pH data is shown in Figure 4.36 plotted against the pore volumes injected. Since no alkali has been used in this flood, the pH remains at or near 7 at all times. The effluent viscosity is shown in figure 4.37 in the form of the viscosity ratio, which is the ratio of the viscosity of the effluent to that of the polymer drive, also plotted against the pore volumes injected. The data indicates that all the viscosity ratios are less than 1 which indicates a favorable mobility ratio between the displacing and the displaced phases.

The ionic conductivities of the effluents were also measured using an ionic conductivity probe. The TDS is assumed to be proportional to the ionic conductivity and is calculated using calibration curves with standard samples of known salinity. The calculated TDS is shown in Figure 4.38 plotted against the pore volumes injected. The

salinity window of the three phase region is also indicated. The data shows that a sufficient salinity gradient has been maintained during the flood.

An HPLC analysis of the effluent was done and no surfactant was detected. The amount of injected surfactant was 1.472 mg surfactant/gm rock. Chemical flooding parameters like the permeability reduction factor and the polymer resistance factor were calculated using Equations 3.20 and 3.21 respectively and are summarized in Table 4.24, along with other chemical flooding parameters.

Summary of the flood

Table 4.25 summarizes the results of core flood experiment S-7. An excellent oil recovery of about 97.7% of the water flood residual oil was obtained in the experiment. However, the surfactant retention was high since 0.294 mg surfactant/gm rock was injected and no surfactant was detected in the effluent by the HPLC analysis.

4.4 DESIGN OF AN ALKALI SURFACTANT POLYMER FORMULATION

As described in the previous section, the Surfactant-Polymer formulation containing 0.75% C_{16-17} 7PO SO_4, 0.25% C_{15-18} IOS and 1% IBA showed a higher surfactant retention than desired. In order to reduce the surfactant retention to minimize the chemical cost of the formulation, it was decided to add a small amount of an alkali to raise the pH. In this case, it was not feasible to use sodium carbonate as the alkali as it would precipitate as calcium carbonate in the presence of about 1300 ppm and 900 ppm Ca^{2+} in the SP slug and the polymer drive respectively. Hence, it was decided to use the novel, hardness tolerant alkali, sodium metaborate for the next core flood experiment.

The purpose of this core flood experiment was to test the ASP formulation containing 0.3% sodium metaborate added to the original SP formulation containing 0.75% C_{16-17} 7PO SO_4, 0.25% of C_{15-18} IOS and 1% IBA using a Berea sandstone core.

4.4.1 Phase Behavior Experiment with Sodium Metaborate

As a first step, a phase behavior experiment was done with the formulation consisting of 0.75% C_{16-17} 7PO SO_4, 0.25% of C_{15-18} IOS and 1% IBA after adding about 0.3% sodium metaborate to the formulation. Figure 4.39 shows the solubilization plot for the above formulation. The optimal salinity for the formulation was about 36500 ppm TDS, with an optimal solubilization ratio of about 28.

4.4.2 Core Properties

The core used for the experiment was a Berea sandstone core of length 28.5 cm and a diameter of 2". Five minute epoxy was used to affix the end pieces. The core was then placed in a Lexan tube of 7.5" diameter and was cast in a slow setting epoxy with a hardener to epoxy ratio of 1:2. Table 4.26 lists the properties of the core.

4.4.3 Preliminary Flooding Experiments

Brine flood

The core was saturated with the synthetic produced brine to measure the brine permeability. The composition of the synthetic produced brine is listed in Table 4.12. Several pore volumes of the brine was injected at a flow rate of 11 ml/min which corresponds to a frontal advance rate of about 130 ft/day, until steady state was reached. Figure 4.40 shows the plot of the pressure drops along different sections of the core.

From the pressure drop data, the corresponding brine permeabilities were calculated using Equation 3.9. Table 4.27 lists the permeabilities of the different sections of the core. The overall brine permeability was 454 md.

Oil flood

The core, which was fully saturated with brine was then flooded with the filtered crude 'S'. The filtration was done through a 0.45 micron cellulose filter paper under a constant pressure of about 50 psi at the reservoir temperature of 25°C. The oil flood was done at a constant pressure of about 91 psi at the reservoir temperature of 25°C. The viscosity of the filtered oil was measured to be 5.6 cp. Figure 4.41 shows the pressure drop across the core during the oil flood. From the pressure drop and flow rate data, the oil permeability and oil relative permeability were calculated using equations 3.10 and 3.11 respectively. The initial oil saturation was calculated from the volume of water collected in the burette at the effluent and was found to be 63%. Table 4.28 lists the different properties of the core calculated from the oil flood data.

Water flood

The oil saturated core at the initial oil saturation was flooded with the synthetic produced brine at a flow rate of about 0.88 ml/min (~10 ft/day). The pressure drops along different sections of the core during the water flood is shown in Figure 4.42. From the pressure drop data, the water permeability and relative permeability were calculated using Equations 3.12 and 3.13 respectively. From the volume of oil collected in the burette at the effluent, the residual oil saturation was calculated and was found to be 37%. Table 4.29 lists the properties of the core calculated from the water flood data.

4.4.4 Chemical Flood

Design of the chemical flood

The formulation used for the alkali surfactant polymer slug was the formulation identified in the phase behavior experiment S-202 described earlier in Section 4.4.1. The solubilization plot for the formulation is shown in Figure 4.39 and consisted of a mixture of 0.75% C_{16-17} 7PO SO_4, 0.25% of C_{15-18} IOS and 1% IBA with 0.3% sodium metaborate at a salinity of 35000 ppm TDS, which is close to the optimal salinity of the formulation of 36500 ppm. The polymer drive was injected at a salinity of 22000 ppm TDS to ensure sufficient salinity gradient.

The concentration of the polymer used in the SP slug and the polymer drive was determined using the apparent viscosity concept described in Section 3.4.5. A polymer concentration of 3000 ppm TDS was used for both the SP slug and the polymer drive.

Precipitation in the ASP slug

Precipitation was observed at the bottom of the container in which the ASP slug was stored a couple of hours after the ASP slug was prepared. Filtration of the sample removed the precipitate giving a clear filtrate. However, on keeping for a few hours, precipitation was again observed. Experiments performed to determine the cause of the observed precipitation are discussed in the next section.

4.4.5 Experiments to determine the cause of the precipitation

A series of experiments were performed to identify the cause of the precipitation in the ASP slug. These are described in this section.

Identification of the component of the ASP slug causing precipitation

The first step to determine the cause of the precipitation observed was to determine the component in the slug causing precipitation. The ASP slug was prepared by mixing three components in addition to the polymer, namely

i.   The brine at the optimal salinity of 35000 ppm TDS, inclusive of a Ca^{2+} concentration of 1300 ppm,

ii.   The surfactant stock solution containing the surfactant slug which is four times as concentrated as the concentration in the slug,

iii. The alkali (sodium metaborate) solution

In the first set of experiments, the above components were added two at a time to determine the incompatible pairs among them. The order of addition of the respective components was also taken into account. The pH of the mixture was also determined in each case. Table 4.30 lists the results of these experiments. The results show that precipitation occurred for the case where the brine and the surfactant stock solution were mixed together, irrespective of the order of addition.

The above experiments were repeated in the presence of the polymer. Table 4.31 lists the results. The results were similar to that of the experiments in the absence of the polymer.

In the next set of experiments all the three components were added together. All the possible orders of addition of the three components were tested. Table 4.32 lists the results of these experiments in the absence of polymer. Table 4.33 lists the results of another set of experiments which were done in the presence of the polymer. All the

samples invariably showed precipitation, irrespective of the order of addition or the presence and absence of the polymer.

It was also observed that the quantity of precipitates generated was greater in the presence of all three components as compared to the cases where only the brine and the stock solution were present suggesting that the higher pH caused by the addition of the alkali favored the precipitation reaction.

In order to test the above hypothesis, the experiments listed in Tables 4.32 and 4.33 were repeated after substituting the sodium metaborate with an equivalent concentration of sodium hydroxide. The results are tabulated in Table 4.34. As expected, all the samples showed precipitation. Moreover, the quantity of precipitates was found to be more than that for the cases where sodium metaborate was used as the alkali. This observation can be easily explained by the fact that the pH of the solution when sodium hydroxide is used as the alkali is higher than that where sodium metaborate is used as the alkali. These observations indicate that the precipitation reactions are favored at higher pH.

Two conclusions can be drawn from the results of the experiments in this section.

- The precipitation is caused by the incompatibility between the brine and the surfactant stock solution, in particular that between the Ca^{2+} ions present in the brine and the surfactant stock solution in the presence of metaborate.

- The precipitation reaction is favored under high pH conditions.

Identification of the component of the surfactant stock solution causing precipitation

The next step towards determining the cause of the precipitation was to determine the component of the surfactant stock solution that was incompatible with the Ca^{2+} ions present in the formation brine. The surfactant stock solution consisted of a mixture of,

67

i.   The primary surfactant, C_{16-17} 7PO SO_4,

ii.   The secondary surfactant, C_{15-18} IOS

iii.   The co-solvent, Isobutyl Alcohol (IBA)

Of these, IBA was ruled out as a cause of the precipitation. To determine the component among the surfactant and the co-surfactant that is incompatible with the brine, both the surfactants were tested individually for compatibility with the formation brine in the presence of the co-solvent and the alkali. An experiment with both the surfactants added together was also performed for the sake of comparison. The results are tabulated in Table 4.35.

The results indicate that precipitation was observed for the cases where the C_{15-18} IOS was used separately as well as for the case where both the surfactants were used separately. The case in which the C_{16-17} 7PO SO_4 was tested separately did not show any precipitation.

Conclusions

The above experiments show that sulfate ions in the sample of the co-surfactant used for the preparation of the surfactant slug was incompatible with the Ca^{2+} ions present in the brine under the high pH conditions in the presence of metaborate. This caused the precipitation of the Ca^{2+} ions present in the brine as calcium sulfate.

It was also observed that the precipitation reaction was favored at high pH. This is explained by the pH dependent equilibrium that exists between the SO_4^{2-} and the HSO_4^{-} ions in the solution. This equilibrium is given by

$$H^+ + SO_4^{2-} \rightleftharpoons HSO_4^-$$
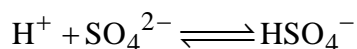
The reverse reaction is favored under high pH conditions wherein the concentration of H^+ ions in the solution decreases, leading to an increase in the concentration of SO_4^{2-} ions in the solution, thereby favoring the precipitation reaction which is given by,

$$Ca^{2+} + SO_4^{2-} \rightleftharpoons CaSO_4$$
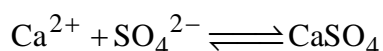
To summarize, the results imply that there was sufficient free calcium present in the solution in the presence of sodium metaborate that precipitation of calcium sulfate occurred. This shows a major limitation in the ability of sodium metaborate to sequester calcium ions in the presence of sulfate ions.

Mitigation of the problem

One way of reducing the tendency to precipitate is to decrease the concentration of Ca^{2+} in the solution. A fresh sample of the synthetic produced brine was prepared which had the same TDS of 65000 ppm, but the concentration of Ca^{2+} was reduced by half, namely 1350 ppm TDS. Table 4.36 lists the ionic compositions of both the original synthetic produced brine (designated as Brine 1 and originally listed in Table 4.12) and the new sample of the synthetic produced brine (designated as Brine 2) alongside each other. At the optimal salinity of 35000 ppm TDS, Brine 2 had a Ca^{2+} concentration of about 750 ppm TDS compared to brine 1 which had a Ca^{2+} concentration of about 1500 ppm TDS. At the salinity of the polymer drive (22000 ppm TDS), the Ca^{2+} concentrations were about 475 ppm and 950 ppm for brines 2 and 1 respectively.

A new sample of the surfactant slug was prepared using the new brine. This was kept for about a day to observe any signs of precipitation and was found to be clear. The chemical flooding experiment was done using this surfactant slug. This is described in the next section.

4.4.6 Chemical Flood with the new ASP slug

The viscosities of the ASP slug and the polymer drive prepared using the brine with reduced concentration of Ca^{2+} were measured to be 18.7 cp and 18.3 cp respectively. Figures 4.43 and 4.44 show the viscosity vs. shear rate plots for the SP slug and the polymer drive respectively. The core at residual oil saturation was injected with 0.3 PV of the alkali-surfactant-polymer slug followed by about 2 PV polymer drive. The formulation used for the alkali-surfactant-polymer slug consisted of a mixture of 0.75% C_{16-17} 7PO SO_4, 0.25% of C_{15-18} IOS 1% IBA, 0.3% sodium metaborate and 3000 ppm of FP3330S at a salinity of 35000 ppm TDS. The polymer drive consisted of a solution of 3000ppm FP 3330S and was injected at a salinity of 22000 ppm TDS to ensure sufficient salinity gradient. The ionic composition of the ASP slug and the polymer drive are listed in Tables 4.37.

The injection was done at a rate of 0.17 ml/min which corresponds to a frontal advance rate of 2 ft/day. Effluent samples were collected in graduated tubes every 18 minutes giving a sample size of nearly 3ml. Figure 4.45 shows the pressure drop across different sections of the core during the chemical flood plotted against the pore volumes injected.

Oil Recovery

The cumulative oil recovered is shown in Figure 4.46 plotted against the pore volumes injected along with the corresponding oil cut and the residual oil saturation. An oil bank was seen between 0.28 PV and 0.95 PV, when the emulsion breakthrough occurs. Microemulsion was produced between 0.95 PV and 1.46 PV. The cumulative oil recovered during the chemical flood was 84.2%. About 74.3% of the residual oil was produced in the oil bank as free oil while about 9.9% was recovered during the microemulsion production. The residual oil saturation after the chemical flood was about 0.058.

Chemical Flood Effluent Analysis and Calculations

The pH and viscosities of the effluent samples were measured. The pH data is shown in figure 4.47 plotted against the pore volumes injected. A pH of about 9.5 is produced due to the use of sodium metaborate as the alkali in this flood. The effluent viscosity is shown in figure 4.48 in the form of the viscosity ratio, which is the ratio of the viscosity of the effluent to that of the polymer drive, also plotted against the pore volumes injected. The data indicates that all the viscosity ratios were less than 1 which indicates a favorable mobility ratio between the displacing and the displaced phases.

The ionic conductivities of the effluent samples were also measured using an ionic conductivity probe. The TDS is assumed to be proportional to the ionic conductivity and is calculated using calibration curves with standard samples of known salinity. The calculated TDS is shown in figure 4.49 plotted against the pore volumes injected. The salinity window of the three phase region is also indicated. The data shows that a sufficient salinity gradient has been maintained during the flood.

An HPLC analysis of the effluent was done and no surfactant was detected (0.289 mg surfactant/gm rock was injected). Chemical flooding parameters like the permeability reduction factor and the polymer resistance factor were calculated using Equations 3.20 and 3.21 respectively and are summarized in Table 4.38, along with other chemical flooding parameters.

Summary of the flood

Table 4.39 summarizes the results of the core flood experiment S-8. The final oil recovery was 84.2% of the water flood residual oil.

4.5 SUMMARY AND CONCLUSIONS

This research was aimed at designing an optimal chemical formulation for a light oil in sandstone reservoir at low temperature using hard brines. An initial surfactant-polymer formulation was developed through phase behavior experiments. This formulation used the surfactants C_{16-17} 7PO SO_4 and C_{15-18} IOS and showed a good oil recovery of nearly 98% from a Berea sandstone core. In an effort to reduce the high surfactant retention (0.294 mg/gm rock), an Alkali-Surfactant-Polymer (ASP) formulation was designed using the hardness tolerant alkali, sodium metaborate with the hard brine. The ASP slug showed precipitation. Experiments to determine the cause of the precipitation showed the precipitating species to be calcium sulfate at high pH caused by the metaborate. The co-surfactant sample C_{15-18} IOS had an excess sulfate ion concentration. Reducing the calcium concentration produced a clear slug without precipitation.

This study showed a major limitation of sodium metaborate with respect to its ability to sequester divalent ions in the presence of sulfate ions. Under the experimental conditions, the calcium tolerance in the presence of about 50 ppm of sulfate ions was found to be less than 1500 ppm when the salinity of the solution was 35000 ppm TDS. This turns out to be a major limitation for a successful field application of sodium metaborate as an alkali.

Table 4.1: Ionic Composition of the Synthetic Formation Brine and the Synthetic Injection Water for Crude 'S'

Ion	Synthetic Formation Brine (ppm)	Synthetic Injection Water (ppm)
Na+	17100	14
Ca++	2003	36
Mg++	885	19
K+	127	4
Cl-	32904	145
TDS	53019	218

Table 4.2: Phase Behavior Experiments for the initial screening of surfactants for Crude 'S'

Expt #	Surfactant		Co-surfactant		Co-solvent		Sol. Ratio (cc/cc)	Opt. Salinity (% Na2CO3)	Aq. Stability limit (% Na2CO3)
	Name	Wt. %	Name	Wt. %	Name	Wt. %			
S - 1	C_{16-17} 7PO SO4	1.50	C_{15-18} IOS	0.50	SBA	2.00	8	6.50%	5%
S - 3	C_{16-18} PO COOH	1.50	C_{15-18} IOS	0.50	SBA	2.00	NA	All Type I	5%
S - 4	C18 IOS COOH	1.50	C_{15-18} IOS	0.50	SBA	2.00	NA	All Type I	5%
S - 5	C_{16-17} 7PO SO4	2.00	-	-	SBA	2.00	6	3.50%	2%
S - 7	C_{16-17} 7PO SO4	1.50	C_{20-24} IOS	0.50	SBA	2.00	11	3.80%	3%

Table 4.3: Aqueous Stability Experiments for screening co-surfactants using C_{16-17} 7PO SO_4 as the primary surfactant for Crude 'S'

Expt #	Surfactant		Co-surfactant		Co-solvent		Aq. Stability limit (ppm TDS)
	Name	Wt. %	Name	Wt. %	Name	Wt. %	
S - 12	C_{16-17} 7PO SO4	1.00	C_{20-24} IOS	1.00	IBA	2.00	5301
S - 15	C_{16-17} 7PO SO4	1.00	C15+ ABS	1.00	IBA	2.00	10000
S - 17	C_{16-17} 7PO SO4	1.00	C16-17 4EO 7PO COOH	1.00	IBA	2.00	15900
S - 18	C_{16-17} 7PO SO4	1.00	C16-17 2EO 7PO COOH	1.00	IBA	2.00	5301
S - 19	C_{16-17} 7PO SO4	1.50	C_{15-18} IOS	0.50	IBA	2.00	39764

Table 4.4: Phase Behavior Experiments for optimizing the total surfactant concentration for crude 'S'

Expt #	Surfactant		Co-surfactant		Co-solvent		Sol. Ratio (cc/cc)	Opt. Salinity (ppm TDS)	Aq. Stability limit (ppm TDS)
	Name	Wt. %	Name	Wt. %	Name	Wt. %			
S - 19	C_{16-17} 7PO SO4	1.50	C_{15-18} IOS	0.50	IBA	2.00	13	38500	39764
S - 20	C_{16-17} 7PO SO4	0.75	C_{15-18} IOS	0.25	IBA	2.00	14	36500	45066
S - 21	C_{16-17} 7PO SO4	0.38	C_{15-18} IOS	0.13	IBA	2.00	17	35000	45066

Table 4.5: Aqueous stability experiments for screening co-solvents for crude 'S' at 2% total surfactant concentration

Expt #	Surfactant		Co-surfactant		Co-solvent		Aq. Stability limit (ppm TDS)
	Name	Wt. %	Name	Wt. %	Name	Wt. %	
S - 10	C_{16-17} 7PO SO4	1.50	C_{15-18} IOS	0.50	DGBE	1.00	2%
S - 11	C_{16-17} 7PO SO4	1.50	C_{15-18} IOS	0.50	IBA	1.00	3%

Table 4.6: Aqueous stability experiments for screening co-solvents for crude 'S' at 0.3% total surfactant concentration and 0.5% co-solvent concentration

Expt #	Surfactant		Co-surfactant		Co-solvent		Aq. Stability limit (ppm TDS)
	Name	Wt. %	Name	Wt. %	Name	Wt. %	
S - 44	C_{16-17} 7PO SO4	0.20	C_{15-18} IOS	0.10	IBA	0.50	37113
S - 45	C_{16-17} 7PO SO4	0.20	C_{15-18} IOS	0.10	DGBE	0.50	47717
S - 56	C_{16-17} 7PO SO4	0.20	C_{15-18} IOS	0.10	TEGBE	0.50	53019

Table 4.7: Aqueous stability experiments for screening co-solvents for crude 'S' at 0.3% total surfactant concentration and 0.25% co-solvent concentration

Expt #	Surfactant		Co-surfactant		Co-solvent		Aq. Stability limit (ppm TDS)
	Name	Wt. %	Name	Wt. %	Name	Wt. %	
SL-55	C_{16-17} 7PO SO4	0.2	C_{15-18} IOS	0.10	DGBE	0.25	47717
SL-57	C_{16-17} 7PO SO4	0.2	C_{15-18} IOS	0.10	TEGBE	0.25	47717

Table 4.8: Aqueous Stability Experiments for screening non ionic co-surfactants as co-solvents for Crude 'S'

Expt #	Surfactant		Co-surfactant		Co-solvent		Aq. Stability limit (ppm TDS)
	Name	Wt. %	Name	Wt. %	Name	Wt. %	
S - 36	C_{16-17} 7PO SO4	0.75	C_{15-18} IOS	0.25	Neodol 25-12	0.10	42415
S - 38	C_{16-17} 7PO SO4	0.20	C_{15-18} IOS	0.10	Neodol 25-12	0.10	47717
S - 39	C_{16-17} 7PO SO4	0.20	C_{15-18} IOS	0.10	Neodol 25-12	0.20	47717
S - 40	C_{16-17} 7PO SO4	0.20	C_{15-18} IOS	0.10	TDA 18 EO	0.10	53019
S - 46	C_{16-17} 7PO SO4	0.20	C_{15-18} IOS	0.10	TDA 6 EO	0.10	21206

Table 4.9: Aqueous Stability Experiments for screening mixtures of non ionic co-surfactants and co-solvents as solvents for Crude 'S'

Expt #	Surfactant		Co-surfactant		Co-solvent		Aq. Stability limit (ppm TDS)
	Name	Wt. %	Name	Wt. %	Name	Wt. %	
S - 54	C_{16-17} 7PO SO_4	0.20	C_{15-18} IOS	0.1	Neodol 25-12	0.10	21207
					IBA	0.25	
S - 47	C_{16-17} 7PO SO_4	0.30	C_{15-18} IOS	0.15	Neodol 25-12	0.10	47717
					IBA	0.25	
S - 48	C_{16-17} 7PO SO_4	0.25	C_{15-18} IOS	0.05	Neodol 25-12	0.10	42415
					IBA	0.25	

Table 4.10: Phase Behavior experiments for optimizing the co-solvent concentration for Crude 'S' at 1% total surfactant concentration

Expt #	Surfactant		Co-surfactant		Co-solvent		Sol. Ratio (cc/cc)	Opt. Salinity (ppm TDS)	Aq. Stability limit (ppm TDS)
	Name	Wt. %	Name	Wt. %	Name	Wt. %			
S - 20	C_{16-17} 7PO SO4	0.75	C_{15-18} IOS	0.25	IBA	2.00	14	36500	45066
S - 24	C_{16-17} 7PO SO4	0.75	C_{15-18} IOS	0.25	IBA	1.00	23	36000	42415
S - 25	C_{16-17} 7PO SO5	0.75	C_{15-18} IOS	0.25	IBA	0.50	24	32000	26509

Table 4.11: Phase Behavior experiments for optimizing the co-solvent concentration for Crude 'S' at 0.5% total surfactant concentration

Expt #	Surfactant		Co-surfactant		Co-solvent		Sol. Ratio (cc/cc)	Opt. Salinity (ppm TDS)	Aq. Stability limit (ppm TDS)	Remarks
	Name	Wt. %	Name	Wt. %	Name	Wt. %				
SL - 21	C_{16-17} 7PO SO4	0.38	C_{15-18} IOS	0.13	IBA	2.00	17	35000	45066	
SL - 26	C_{16-17} 7PO SO4	0.38	C_{15-18} IOS	0.13	IBA	1.00	NA	NA	45066	Forms gels
SL - 27	C_{16-17} 7PO SO4	0.38	C_{15-18} IOS	0.13	IBA	0.50	39	32250	29160	

Table 4.12: Ionic Composition of the Synthetic Produced Brine for Crude 'S'

Ion	Synthetic Produced Brine (ppm)
Na+	22501
Ca++	2800
Cl-	39699
TDS	65000

Table 4.13: Core properties for the core flood experiment S-5 with crude 'S'

Core	S - 5	
Mass	1172.7	g
Porosity	0.2137	
Length	28.5	cm
Length to Tap 1	7.62	cm
Length to Tap 2	15.24	cm
Length to Tap 3	22.86	cm
Length to Outlet	28.5	cm
Diameter	5.03	cm
Area	19.86	cm^2
Temperature	25	^{o}C
Air permeability	*963*	md
Brine permeability	*433*	md
PV	*121*	ml

Table 4.14: Absolute Permeabilities of the different sections of the core obtained from the brine flood for the experiment S-5

Section	Brine Permeability (md)
Whole core	433
Inlet	391
Middle Section	456
Outlet	400

Table 4.15: Results of the oil flooding experiment on core S-5

Initial Oil Saturation	S_{oi}	0.634
Residual Water Saturation	S_{wr}	0.366
Core Inlet Pressure	P_{max}	88.2 psi
Oil Permeability	k_{oil}	349 md
Oil Relative Permeability	k_{ro}	0.82

Table 4.16: Results of the water flood experiment on core S-5

Residual Oil Saturation	S_{orw}	0.368
Water Permeability	k_{water}	17.8 md
Water Relative Permeability	k_{rw}	0.042

Table 4.17: Results of the Chemical flood experiment on core S-5

Residual Oil Saturation after Chemical Flood	S_{orc}	0.104
Chemical Flood Permeability	$k_{chemical}$	142 md
Permeability Reduction Factor	R_k	3.05
Resistance Factor	Rf	60.99
Cumulative Oil Recovery	f	71%

Table 4.18: Summary of the results of the core flood experiment S-5

Rock Type	Berea Sandstone
Pore volume, PV [ml]	121
Porosity	0.2137
K_{brine} [md]	433
K_{ro}	0.82
K_{rw}	0.042
S_{oi}	0.634
S_{orw}	0.368
SP slug	
Conc. of surf. [wt%]	1
Conc. of polymer [ppm]	2500
Salinity [ppm TDS]	22000
Vol. Injected [PV]	0.3
Front Adv. Rate [ft/day]	1
Viscosity [cP], 10s-1	17.3
Polymer Drive	
Conc. of polymer [ppm]	2500
Vol. Injected [PV]	2
Front Adv. Rate [ft/day]	1
viscosity [cP], 10s-1	20
Results	
S_{orc} [%]	11
Oil breakthrough, [PV]	0.3
Surf. Breakthrough [PV]	0.83
% Oil Recovery	70
Adsorption/Retention [mg/g rock]	0.31

Table 4.19: Core properties for the core flood experiment S-7 with crude 'S'

Mass	1167.5	g
Porosity	0.2	
Length	28.5	cm
Length to Tap 1	*7.62*	cm
Length to Tap 2	*15.24*	cm
Length to Tap 3	*22.86*	cm
Length to Outlet	*28.5*	cm
Diameter	5.05	cm
Area	20.07	cm^2
Temperature	25	^oC
Air permeability	*1172*	md
Brine permeability	*429*	md
PV	*114.6*	ml

Table 4.20: Absolute Permeabilities of the different sections of the core obtained from the brine flood for the experiment S-7

Section	Brine Permeability (md)
Whole core	429
Inlet	456
Middle Section	447
Outlet	331

Table 4.21: Results of the oil flooding experiment on core S-7

Initial Oil Saturation	S_{oi}	0.58
Residual Water Saturation	S_{wr}	0.42
Oil Permeability	k_{oil}	347
Oil Relative Permeability	k_{ro}	0.74

Table 4.22: Results of the water flooding experiment on core S-7

Residual Oil Saturation	S_{orw}	0.294
Water Permeability	k_{water}	46
Water Relative Permeability	k_{rw}	0.098

Table 4.23: Ionic Composition of the SP slug and the Polymer drive used for the core flood experiment S-7

Ion	SP Slug (ppm)	Polymer Drive (ppm)
Na+	11257.5	6872.535
Ca++	1426.5	890.835
Cl-	19922	12208.97
TDS	32606	19972.34

Table 4.24: Results of the Chemical flood experiment on core S-7

Residual Oil Saturation after Chemical Flood	S_{orc}	0.007
Chemical Flood Permeability	$k_{chemical}$	267 md
Permeability Reduction Factor	R_k	1.75
Resistance Factor	Rf	29.98
Cumulative Oil Recovery	f	97.70%

Table 4.25: Summary of the results of the core flood experiment S-7

Rock Type		Berea sandstone
pore volume, PV	[ml]	114.6
porosity		0.2011
Kbrine	[md]	429
K_{ro}		0.74
K_{rw}		0.098
Soi		0.58
Sorw		0.294
SP slug		
Conc. of surf.	[wt%]	1
Conc. of polymer	[ppm]	3000
Salinity	[ppm TDS]	33000
Vol. Injected	[PV]	0.3
Front Adv. Rate	[ft/day]	2.11
viscosity [cP], 10s-1		17.6
Polymer Drive		
Conc. of polymer	[ppm]	3000
Vol. Injected	[PV]	2
Front Adv. Rate	[ft/day]	2.11
viscosity [cP], 10s-1		17.1
Results		
Sorc	[%]	0.7
Oil breakthrough,	[PV]	0.28
Surf. Breakthrough	[PV]	0.71
% Oil Recovery		97.7
Adsorption/Retention	[mg/g rock]	0.294

Table 4.26: Core properties for the core flood experiment S-8 with crude 'S'

Mass	1167.5	g
Porosity	0.203	
Length	28.5	cm
Length to Tap 1	7.62	cm
Length to Tap 2	15.24	cm
Length to Tap 3	22.86	cm
Length to Outlet	28.5	cm
Diameter	5	cm
Area	19.66	cm^2
Temperature	25	^oC
Air permeability	983	md
Brine permeability	454	md
PV	112.5	ml

Table 4.27: Absolute Permeabilities of the different sections of the core
obtained from the brine flood for the experiment S-8

Section	Brine Permeability (md)
Whole core	454
Inlet	353
Middle Section	648
Outlet	250

Table 4.28: Results of the oil flooding experiment on core S-8

Initial Oil Saturation	S_{oi}	0.63
Residual Water Saturation	S_{wr}	0.37
Oil Permeability	k_{oil}	336 md
Oil Relative Permeability	k_{ro}	0.77

Table 4.29: Results of the water flooding experiment on core S-8

Residual Oil Saturation	S_{orw}	0.37
Water Permeability	k_{water}	36 md
Water Relative Permeability	k_{rw}	0.082

Table 4.30: Experiments to determine the component of the ASP slug causing precipitation with components added two at a time (in the absence of polymer)

Expt #	Component 1	Component 2	Component 3	Polymer present	pH	Solution state
1	Surfactant stock	Sodium metaborate	-	N	10.23	Clear
2	Surfactant stock	Brine	-	N	7.93	Precipitates
3	Brine	Sodium metaborate	-	N	10.21	Clear
4	Brine	Surfactant stock	-	N	7.97	Precipitates
5	Sodium metaborate	Surfactant stock	-	N	10.40	Clear
6	Sodium metaborate	Brine	-	N	10.14	Clear

Table 4.31: Experiments to determine the component of the ASP slug causing precipitation with components added two at a time (in the presence of polymer)

Expt #	Component 1	Component 2	Component 3	Polymer present	pH	Solution state
13	Surfactant stock	Sodium metaborate	-	Y	10.01	Clear
14	Surfactant stock	Brine	-	Y	8.01	Precipitates
15	Brine	Sodium metaborate	-	Y	9.96	Clear
16	Brine	Surfactant stock	-	Y	7.98	Precipitates
17	Sodium metaborate	Surfactant stock	-	Y	9.97	Clear
18	Sodium metaborate	Brine	-	Y	9.97	Clear

Table 4.32: Experiments to determine the component of the ASP slug causing precipitation with all the three components added together (in the absence of polymer)

Expt #	Component 1	Component 2	Component 3	Polymer present	pH	Solution state
7	Surfactant stock	Sodium metaborate	Brine	N	10.13	Precipitates
8	Surfactant stock	Brine	Sodium Metaborate	N	10.02	Precipitates
9	Brine	Sodium metaborate	Surfactant stock	N	9.86	Precipitates
10	Brine	Surfactant stock	Sodium Metaborate	N	10.05	Precipitates
11	Sodium metaborate	Surfactant stock	Brine	N	10.13	Precipitates
12	Sodium metaborate	Brine	Surfactant stock	N	9.88	Precipitates

Table 4.33: Experiments to determine the component of the ASP slug causing precipitation with all the three components added together (in the presence of polymer)

Expt #	Component 1	Component 2	Component 3	Polymer present	pH	Solution state
19	Surfactant stock	Sodium metaborate	Brine	Y	9.77	Precipitates
20	Surfactant stock	Brine	Sodium Metaborate	Y	9.82	Precipitates
21	Brine	Sodium metaborate	Surfactant stock	Y	9.78	Precipitates
22	Brine	Surfactant stock	Sodium Metaborate	Y	9.76	Precipitates
23	Sodium metaborate	Surfactant stock	Brine	Y	9.72	Precipitates
24	Sodium metaborate	Brine	Surfactant stock	Y	9.77	Precipitates

Table 4.34: Experiments to determine the component of the ASP slug causing precipitation using sodium hydroxide as an alkali

Expt #	Component 1	Component 2	Component 3	Polymer present	pH	Solution state
25	Brine	Surfactant stock	Sodium Hydroxide	Y	12.34	Precipitates
26	Surfactant stock	Brine	Sodium Hydroxide	Y	12.35	Precipitates
27	Brine	Surfactant stock	Sodium Hydroxide	N	12.32	Precipitates
28	Surfactant stock	Brine	Sodium Hydroxide	N	12.31	Precipitates

Figure 4.35: Experiments to identify the component of the surfactant stock solution causing precipitation

Expt #	Surfactant		Co-surfactant		Co-solvent		Alkali		Result
	Name	Wt. %	Name	Wt. %	Name	Wt. %	Name	Wt. %	
S-202	C_{16-17} 7PO SO4	0.75%	C_{15-18} IOS	0.25%	IBA	1%	Sodium Metaborate	0.3%	Precipitation occurs
S-203	-	-	-	-	IBA	1%	Sodium Metaborate	0.3%	No Precipitation
S-204	C_{16-17} 7PO SO4	0.75%	-	-	IBA	1%	Sodium Metaborate	0.3%	No Precipitation
S-205	-	-	C_{15-18} IOS	0.25%	IBA	1%	Sodium Metaborate	0.3%	Precipitation occurs

Table 4.36: Ionic compositions of the old and the new synthetic produced brines

Ion	Synthetic Produced Brine	
	Old Brine (ppm)	New Brine (ppm)
Na+	22501	23901
Ca++	2800	1400
Cl-	39699	39699
TDS	65000	65000

Figure 4.37: Ionic Composition of the ASP Slug and the Polymer Drive for the Core Flood experiment S-8

Ion	SP Slug (ppm)	Polymer Drive (ppm)
Na+	11957.5	7299.535
Ca++	726.5	463.835
Cl-	19922	12208.97
TDS	32606	19972.34

Table 4.38: Results of the chemical flooding experiment on core S-8

Residual Oil Saturation after Chemical Flood	S_{orc}	0.057
Chemical Flood Permeability	$k_{chemical}$	327 md
Permeability Reduction Factor	R_k	1.33
Resistance Factor	Rf	24.3
Cumulative Oil Recovery	f	84.20%

Table 4.39: Summary of the results of the core flood experiment S-8

Rock Type		Berea sandstone
Pore volume, PV	[ml]	112.5
Porosity		0.2007
K_{brine}	[md]	454
K_{ro}		0.77
K_{rw}		0.082
Soi		0.63
Sorw		0.37
SP slug		
Conc. of surf.	[wt%]	1
Conc. of polymer	[ppm]	3000
Salinity	[ppm TDS]	35000
Vol. Injected	[PV]	0.3
Front Adv. Rate	[ft/day]	2.03
Viscosity [cP], 10s-1		18.7
Polymer Drive		
Conc. of polymer	[ppm]	3000
Vol. Injected	[PV]	2
Front Adv. Rate	[ft/day]	2.03
Viscosity [cP], 10s-1		18.3
Results		
Sorc	[%]	5.7
Oil breakthrough,	[PV]	0.28
Surf. Breakthrough	[PV]	0.95
% Oil Recovery		84.2
Adsorption/Retention	[mg/g rock]	0.289

Figure 4.1: Solubilization ratio plot of the Phase Behavior Experiment S-6 using Crude 'S' at 25 C. The formulation contained 2% C_{16-17} 7PO SO_4, 2% IBA in 218 ppm TDS mixing brine.
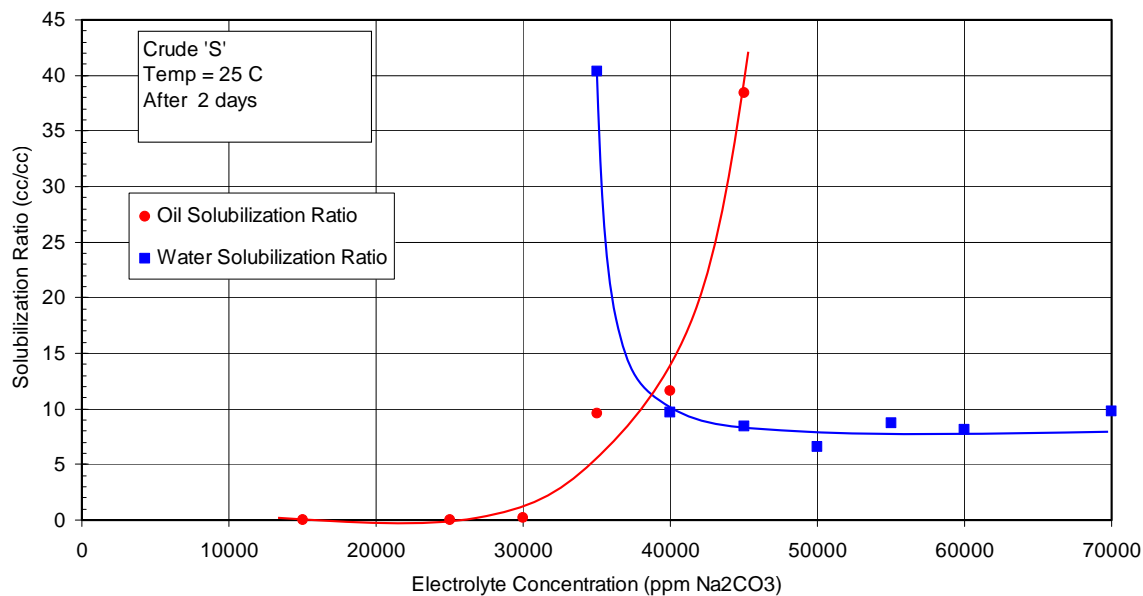
Figure 4.2: Solubilization ratio plot of the Phase Behavior Experiment S - 7 using Crude 'S' at 25 C. The formulation contained 1.5% C_{16-17} 7PO SO_4, 0.5% C_{20-24} IOS, 2% IBA in 218 ppm TDS mixing brine.
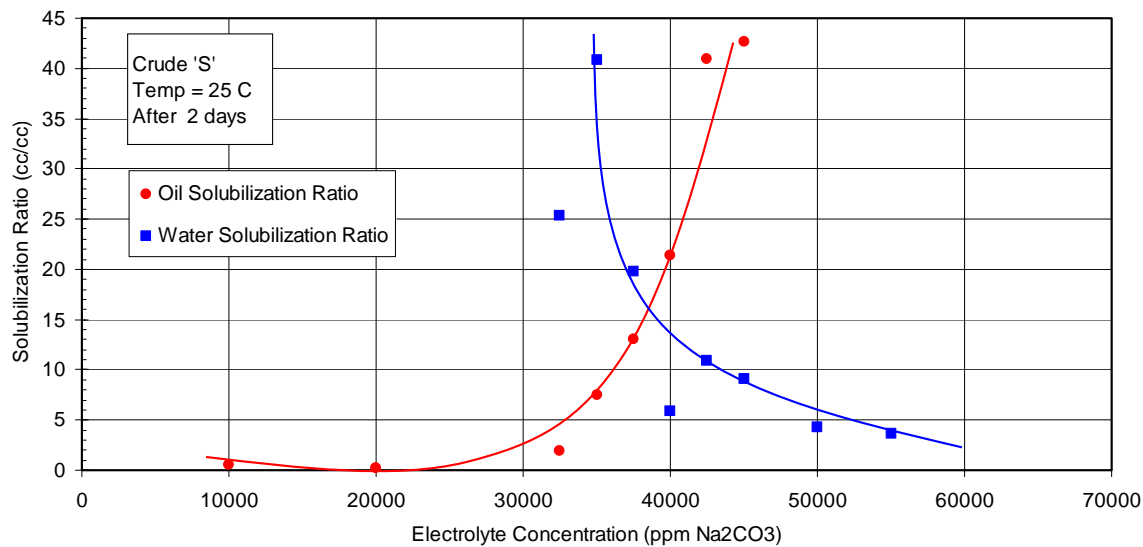
Figure 4.3: Solubilization ratio plot of the Phase Behavior Experiment S - 9 using 50% Crude 'S' at 25 C. The formulation contained 1.5% C_{16-17} 7PO SO_4, 0.5% C_{20-24} IOS, 2% IBA in 218 ppm TDS mixing brine.
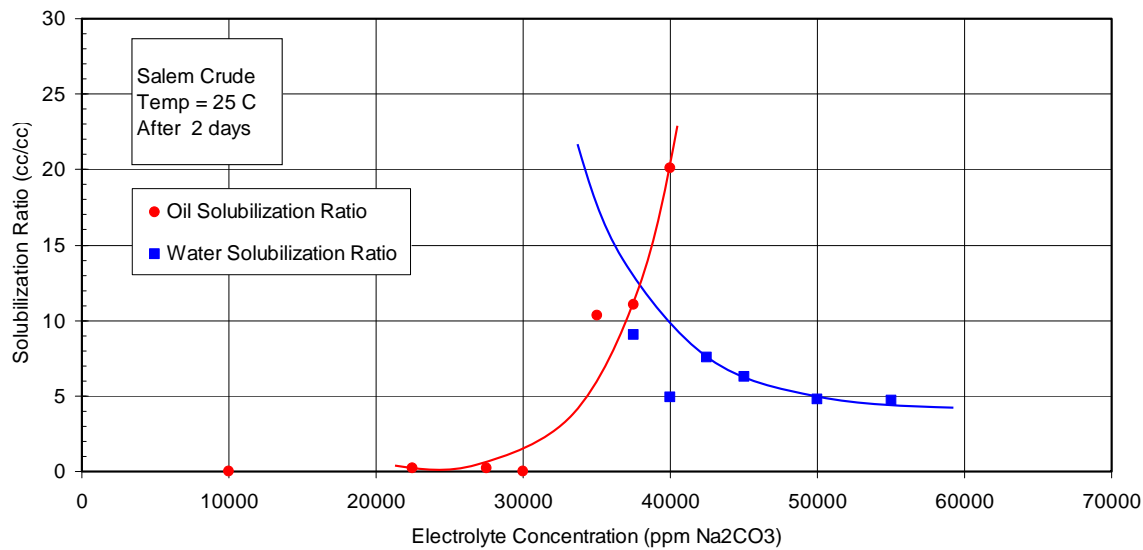
Figure 4.4: Solubilization ratio plot of the Phase Behavior Experiment S - 9 using 40% Crude 'S' at 25 C. The formulation contained 1.5% C_{16-17} 7PO SO_4, 0.5% C_{20-24} IOS, 2% IBA in 218 ppm TDS mixing brine.

Figure 4.5: Solubilization ratio plot of the Phase Behavior Experiment S - 9 using 30% Crude 'S' at 25 C. The formulation contained 1.5% C_{16-17} 7PO SO_4, 0.5% C_{20-24} IOS, 2% IBA in 218 ppm TDS mixing brine.

Figure 4.6: Solubilization ratio plot of the Phase Behavior Experiment S - 9 using 20% Crude 'S' at 25 C. The formulation contained 1.5% C_{16-17} 7PO SO_4, 0.5% C_{20-24} IOS, 2% IBA in 218 ppm TDS mixing brine.
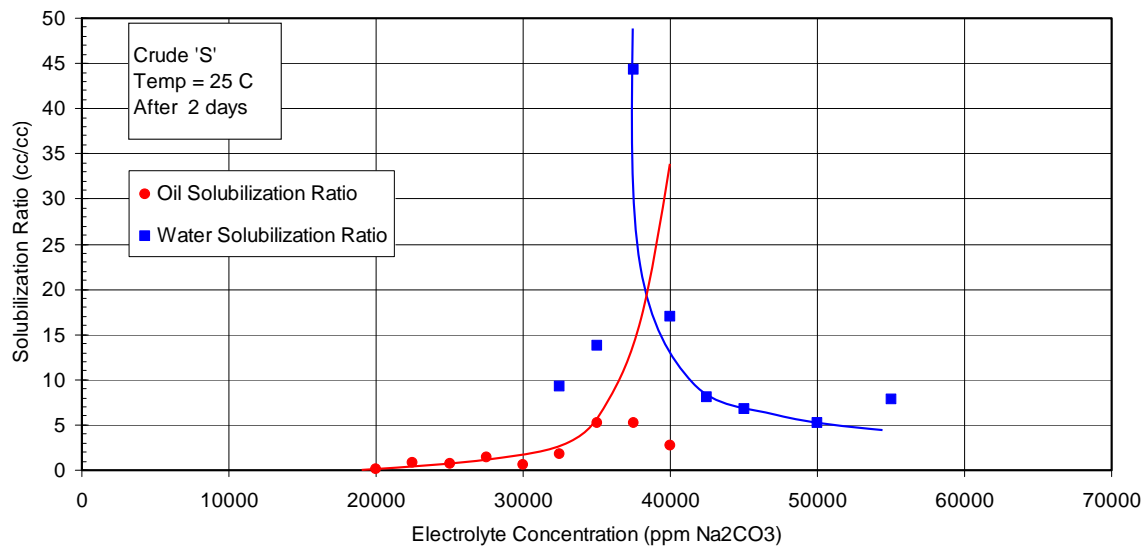
Figure 4.7: Solubilization ratio plot of the Phase Behavior Experiment S - 9 using 10% Crude 'S' at 25 C. The formulation contained 1.5% C_{16-17} 7PO SO_4, 0.5% C_{20-24} IOS, 2% IBA in 218 ppm TDS mixing brine.
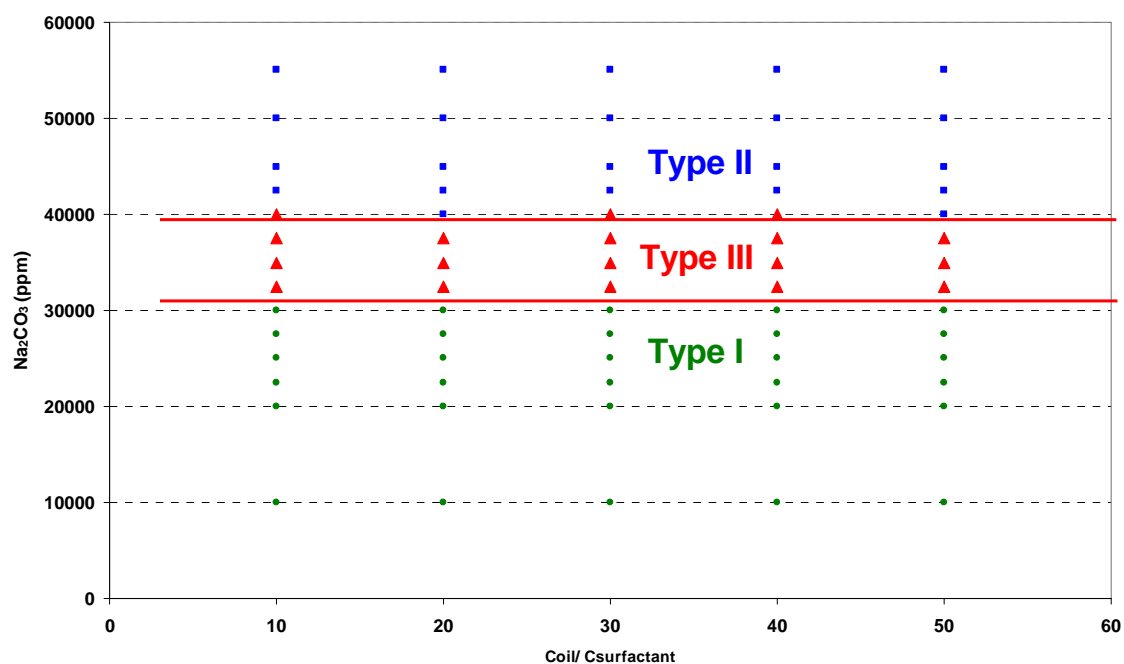
Figure 4.8: Activity Map of the Phase Behavior Experiment S-9 using Crude 'S' at 25 C. The formulation contained 1.5% C_{16-17} 7PO SO_4, 0.5% C_{20-24} IOS, 2% IBA in 218 ppm TDS mixing brine.
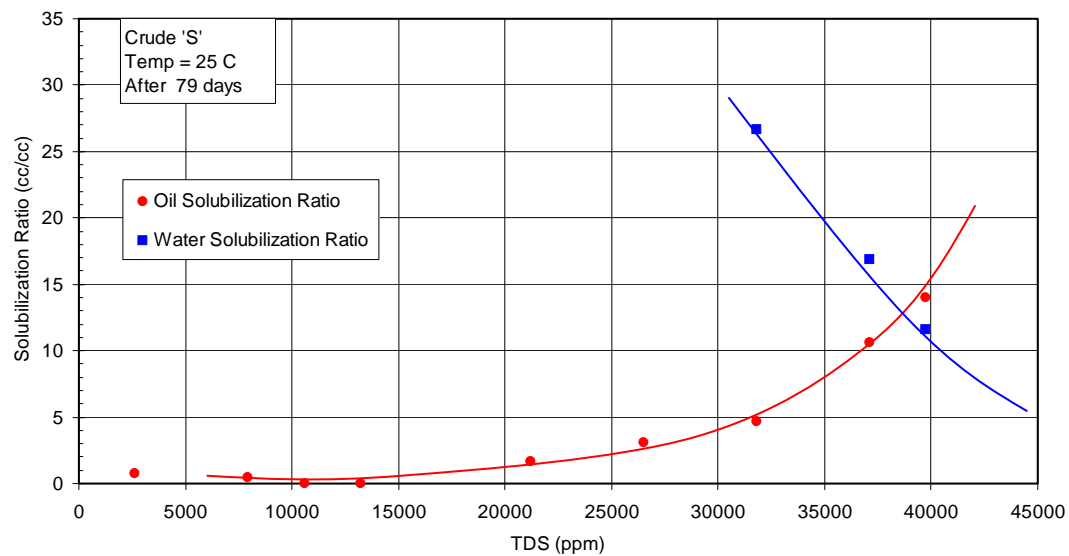
Figure 4.9: Solubilization ratio plot of the Phase Behavior Experiment S - 19 using Crude 'S' at 25C. The formulation contained 1.5% C_{16-17} 7PO SO_4, 0.5% C_{15-18} IOS, 2% IBA in 218 ppm TDS mixing brine.

Figure 4.10: Solubilization plot of the Phase Behavior Experiment S - 20 usinf Crude 'S' at 25 C. The formulation contained 0.75% C_{16-17} 7PO SO_4, 0.25% C_{15-18} IOS, 2% IBA in 218 ppm TDS mixing brine.
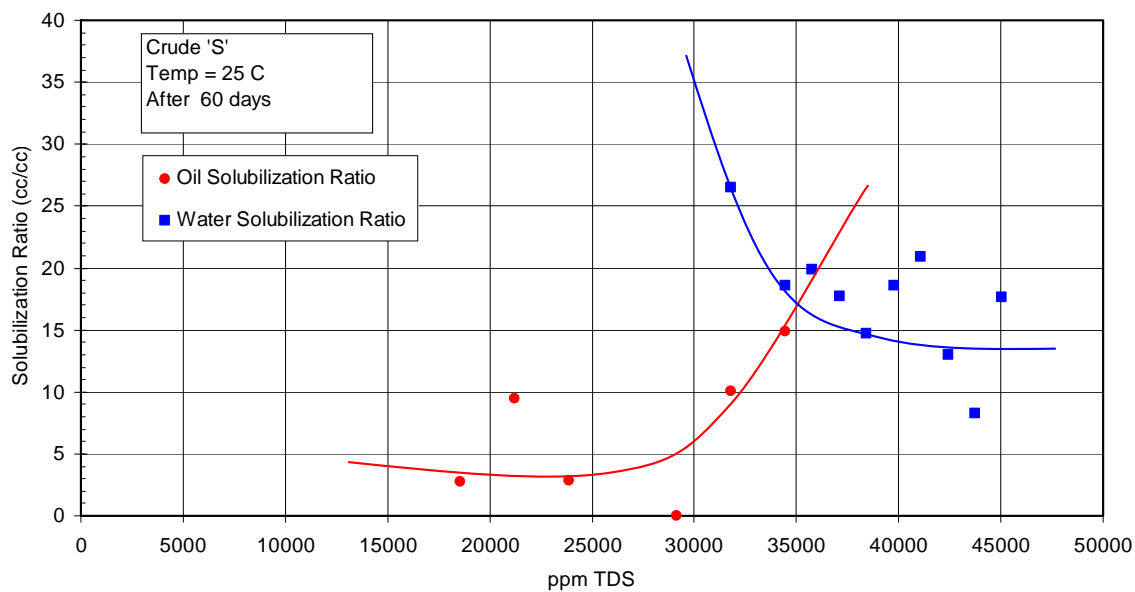
Figure 4.11: Solubilization ratio plot of the Phase Behavior Experiment S - 21 usinf Crude 'S' at 25 C. The formulation contained 0.375% C_{16-17} 7PO SO_4, 0.125% C_{15-18} IOS, 2% IBA in 218 ppm TDS mixing brine.
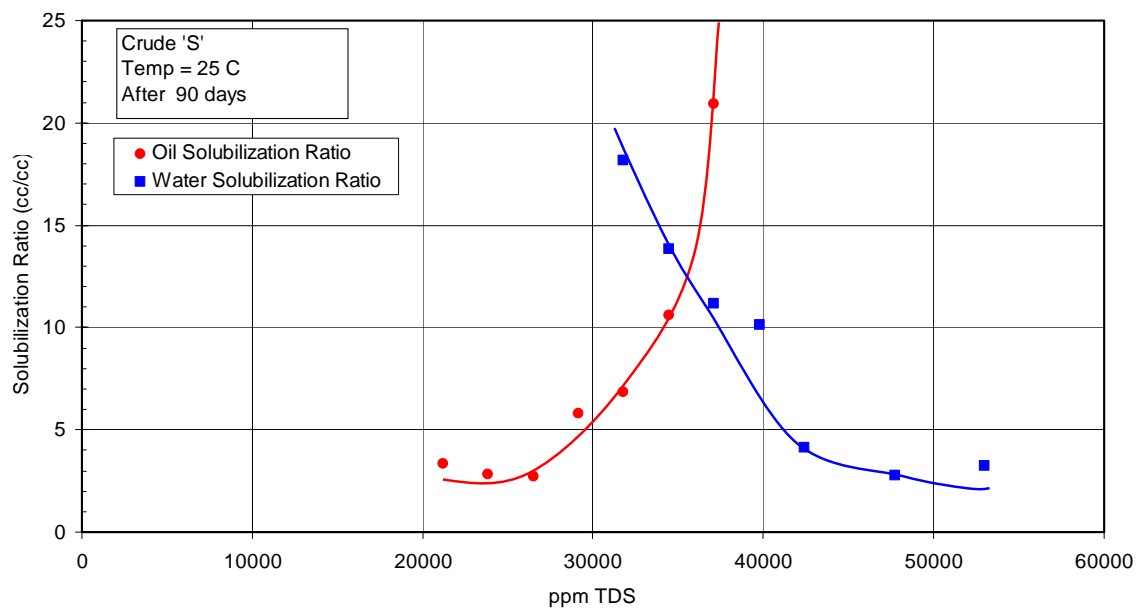
Figure 4.12: Solubilization ratio plot for the Phase Behavior Experiment S - 24 using Crude 'S' at 25C. The formulation contained 0.75% C_{16-17} 7PO SO_4, 0.25% C_{15-18} IOS, 1% IBA in 218 ppm TDS mixing brine.
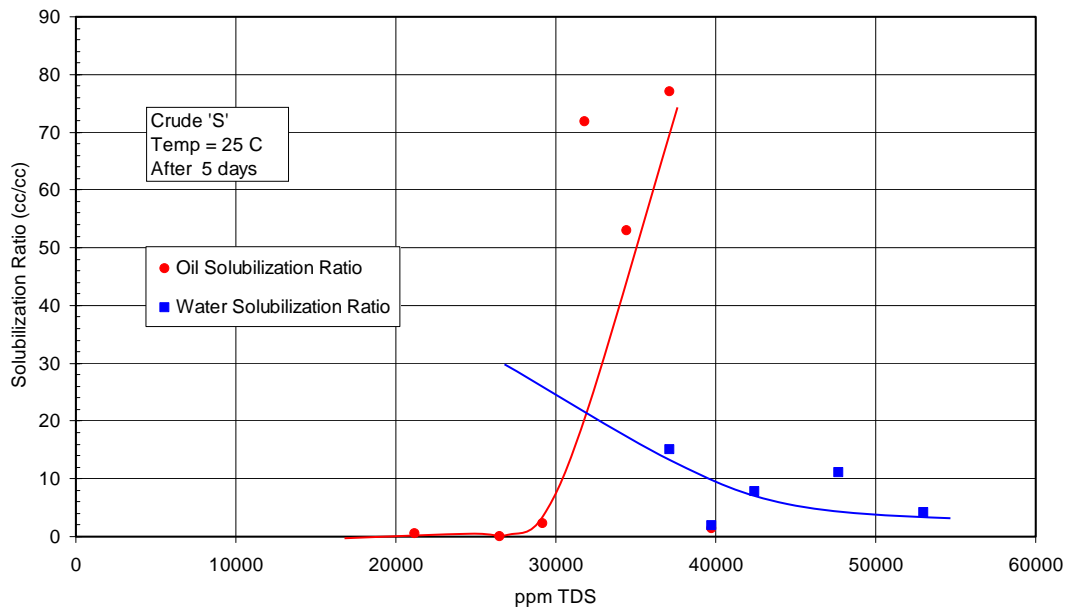
Figure 4.13: Solubilization ratio plot of the Phase Behavior Experiment S - 25 using Crude 'S' at 25 C. The formulation contained 0.75% C_{16-17} 7PO SO_4, 0.25% C_{15-18} IOS, 0.5% IBA in 218 ppm TDS mixing brine.
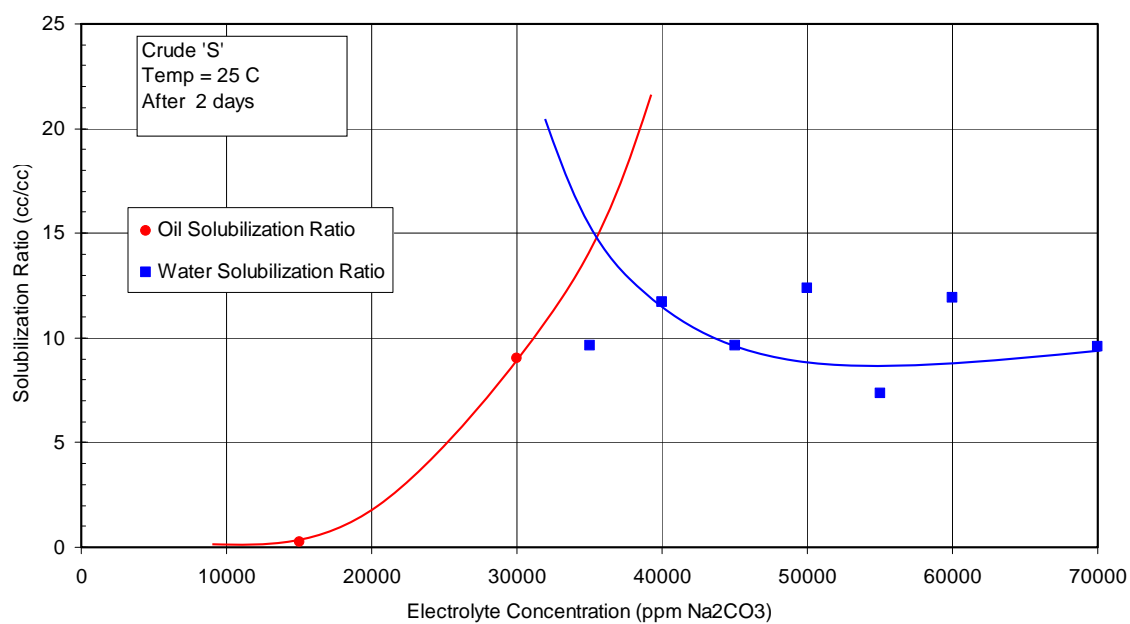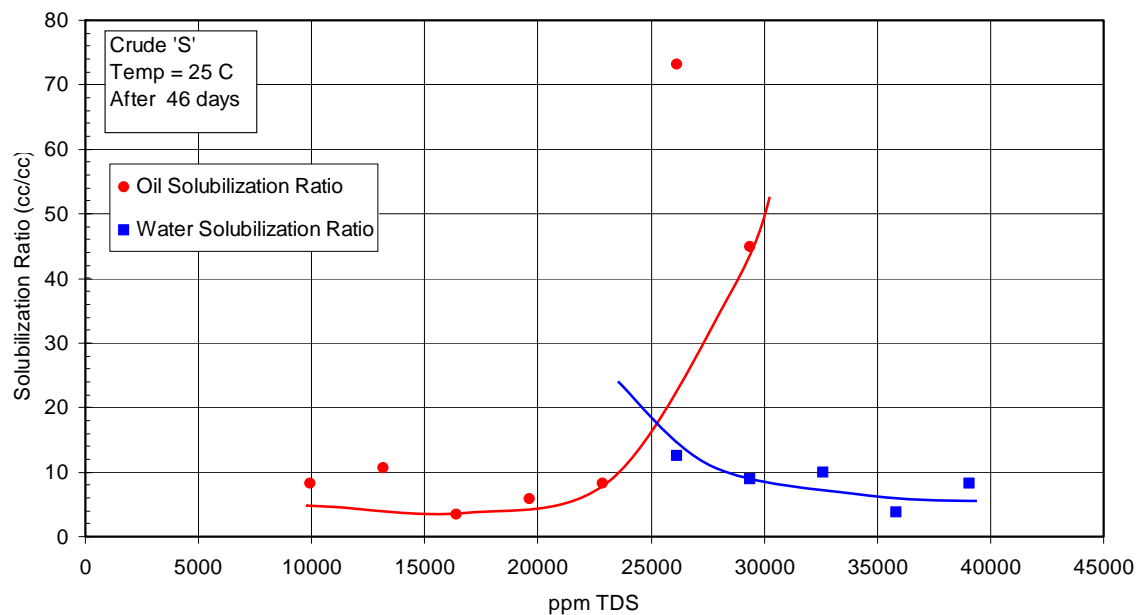
Figure 4.14: Solubilization ratio plot of the Phase Behavior Experiment S - 100 using Crude 'S' at 25 C. The formulation contained 0.75% C_{16-17} 7PO SO_4, 0.25% C_{15-18} IOS, 1% IBA in 218 ppm TDS mixing brine.
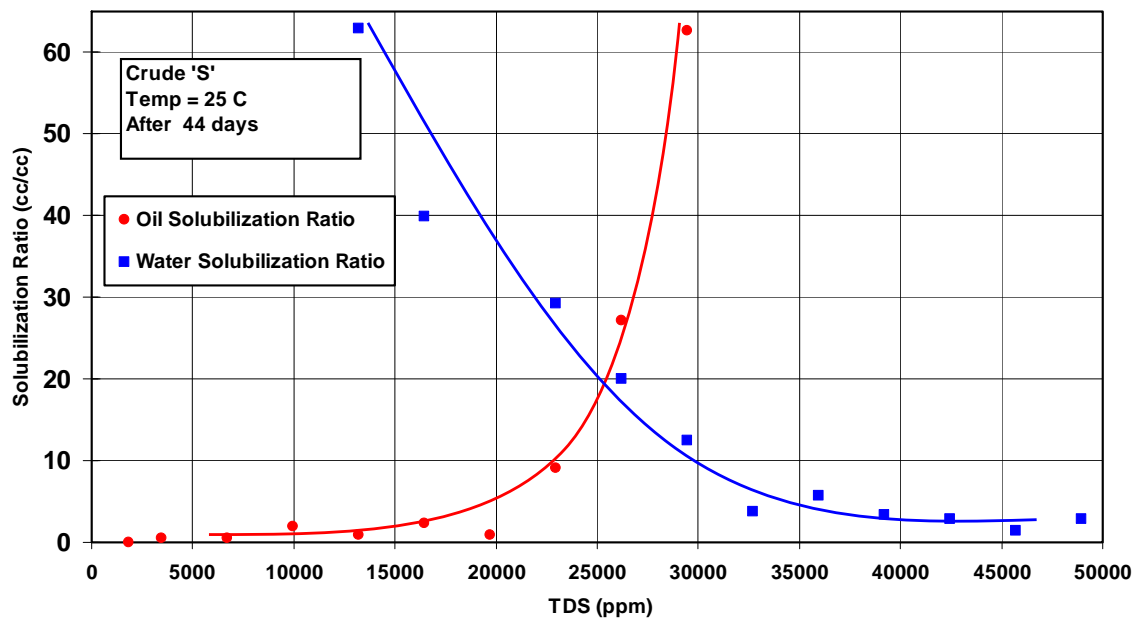
Figure 4.15: Solubilization plot for the Phase Behavior Experiment S - 131 for the formulation 0.75% C_{16-17} 7PO SO_4, 0.25% C_{15-18} IOS, 1% IBA in 218 ppm TDS mixing brine with Crude 'S' at 25°C
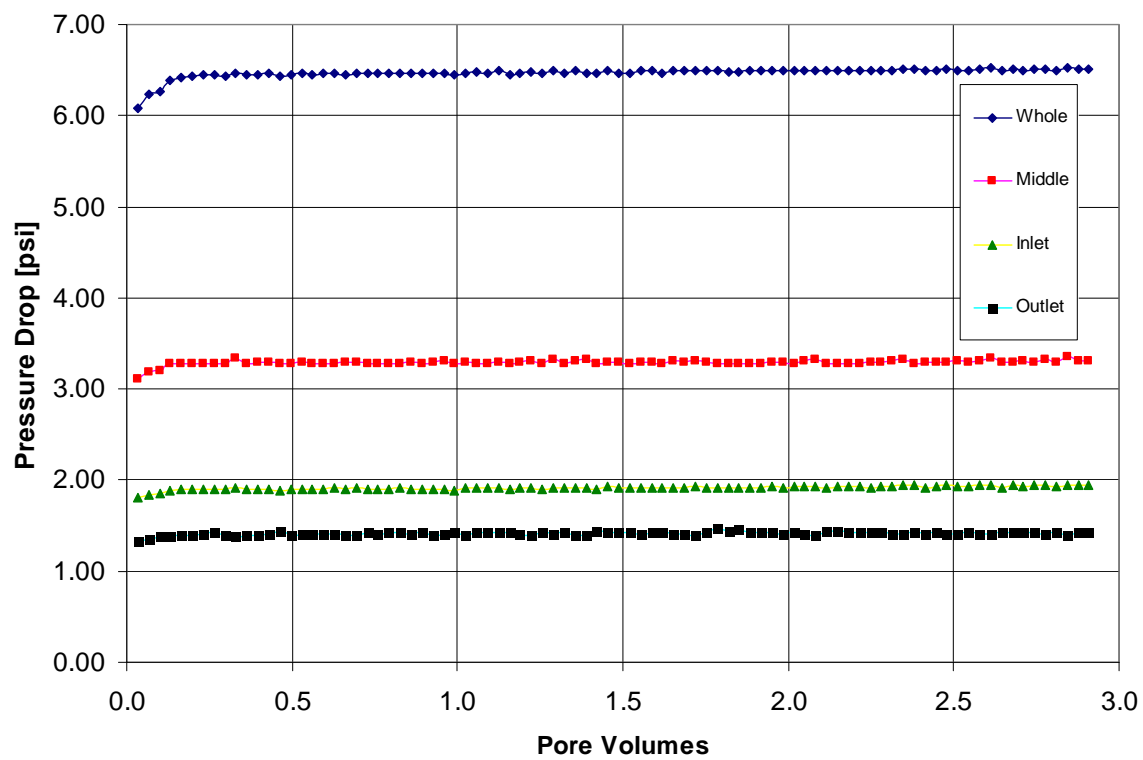
Figure 4.16: Pressure drops across different sections of the core during the brine flooding experiment on core S-5
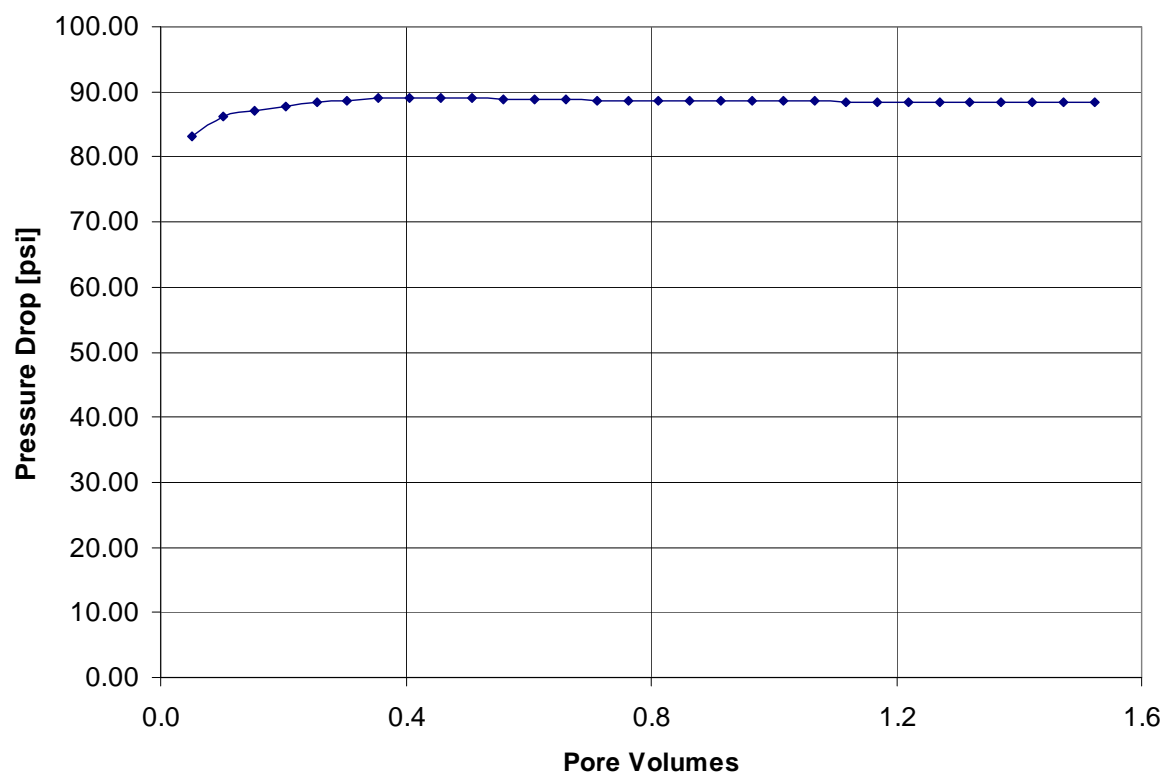
Figure 4.17: Pressure drop across the core during the first oil flooding experiment on core S-5
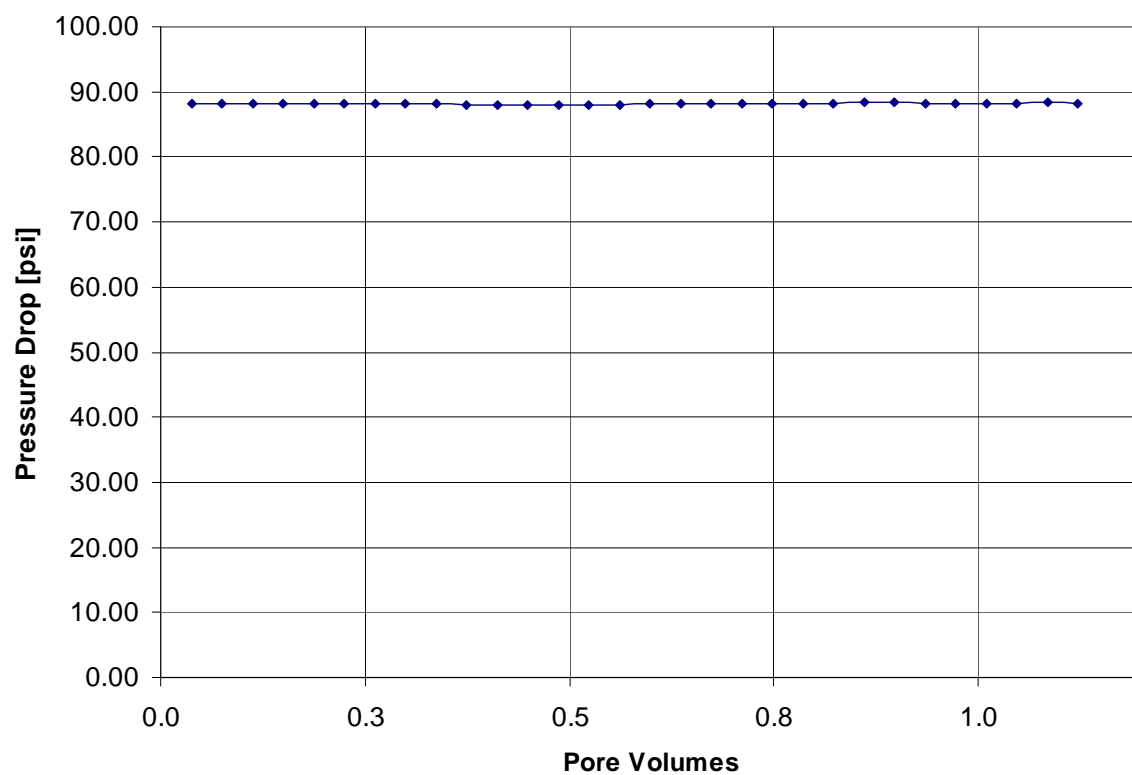
Figure 4.18: Pressure drop across the core during the second oil flooding experiment on
core S-5
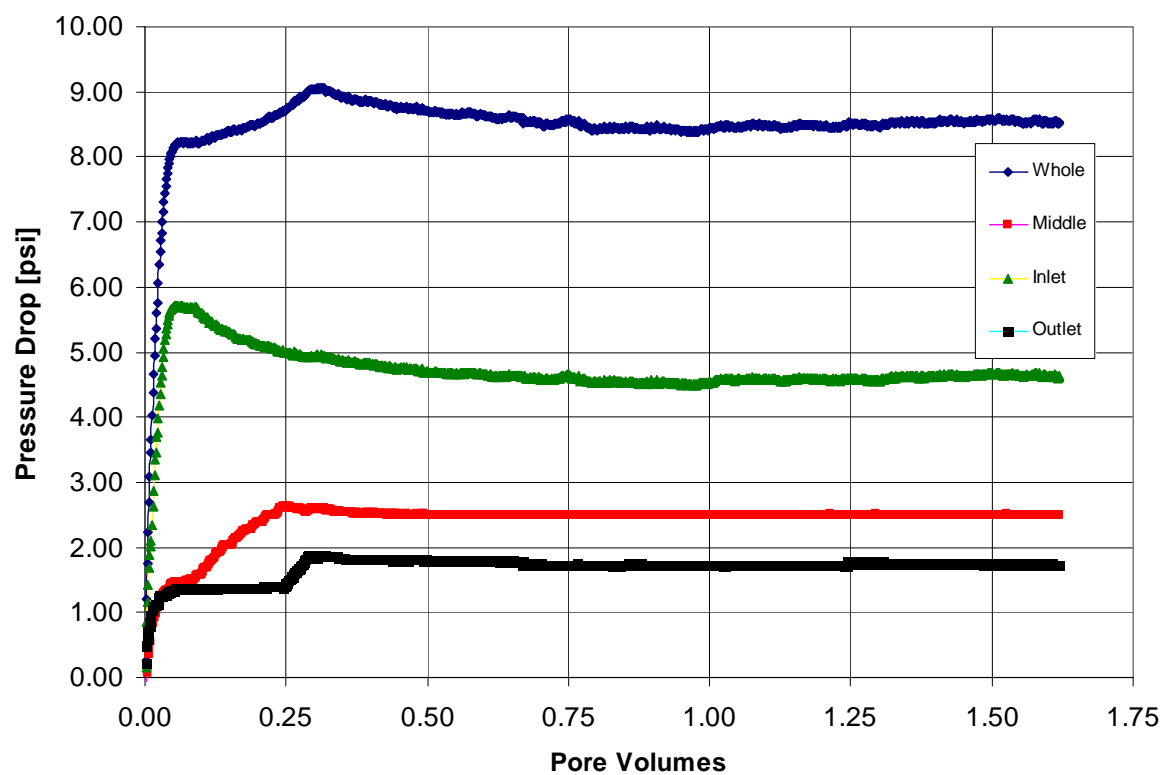
Figure 4.19: Pressure drops across different sections of the core during the water flooding experiment on core S-5
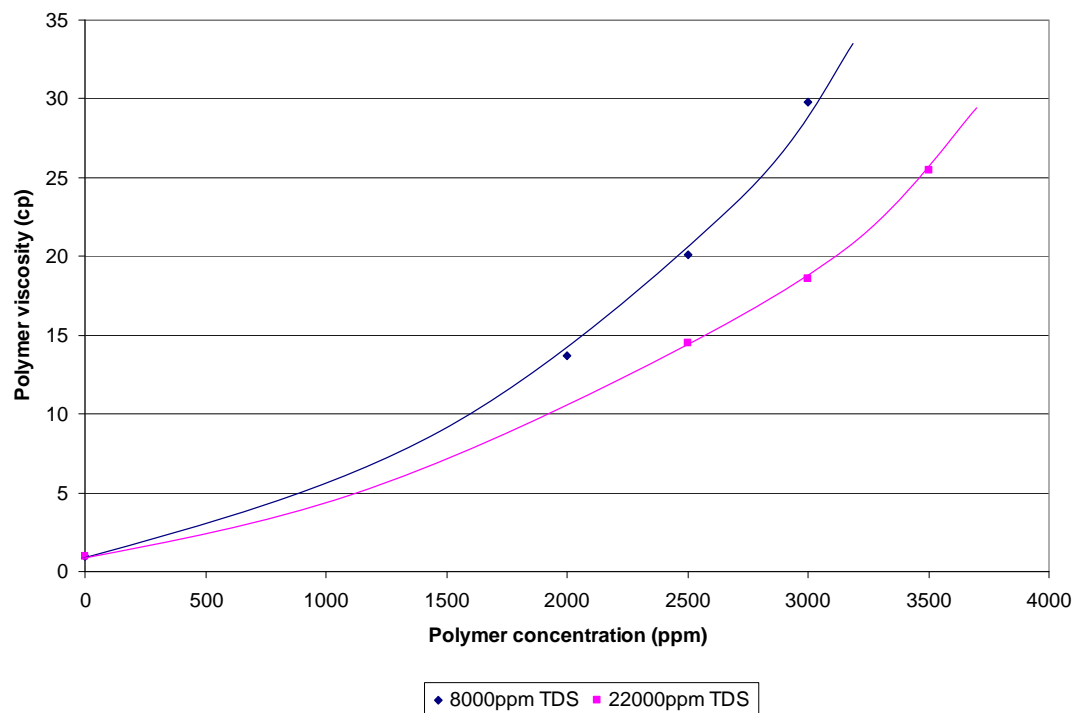
Figure 4.20: FP3330S polymer viscosities at different polymer concentrations at the salinities of the SP slug (22000 ppm TDS) and the Polymer drive (8000 ppm TDS) of the core flood experiment S-5 at $10s^{-1}$ shear rate at 25C

114
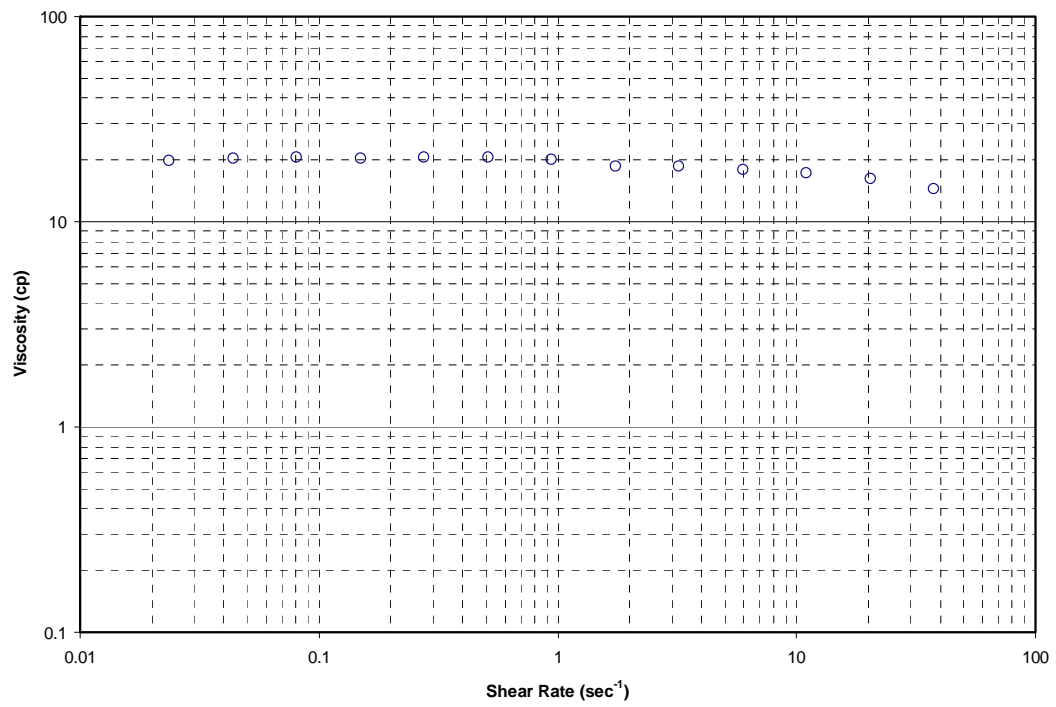
Figure 4.21: Viscosity measurement for the Surfactant Polymer slug at 25 C for the core flood experiment S-5
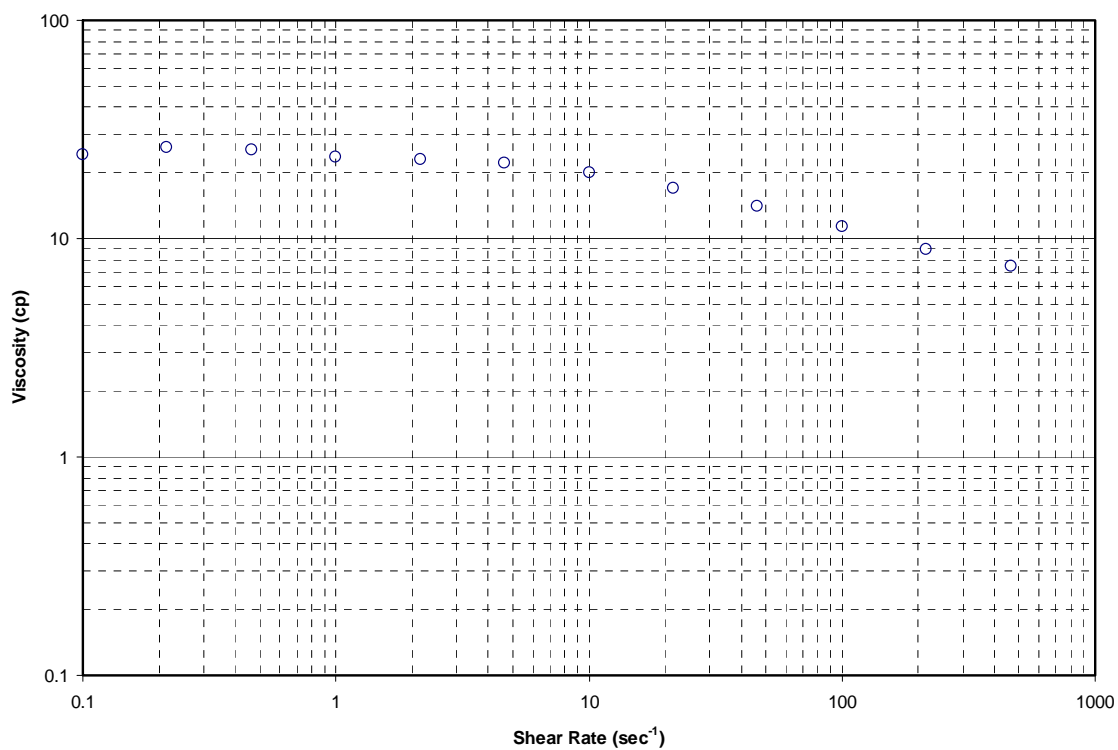
Figure 4.22: Viscosity measurement for the Polymer drive at 25 C for the core flood experiment S-5
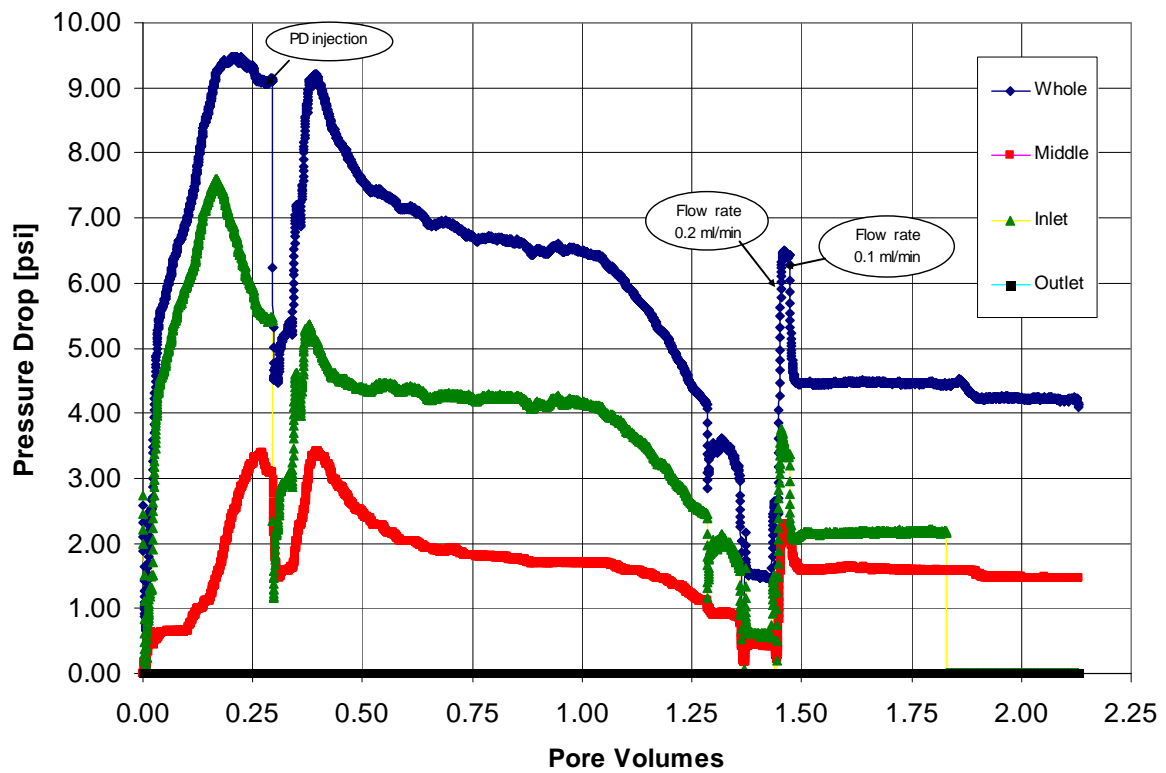
Figure 4.23: Pressure drops across the different sections of the core during the chemical flooding experiment on core S-5
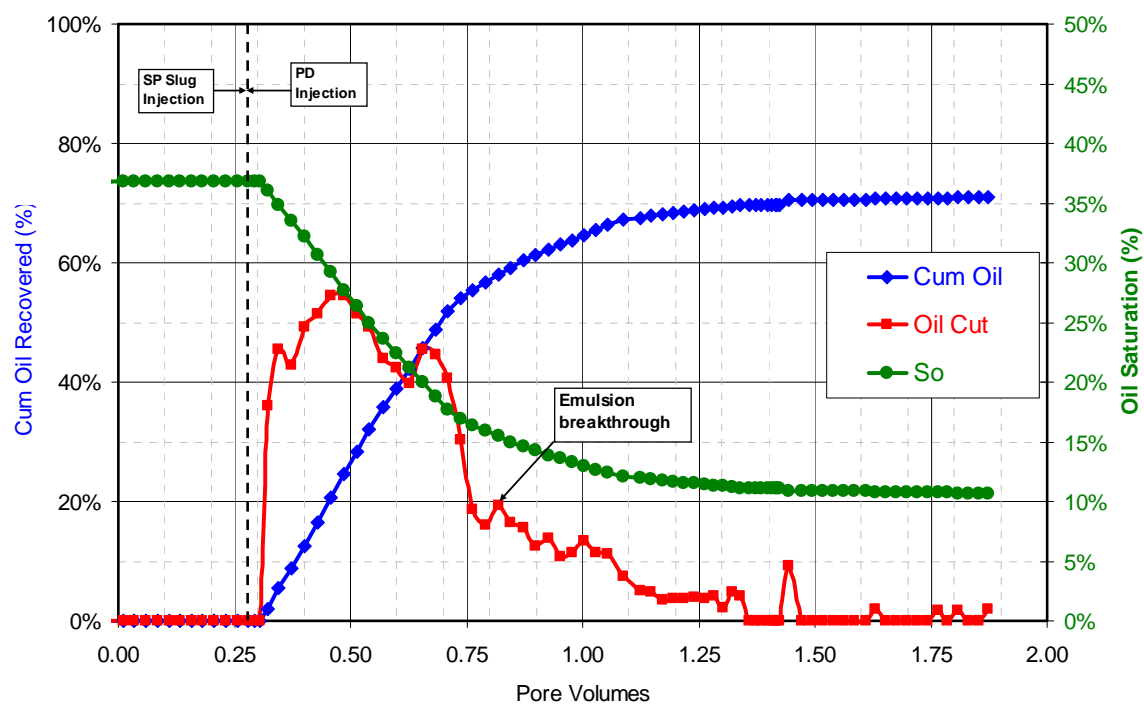
Figure 4.24: Cumulative Oil Recovery, Oil Cut and the Oil Saturation in the core during
the chemical flooding experiment on core S-5
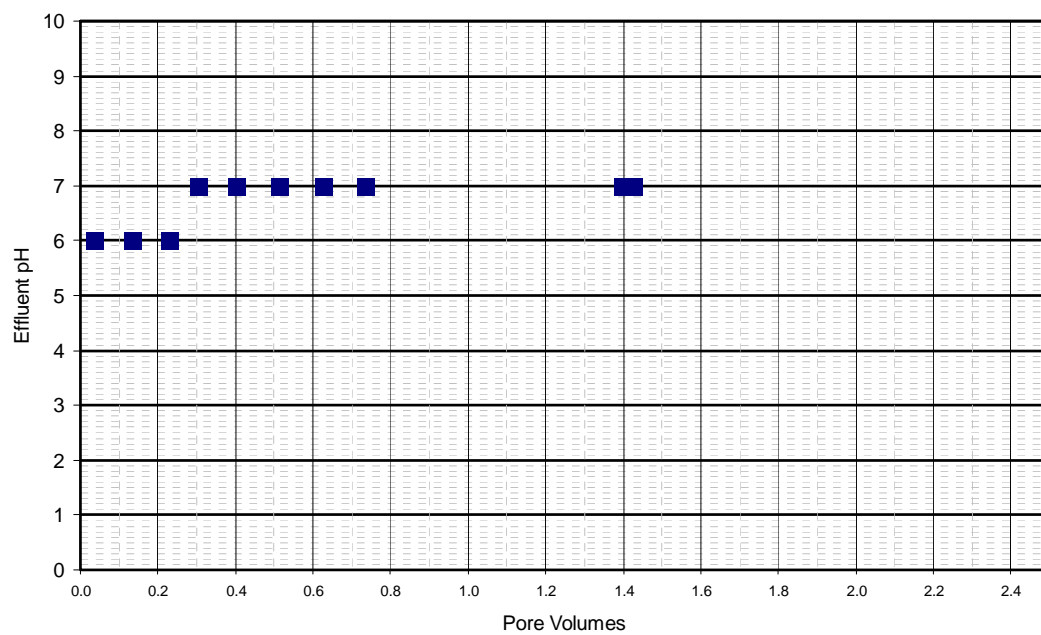
Figure 4.25: Effluent pH during the chemical flooding experiment on core S-5
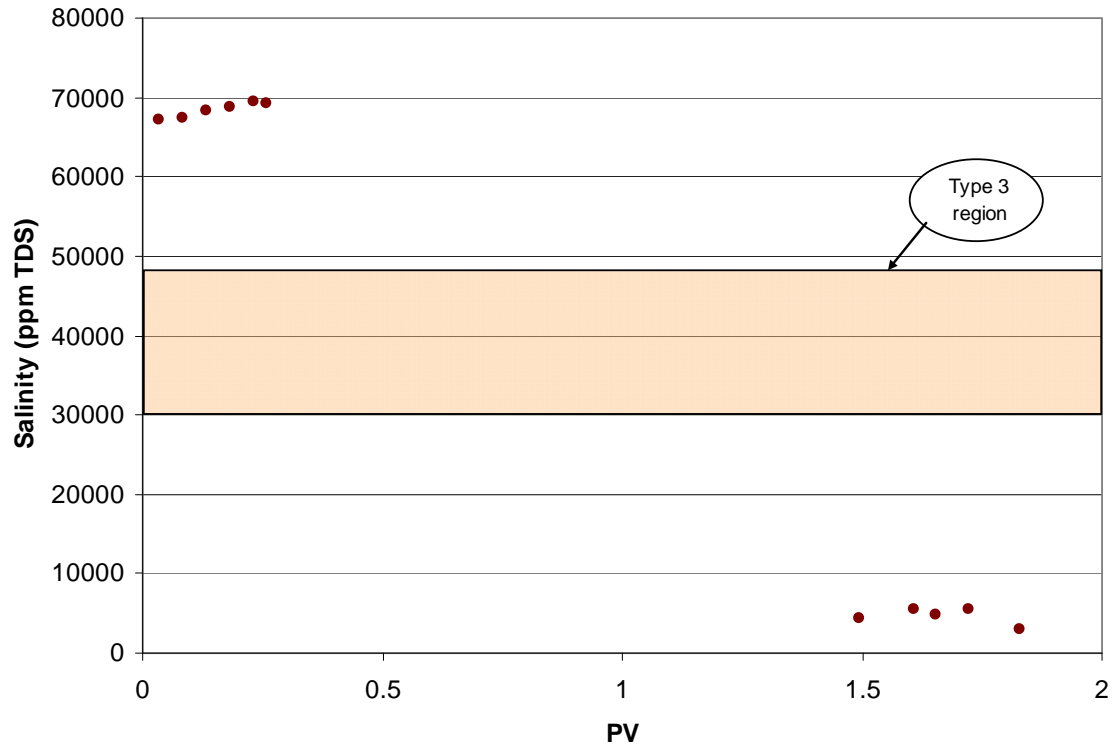
Figure 4.26: Effluent salinity during the chemical flooding experiment on core S-5
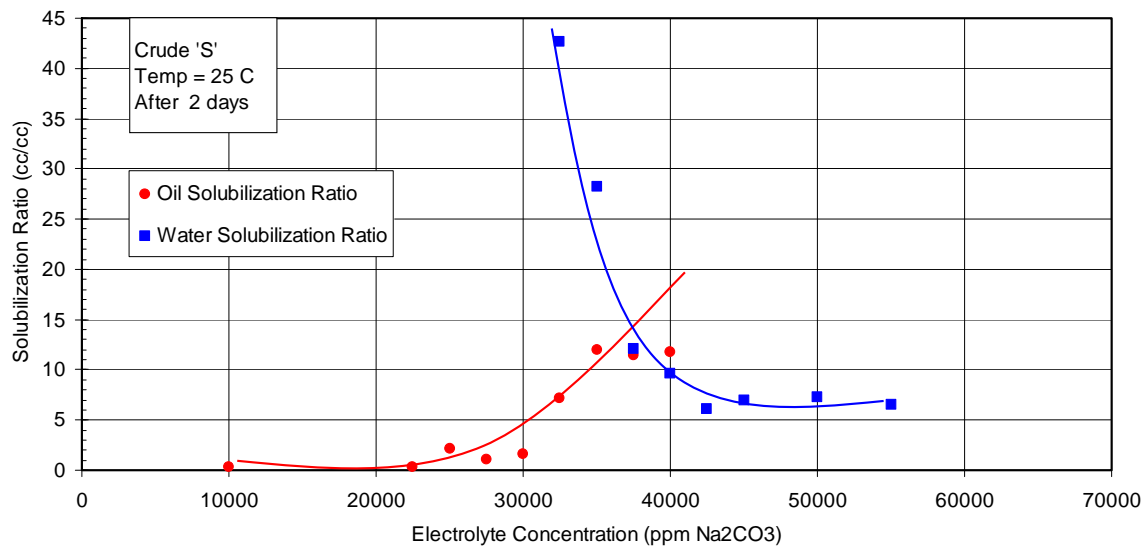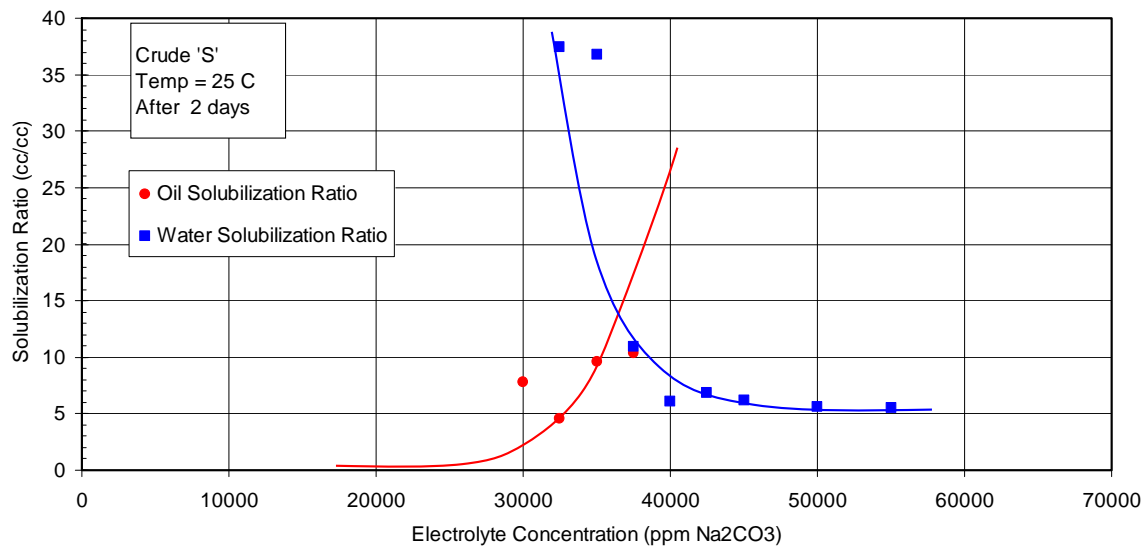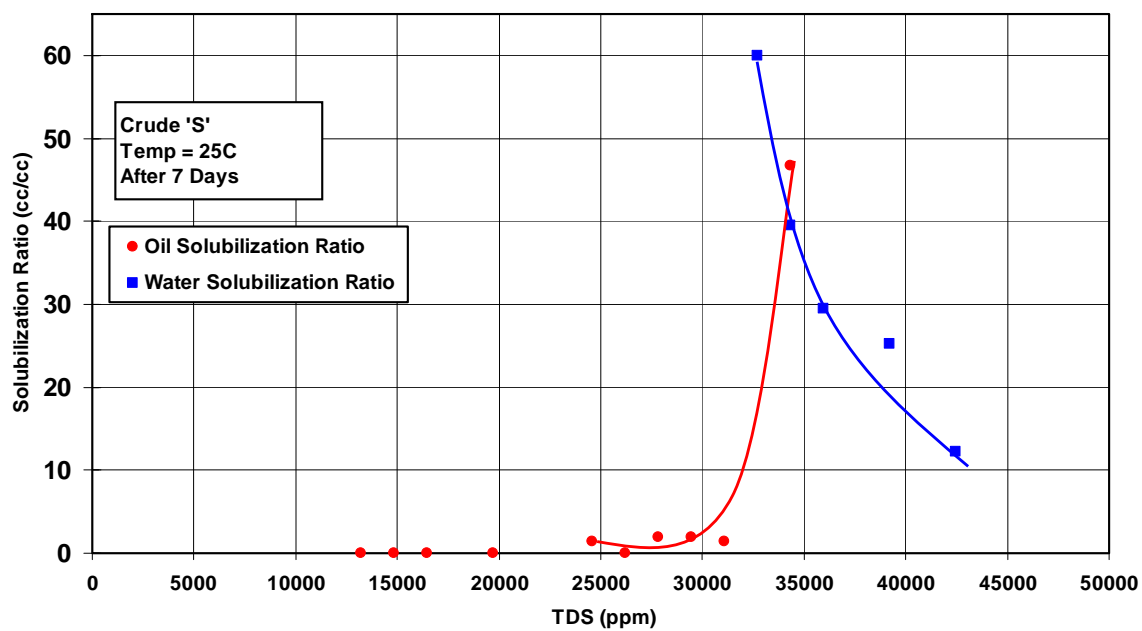
Figure 4.27: Solubilization ratio plot of the Phase Behavior Experiment S - 200 using the Crude 'S' at 25 C. The formulation contained 0.75% C_{16-17} 7PO SO_4, 0.25% C_{15-18} IOS, 1% IBA in 218 ppm TDS mixing brine.
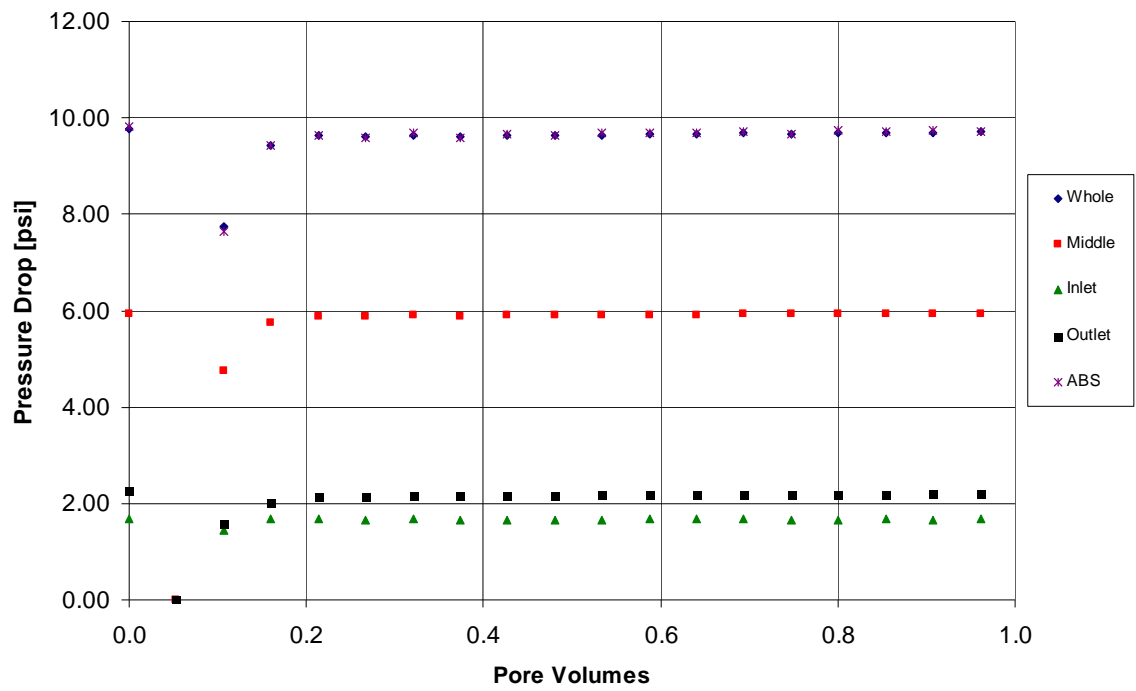
Figure 4.28: Pressure drops across different sections of the core during the brine flooding
experiment on the core S-7
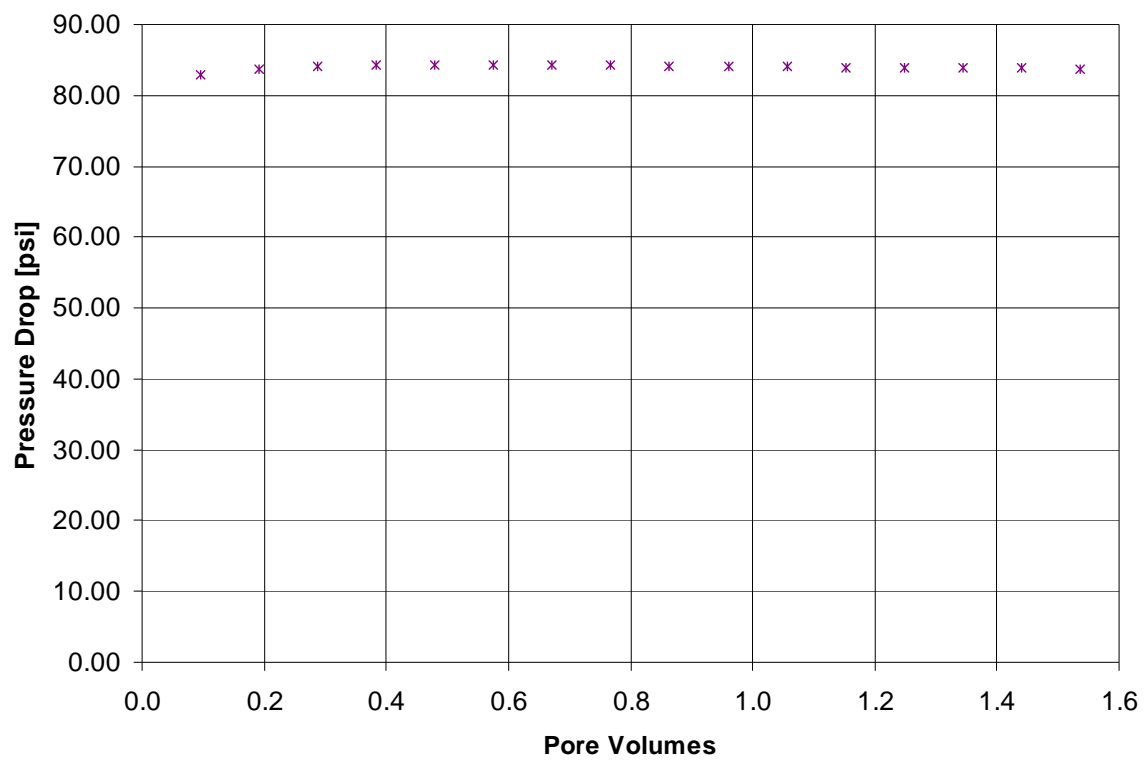
Figure 4.29: Pressure drops across the core during the oil flooding experiment on the core S-7
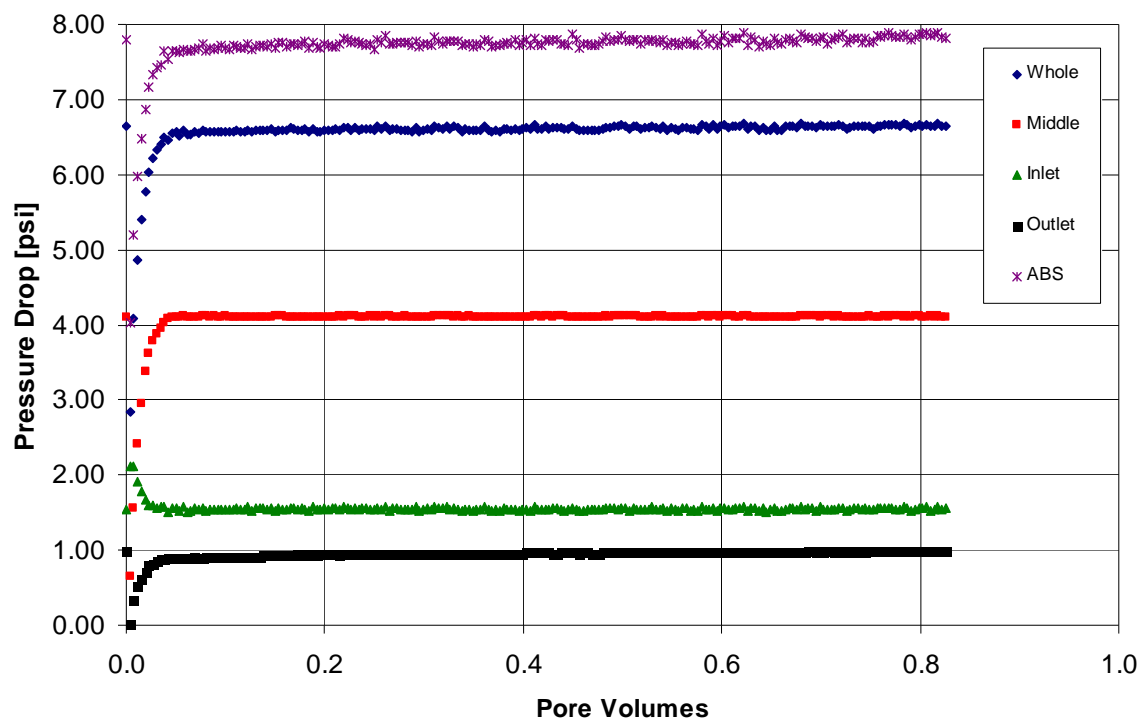
Figure 4.30: Pressure drops across different sections of the core during the water flooding experiment on the core S-7
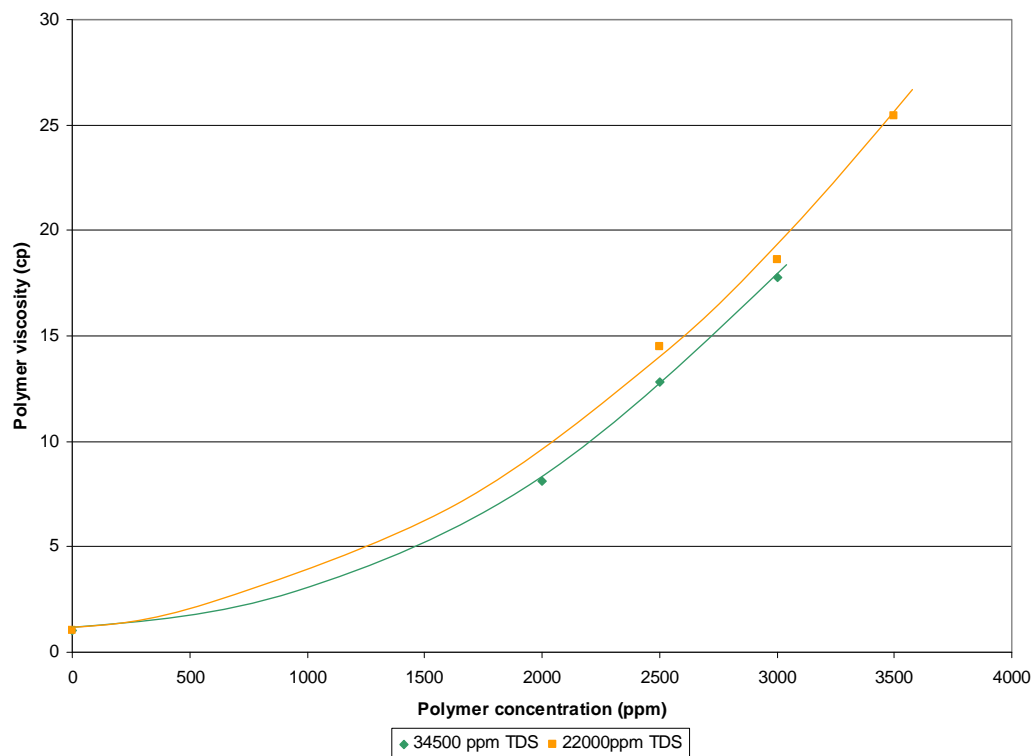
Figure 4.31: FP3330S polymer viscosities at different polymer concentrations at the salinities of the SP slug (34500 ppm TDS) and the Polymer drive (22000 ppm TDS) of the core flood experiment S-7 at $10s^{-1}$ shear rate at 25C
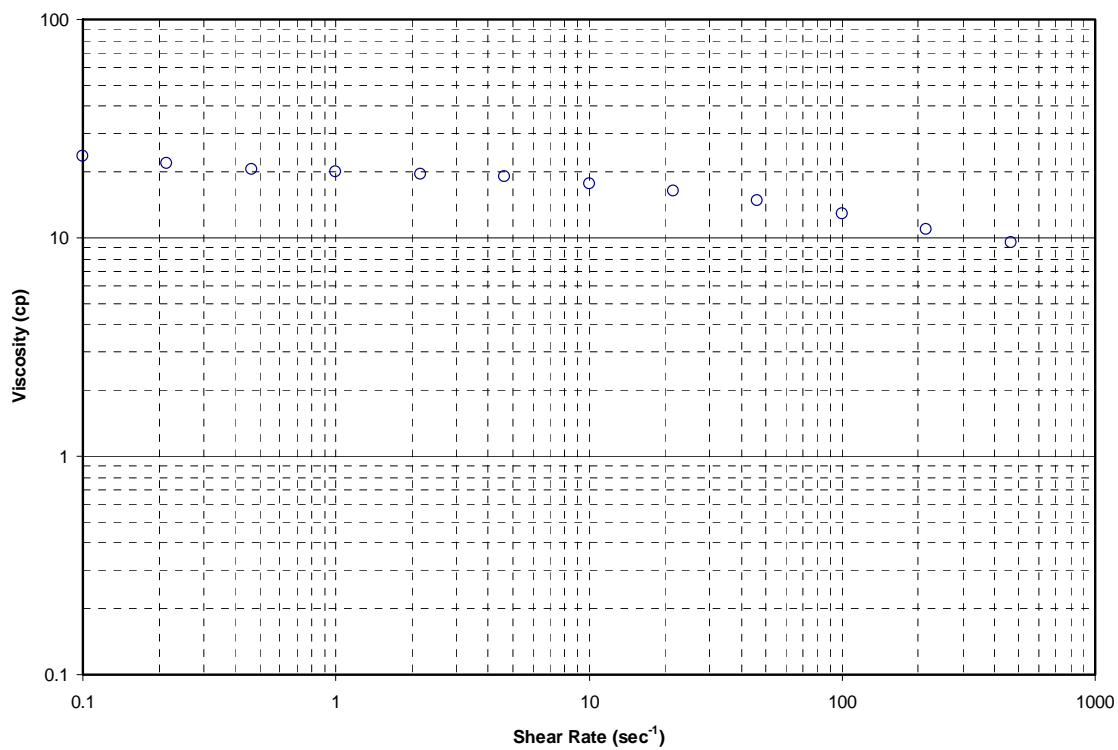
Figure 4.32: Viscosity measurement for the Surfactant Polymer slug at 25 C for the core
flood experiment S-7
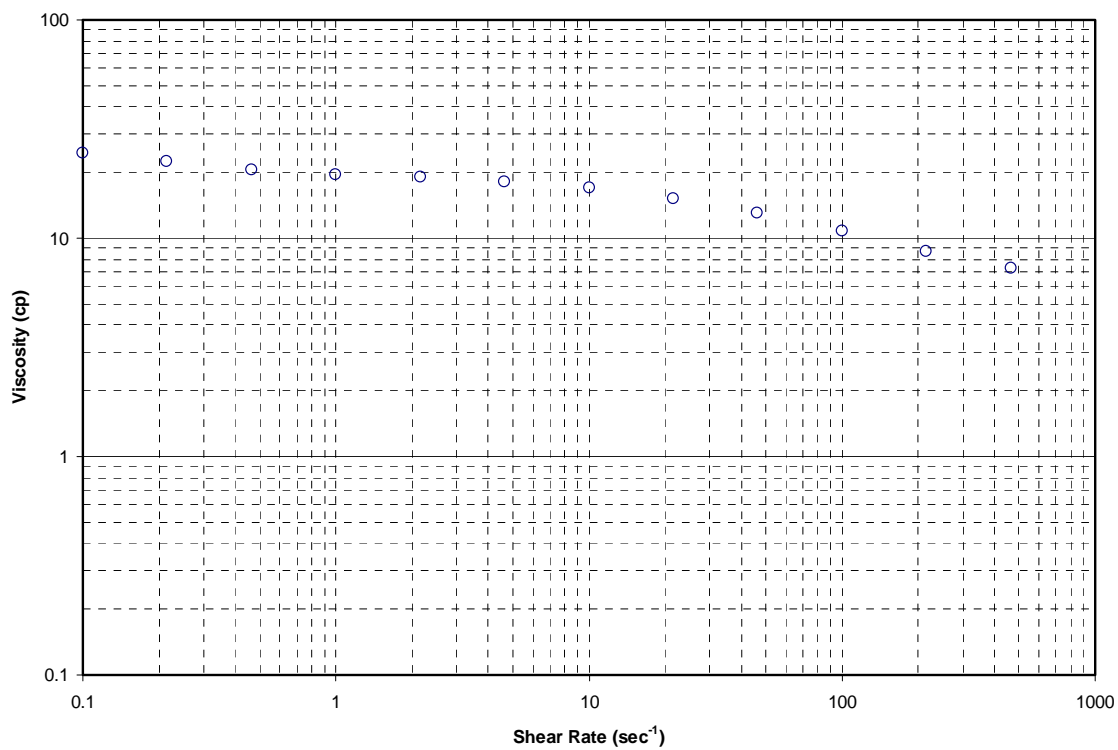
Figure 4.33: Viscosity measurement for the Polymer drive at 25 C for the core flood
experiment S-7
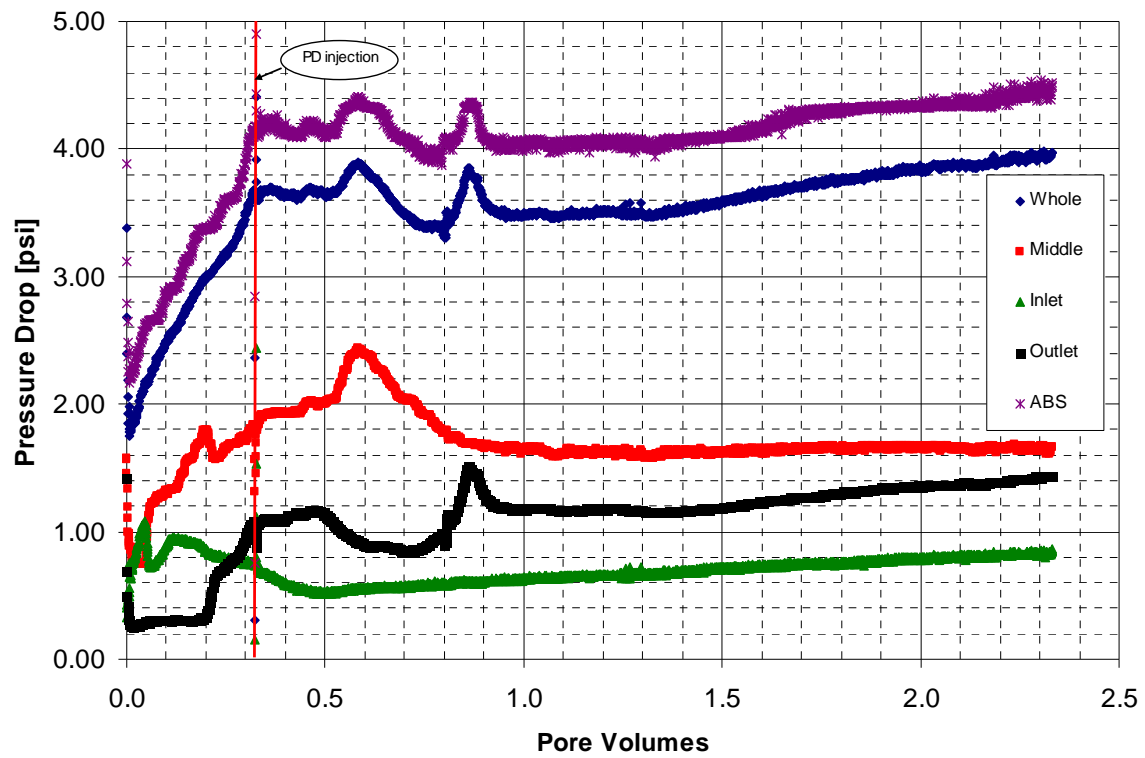
Figure 4.34: Pressure drops across different sections of the core during the chemical
flooding experiment on the core S-7
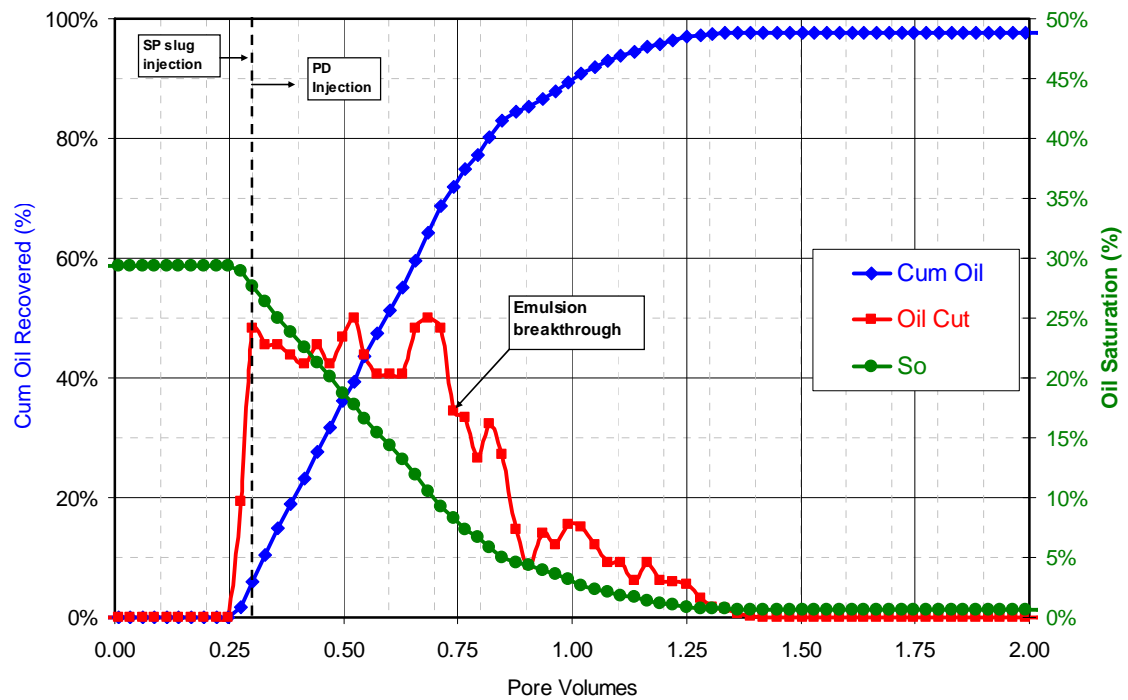
Figure 4.35: Cumulative Oil Recovery, Oil Cut and the Oil Saturation in the core during the chemical flooding experiment on the core S-7
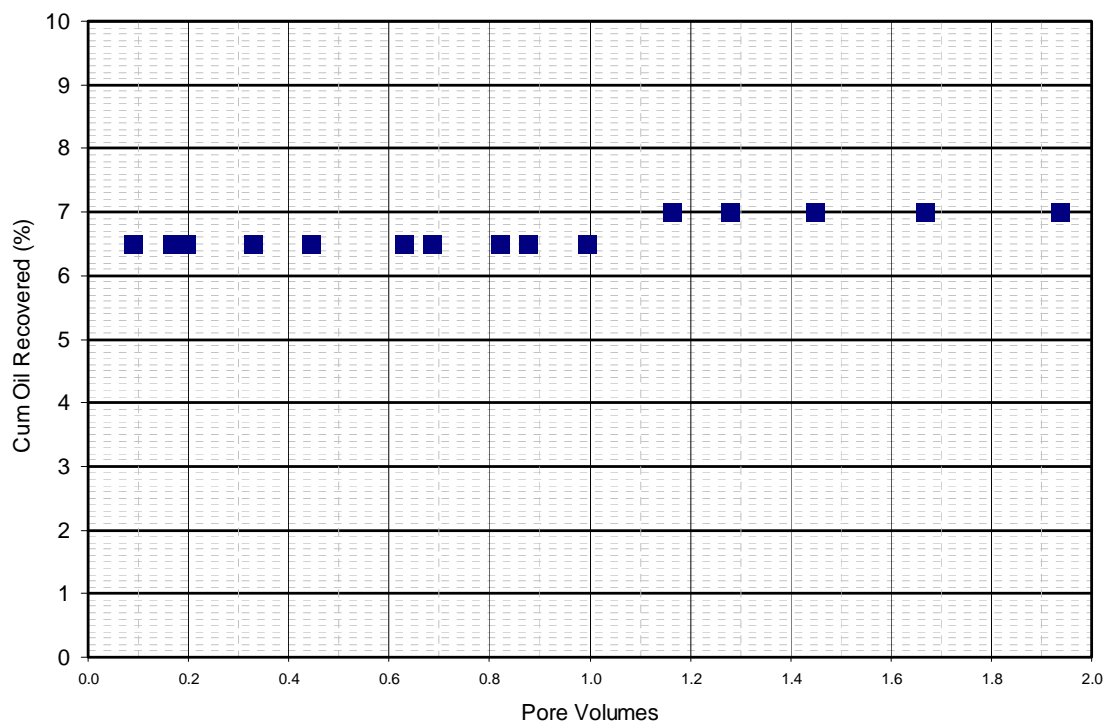
Figure 4.36: Effluent pH during the chemical flooding experiment on the core S-7
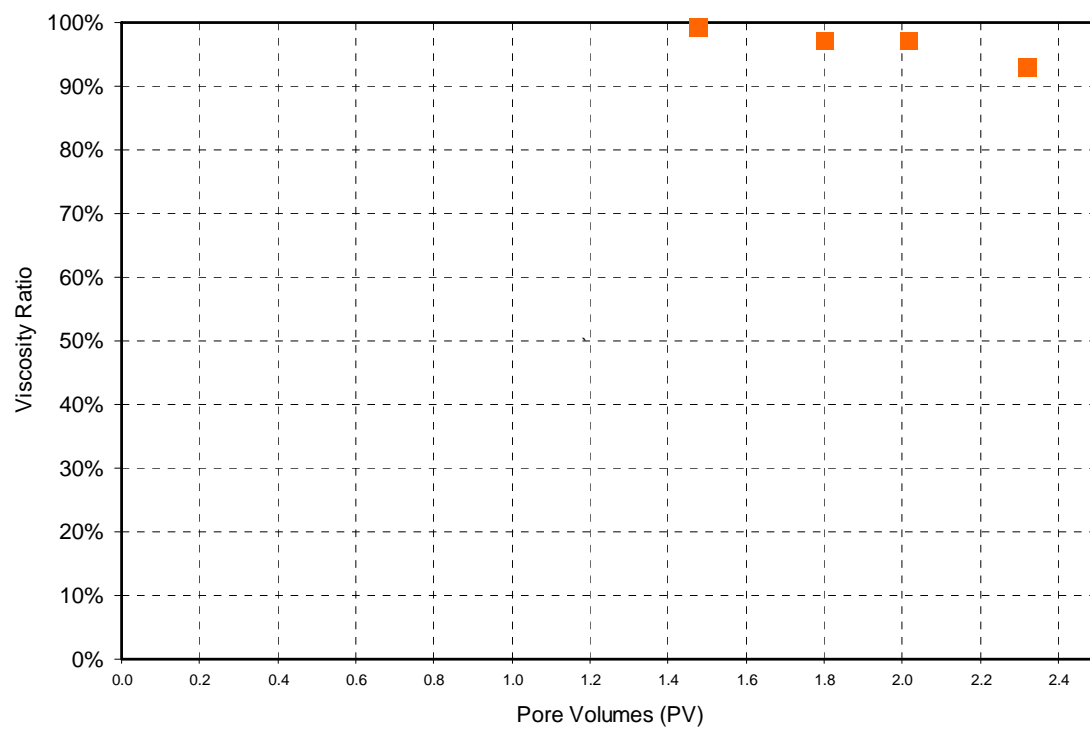
Figure 4.37: Effluent Viscosity Ratio during the chemical flooding experiment on the core S-7
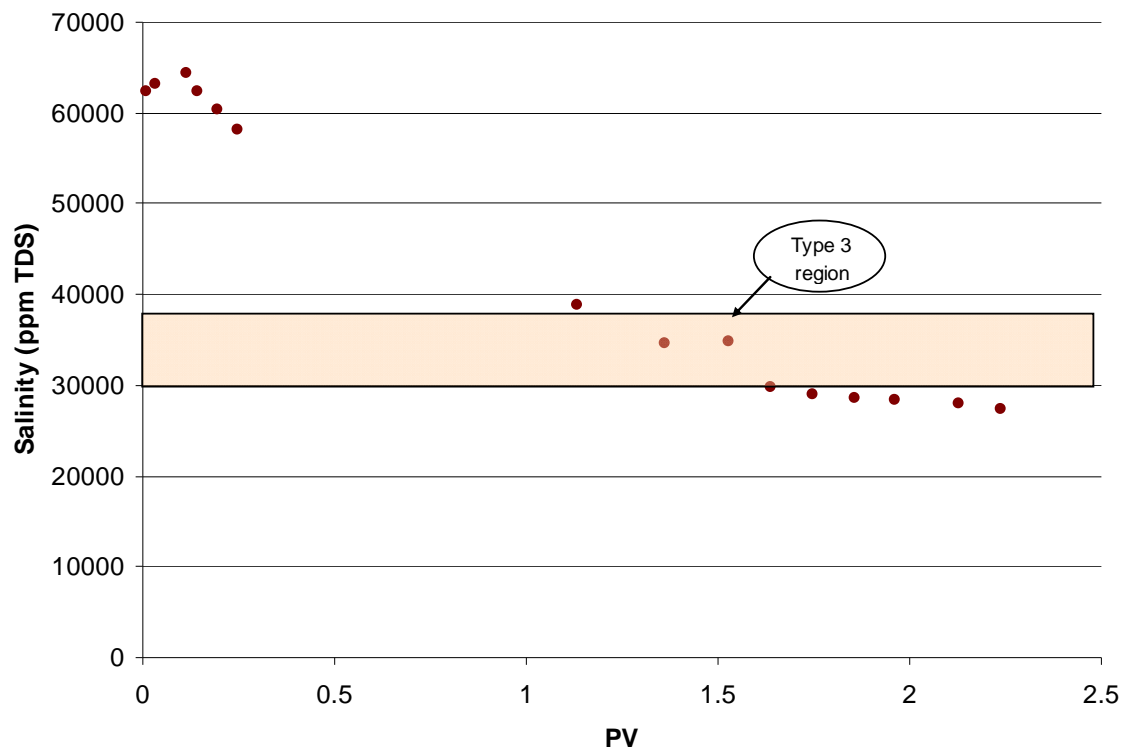
Figure 4.38: Effluent salinity during the chemical flooding experiment on the core S-7
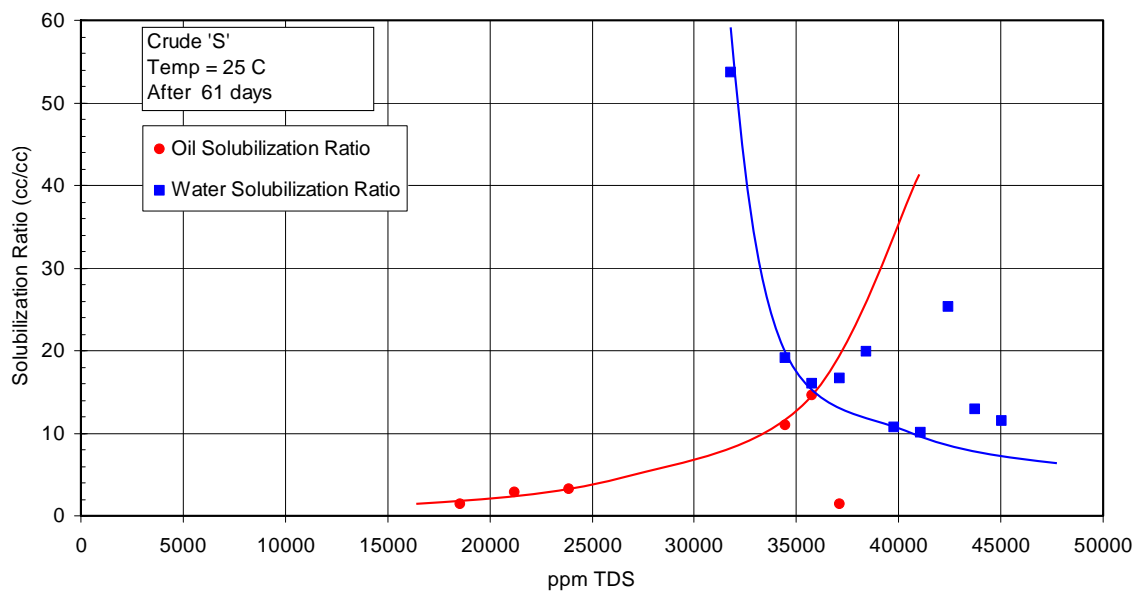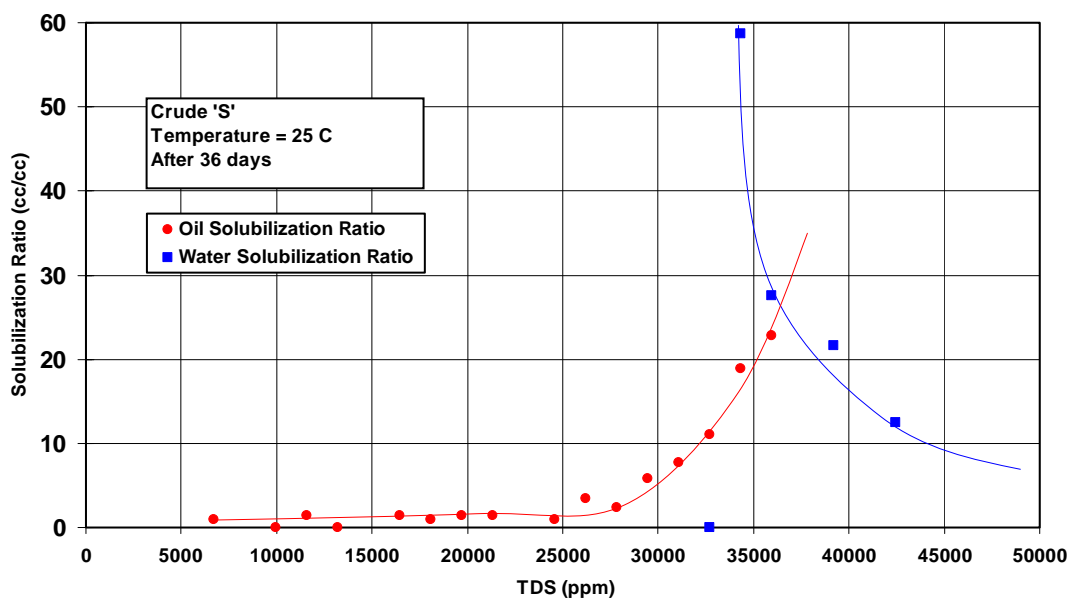
Figure 4.39: Solubilization plot for the Phase Behavior Experiment S - 202 with Crude 'S' at 25 C. The formulation contained 0.75% C_{16-17} 7PO SO_4, 0.25% C_{15-18} IOS, 1% IBA 0.3 % sodium metaborate in 218 ppm TDS mixing brine.
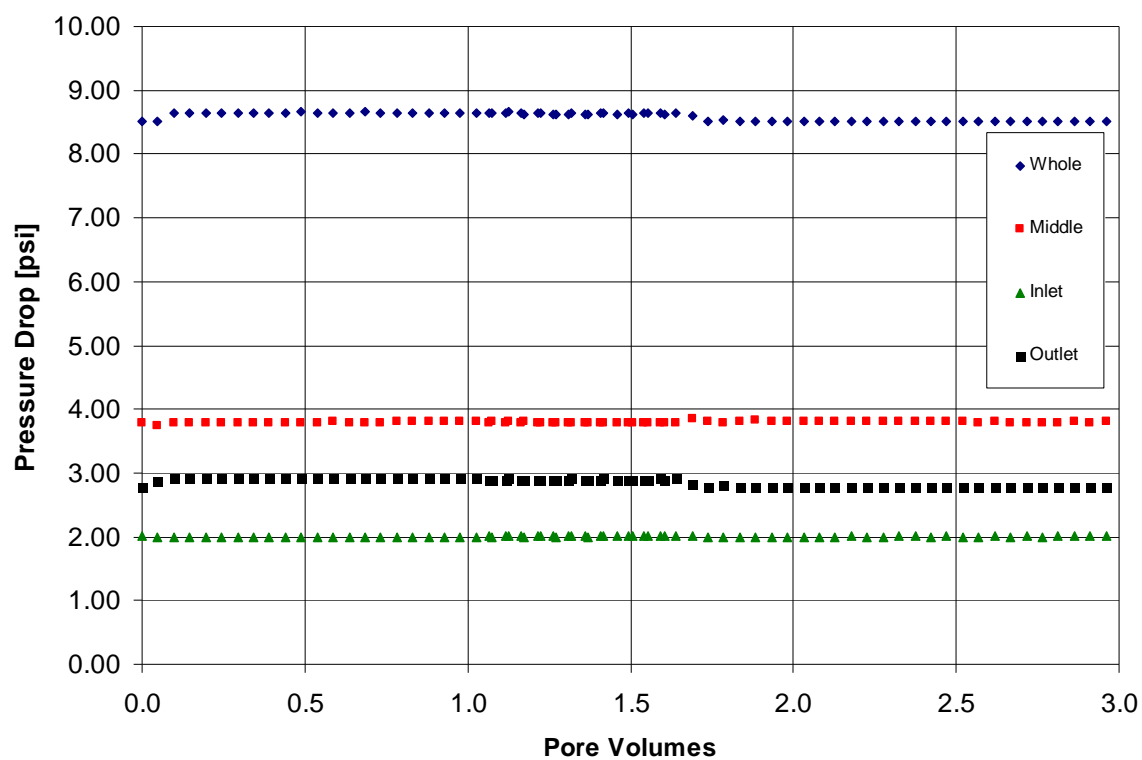
Figure 4.40: Pressure drops across different sections of the core during the brine flooding experiment on the core S-8
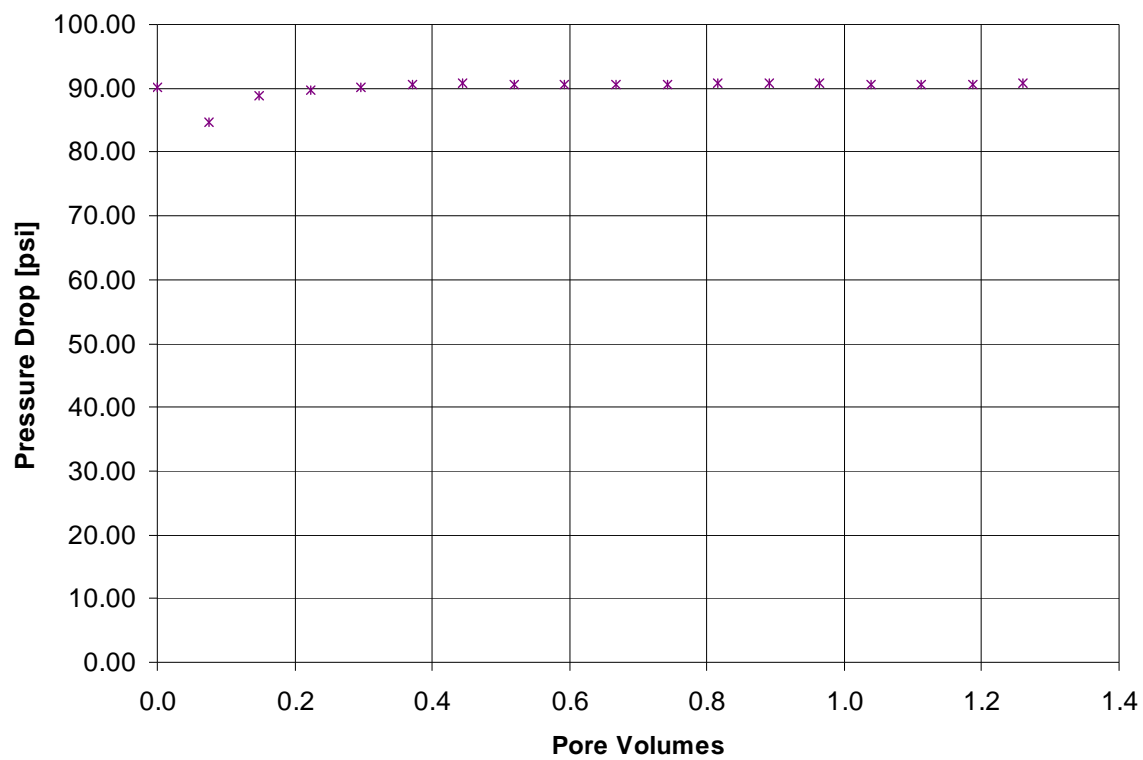
Figure 4.41: Pressure drops across the core during the oil flooding experiment on the core S-8
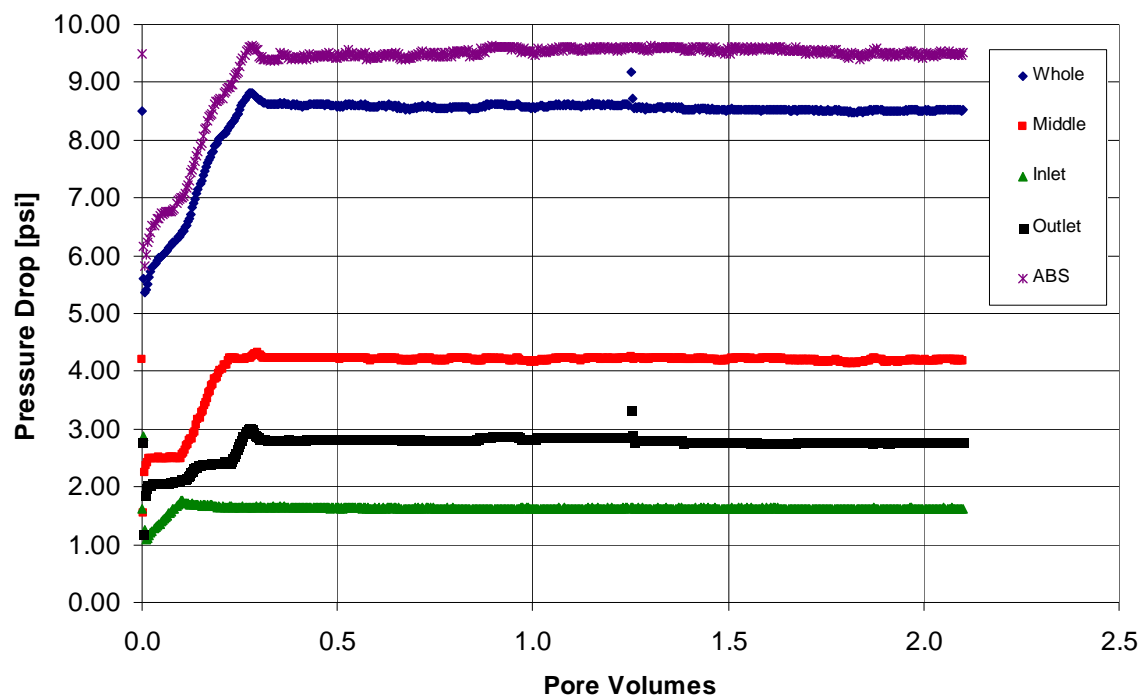
Figure 4.42: Pressure drops across different sections of the core during the water flooding experiment on the core S-8
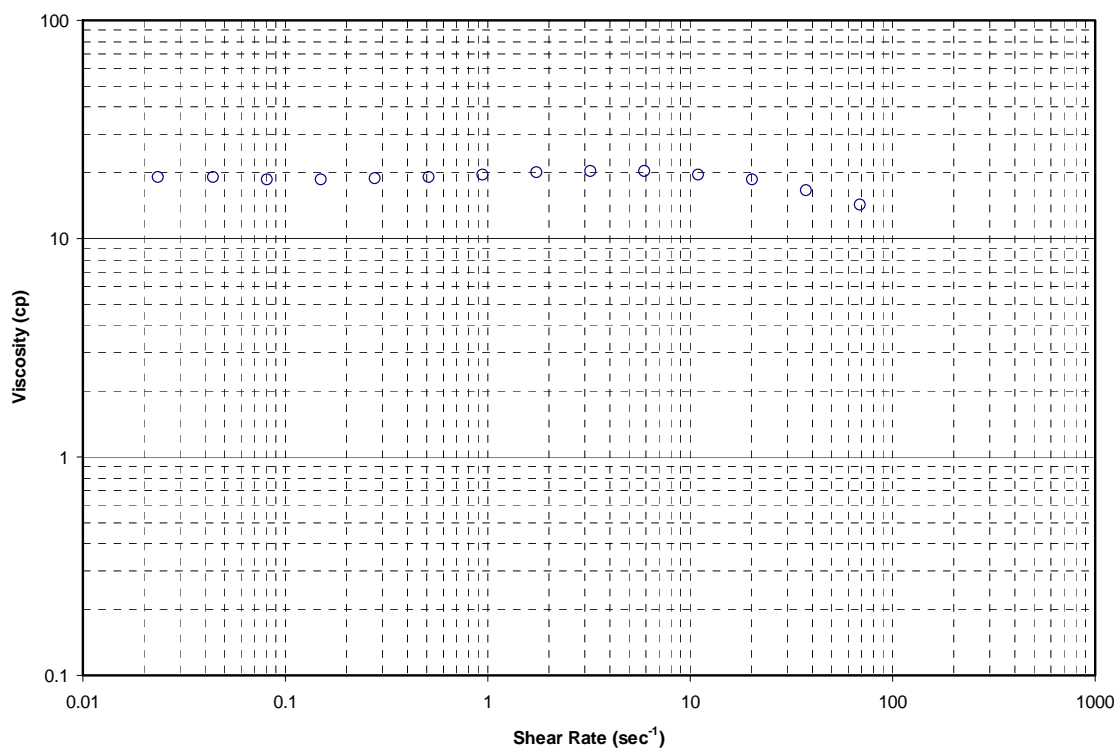
Figure 4.43: Viscosity measurement for the Alkali Surfactant Polymer slug at 25 C for the core flood experiment S-8
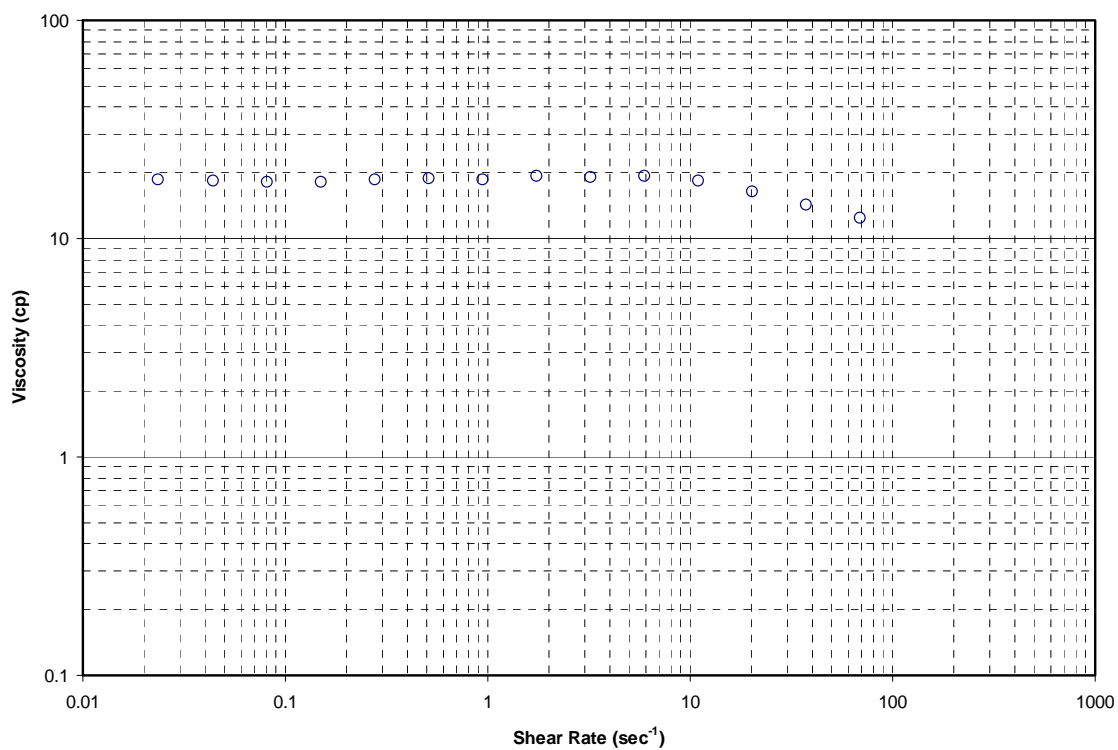
Figure 4.44: Viscosity measurement for the Polymer Drive at 25 C for the core flood
experiment S-8
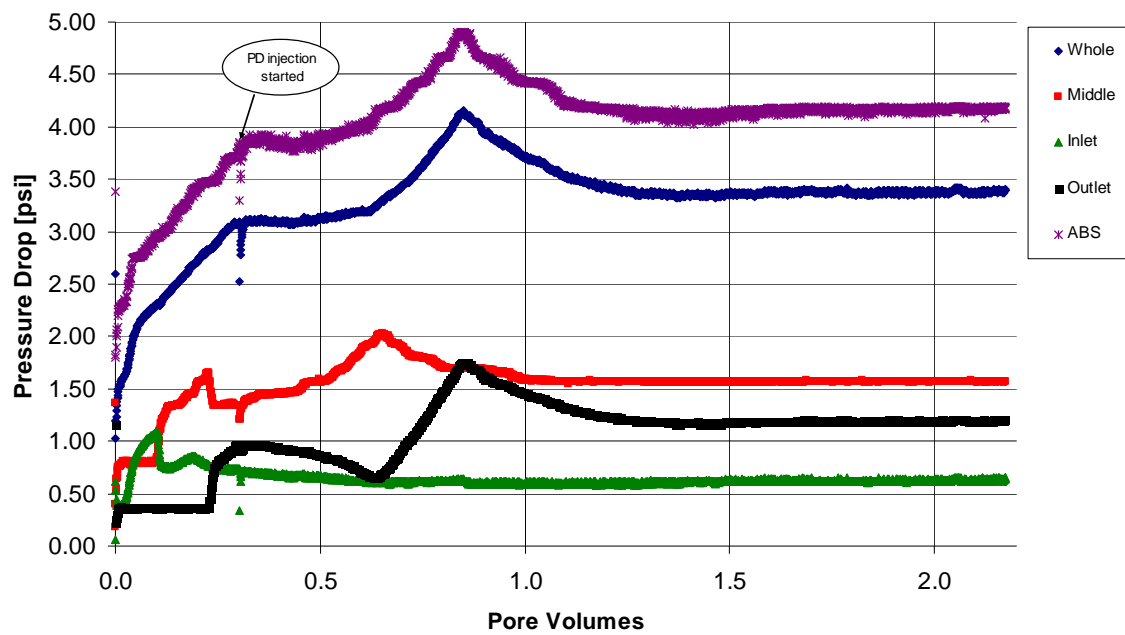
Figure 4.45: Pressure drops across different sections of the core during the chemical
flooding experiment on the core S-8
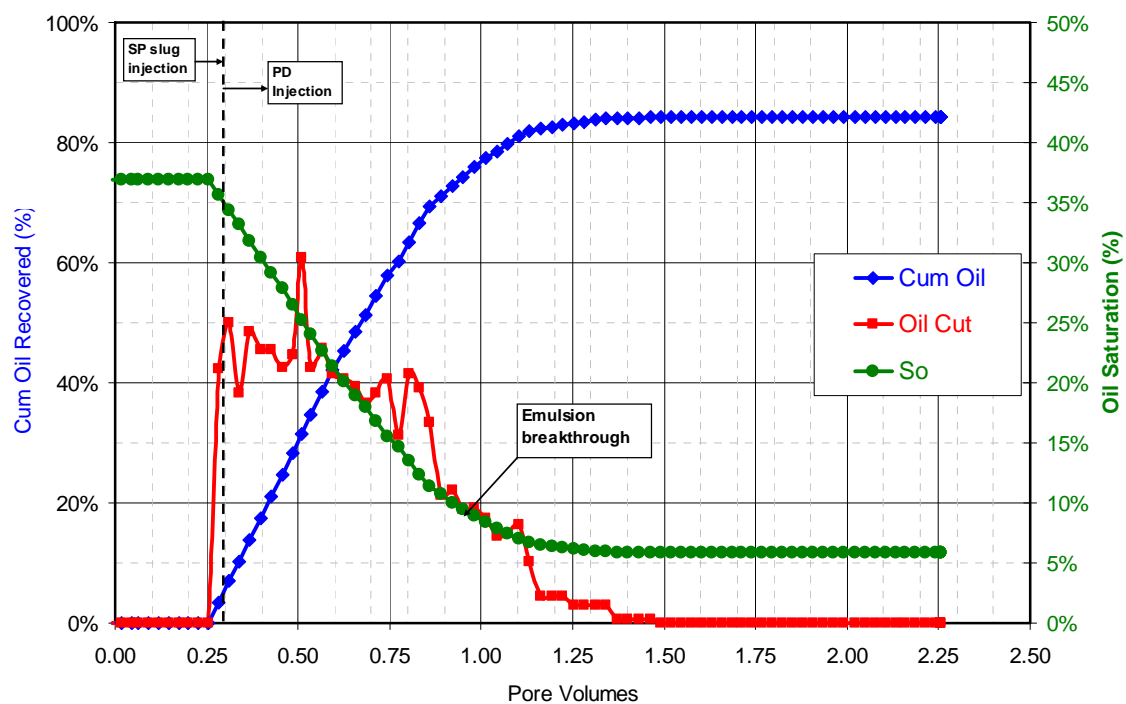
Figure 4.46: Cumulative Oil Recovery, Oil Cut and the Oil Saturation in the core during the chemical flooding experiment on the core S-8
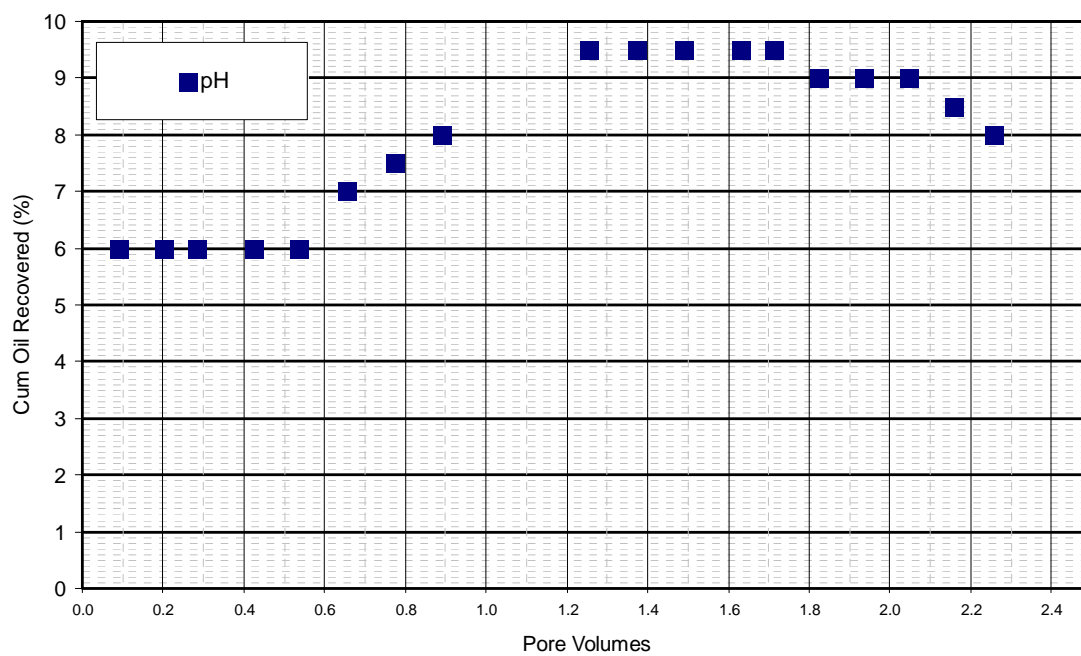
Figure 4.47: Effluent pH during the chemical flooding experiment on the core S-8
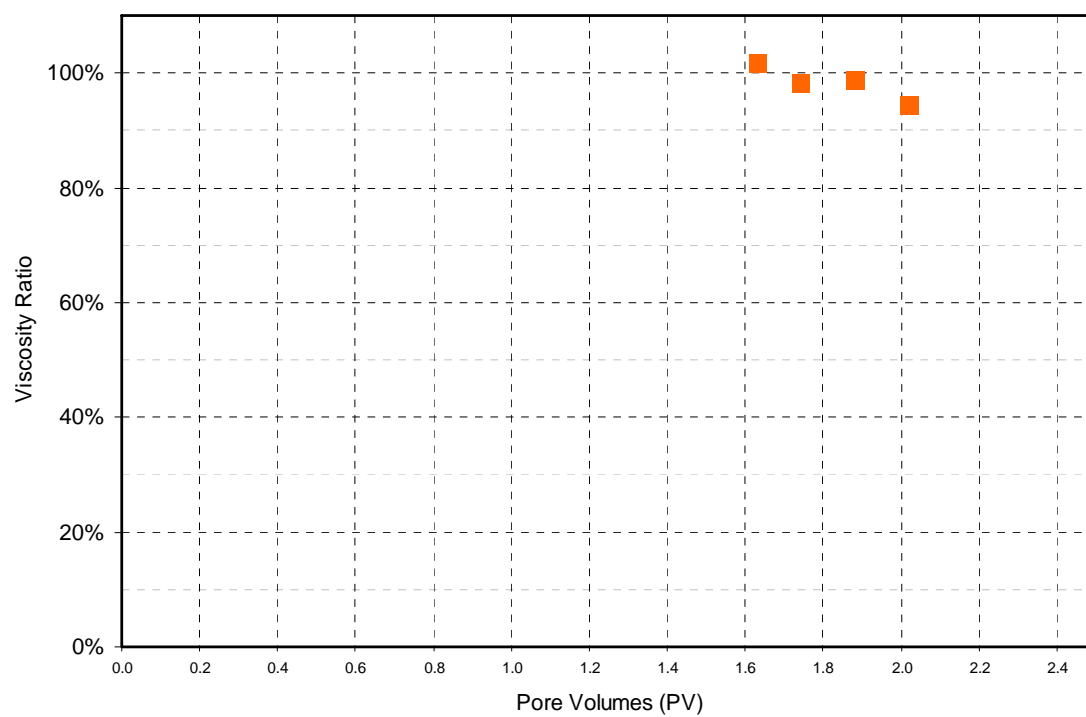
Figure 4.48: Effluent Viscosity Ratio during the chemical flooding experiment on the core S-8
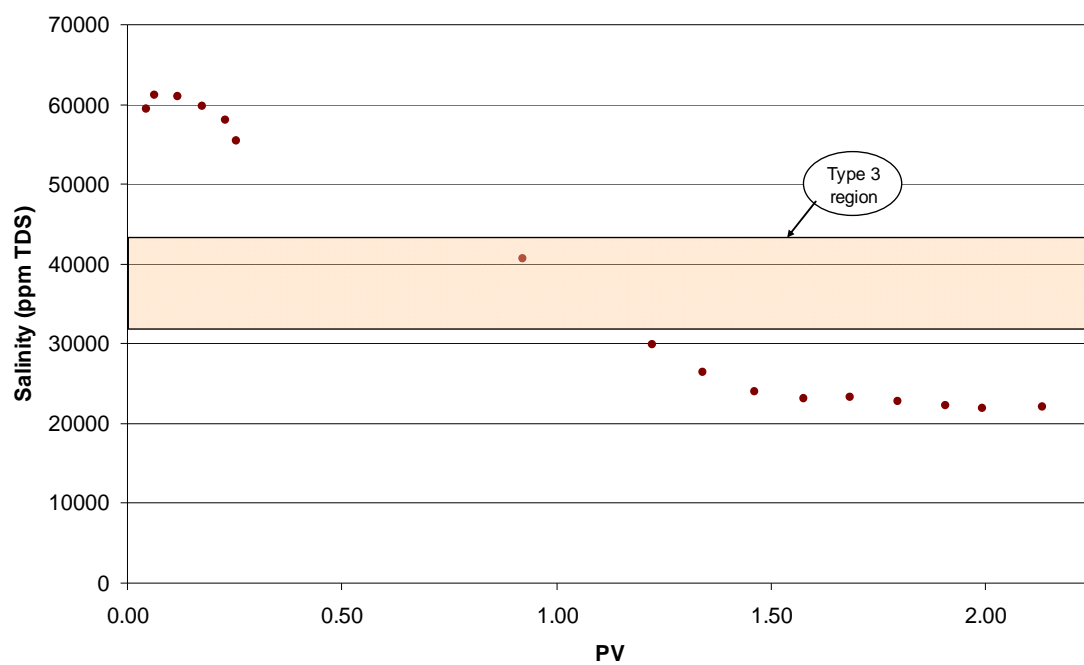
Figure 4.49: Effluent salinity during the chemical flooding experiment on the core S-8

Chapter 5: Simulation of Geochemical Species in Aqueous Systems

Sodium metaborate has been proposed as a novel alkali for ASP flooding without the need for soft water (Flaaten, 2008). However, precipitation was observed to occur in the presence of sulfate ions that are present in some commercial surfactant products in solution. Moreover, the presence of bicarbonate ions is also known to reduce the divalent ion tolerance in the presence of sodium metaborate. The principal aim of this chapter is to gain an understanding of the performance of novel alkali and chelating agents like sodium metaborate and tetrasodium EDTA with respect to their ability to sequester divalent ions in the form of soluble complexes. A study of the geochemical species present under different conditions was done with this objective in mind. This study used PHREEQC, a computer program developed by USGS which is capable of simulating the different aqueous phase geochemical species. The next section gives a brief overview of PHREEQC. The subsequent sections discuss the results of this study.

5.1 OVERVIEW OF PHREEQC

PHREEQC (Parkhurst, 1995) is a computer program capable of performing a variety of low temperature geochemical calculations. Based on the program PHREEQE (Parkhurst et al., 1980), PHREEQC can be used as a speciation program to calculate saturation indices and the distribution of aqueous species in solution. PHREEQC is based on the equilibrium chemistry of aqueous solutions interacting with minerals, gases, solid solutions and exchangers among others and uses an ion association model and Debye Huckel expressions to account for the non ideality of aqueous solutions.

5.2 SPECIATION STUDIES IN THE PRESENCE OF SODIUM METABORATE

       This section discusses the results of a study of aqueous phase geochemical species in the presence of sodium metaborate as an alkali. The first part of this study investigated the effectiveness of sodium metaborate in forming soluble borate complexes with the calcium and magnesium ions in solution. A sensitivity study of the effect of the presence of different aqueous solution species on the formation of these soluble complexes was done. The second part of this study focused on the factors affecting the tolerance for divalent ions in the presence of sodium metaborate. The effect of the presence of different species in solution on these tolerance limits was investigated. The results were verified with experiments on the calcium and magnesium ion tolerance limits and attempts were made to explain any discrepancies between the simulated and experimental tolerance limits.

5.2.1 Reactions Modeled

       The list of reactions modeled for the current study is shown below. These include the aqueous phase reactions as well as the precipitation reactions.

Aqueous phase Reactions

$$B(OH)_3 + H_2O \rightleftharpoons [B(OH)_4]^- + H^+$$

$$3B(OH)_3 \rightleftharpoons [B_3O_3(OH)_4]^- + 2H_2O + H^+$$

$$4B(OH)_3 \rightleftharpoons [B_4O_5(OH)_4]^- + 3H_2O + 2H^+$$

$$Ca^{2+} + B(OH)_3 + H_2O \rightleftharpoons Ca[B(OH)_4]^+ + H^+$$

$$Mg^{2+} + B(OH)_3 + H_2O \rightleftharpoons Mg[B(OH)_4]^+ + H^+$$

$$Ca^{2+} + CO_3^{2-} \rightleftharpoons CaCO_3$$

$$Ca^{2+} + H^+ + CO_3^{2-} \rightleftharpoons CaHCO_3^+$$

$$Mg^{2+} + CO_3^{2-} \rightleftharpoons MgCO_3$$

$$Mg^{2+} + H^+ + CO_3^{2-} \rightleftharpoons MgHCO_3^+$$

$$H^+ + CO_3^{2-} \rightleftharpoons HCO_3^-$$

$$SO_4^{2-} + H^+ \rightleftharpoons HSO_4^-$$

$$Ca^{2+} + SO_4^{2-} \rightleftharpoons CaSO_4$$

$$Mg^{2+} + SO_4^{2-} \rightleftharpoons MgSO_4$$

$$H_2O \rightleftharpoons H^+ + OH^-$$

$$Ca^{2+} + OH^- \rightleftharpoons CaOH^+$$

$$Mg^{2+} + OH^- \rightleftharpoons MgOH^+$$

Precipitation Reactions

$$Calcite(CaCO_3) \rightleftharpoons Ca^{2+} + CO_3^{2-}$$

$$Aragonite(CaCO_3) \rightleftharpoons Ca^{2+} + CO_3^{2-}$$

$$Anhydrite(CaSO_4) \rightleftharpoons Ca^{2+} + SO_4^{2-}$$

$$Gypsum(CaSO_4.2H_2O) \rightleftharpoons Ca^{2+} + SO_4^{2-} + 2H_2O$$

$$Portlandite(Ca(OH)_2) \rightleftharpoons Ca^{2+} + 2OH^-$$

$$Brucite(Mg(OH)_2) \rightleftharpoons Mg^{2+} + 2OH^-$$

$$Magnesite(MgCO_3) \rightleftharpoons Mg^{2+} + CO_3^{2-}$$

$$Borax(Na_2[B_4O_5(OH)_4].8H_2O) + 2H^+ \rightleftharpoons 4B(OH)_3 + 2Na^+ + 5H_2O$$
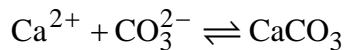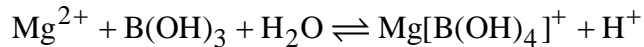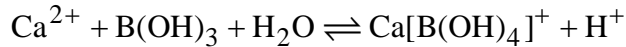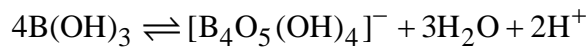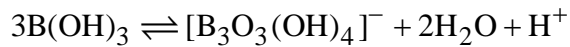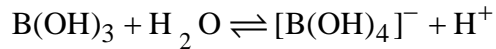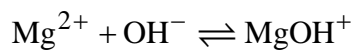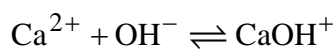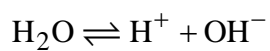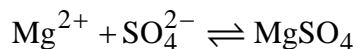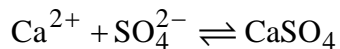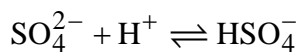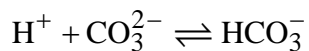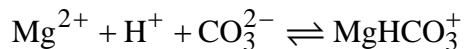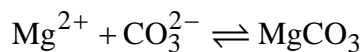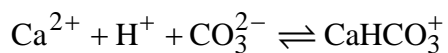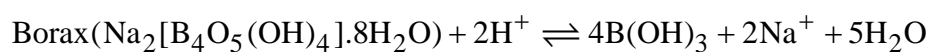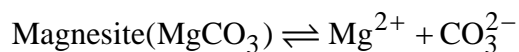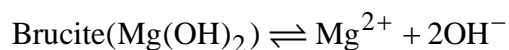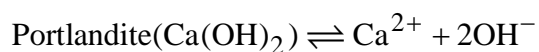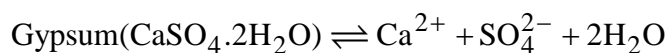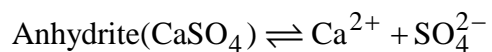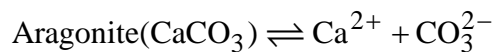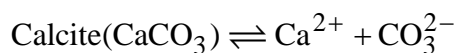
Table 5.1 and 5.2 show the thermodynamic equilibrium data for the aqueous and solid species modeled. These were obtained from the database Pitzer.dat (Plummer et al., 1988).

146

5.2.1 Effectiveness of sodium metaborate in forming soluble complexes

The first geochemical calculations were done to understand the effectiveness of sodium metaborate in forming soluble complexes with the calcium and magnesium ions in solution under different conditions. This is directly proportional to the fraction of calcium and magnesium ions present in the soluble borate complex form as compared to that present as free calcium and magnesium ions. The results of these calculations are presented below.

Effect of solution pH

The pH of the solution is expected to have a major influence on the effectiveness of sodium metaborate in forming soluble complexes with calcium and magnesium ions. This is because of the existence of different borate and polyborate chemical species in solution as a function of pH, first described by Ingri (1963) and shown in Figure 5.1. Soluble borate complexes were formed only under high pH conditions when the sodium metaborate exists in the borate form.

The first calculations examined the complexation of calcium and magnesium as a function of pH. Complexation refers to the ratio of the divalent ions present in the form of the soluble borate complex (like $[CaB(OH)_4]^+$ and $[MgB(OH)_4]^+$) to that of the total concentration of the divalent ions in the solution at equilibrium. The case simulated here used a calcium ion concentration of 2700 ppm. The results are plotted in Figure 5.2. No complexation was observed at neutral and acidic pH. Under alkaline pH conditions, the complexation increased with an increase in the pH, peaking at a pH of 14 wherein about 40% of the calcium ions were present in the form of the soluble borate complex.

147

Sensitivity to calcium ion and sodium metaborate concentration

The next calculations analyzed the sensitivity of the calcium complexation to the concentration of calcium ions at constant sodium metaborate concentration. The runs were repeated at different sodium metaborate concentrations. Figure 5.3 shows a plot the of the calcium complexation as a function of the concentration of the calcium ion at different sodium metaborate concentrations. The results indicate that the calcium concentration decreased as the calcium ion concentration increased at a particular sodium metaborate concentration. Moreover, the greater the sodium metaborate concentration, the higher was the complexation of calcium ion at a constant calcium ion concentration. This is also shown in figure 5.4, which shows a plot of the calcium concentration as a function of the sodium metaborate concentration at different calcium ion concentrations. The calcium complexation increased as a function of the sodium metaborate concentration at a particular calcium ion concentration.

Effect of the presence of Magnesium ion

The next case considered the simultaneous presence of both calcium and magnesium ions. Both these ions competed with one another for forming soluble borate complexes with sodium metaborate. The effect of the presence of one of the ions on the complexation of the other ion with sodium metaborate was studied. Figure 5.5 shows the plot of the magnesium complexation as a function of the magnesium ion concentration at different calcium ion concentrations. Figure 5.6 shows the corresponding calcium complexation in the presence of magnesium. The results indicate that both the magnesium as well as the calcium complexation decreased as the concentration of the magnesium ion increased at a constant calcium ion concentration. Moreover, the calcium complexation was substantially higher than the magnesium complexation for the same

148

magnesium and calcium ion concentrations. Figure 5.7 shows the plot of the magnesium complexation as a function of the magnesium ion concentration at different sodium metaborate concentrations. Figure 5.8 shows the corresponding calcium complexation.

In all cases in this section, precipitation of the magnesium hydroxide was observed at a particular magnesium ion concentration. The corresponding precipitation boundary is indicated by the dotted lines in each of the four plots. As the calcium concentration increased, the corresponding magnesium ion tolerance decreased. Also, as the sodium metaborate concentration increased, it was observed that the magnesium ion tolerance increased.

Effect of the presence of the sulfate ion

The next set of runs considered the presence of sulfate ions in the aqueous solution. A sensitivity study of its effect on the complexation of the calcium ion was done. The sulfate ion concentration was varied from 0 to 5000 ppm while maintaining a constant concentration of the calcium ion and sodium metaborate. The cases considered here used a calcium ion concentration of 2700 ppm and a sodium metaborate concentration of 0.3%. The results are shown in figure 5.9 in the form of a plot of the calcium ion complexation as a function of the sulfate ion concentration. The results indicate a slight drop in the calcium ion complexation as the sulfate ion concentration increased.

Effect of the presence of the bicarbonate ion

The presence of the bicarbonate ion is expected to significantly decrease the calcium ion tolerance in the presence of sodium metaborate. This is because of the nature of the carbonate equilibrium given by,

$$H^+ + CO_3^{2-} \rightleftharpoons HCO_3^-$$
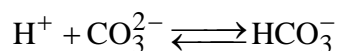
Under high pH conditions, the reverse reaction is expected to be favored, thereby increasing the concentration of the carbonate ion. This increases the precipitation of calcium carbonate and hence decreases the calcium tolerance limit.

The calculations shown in this section considered the effect of the presence of the bicarbonate ion on the calcium complexation. Figure 5.10 shows the plot of the calcium tolerance limit from the simulations using PHREEQC, as a function of the concentration of bicarbonate ion. The calcium tolerance limit decreased drastically as the bicarbonate ion concentration increased.

5.2.2 Factors influencing the performance of sodium metaborate as an alkali

This section discusses the results of a study of the factors affecting the performance of sodium metaborate as an alkali. A series of aqueous tests were done towards this end which investigated the tolerance limits for divalent ions like calcium and magnesium under different conditions. This section aims to explain these observations in terms of the precipitation of different species in the presence of sodium metaborate.

150

Considering the precipitation of calcium carbonate

The first calculations considered calcium carbonate to be the precipitating species. A small concentration of carbonate ion was assumed to be present and precipitated with the free calcium and magnesium ions as the corresponding carbonates when the concentration of calcium/magnesium ions exceeded a threshold limit designated as the tolerance limit. This section describes the results of these calculations and compares them with the corresponding experimental results.

Base Case

The base case considered the presence of only calcium ions at different sodium metaborate concentrations at room temperature. The results are plotted in Figure 5.11 in the form of the calcium ion tolerance with respect to the precipitation of calcium carbonate against the corresponding sodium metaborate concentration, along with the corresponding experimental data. A reasonable match between the experimental and simulated calcium tolerance limits was observed.

At High Temperatures

The next case considered the presence of calcium ions at different sodium metaborate concentrations at elevated temperatures. Two different temperatures were considered, namely 50°C and 80°C. The results have been plotted in Figures 5.12 and 5.13 in the form of the calcium ion tolerance with respect to the precipitation of calcium carbonate against the corresponding sodium metaborate concentration, along with the corresponding experimental data. The results indicate that the predicted calcium tolerance limits deviated significantly from the observed experimental values at lower sodium

151

metaborate concentrations. At higher sodium metaborate concentrations, the experimental and simulated values were reasonably close to one another.

In the presence of sodium chloride

In the case considered next, sodium chloride was present in addition to the calcium ions. The case considered here used a sodium chloride concentration of 3% in the aqueous solution. The calcium tolerance limits with respect to the precipitation of calcium carbonate were determined and have been plotted in Figure 5.14 along with the corresponding experimental data. The results indicate a significant deviation from the experimental values at lower sodium metaborate concentrations. However, at higher sodium metaborate concentrations, the results were reasonably close.

In the presence of sodium hydroxide

The next case considered the presence of the alkali, sodium hydroxide, along with calcium ions. A sodium hydroxide concentration of 0.4% was used. In addition to calcium carbonate, calcium hydroxide was found to be one of the precipitating species under the high pH conditions produced by the addition of sodium hydroxide. The corresponding calcium tolerance limits with respect to the precipitation of calcium hydroxide and calcium carbonate were determined and are shown in figure 5.15 plotted against the sodium metaborate concentration. The results indicate good agreement with the experimental data at lower sodium metaborate concentrations. However, at high sodium metaborate concentrations, the results were found to deviate significantly.

152

In the presence of the sulfate ion

The last case considered the presence of sulfate ions along with the calcium ions. Two different concentrations of sodium sulfate, namely 0.1% and 0.2% were used in this study. The corresponding calcium tolerance limits with respect to the precipitation of calcium carbonate were determined and are shown in Figures 5.16 and 5.17 for the sodium sulfate concentrations of 0.1 and 0.2% respectively along with the corresponding experimental data. The results indicate a reasonable agreement with the experimental data, especially at higher sodium metaborate concentrations for the case with 0.1% sodium sulfate. At lower concentrations, the results were found to deviate significantly from the experimental values, especially for the case with 0.2% sodium sulfate.

Considering the precipitation of calcium carbonate and calcium sulfate

The next set of calculations considered calcium sulfate to be the main precipitating species. However, the calcium tolerance limits so obtained were unrealistically high and hence this model was discarded. The next case considered both calcium carbonate and calcium sulfate to be the precipitating species. A small concentration of carbonate and sulfate ions were assumed to be present in the initial solution which precipitated as the calcium and magnesium ions present in the solution as the respective carbonates and sulfates when the calcium/magnesium ion concentration exceeded a threshold limit called the calcium/magnesium ion tolerance limit. In this case, the calcium/magnesium tolerance limit was defined as the calcium/magnesium ion concentration at which precipitation in the form of either calcium carbonate or calcium sulfate was observed. This section describes the results and compares them with the observed experimental results.

153

Base Case

The base case considered the presence of only calcium ions at different sodium metaborate concentrations at 25 C. In this case, calcium carbonate was found to be the precipitating species. The results have been plotted in Figure 5.18 in the form of the calcium ion tolerance with respect to the precipitation of calcium carbonate against the corresponding sodium metaborate concentration, along with the corresponding experimental data. The results indicated a higher calcium ion tolerance limit as compared to the experimentally observed values. This deviation was found to be especially high at higher sodium metaborate concentrations.

At High Temperature

The next case considered the presence of calcium ions at different sodium metaborate concentrations at two different temperatures which were higher than the temperature of 25°C considered for the base case, namely 50°C and 80°C. In this case too, calcium carbonate was found to be the main precipitating species. The corresponding results have been plotted in Figures 5.19 and 5.20 in the form of the calcium ion tolerance with respect to the precipitation of calcium carbonate against the sodium metaborate concentration, along with the corresponding experimental data. The results were along the lines of that observed during the initial case (Figure 5.12 and 5.13) which considered the precipitation of calcium carbonate alone. The simulated calcium ion tolerance limits deviated significantly from the experimental values at lower sodium metaborate concentrations while they were reasonably close at higher sodium metaborate concentrations.

154

In the presence of Sodium Chloride

This case considered the presence of sodium chloride in the system in addition to calcium ions in the form of calcium chloride. The case considered here had a sodium chloride concentration of 3% in the solution. In this case too, calcium carbonate was found to be the main precipitating species. The calcium tolerance limits with respect to the precipitation of calcium carbonate were determined and have been plotted in Figure 5.21 along with the corresponding experimental data. The results indicate a significant deviation from the experimental values at lower sodium metaborate concentrations. However, at higher sodium metaborate concentrations, the results were reasonably close.

In the presence of Sodium Hydroxide

The next case considered the presence of sodium hydroxide along with calcium ions in the form of calcium chloride. A sodium hydroxide concentration of 0.4% was used in this study. Calcium hydroxide along with calcium carbonate was found to be the precipitating species. The corresponding calcium tolerance limits with respect to the precipitation of calcium hydroxide and calcium carbonate were determined and are shown in Figure 5.22 plotted against the sodium metaborate concentration. The results indicate a good agreement with the experimental data at low concentrations of sodium metaborate. At higher concentrations, the results deviated significantly.

In the presence of the sulfate ion

The last case considered the presence of sulfate ions along with the calcium ions. Two different concentrations of sodium sulfate, namely 0.1% and 0.2% were used in this study. In this case, calcium sulfate was found to be the main precipitating species. The corresponding calcium tolerance limits with respect to the precipitation of calcium sulfate

were determined and are shown in Figures 5.23 and 5.24 for the sodium sulfate concentrations of 0.1 and 0.2% respectively along with the corresponding experimental data. The results indicate a reasonable agreement with the experimental data for all concentrations of sodium metaborate at a sodium sulfate concentration of 0.1%. At a sodium sulfate concentration of 0.2%, the simulated calcium tolerance limits agree with the experimental values at low concentrations of sodium metaborate while at higher concentrations, the results deviated significantly.

5.2.3 Summary and Conclusions

An investigation into the conditions under which soluble borate complexes were formed showed that complexation occurred only under alkaline pH conditions. No complexation was observed under acidic or neutral pH conditions. Moreover, the calcium ions were observed to form soluble complexes more easily as compared to magnesium ions.

A sensitivity study of the effect of the presence of and the variation in the concentration of different species in the solution was done. The fraction of calcium ions present in the form of the soluble complex in the solution:

i. Increased with an increase in the solution pH.
ii. Decreased with an increase in the calcium ion concentration under constant magnesium ion concentration when both ions were present. Similar observations were made for the case when the complexation of the magnesium ions was considered under varying magnesium ion concentrations while maintaining constant calcium ion concentrations.
iii. Increased with an increase in the sodium metaborate concentration.
iv. Decreased slightly with an increase in the sulfate ion concentration when sulfate ions were present in the system.

156

The second part of this study considered the effectiveness of sodium metaborate in forming soluble borate complexes with respect to the tolerance of the calcium and magnesium ions in the presence of sodium metaborate under different conditions. The calcium and magnesium carbonates and sulfates, along with magnesium hydroxide (when magnesium ions were present) were the major precipitating species. The predicted tolerance limits showed reasonably good matches with the results of aqueous phase experiments done in this regard under different conditions at room temperature. However, at elevated temperatures, significant deviations were observed between the experimental and simulated tolerance limits.

5.3 SPECIATION STUDIES IN THE PRESENCE OF TETRASODIUM EDTA

This section discusses the results of a study of geochemical species in the presence of hardness causing ions like calcium and magnesium along with tetrasodium EDTA (Na_4EDTA) as a chelating agent. Specific laboratory aqueous phase experiments involving brines from different reservoirs under different temperature conditions as well as hardness and salinity levels, in the presence of Na_4EDTA as the chelating agent were analyzed using PHREEQC, the geochemical software developed by USGS that is capable of performing aqueous phase geochemical calculations based on equilibrium chemistry. From the concentration and activity data of the different species in the solution, equilibrium calculations were performed to determine whether or not precipitation occurred. If precipitation was predicted, the theoretical quantities of different precipitating species were estimated.

5.3.1 Formation Brine Description

This study considered synthetic injection brines from two different reservoirs differing widely in the reservoir temperature as well as their salinity and hardness levels. These are described in this section.

Reservoir 'U' is a high temperature carbonate formation with a reservoir temperature of 100°C. The synthetic injection brine for this reservoir had a high salinity (58000 ppm TDS) and hardness (2750 ppm TDS). The brine had a high magnesium hardness content (2100 ppm) and moderate calcium hardness (650 ppm). The high magnesium hardness content made it particularly sensitive to precipitation under high pH conditions in the absence of suitable chelating agents like Na_4EDTA. Table 5.3 lists the ionic composition of the synthetic formation brine of the reservoir 'U'.

Reservoir 'C' is a low temperature sandstone reservoir with a reservoir temperature of 30°C. The synthetic formation brine for this reservoir had a low salinity (18700 ppm TDS) and moderate hardness content (900 ppm). This brine had a moderate calcium ion concentration (640ppm) while the magnesium ion content of the brine was fairly low (240 ppm). Table 5.4 lists the ionic composition of the synthetic formation brine of the reservoir 'C'.

5.3.2 Reactions Modeled

The list of reactions modeled for the current study is shown below. These include the aqueous phase reactions as well as the precipitation reactions.

Aqueous Phase Reactions

$$H^+ + EDTA^{4-} \rightleftharpoons H(EDTA)^{3-}$$

$$2H^+ + EDTA^{4-} \rightleftharpoons H_2(EDTA)^{2-}$$

$$3H^+ + EDTA^{4-} \rightleftharpoons H_3(EDTA)^-$$

$$4H^+ + EDTA^{4-} \rightleftharpoons H_4(EDTA)$$

$$5H^+ + EDTA^{4-} \rightleftharpoons H_5(EDTA)^+$$

$$Ca^{2+} + EDTA^{4-} \rightleftharpoons Ca(EDTA)^{2-}$$

$$Mg^{2+} + EDTA^{4-} \rightleftharpoons Mg(EDTA)^{2-}$$

$$H^+ + CO_3^{2-} \rightleftharpoons HCO_3^-$$

$$2H^+ + CO_3^{2-} \rightleftharpoons H_2CO_3$$

$$Ca^{2+} + CO_3^{2-} \rightleftharpoons CaCO_3$$

$$Ca^{2+} + H^+ + CO_3^{2-} \rightleftharpoons CaHCO_3^+$$

$$Mg^{2+} + CO_3^{2-} \rightleftharpoons MgCO_3$$

$$Mg^{2+} + H^+ + CO_3^{2-} \rightleftharpoons MgHCO_3^+$$

$$H^+ + SO_4^{2-} \rightleftharpoons HSO_4^-$$

$$Ca^{2+} + SO_4^{2-} \rightleftharpoons CaSO_4$$

$$Mg^{2+} + SO_4^{2-} \rightleftharpoons MgSO_4$$

$$H_2O \rightleftharpoons H^+ + OH^-$$

$$Ca^{2+} + OH^- \rightleftharpoons CaOH^+$$

$$Mg^{2+} + OH^- \rightleftharpoons MgOH^+$$

Precipitation Reactions

$$\text{Calcite}(CaCO_3) \rightleftharpoons Ca^{2+} + CO_3^{2-}$$

$$\text{Aragonite}(CaCO_3) \rightleftharpoons Ca^{2+} + CO_3^{2-}$$

$$\text{Anhydrite}(CaSO_4) \rightleftharpoons Ca^{2+} + SO_4^{2-}$$

159

$$Gypsum(CaSO_4.2H_2O) \rightleftharpoons Ca^{2+} + SO_4^{2-} + 2H_2O$$

$$Portlandite(Ca(OH)_2) \rightleftharpoons Ca^{2+} + 2OH^-$$

$$Brucite(Mg(OH)_2) \rightleftharpoons Mg^{2+} + 2OH^-$$

$$Magnesite(MgCO_3) \rightleftharpoons Mg^{2+} + CO_3^{2-}$$
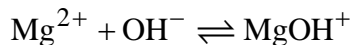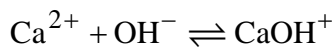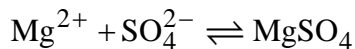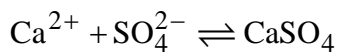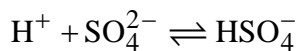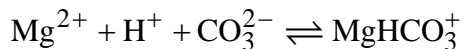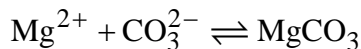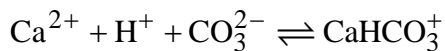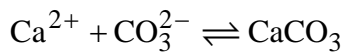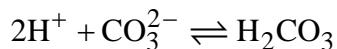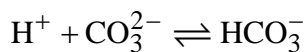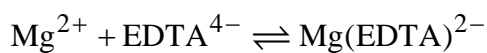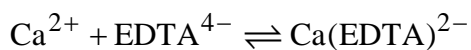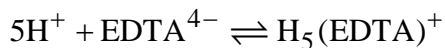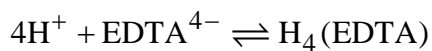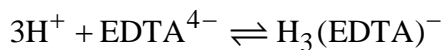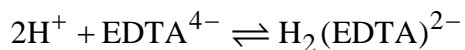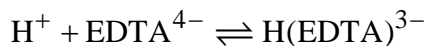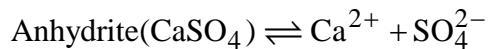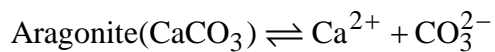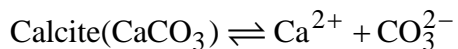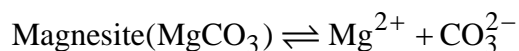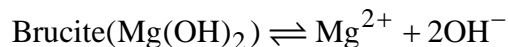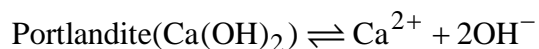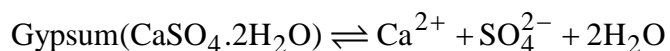
Tables 5.5 and 5.6 shows the thermodynamic equilibrium data for the aqueous and solid species modeled respectively. These were obtained from the database Minteq.dat (Allison et al., 1990).

5.3.2 Speciation studies with reservoir 'U'

This section discusses the results of the solution speciation studies in the presence of Na_4EDTA as the chelating agent for reservoir 'U'. Specific aqueous stability experiments for this reservoir were chosen for this study. These experiments attempted to determine the minimum amount of Na_4EDTA that was required to keep the aqueous solution with the injection water clear without any precipitation, both at the room temperature and at the reservoir temperature of 100°C. The geochemical solution species under the corresponding experimental conditions were simulated using PHREEQC. From the concentration and activity data of the different species in solution, the likelihood of precipitation was predicted. In case precipitation was predicted, the nature of the species precipitating was determined. Also, the theoretical quantity of precipitates of each species expected to precipitate was also calculated by considering the solubility equilibrium of the corresponding precipitating species.

Na₄EDTA scan of the Synthetic Injection Water

The first experiment studied considered the effect of varying the Na₄EDTA concentration while maintaining a constant divalent ion concentration. To this end, a Na₄EDTA scan was done with the synthetic injection brine for the reservoir 'U'. The ionic composition of the synthetic injection brine is shown in Table 5.1. The Na₄EDTA concentration range in which the scan was done ranged from 0 to 4.5%. The scan was done both at room temperature and at the reservoir temperature of 100°C. The experimental results showed that at room temperature, the samples up to 3% Na₄EDTA were cloudy and showed precipitation. When the Na₄EDTA concentration was more than 3%, all the samples were clear and showed no precipitation. At the reservoir temperature of 100°C, all samples up to 4.5% Na₄EDTA were cloudy after a period of 12 hours.

Figures 5.25 and 5.26 show the results of the simulations of geochemical species for this experiment using PHREEQC at room temperature and at the reservoir temperature of 100°C respectively. The results have been presented in the form of the predicted precipitation amount, i.e. the mass of precipitates per unit volume of the solution for each individual species as well as the total precipitation for all species. The results indicate that at the room temperature, magnesium carbonate and magnesium hydroxide were the main precipitating species under the experimental conditions. At low Na₄EDTA concentrations, magnesium carbonate was found to be the main precipitating species. However, at higher Na₄EDTA concentrations and hence high pH conditions, magnesium hydroxide was also found to precipitate along with magnesium carbonate. At 4% Na₄EDTA concentration, magnesium hydroxide was found to be the sole precipitating species.

The above observations can be explained by considering the percentage of calcium and magnesium ions present in the chelated form with EDTA, at different

concentrations of Na_4EDTA. These are shown in Figures 5.27 and 5.28 for the cases at room temperature and the reservoir temperature of 100°C respectively. The chelating ability of Na_4EDTA decreased drastically as the temperature increased from 25 C to 100°C. This explains the observed increase in the total precipitation at higher temperature. Moreover, the calcium ion formed soluble chelates with the EDTA more easily compared to the magnesium ion, especially at low temperatures. This explains the fact that no calcium precipitation was predicted to occur under the given experimental conditions.

Varying the divalent ion concentration at constant Na_4EDTA concentration

The next experiment considered the effect of varying the divalent ion concentration while maintaining a constant Na_4EDTA concentration. This was done by mixing varying proportions of the synthetic injection brine and deionized water, thereby producing solutions with varying TDS content and hence divalent ion concentrations. The divalent ion concentrations so tested ranged from 835 ppm (640 ppm of Mg^{2+}, 195ppm Ca^{2+} and a total salinity of 17435 ppm TDS) to 2785 ppm (2134 ppm of Mg^{2+}, 651 ppm of Ca^{2+} and a total salinity of 57818 ppm TDS). A 3% Na_4EDTA concentration was used, which was close to the calculated theoretical requirement of Na_4EDTA to chelate all the divalent ions present in solution. The solution was pre treated to remove the bicarbonates present. The scan was done at room temperature. The experimental results showed that the samples were clear without any signs of precipitation up to a total divalent ion concentration of 1393 ppm (1067 ppm of Mg^{2+}, 326 ppm of Ca^{2+} and a total salinity of 28909 ppm TDS).

Figure 5.29 shows the results of the simulation studies of the geochemical species for this experiment in the form of a plot of the predicted precipitation rate, i.e mass of

precipitates per unit volume of the solution. The results indicate that little or no precipitation occurred up to a total divalent ion concentration of about 1671 ppm (1280 ppm Mg^{2+}, 391 ppm Ca^{2+} and a total salinity of 34691 ppm TDS). Beyond this, precipitation was observed. In the absence of the bicarbonate ion, the only precipitating species was found to be magnesium hydroxide. The observed precipitation rate reached a maximum at a total divalent ion concentration of 2228 ppm after which it showed a decrease.

Figure 5.30 shows a plot of the percentage of the calcium and magnesium ions presented in the chelated state with EDTA as a function of the total divalent ion concentration. The simulated solution pH is also plotted in the same plot. For a divalent ion concentration of 1949 ppm, nearly all the calcium and magnesium ions were present in the chelated form, thereby preventing their precipitation. Beyond this concentration, a significant proportion of the magnesium ions were present as free magnesium, thereby causing the precipitation of magnesium hydroxide. An observation of the solution pH shows that it fell drastically from a very high value of about 11.5 to a much lower value of 10 at and above a total divalent ion concentration of 2228 ppm. This explains the observed fall in the precipitation rate in the simulation results in spite of the increasing amount of free magnesium present in the solution. Also, the fact that nearly all the calcium was present in the chelated form in all samples explains the absence of any calcium hydroxide precipitates.

Na$_4$EDTA scan of the Synthetic Injection Water at lower solution pH

The last experiment studied for the reservoir 'U' considered an Na_4EDTA scan of the synthetic injection brine. However, in this case, the solution pH was maintained at a low value of 10.5 to minimize the precipitation of magnesium hydroxide. The Na_4EDTA

concentration range in which the scan was done ranged from 2 to 4%. The solution was pre treated and filtered to remove any precipitates present in the samples. The experimental results showed that precipitation was observed up to a Na_4EDTA concentration of 3.5% beyond which the solutions were clear and no precipitation was observed.

Figure 5.31 shows the results of the geochemical simulation studies for this experiment. The results are plotted in the form of a plot of the predicted precipitation, i.e. mass of precipitates per unit volume of the solution. The results indicate precipitation in all the samples. However, the precipitation rate increased up to a Na_4EDTA concentration of 3.5%, beyond which it showed a drastic decrease to very low values. Also, magnesium hydroxide was found to be the only precipitating species in the absence of bicarbonate ions.

The above observations can be explained by considering the plot of the percentage of calcium and magnesium ions present in the chelated state in the experimental conditions. These are plotted in figure 5.32 as a function of the Na_4EDTA concentration. Nearly all the calcium ions were present in the chelated form at all concentrations of Na_4EDTA. This explains the absence of calcium hydroxide precipitates. Also, the fraction of magnesium ions present in the chelated form showed an increase from nearly 40% at 2% Na_4EDTA concentration to nearly 100% at 4% concentration. This explains the observed drastic decrease in the magnesium hydroxide precipitation at an Na_4EDTA concentration of more than 3.5%.

5.3.3 Speciation studies with reservoir 'C'

This section discusses the results of the solution speciation studies in the presence of Na_4EDTA as the chelating agent for reservoir 'C'. Two aqueous stability experiments

for this reservoir were chosen for this study. The geochemical solution species under the corresponding experimental conditions were simulated using PHREEQC. From the concentration and activity data of the different species in solution, the likelihood of precipitation was predicted. In case precipitation was predicted, the nature of the species precipitating was determined. Also, the quantity of precipitates of each species theoretically expected to precipitate was also calculated by considering the solubility equilibrium of the corresponding precipitating species.

Na$_4$EDTA scan of the Synthetic Formation Brine

This experiment considered the effect of varying the concentration of Na$_4$EDTA while maintaining a constant divalent ion concentration. This was done by performing an Na$_4$EDTA scan with the synthetic formation brine for the reservoir 'C'. This was done both at the room temperature as well as at the reservoir temperature of 30°C. The Na$_4$EDTA concentration for which the scan was done ranged from 0 to 1.80%. The experimental results indicated that the samples were cloudy and showed precipitation up to a Na$_4$EDTA concentration of 0.6%. Beyond this, no precipitation was observed and the samples were clear.

Figures 5.33 and 5.34 show the results of simulation studies using PHREEQC at the room temperature and at the reservoir temperature of 87°F respectively. Magnesium hydroxide was found to be the only precipitating species. The results have been plotted in the form of the expected precipitation of magnesium hydroxide per unit volume of the solution at different concentrations of Na$_4$EDTA in the system. These results indicate that precipitation occurred till an EDTA concentration of 1% at both the room temperature and at the reservoir temperature of 87°F, beyond which no precipitation was observed. The amount of precipitates is expected to increase with an increase in the

Na$_4$EDTA concentration up to a concentration of 1%. Moreover, more precipitation is expected to occur at the reservoir temperature of 87°F as compared to that at the room temperature.

Figures 5.35 and 5.36 show plots of the fraction of calcium and magnesium ions present in the chelated form at different concentrations of EDTA under the experimental conditions at the room temperature and at the reservoir temperature of 87°F respectively. The expected solution pH is also plotted alongside. A far greater fraction of calcium ions was observed to be present in the chelated form as compared to the magnesium ions, irrespective of the temperature. This, coupled with the lower solubility product of magnesium hydroxide as compared to that of calcium hydroxide explains the fact that calcium hydroxide does not precipitate under the experimental conditions. At an Na$_4$EDTA concentration of greater than or equal to 1%, nearly all the calcium and magnesium ions were present in the chelated form, thereby preventing any precipitation.

Sodium carbonate scan of the synthetic formation brine in the presence of Na$_4$EDTA

This experiment considered the effect of the presence of the carbonate ion on the divalent ion tolerance in the presence of Na$_4$EDTA. A sodium carbonate scan of the synthetic formation brine was done in the presence of 1% Na$_4$EDTA both at the room temperature and at the reservoir temperature of 87°F. The range of sodium carbonate concentrations in which the scan was done ranged from 0% to 3.5%. The experimental results showed that all samples were cloudy at the reservoir temperature of 87°F. At the room temperature, the samples were clear up to a sodium carbonate concentration of 0.5% while they were cloudy at higher sodium carbonate concentrations.

Figures 5.37 and 5.38 show the results of geochemical calculations for this experiment at the room temperature and at the reservoir temperature of 87°F respectively.

The results have been plotted in the form of the expected theoretical precipitation per unit volume of the solution at different concentrations of sodium carbonate. The results indicate that theoretically, precipitation would be expected in all the samples. Magnesium hydroxide was found to be the only precipitating species in the absence of sodium carbonate. In the presence of sodium carbonate, calcium and magnesium carbonates were also found to precipitate. The amount of precipitates was found to reach a maximum at a sodium carbonate concentration of 0.5%. At higher sodium carbonate concentrations, the amount of precipitates showed a decrease with an increase in the sodium carbonate concentration.

Figures 5.39 and 5.40 show the fractions of the calcium and magnesium ions present in the chelated form at different sodium carbonate concentrations at the room temperature and at the reservoir temperature of 87°F respectively. The expected solution pH is also plotted alongside. The results show a marginal increase in the fraction of magnesium ions existing in the chelated state as the sodium carbonate concentration increased. This explains the observed decrease in the precipitation with an increase in the concentration of sodium carbonate.

5.3.4 Summary and Conclusions

To summarize, a study was done of the geochemical species in the presence of hardness causing divalent ions calcium and magnesium and Na_4EDTA as the chelating agent. From the results of this study, a few general conclusions can be made.

- The chelating ability of Na_4EDTA decreased drastically as the temperature increased.
- Calcium formed soluble chelates with Na_4EDTA more easily than magnesium. This effect was more pronounced at lower temperatures.

167

A sensitivity study about the effect of the presence of different solution species on the chelating ability of Na_4EDTA showed that the fraction of calcium/magnesium ions present in the chelated form,

- Increased drastically with an increase in the Na_4EDTA concentration. This effect was more pronounced at lower Na_4EDTA concentrations and lower temperatures.
- Decreased as the concentration of divalent ions increased at constant Na_4EDTA concentrations. This effect was more pronounced for magnesium ions as compared to that for calcium ions.

The qualitative experimental observations of precipitation/cloudiness under different conditions were successfully explained by the model. Quantitative calculations of the amount of precipitates under different conditions were also done as a part of this study.

Table 5.1: Equilibrium Constants for the modeled Aqueous Species at 25°C for the case where sodium metaborate was used as the alkali

Aqueous Species	Equilibrium Constant
$[B(OH)_4]^-$	5.77E-10
$[B_4O_3(OH)_4]^-$	2.96E-08
$[B_4O_5(OH)_4]^-$	7.35E-17
$Ca[B(OH)_4]^+$	2.58E-08
$Mg[B(OH)_4]^+$	1.45E-08
$CaCO_3$	1.42E+03
$CaHCO_3^+$	2.72E+11
$MgCO_3$	8.47E+02
$MgHCO_3^+$	2.51E+11
HCO_3^-	2.18E+10
HSO_4^-	9.53E+01
$CaSO_4$	2.00E+02
$MgSO_4$	2.34E+02
OH^-	1.00E-14
$MgOH^+$	1.55E-12

Table 5.2: Equilibrium Constants for the modeled Solid Species at the room temperature
for the case where sodium metaborate was used as the alkali

Solid Species	Equilibrium Constant
Calcite ($CaCO_3$)	3.93E-09
Aragonite (CaCO3)	4.61E-09
Anhydrite ($CaSO_4$)	4.35E-05
Gypsum ($CaSO_4.2H_2O$)	2.62E-05
Portlandite ($Ca(OH)_2$)	6.46E-06
Brucite ($Mg(OH)_2$)	1.32E-11
Magnesite ($MgCO_3$)	1.47E-08

Table 5.3: Ionic composition of the Synthetic Injection Brine for the Reservoir 'U'

Ion	Concentration (mg/L)
Na+	18,300
Ca++	650
Mg++	2,110
SO4--	4,290
Cl-	32,200
HCO3-	120
TDS	57,670

Table 5.4: Ionic composition of the Synthetic Formation Brine for the Reservoir 'C'

Ion	Concentration (mg/L)
Na+	6300
Cl-	11606
Mg++	260
Ca++	640

Table 5.5: Equilibrium Constants for the modeled Aqueous Species for the cases where tetrasodium EDTA was used as the chelating agent

Aqueous Species	Equilibrium Constant		
	25^oC	31^oC	100^oC
$H(EDTA)^{3-}$	8.87E+10	7.36E+10	1.32E+10
$H_2(EDTA)^{2-}$	1.66E+17	1.20E+17	5.97E+15
$H_3(EDTA)^-$	2.19E+20	1.65E+20	1.22E+19
$H_4(EDTA)$	3.16E+22	2.41E+22	1.95E+21
$H_5(EDTA)^+$	1.00E+24	7.74E+23	7.32E+22
$Ca(EDTA)^{2-}$	2.63E+12	2.15E+12	3.31E+11
$Mg(EDTA)^{2-}$	9.33E+14	1.04E+15	2.86E+15
HCO_3^-	2.13E+10	1.90E+10	6.52E+09
H_2CO_3	4.80E+16	3.97E+16	6.98E+15
$CaCO_3$	1.58E+03	1.80E+03	5.81E+03
$CaHCO_3^+$	3.97E+11	4.15E+11	6.16E+11
$MgCO_3$	8.32E+02	9.15E+02	2.20E+03
$MgHCO_3^+$	3.97E+11	4.35E+11	9.97E+11
HSO_4^-	9.77E+01	1.16E+02	5.83E+02
$CaSO_4$	2.29E+02	2.42E+02	4.08E+02
$MgSO_4$	1.82E+02	1.91E+02	2.91E+02
OH^-	1.01E-14	1.57E-14	9.33E-13
$CaOH^+$	2.01E-13	3.35E-13	3.65E-11
$MgOH^+$	4.01E-12	6.88E-12	9.84E-10

Table 5.6: Equilibrium Constants for the modeled Solid Species for the cases where tetrasodium EDTA was used as the chelating agent

Solid Species	Equilibrium Constant		
	25^oC	31^oC	100^oC
Calcite ($CaCO_3$)	3.31E-09	3.11E-09	1.73E-09
Aragonite (CaCO3)	5.01E-09	4.55E-09	1.89E-09
Anhydrite ($CaSO_4$)	4.37E-05	4.12E-05	2.43E-05
Gypsum ($CaSO_4.2H_2O$)	2.45E-05	2.47E-05	2.66E-05
Portlandite ($Ca(OH)_2$)	6.46E-06	2.32E-06	1.89E-10
Brucite ($Mg(OH)_2$)	7.08E-12	2.86E-12	6.79E-16
Magnesite ($MgCO_3$)	3.47E-08	4.07E-08	1.76E-07
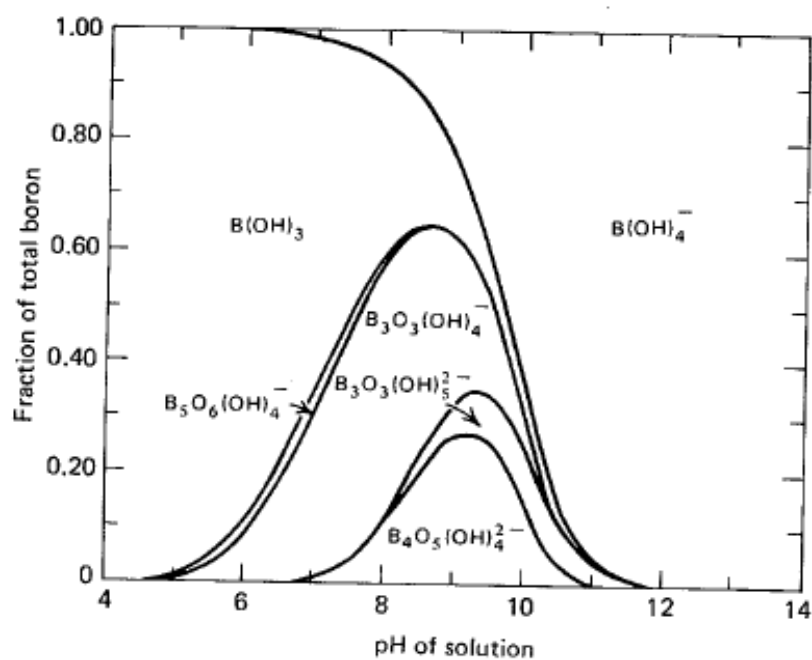
Figure 5.1: Speciation of the borate ion at different solution pH (Ingri, 1963)
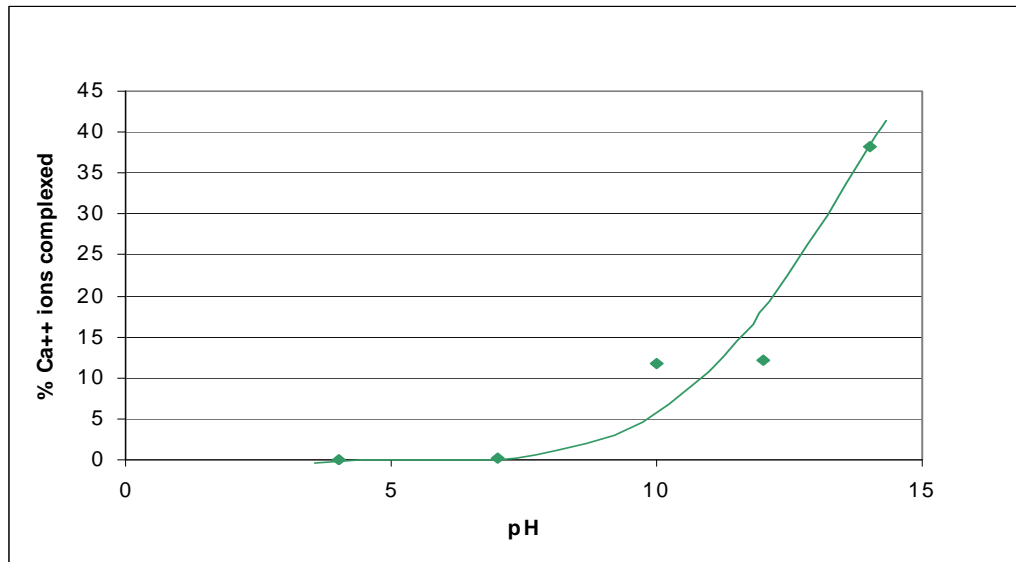
Figure 5.2: Effect of the solution pH on the calcium ion complexation with sodium metaborate
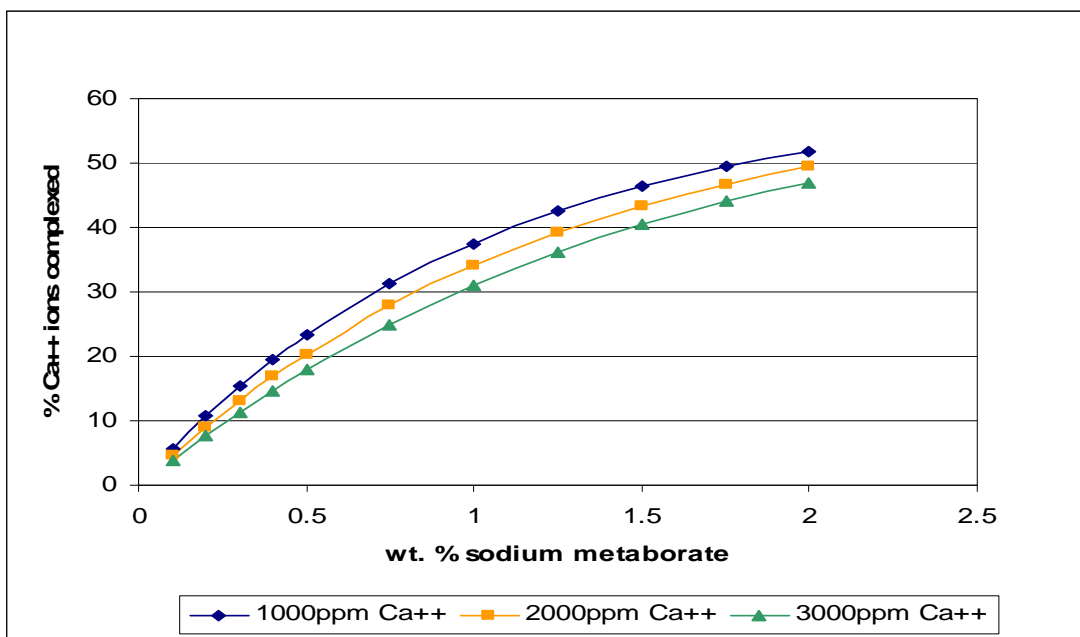
Figure 5.3: Effect of the sodium metaborate concentration on the complexation of the calcium ion (at different calcium ion concentrations)
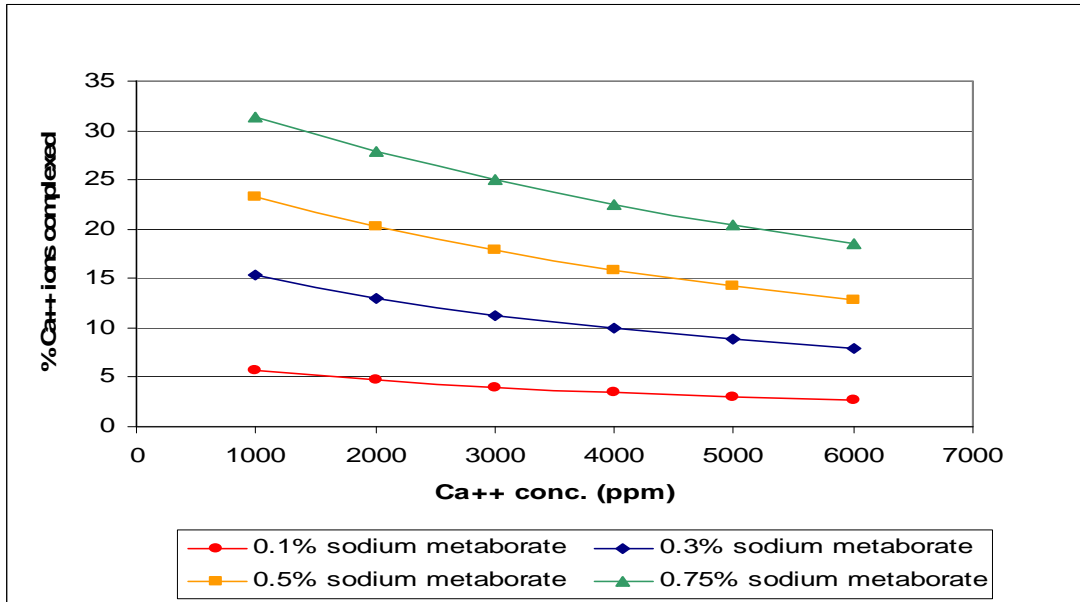
Figure 5.4: Effect of the calcium ion concentration on the complexation of the calcium ion (at different sodium metaborate concentrations)
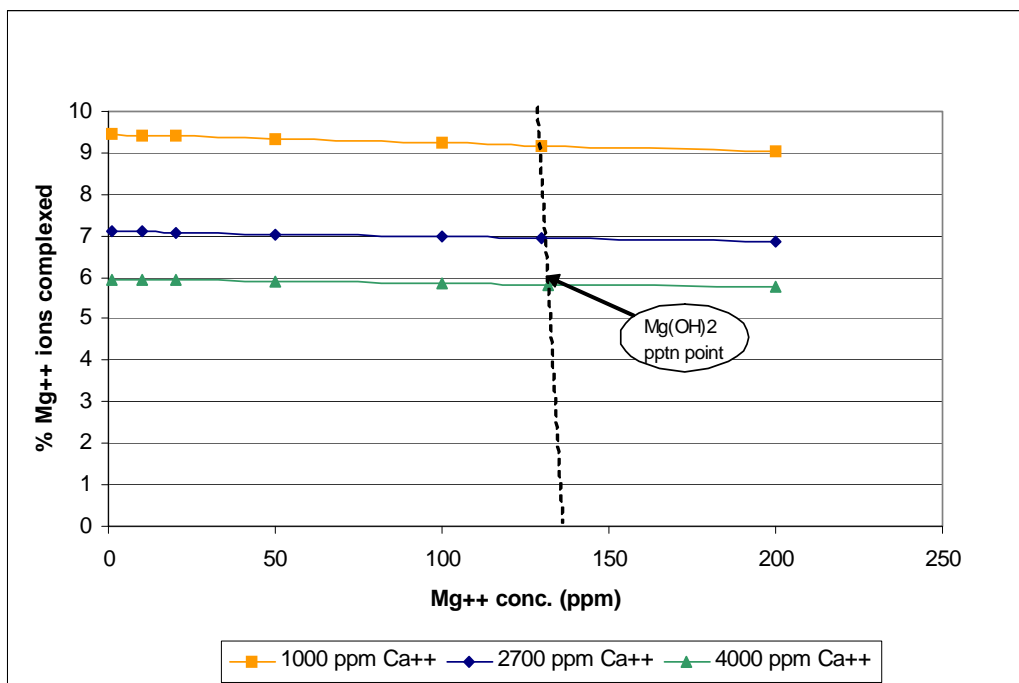
Figure 5.5: Effect of the magnesium ion concentration on the complexation of the magnesium ion (at different calcium ion concentrations)
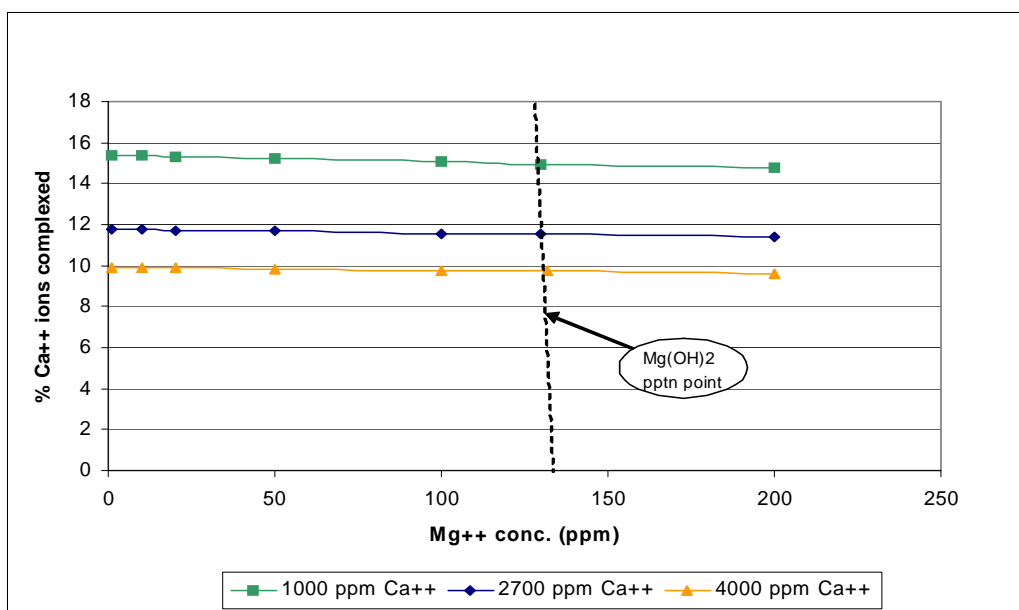
Figure 5.6: Effect of the magnesium ion concentration on the complexation of the calcium ion (at different calcium ion concentrations)

175
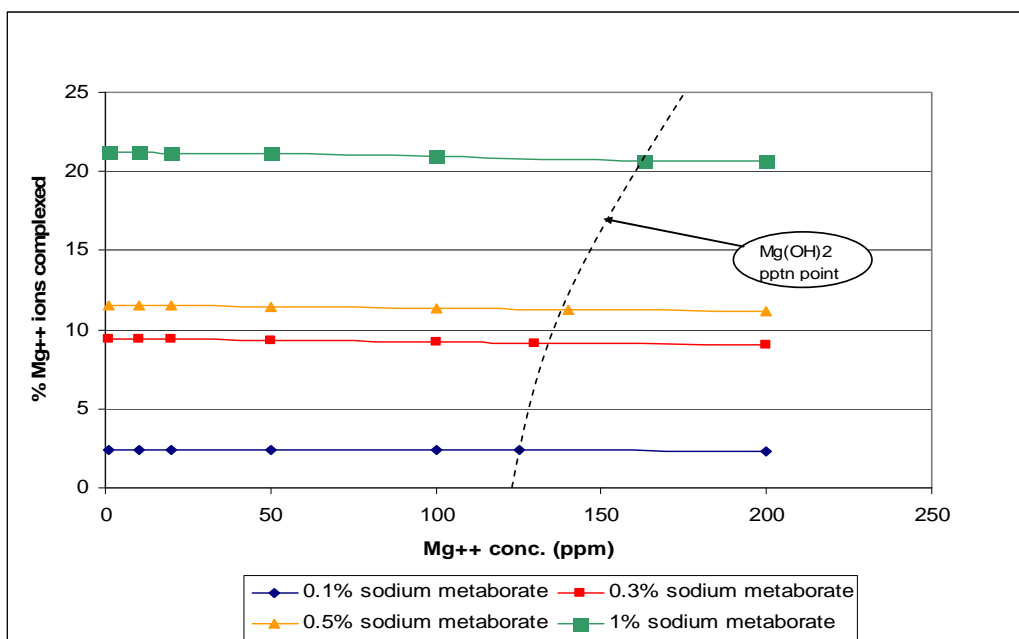
Figure 5.7: Effect of the magnesium ion concentration on the complexation of the magnesium ion (at different sodium metaborate concentrations)
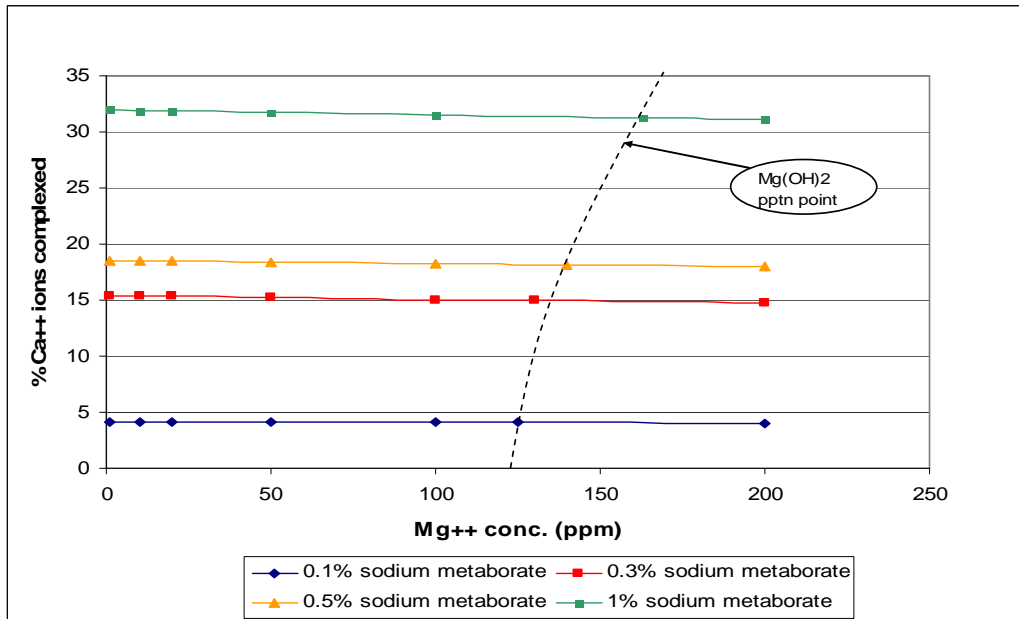
Figure 5.8: Effect of the magnesium ion concentration on the complexation of the calcium ion (at different sodium metaborate concentrations)

176
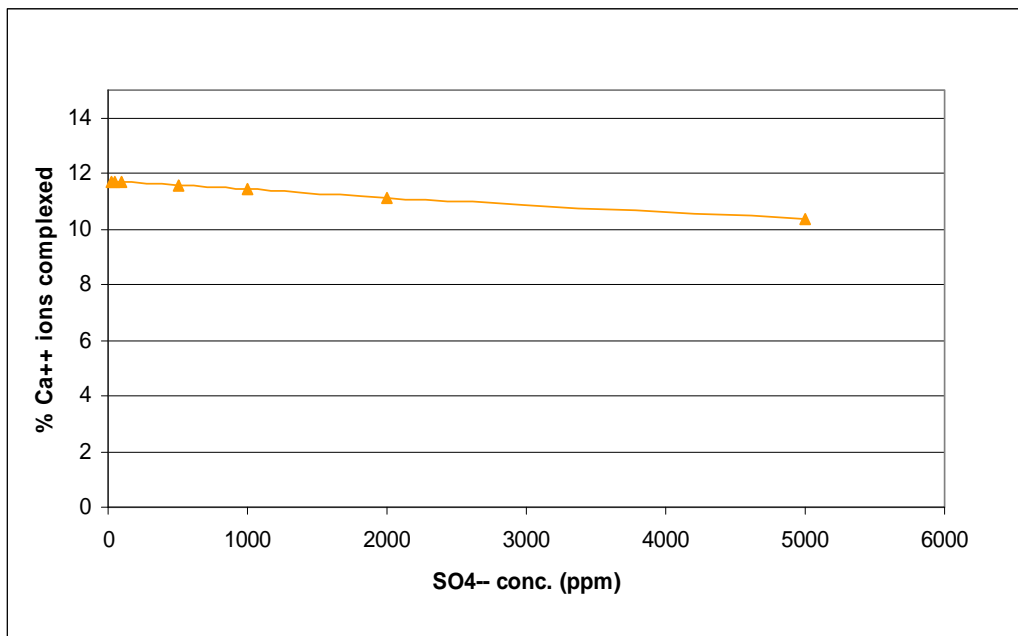
Figure 5.9: Effect of the sulfate ion on the complexation of the calcium ion
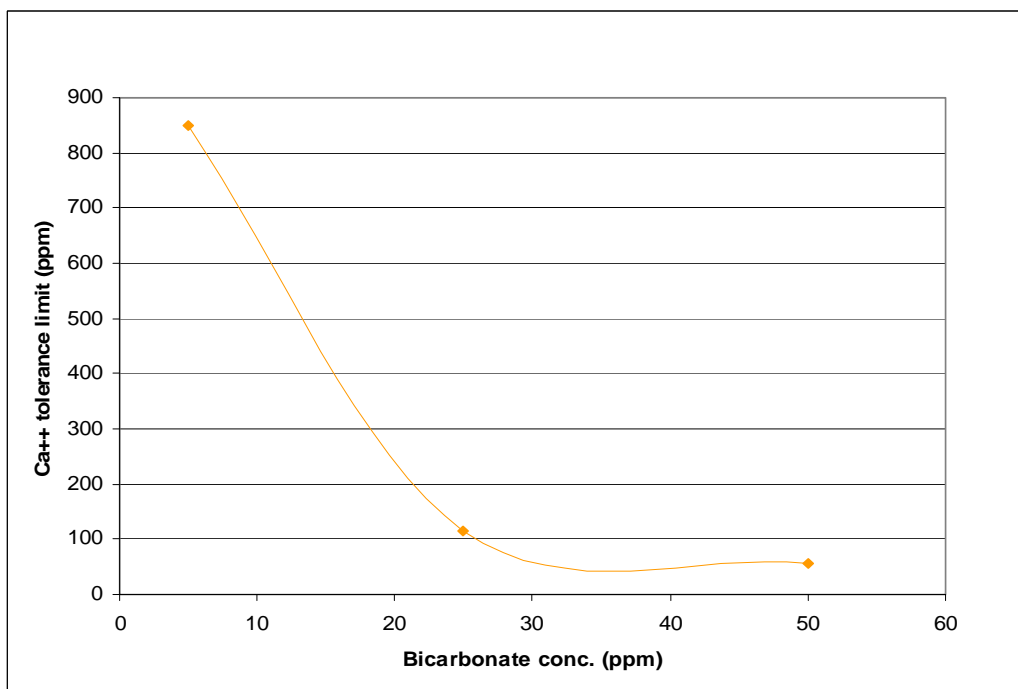
Figure 5.10: Effect of the bicarbonate ion on the calcium ion tolerance limit

177
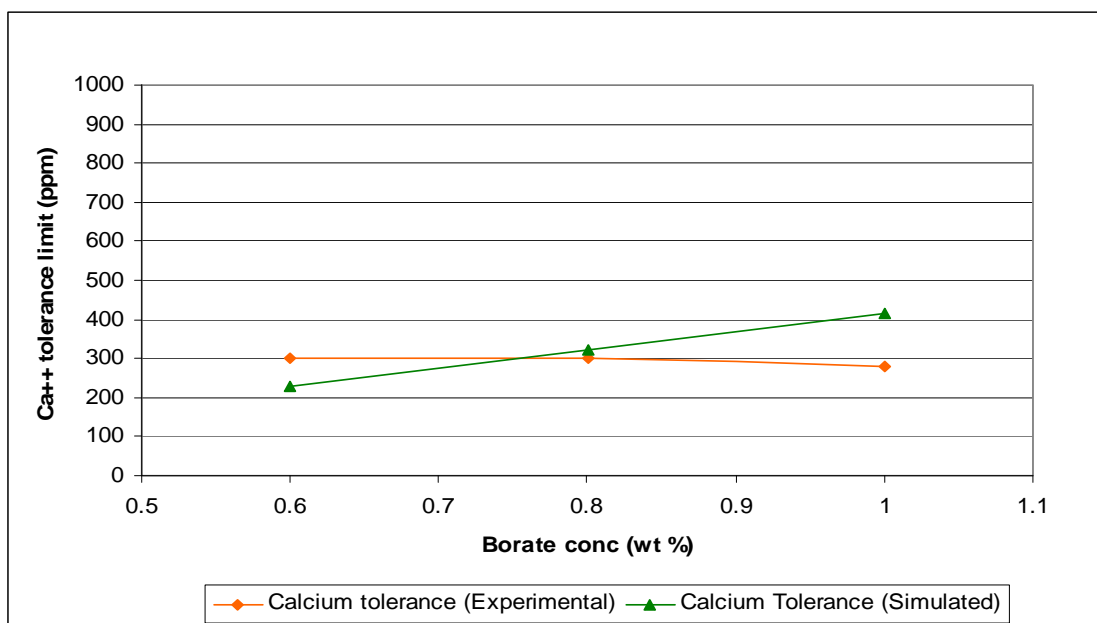
Figure 5.11: Calcium ion tolerance in the presence of sodium metaborate at the room temperature
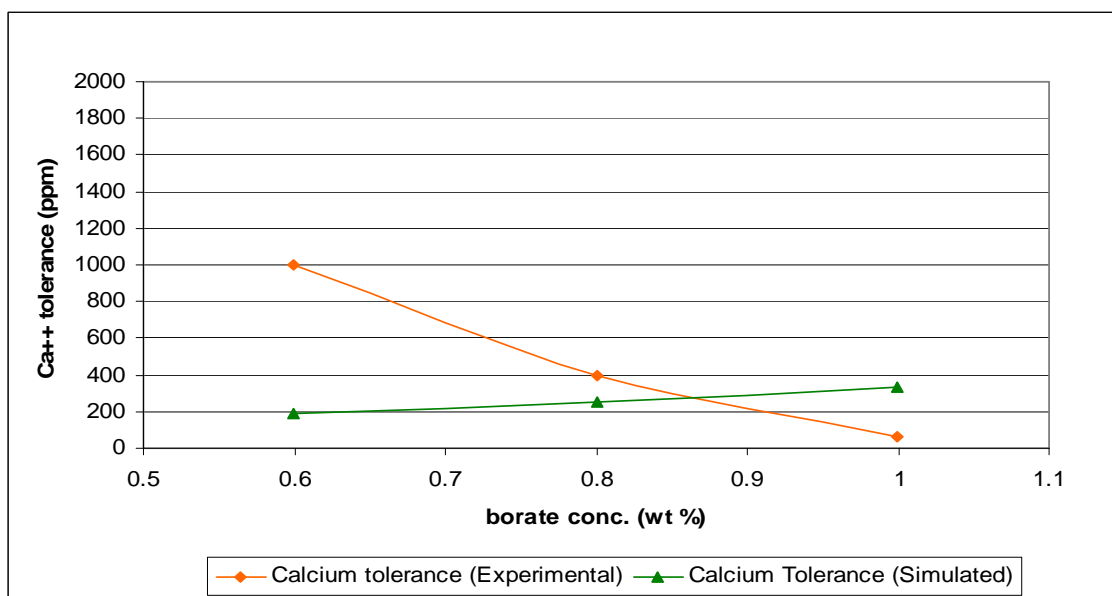
Figure 5.12: Calcium ion tolerance in the presence of sodium metaborate at a temperature of 50°C

178
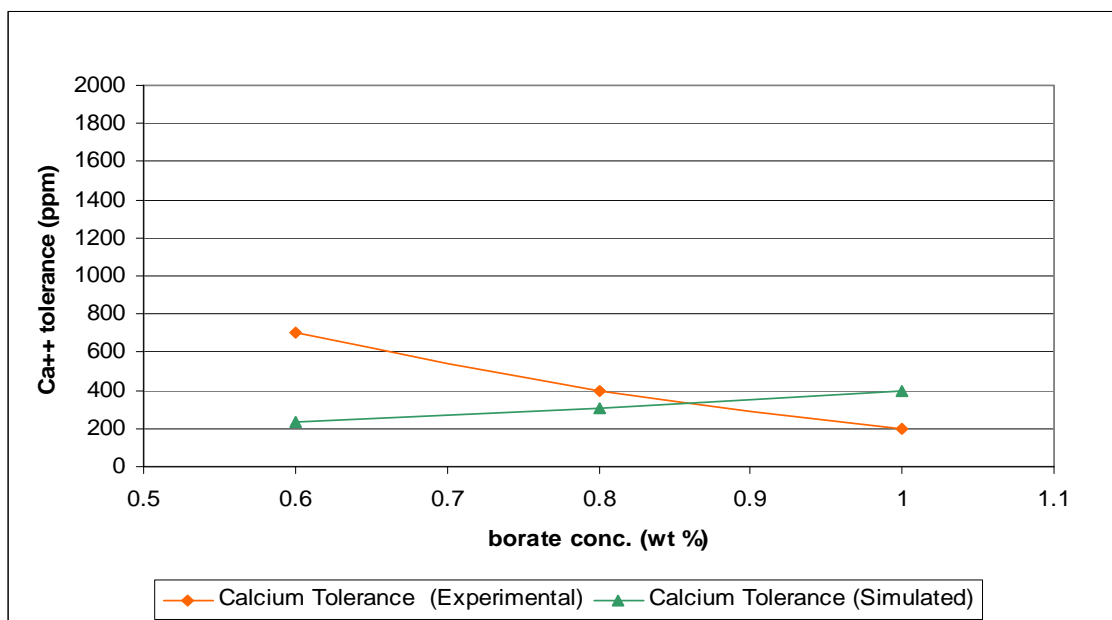
Figure 5.13: Calcium ion tolerance in the presence of sodium metaborate at a temperature of 80°C
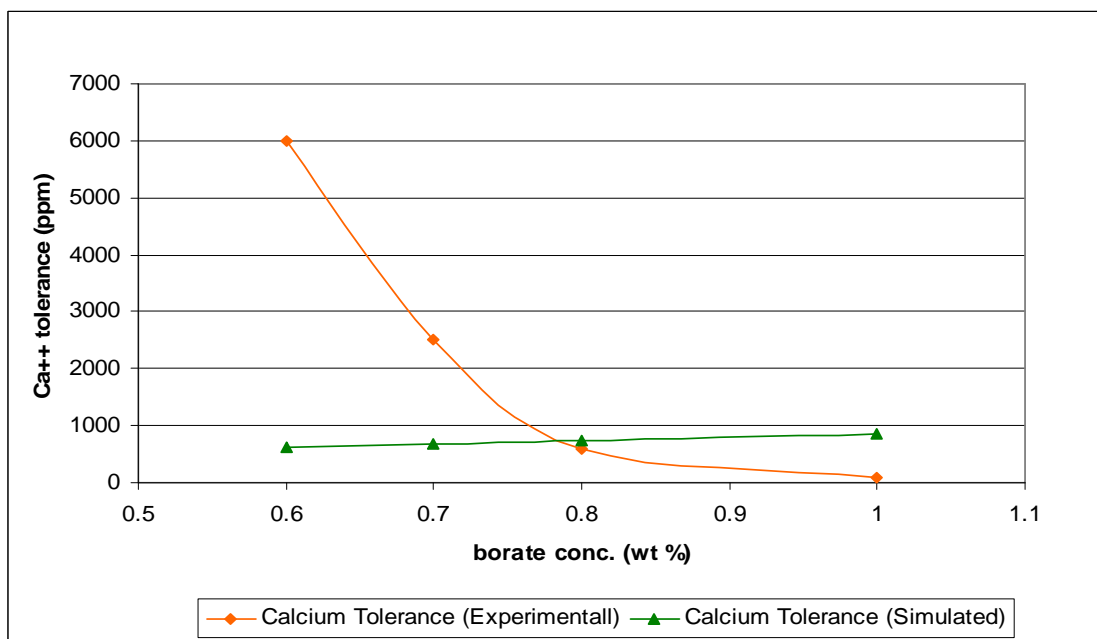
Figure 5.14: Effect of the sodium metaborate concentration on the calcium ion tolerance in the presence of 3% sodium chloride

179
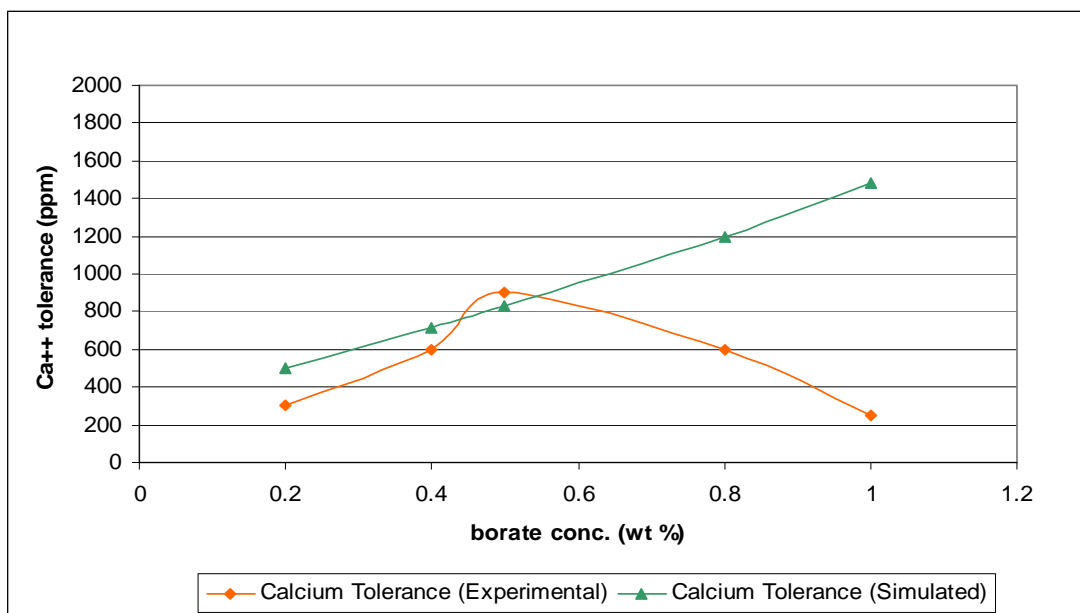
Figure 5.15: Effect of sodium metaborate concentration on the calcium ion tolerance in the presence of 0.4% sodium hydroxide
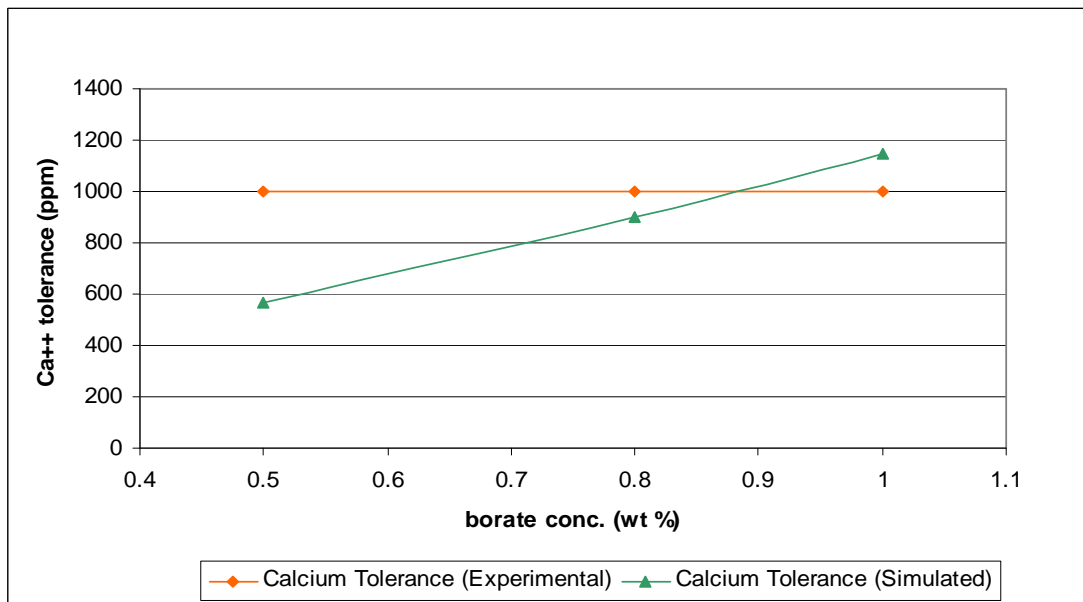
Figure 5.16: Effect of sodium metaborate concentration on the calcium ion tolerance in the presence of 0.1% sodium sulfate
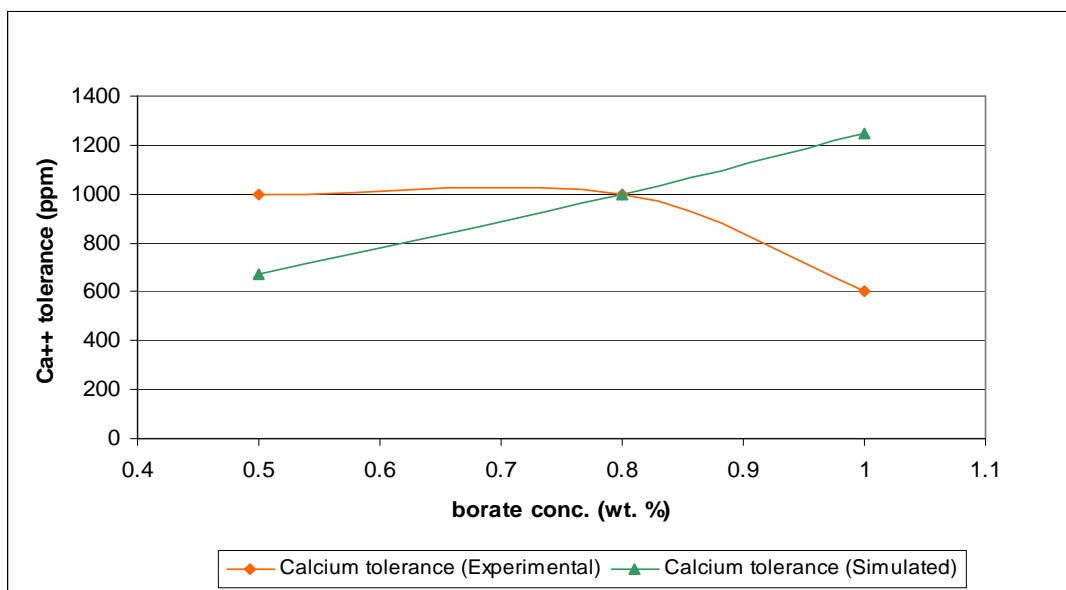
Figure 5.17: Effect of sodium metaborate concentration on the calcium ion tolerance in the presence of 0.2% sodium sulfate
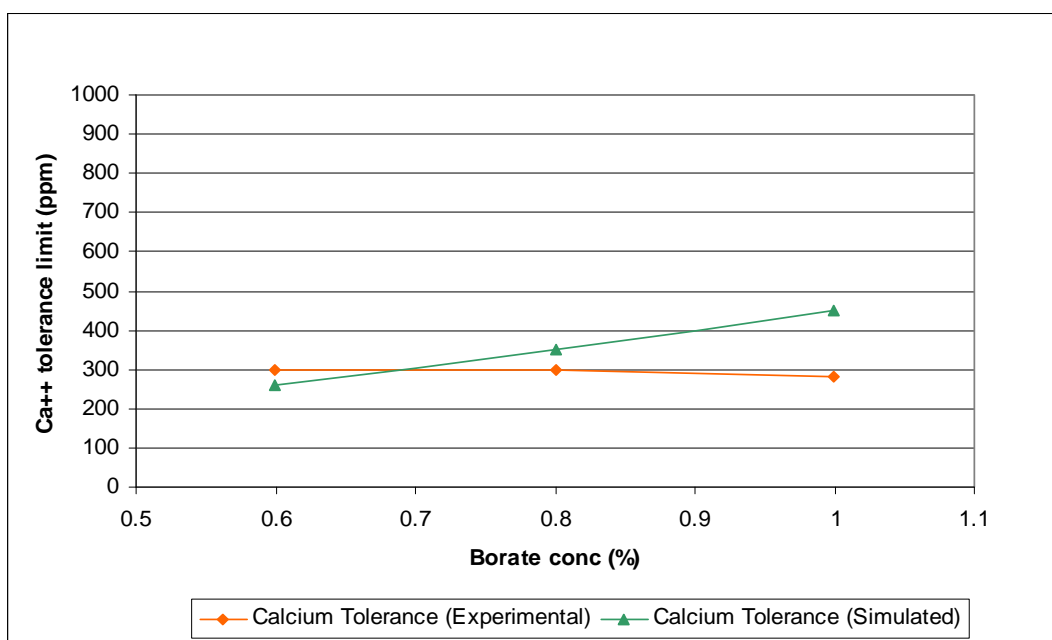
Figure 5.18: Calcium ion tolerance in the presence of sodium metaborate at the room temperature

181
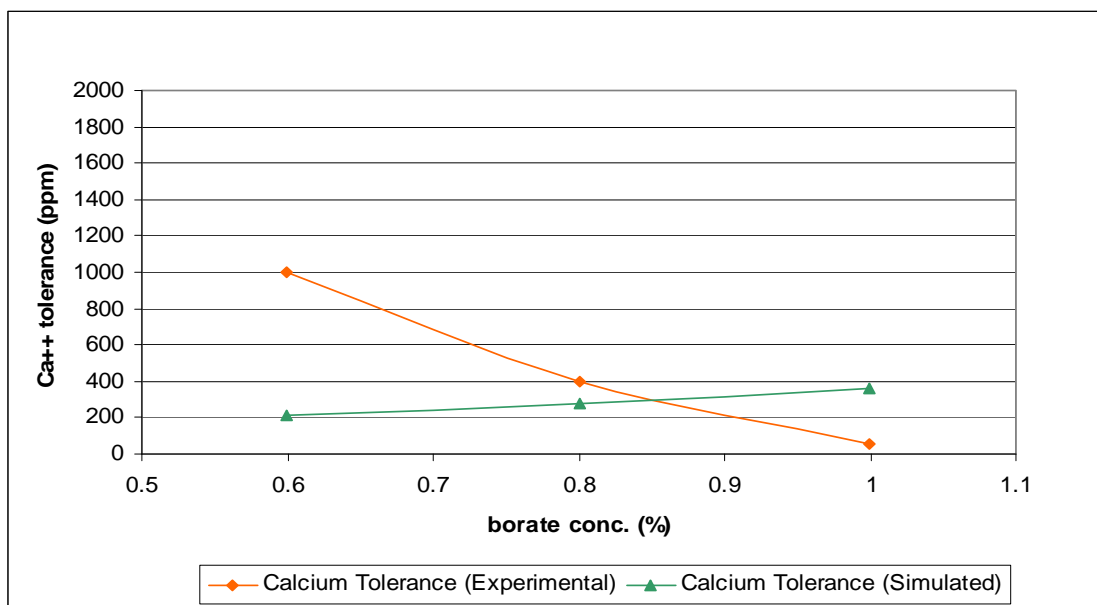
Figure 5.19: Calcium ion tolerance in the presence of sodium metaborate at a temperature of 50°C
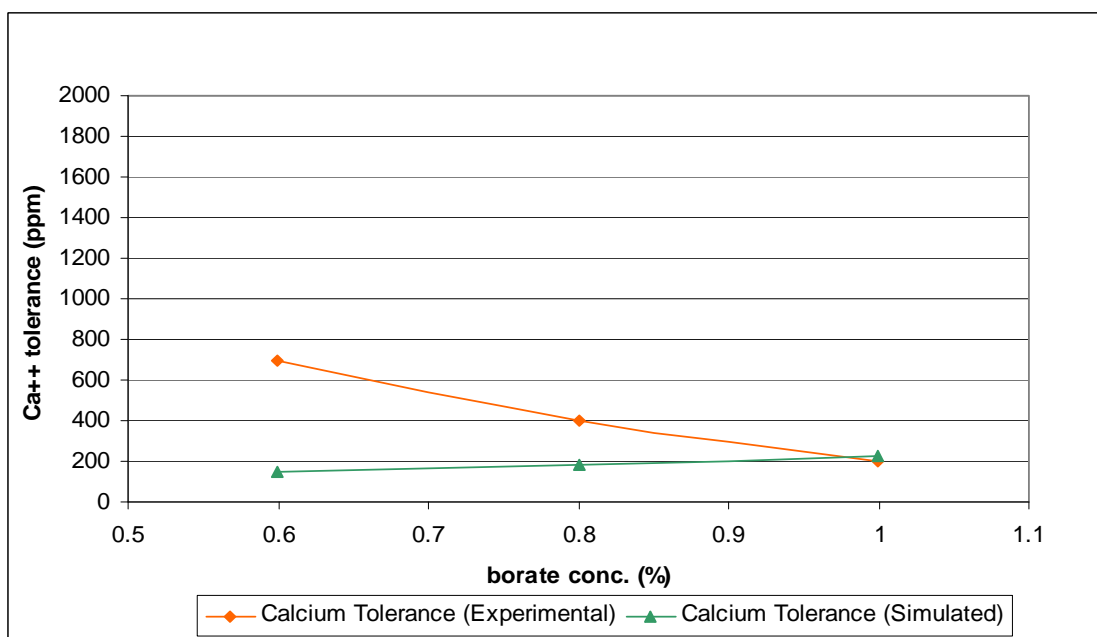
Figure 5.20: Calcium ion tolerance in the presence of sodium metaborate at a temperature of 80°C
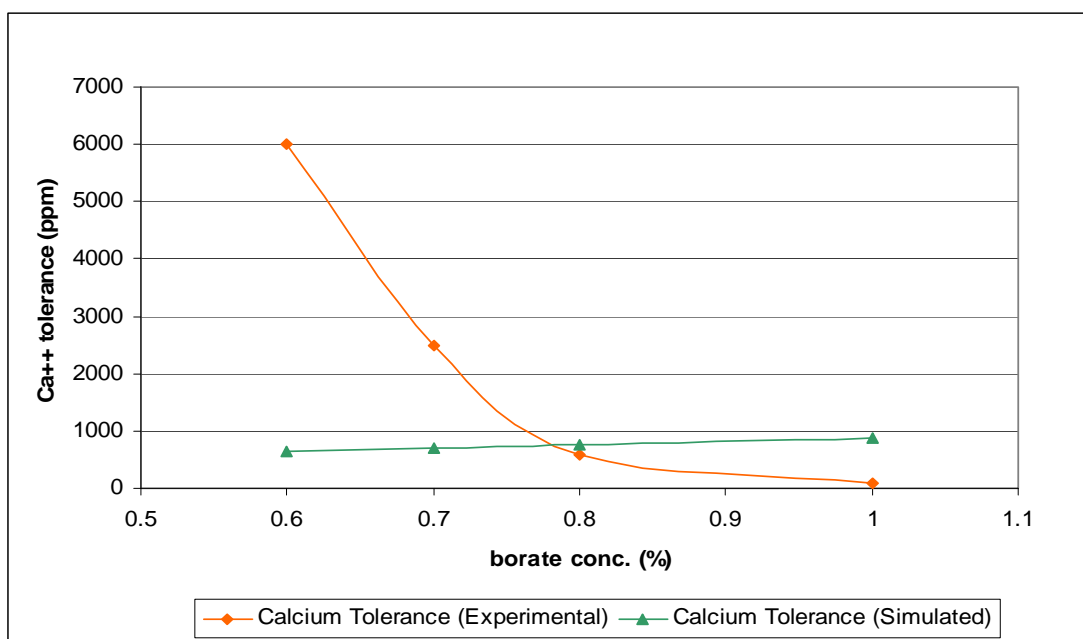
Figure 5.21: Effect of the sodium metaborate concentration on the calcium ion tolerance
in the presence of 3% sodium chloride
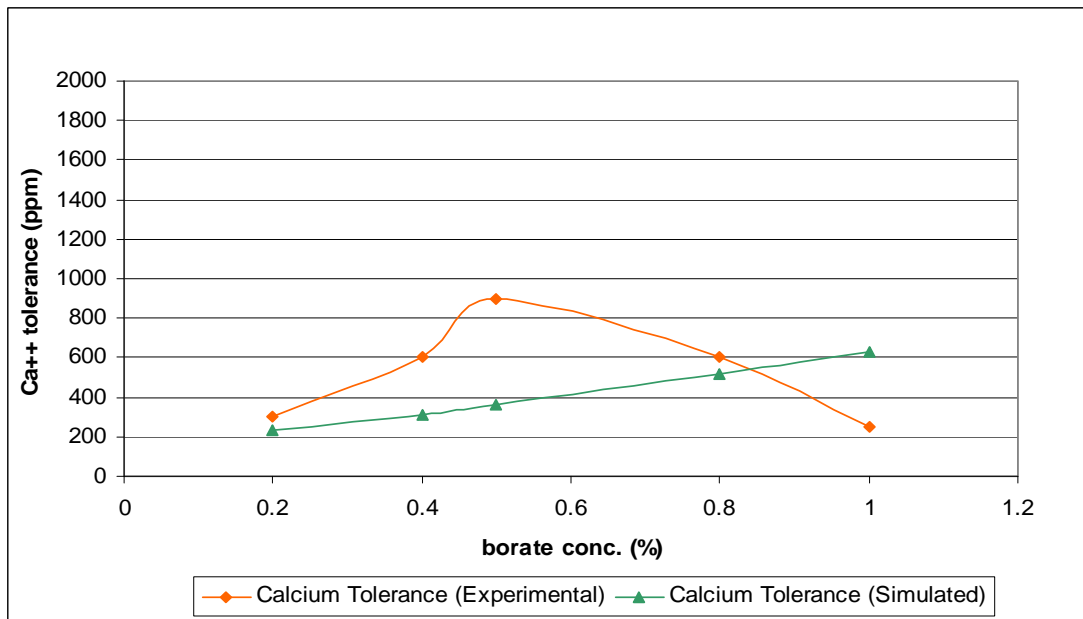
Figure 5.22: Effect of sodium metaborate concentration on the calcium ion tolerance in
the presence of 0.4% sodium hydroxide
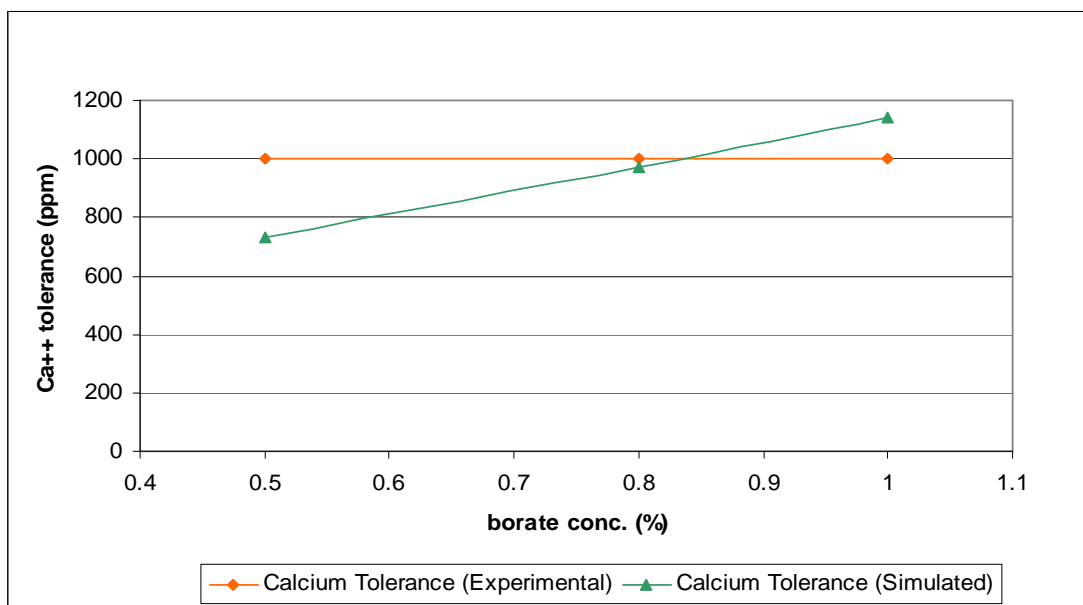
Figure 5.23: Effect of sodium metaborate concentration on the calcium ion tolerance in the presence of 0.1% sodium sulfate
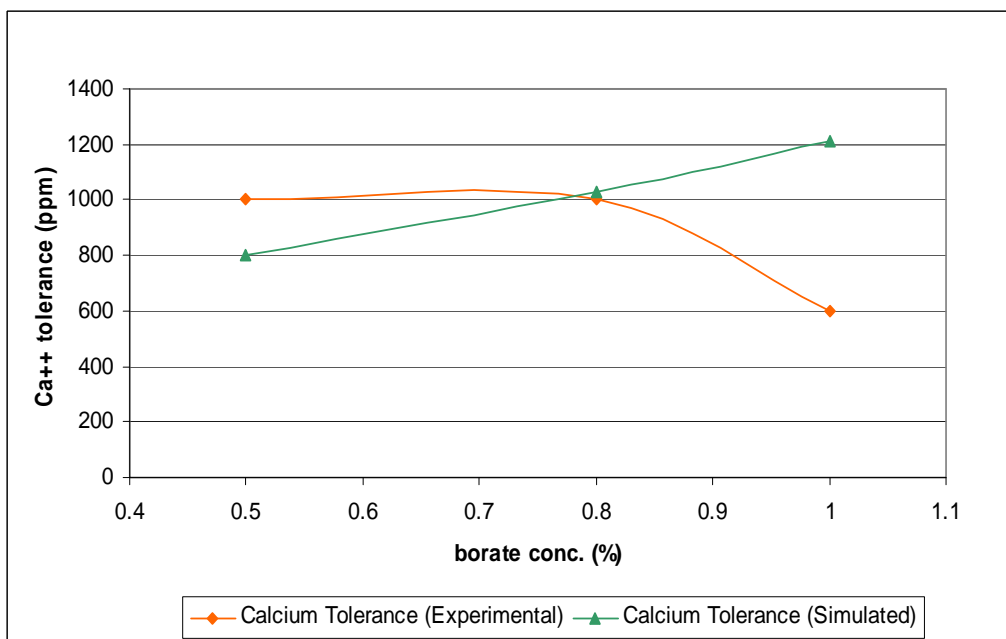
Figure 5.24: Effect of sodium metaborate concentration on the calcium ion tolerance in the presence of 0.2% sodium sulfate
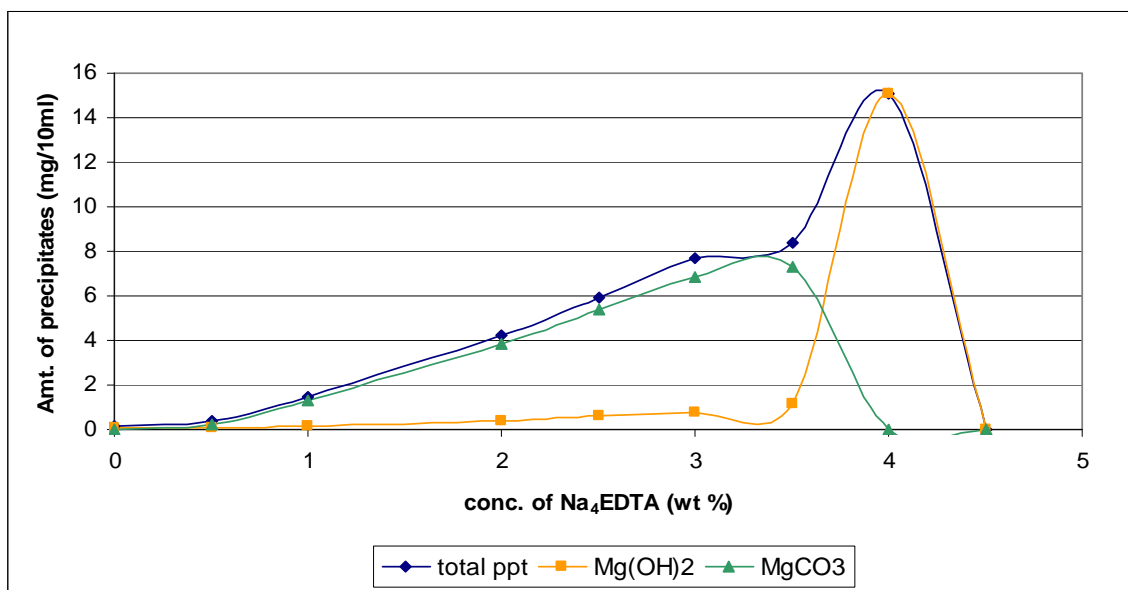
Figure 5.25: Precipitation of Magnesium Hydroxide and Magnesium Carbonate in the presence of varying concentrations of Na₄EDTA for the Reservoir 'U' at the room temperature
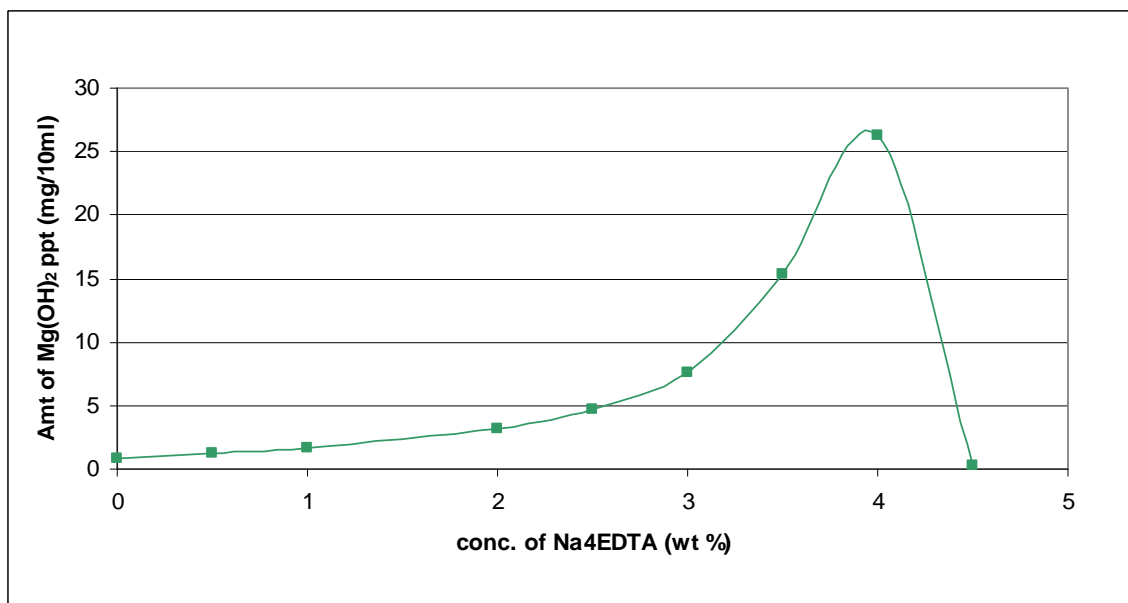
Figure 5.26: Precipitation of magnesium hydroxide in the presence of varying concentrations of Na₄EDTA for the Reservoir 'U' at the reservoir temperature (100°C)
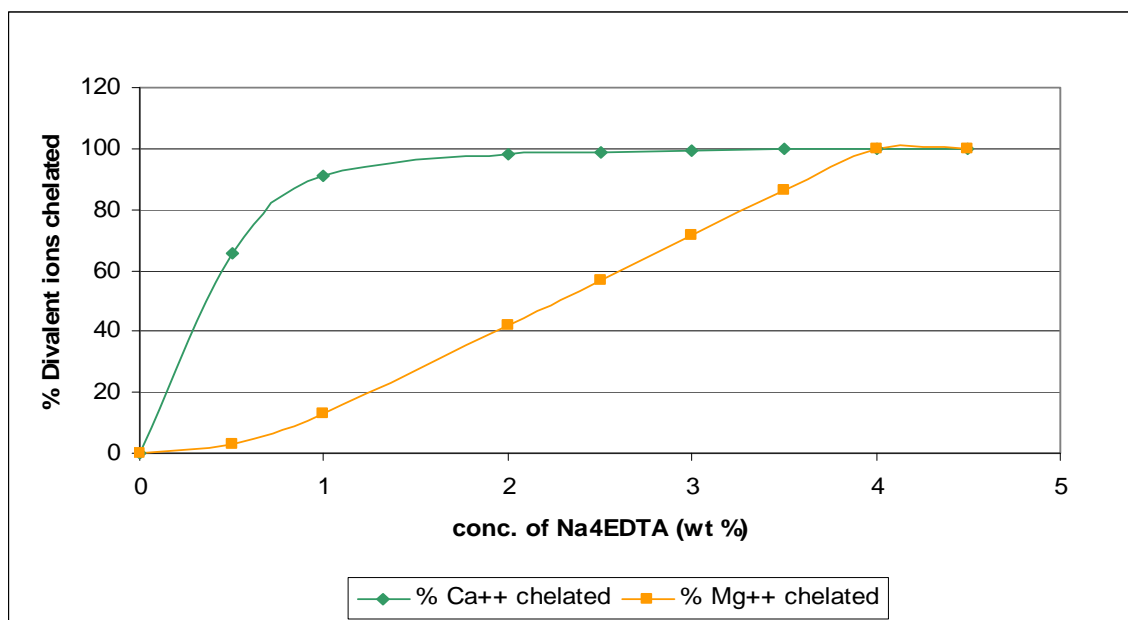
Figure 5.27: Chelation of calcium and magnesium ions in the presence of varying
concentrations of Na_4EDTA for the Reservoir 'U' at the room temperature
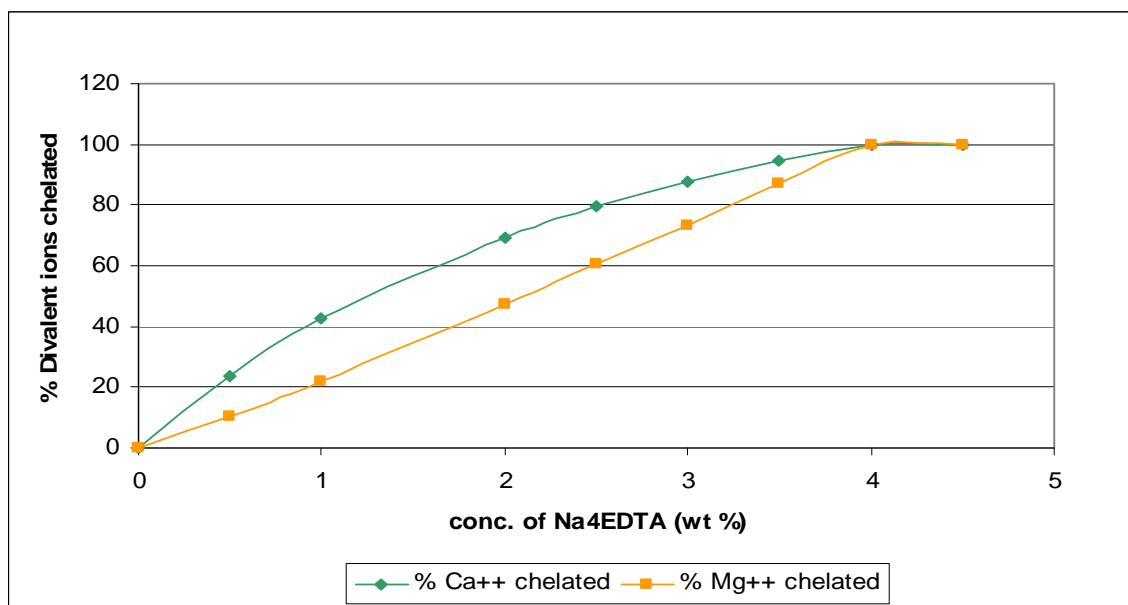
Figure 5.28: Simulated chelation of calcium and magnesium ions in the presence of
varying concentrations of Na_4EDTA for the Reservoir 'U' at the reservoir
temperature (100°C)

186
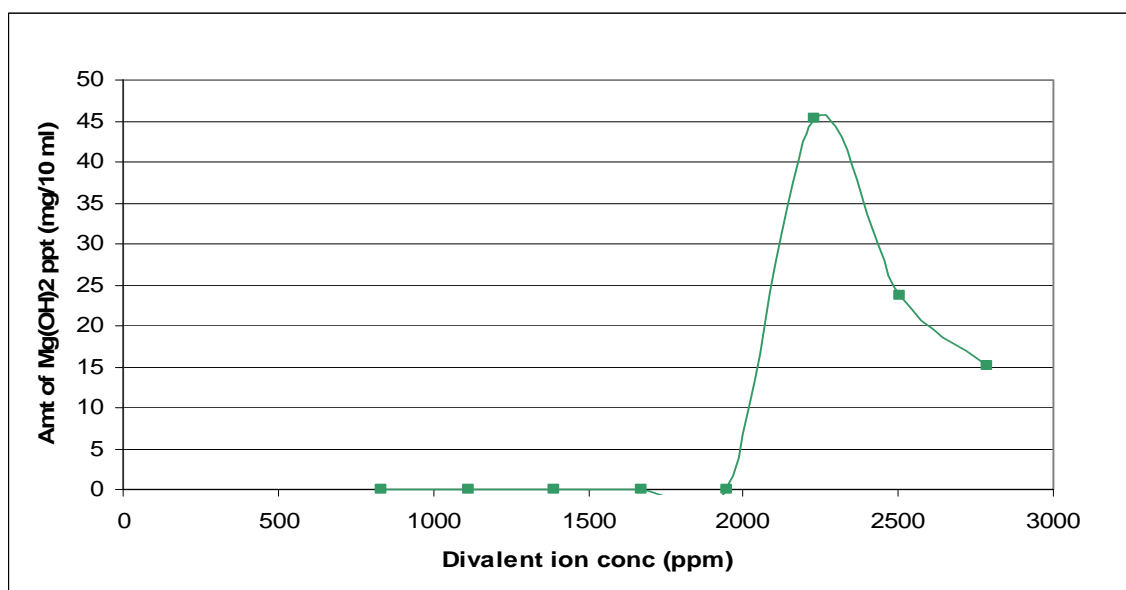
Figure 5.29: Precipitation of magnesium hydroxide in the presence of 3% Na4EDTA in the presence of varying concentrations of the divalent ion (Ca++ and Mg++) for the Reservoir 'U' at the room temperature
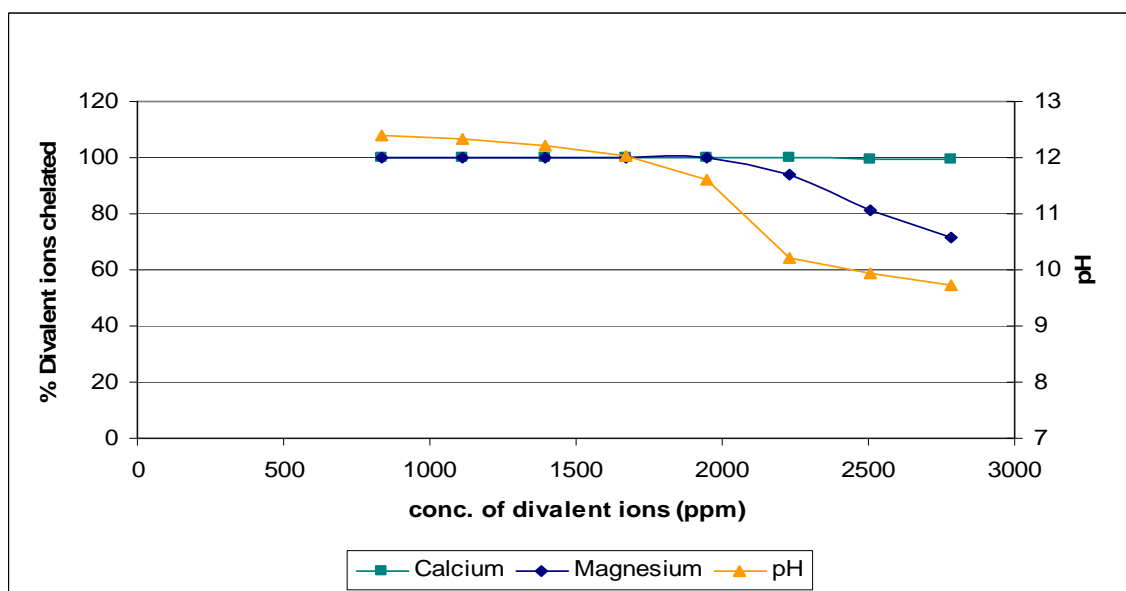
Figure 5.30: Chelation of calcium and magnesium ions in the presence of 3% Na4EDTA in the presence of varying concentrations of the divalent ion (Ca++ and Mg++) for the Reservoir 'U' at the room temperature
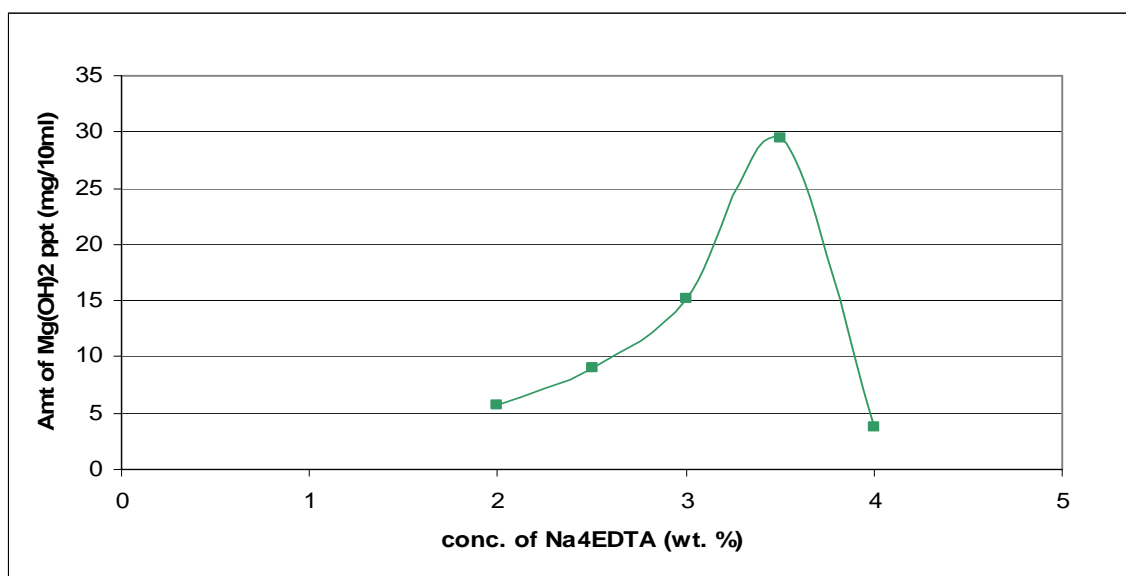
Figure 5.31: Precipitation of magnesium hydroxide in the presence of varying
concentrations of Na4EDTA for the Reservoir 'U' at room temperature (with
the solution pH lowered to 10.5)
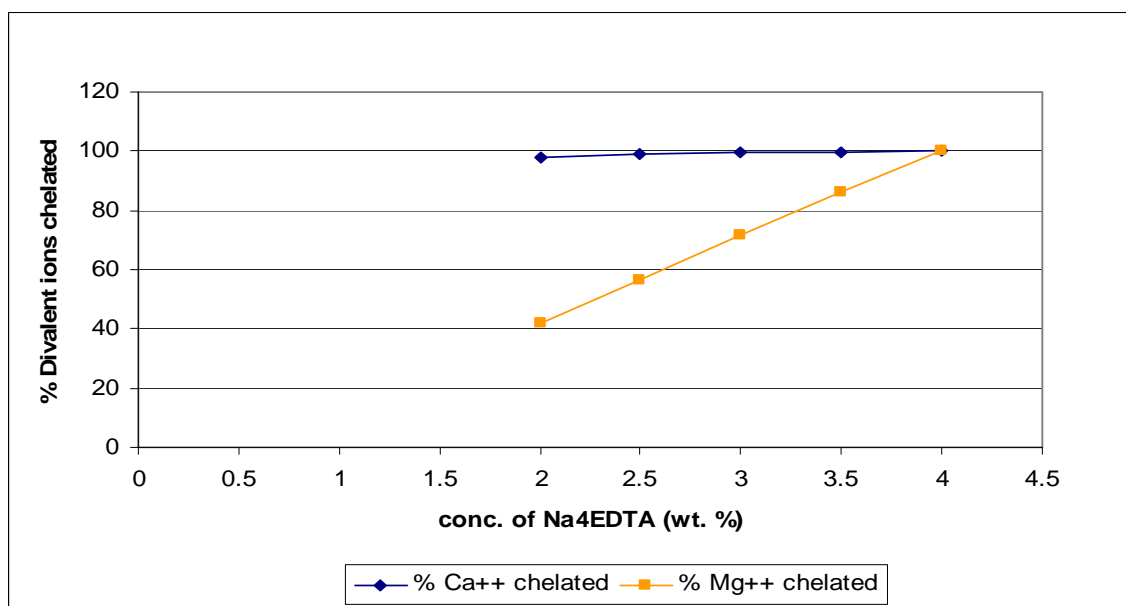
Figure 5.32: Chelation of calcium and magnesium ions in the presence of varying
concentrations of Na4EDTA for the Reservoir 'U' at room temperature (with
the solution pH lowered to 10.5)
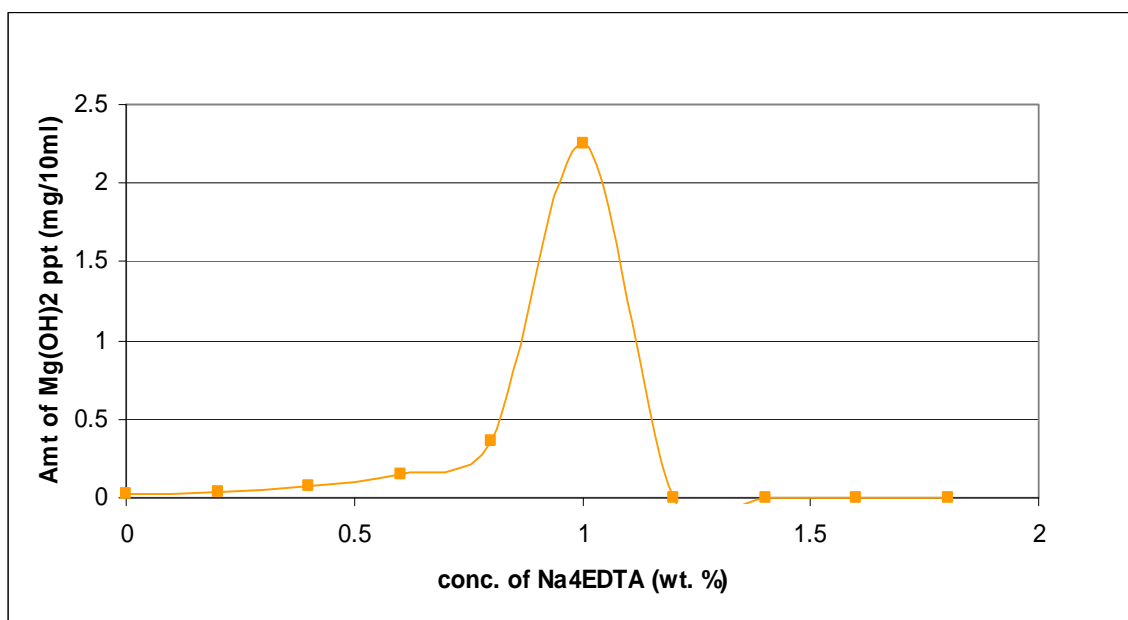
Figure 5.33: Precipitation of magnesium hydroxide in the presence of varying
concentrations of Na4EDTA for the Reservoir 'C' at room temperature
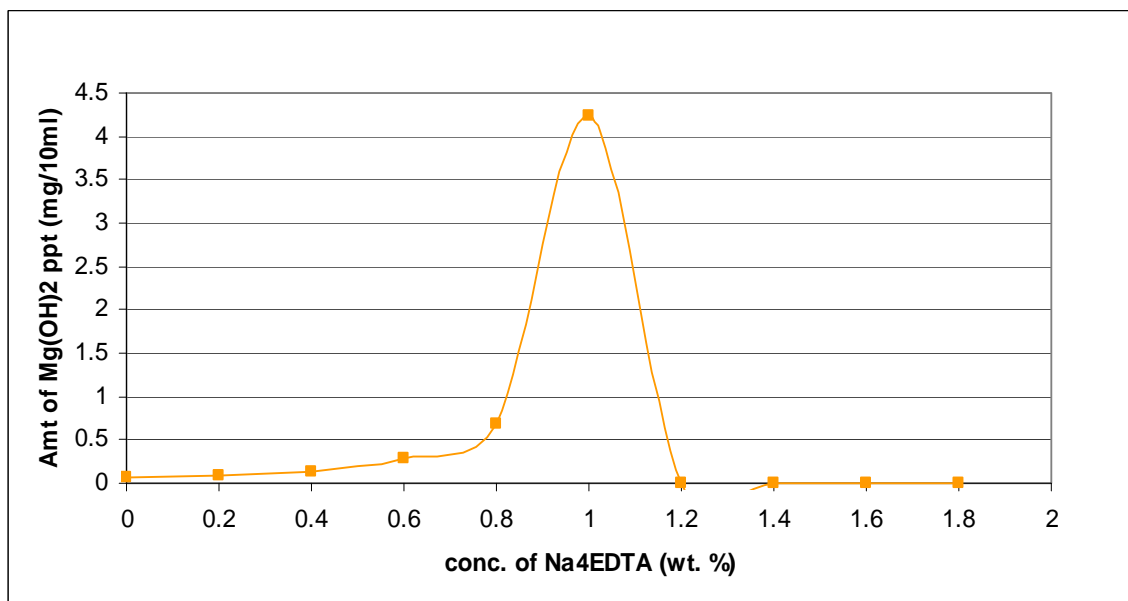
Figure 5.34: Precipitation of magnesium hydroxide in the presence of varying
concentrations of Na4EDTA for the Reservoir 'C' at the reservoir
temperature (87°F)

189
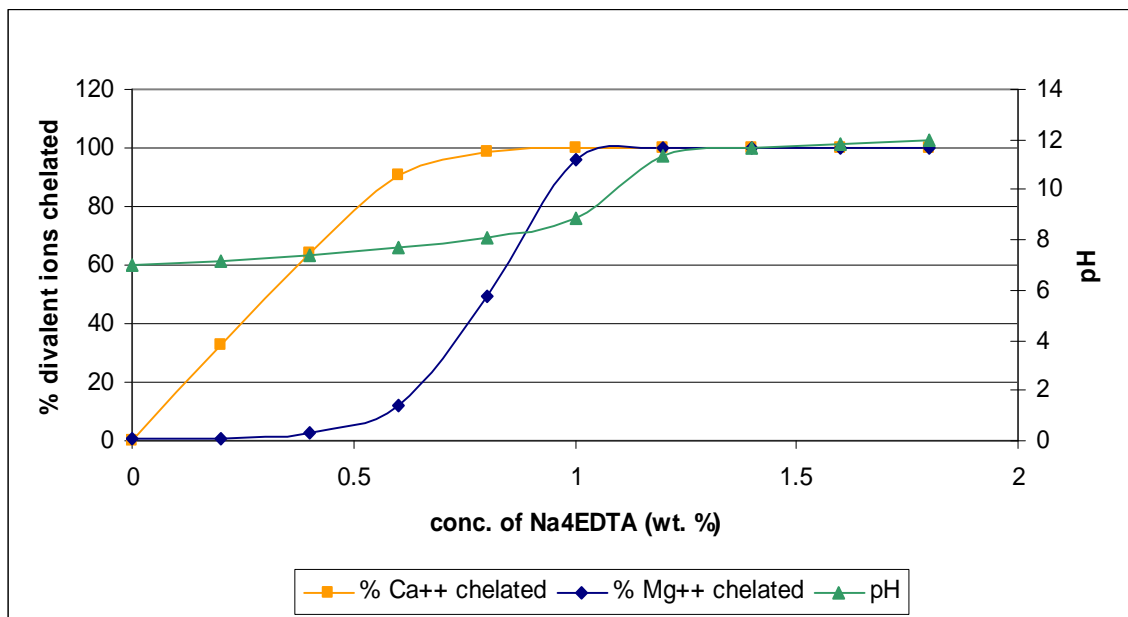
Figure 5.35: Chelation of calcium and magnesium ions in the presence of varying concentrations of Na4EDTA for the Reservoir 'C' at room temperature
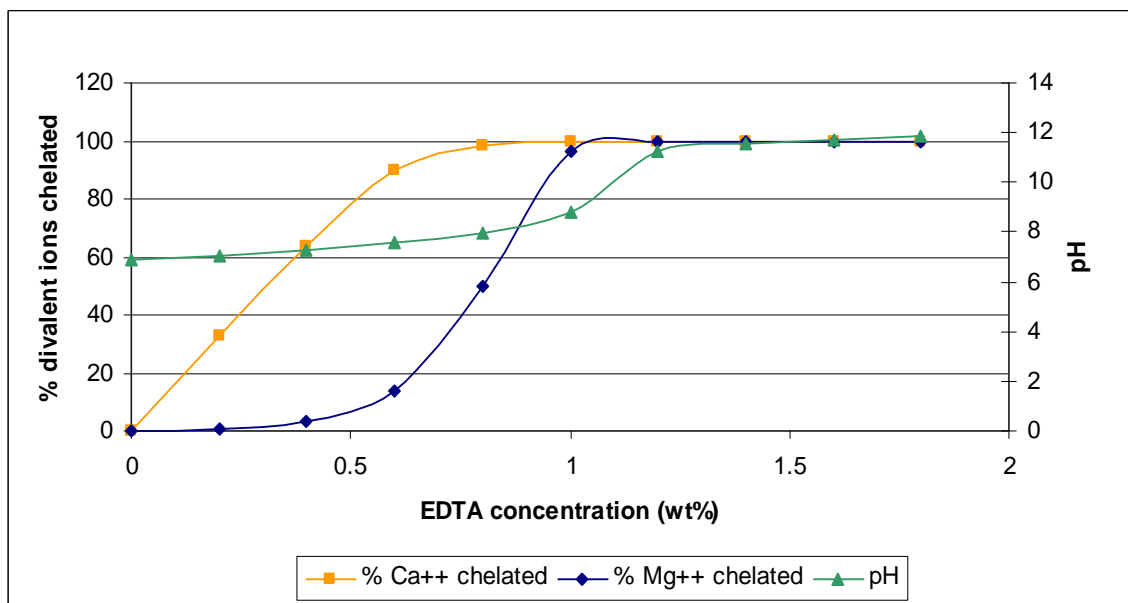
Figure 5.36: Chelation of calcium and magnesium ions in the presence of varying concentrations of Na4EDTA for the Reservoir 'C' at the reservoir temperature (87°F)
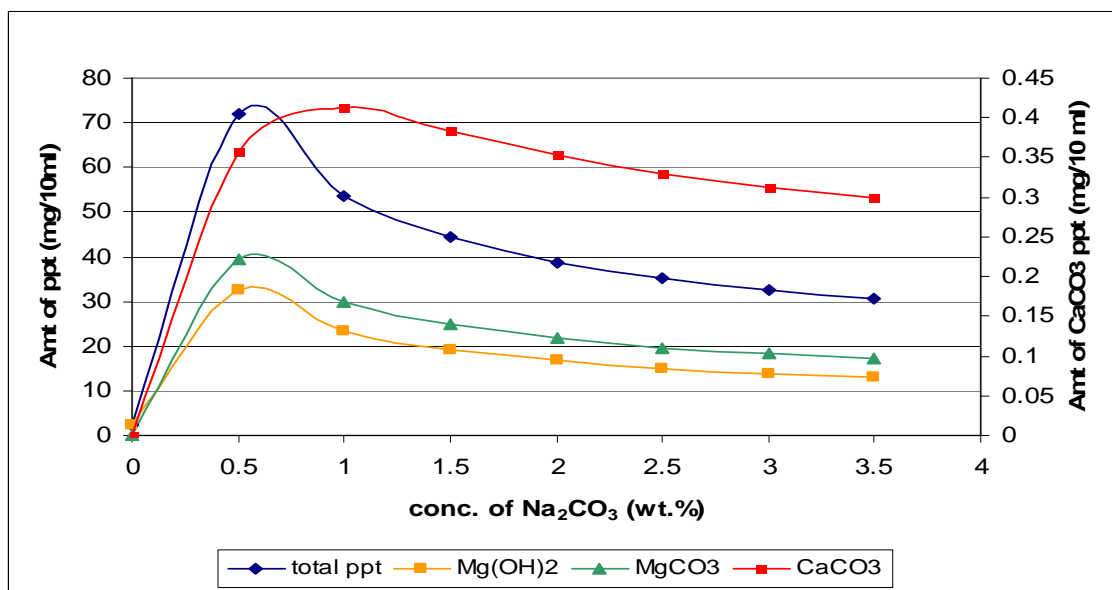
Figure 5.37: Precipitation of different chemical species in the presence of 1% Na4EDTA along with varying concentrations of sodium carbonate for the Reservoir 'C' at the room temperature
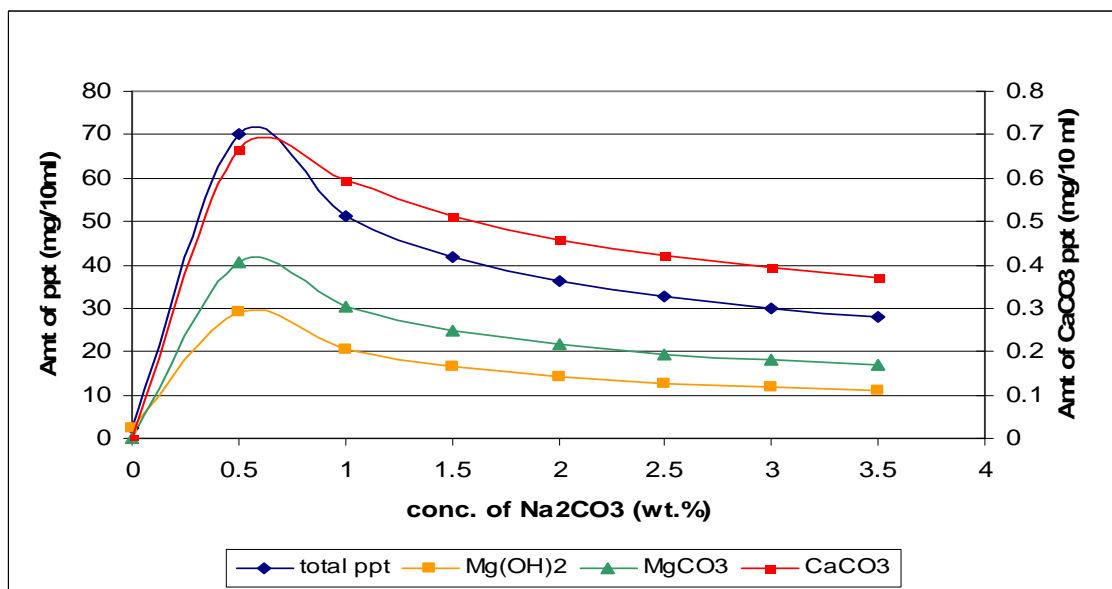
Figure 5.38: Precipitation of different chemical species in the presence of 1% Na4EDTA along with varying concentrations of sodium carbonate for the Reservoir 'C' at the reservoir temperature (87°F)

191
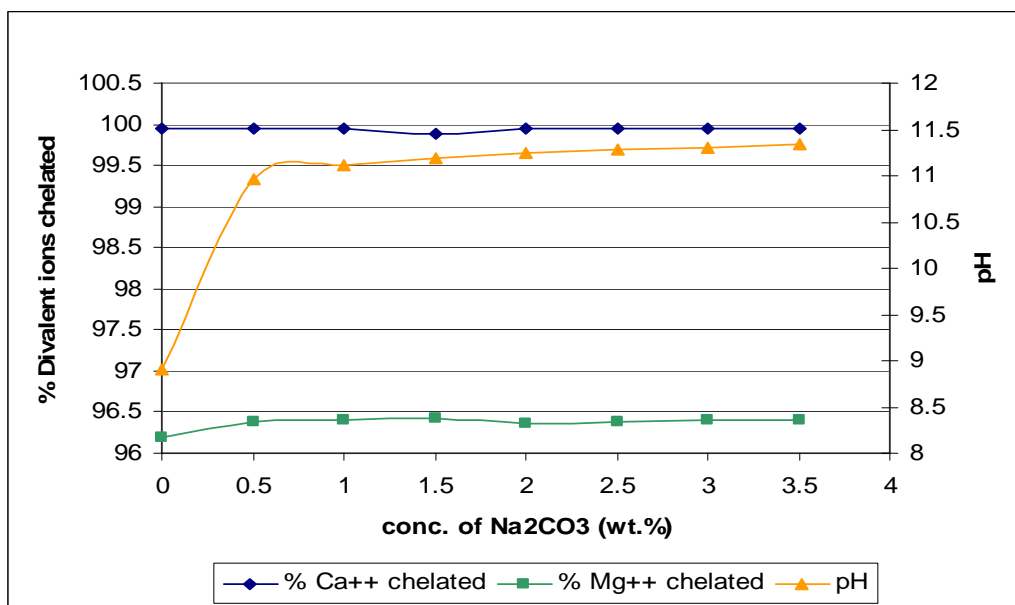
Figure 5.39: Chelation of calcium and magnesium ions in the presence of 1% Na4EDTA
along with varying concentrations of sodium carbonate for the Reservoir 'C'
at the room temperature
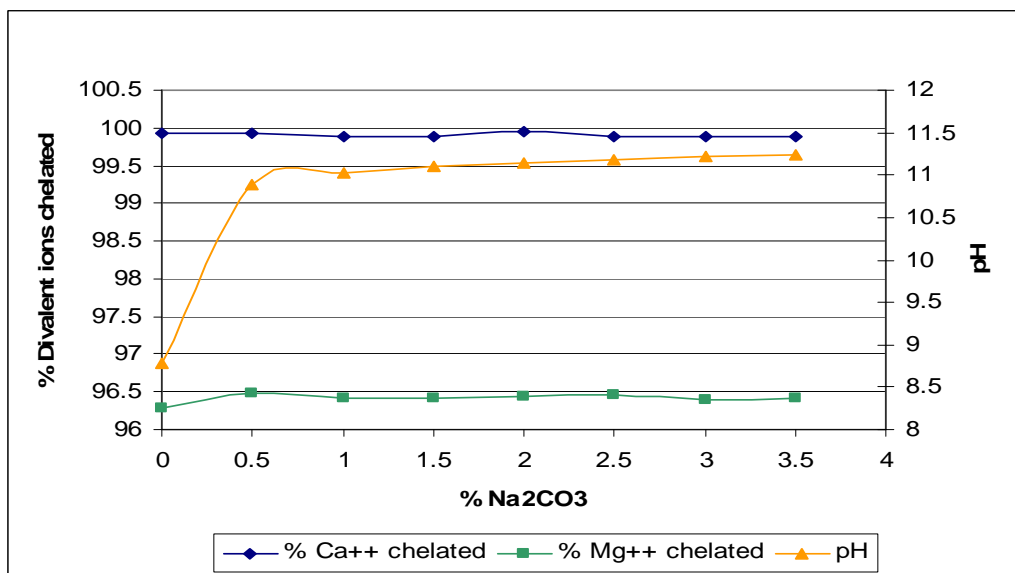
Figure 5.40: Chelation of calcium and magnesium ions in the presence of 1% Na4EDTA
along with varying concentrations of sodium carbonate for the Reservoir 'C'
at the reservoir temperature (87°F)

Chapter 6: Mechanistic Simulation of Geochemical Scaling during ASP Flooding

6.1 INTRODUCTION

The use of alkaline chemicals like sodium carbonate in EOR has several beneficial effects like reducing surfactant adsorption and generating in situ soap with acidic crudes. However, an undesirable consequence of the use of alkaline chemicals is the phenomenon of geochemical scaling in the presence of hard formation brines. This occurs as a result of the precipitation of sparingly soluble minerals like the carbonates, sulfates and silicates of alkaline earth metals like calcium, magnesium and barium. These minerals are formed at the ASP flood front where CO_3^{2-} ions from the sodium carbonate in the ASP slug mixes with the formation water containing divalent ions present as connate water in the pores of the formation, thereby precipitating the sparingly soluble divalent metal carbonates as scale.

This chapter discusses the results of a mechanistic simulation study of geochemical scaling. This study was done using the compositional chemical flooding simulator, UTCHEM. The first section reviews relevant literature and gives a brief overview of UTCHEM. The second section discusses the simulation of an ASP Core Flooding experiment to history match the data and to determine the simulation parameters for use with the field scale simulations. The third section discusses the results of 3D field scale simulations aimed at determining the extent of scaling under different conditions. A sensitivity study to determine the effect of key reservoir and process parameters like physical dispersion and the alkali concentration on the extent of scaling in the reservoir and in the well bores was done. The final section provides a summary of the results and conclusions from this study.

6.2 REVIEW OF LITERATURE

Geochemical scaling is one of the major challenges faced by the oil and gas industry. Extensive scaling in the near well bore region, near production wells may render the formation impermeable to the flow of any kinds of fluids due to plugging. This causes flow restriction and hence severely reduces the oil and gas production (Moghadasi, 2004). Deposition of scale in the near well bore region of injection wells can lead to a rapid decrease in the well injectivity, which can ultimately lead to the shutting of the well (Moghadasi, 2003). Scale can also be deposited in the downstream production equipment and facilities like downhole pumps, subsurface safety valves, tubing, flow lines and storage tanks, where it leads to operational problems because of fouling as well as safety issues (Krueger, 1986; Mackay et al., 2005).

6.2.1 Field Experiences of Scaling

Several cases of scaling in the field scale have been documented in literature. Some of them are discussed in this section.

Raimondi et al. (1977) reported the plugging of production wells due to gypsum scale deposition during the caustic flooding pilot of the North Ward- Estes field. At least three wells were reported to have either been shut down or have experienced a production decline due to plugging caused by gypsum scaling under high pH conditions. Scaling was reported to occur in the well bore as well as in the production equipment.

Krumine (1985) reported severe scaling in the production wells of the alkaline injection pilot at the Long Beach Unit of the Wilmington field, California. A mixture of sodium silicate and sodium hydroxide was used as the alkali and the scales were found to be composed of a mixture of calcium carbonate, magnesium silicate and amorphous silica. The cause of the scaling was reported to be the mixing of the hard brines from one

194

subzone of the reservoir with the moderately alkaline water from other subzones. Precipitation was most severe in the producers located closest to the injectors.

More recently, several papers on the Daqing ASP pilot project have reported severe scaling problems. Wang et al. (2004) reported severe scaling in the production well bore as well as in the surface gathering and delivery system. Scaling was observed in the artificial lift system resulting in pump failures when the pilot entered its peak period of response. This resulted in a substantial reduction in the oil production. Gang et al. (2007) reported severe scaling in the production system, especially the downhole artificial lift systems, resulting in the abnormal operation of the producers. The chemical composition of the scale was found to be a mixture of calcium carbonate and calcium silicate.

6.2.2 Modeling Geochemical Scaling

Historically, geochemical flow models have assumed either a local thermodynamic equilibrium or a kinetically controlled process. Walsh et al. 1984 developed a model based on the equilibrium approach. This model predicted the mineral and aqueous phase compositions as a function of time and position assuming a chemical equilibrium in the mineral and aqueous phases by considering dissolution and precipitation reactions, redox reactions and adsorption. Araque-Martinez et al. (2001) developed a model based on the method of characteristics which included reaction kinetics to describe fluid solid reactions and thermodynamic equilibria to describe fluid fluid reactions. This model however is appropriate only for the near injection wellbore calculations and does not include physical dispersion (Delshad et al., 2003). Rocha et al. (2003) developed a salt precipitation model which was coupled with an ion transport equation describing the ion movements and reaction through porous media by a finite

element method to predict precipitation around the well bore. However, this model is applicable only for the single phase flow of water.

Delshad et al (2003) simulated a field scale water flood to investigate the flow and transport of barium and sulfate ions. They analyzed the scaling potential for barium sulfate in a reservoir and determined the effect of physical dispersion on the extent of scaling. Mohammedi (2008) did a 1-D mechanistic simulation study of alkali consumption, especially with respect to its effect on alkali propagation through the rock for different alkali and rock types. Both these studies used the compositional chemical flooding simulator, UTCHEM to simulate the geochemical reactive flow problem.

6.2.3 Overview of UTCHEM

The three dimensional multiphase, multicomponent, compositional Chemical Flooding simulator, UTCHEM was used to mechanistically simulate geochemical scaling in this research. The simulator uses an IMPEC solution scheme wherein the pressure is solved implicitly and the concentration is solved explicitly. The simulator has the capability to model phenomena like multiphase flow, water reaction chemistry with the rock and species transport equations. Physical phenomena like velocity dependent dispersion, molecular diffusion, adsorption and cation exchange on the surface of the matrix as well as the surfactant micelles which are expected to significantly affect the extent of geochemical scaling among others are also modeled in UTCHEM (Delshad et al., 1996). The geochemical module in UTCHEM is based on the assumption of local thermodynamic equilibrium and can model chemical reactions among the injected chemical species, in-situ fluids and reservoir rocks. The sections below describe the geochemical module in UTCHEM, along with the models describing some of the physical phenomena that are most significant with regards to the problem under

196

consideration. A detailed description of the various models used in UTCHEM can be found in the UTCHEM Technical Documentation (UTCHEM Vol. II, 2000)

Geochemical Module in UTCHEM

The geochemical module in UTCHEM is based on the work done by Bhuyan (1989) and Bhuyan et al. (1990). This was later generalized to model any number of elements and fluid species (Delshad et al., 1998). UTCHEM has the capability of modeling aqueous electrolyte chemistry, precipitation/dissolution of minerals, ion exchange reactions with the matrix and surfactant micelles and the reaction of acidic components of oil with the alkali in the aqueous solution. Some of the assumptions made in developing the geochemical module relevant to the problem under consideration are,

    i.   All reactions attain thermodynamic equilibrium.

    ii.   Activity coefficients of all the reactive species are unity. Hence molar concentrations replace activities in all equilibrium calculations.

    iii.   Supersaturation of aqueous species is not allowed.

    iv.   Solid precipitates are stationary and are not allowed to migrate.

    v.   Precipitation/dissolution and cation exchange reactions have a negligible effect on the porosity and permeability.

Cation Exchange

Cation exchange between the brine and the clays in a formation occurs when the cations in the injected brine is not in equilibrium with the clays in the formation. The difference between the injected and equilibrium concentrations sets off cation exchange

waves that move slower than the salinity wave. Pope et al., 1978 described the basic theory of cation exchange during chemical flooding. Lake et al., 1978 extended the theory to include the effects of fluid dynamic dispersion. The change in the cation concentrations (e.g. Na+ and Ca++ ions) affects the surfactant properties to various degrees depending on the type of surfactant and many other variables. The effect may be large if the cation exchange capacity is large, the optimum salinity is low, the surfactant has a low Ca++ tolerance and so forth, but with many of the newer surfactants the effect is small, especially if a salinity gradient is used to mitigate such effects.

The cation exchange model implemented in UTCHEM is based on Hirasaki's model (Hirasaki, 1982), which describes ion exchange with clays in the presence of surfactant. Cations exist in the form of free ions and are either adsorbed on the clay surfaces or associated with the surfactant micelles or the adsorbed surfactant. The mass action equations describing the exchange of calcium and sodium is given by,

$$\frac{(C_{12}^s)^2}{C_6^s} = \beta^s C_3^m \frac{(C_{12}^f)^2}{C_6^f} \ldots\ldots\ldots\ldots\ldots\ldots\ldots\ldots\ldots\ldots\ldots\ldots\ldots\ldots \text{(6.1)}$$

$$\frac{(C_{12}^c)^2}{C_6^c} = \beta^c Q_v \frac{(C_{12}^f)^2}{C_6^f} \ldots\ldots\ldots\ldots\ldots\ldots\ldots\ldots\ldots..\ldots\ldots\ldots.. \text{(6.2)}$$

where the subscripts c, s and f denote adsorbed cation on clay, adsorbed cation on micelles and free cation respectively. The subscripts 6 and 12 refer to calcium and sodium respectively. The simulator input parameters are Q_v, the cation exchange capacity of the rock, β^c and β^s, the ion exchange constants for the clay and the surfactant respectively, and C_3^m, the initial surfactant concentration in meq/ml.

The geochemical module of UTCHEM also takes into account the reversible hydrogen exchange and the pH dependence of the cation exchange.

198

Effective Salinity

At constant temperature, the effective salinity increases with the presence of divalent ions bound to the micelles (Glover et al., 1979, Hirasaki, 1982). This is given by

$$C_{SE} = \frac{C_{51}}{(1 - \beta_6 f_6^s)(1 + \beta_T (T - T_{ref}))} \quad \text{..............................} \quad (6.3)$$

where, C_{51} is the aqueous phase anionic concentration, β_6 is a positive constant and f_6^s is the fraction of total divalent ions bound to the micelles given by,

$$f_6^s = \frac{C_6^s}{C_3^m} \quad \text{...} \quad (6.4)$$

and β_T is a positive temperature co-efficient used to model the effect of temperature changes on the optimal salinity.

Dispersion

Dispersion is the in-situ mixing of chemical components as they are transported through the porous media and includes the effects of molecular diffusion as well as fluid velocity gradients (Taylor, 1953). Physical Dispersion in UTCHEM is accounted for in the mass conservation equations in the form of the dispersive flux. The dispersive flux is assumed to be of the Fickian form and is given by

$$\overline{\overline{D}}_{\kappa\ell,x} = \phi S_\ell \overline{\overline{K}}_{\kappa\ell} . \vec{\nabla} C_{\kappa\ell} \quad \text{......................................} \quad (6.5)$$

199

where,

$\overrightarrow{D}_{\kappa\ell,x}$ = Dispersive flux of the species κ in phase ℓ

ϕ = Porosity

S_ℓ = Saturation of the Phase ℓ

$\overrightarrow{\overrightarrow{K}}_{\kappa\ell}$ = Dispersion tensor for the species κ in phase ℓ

$.\overrightarrow{\nabla}C_{\kappa\ell}$ = Concentration Gradient of the species κ in phase ℓ

The dispersion tensor, $\overrightarrow{\overrightarrow{K}}_{\kappa\ell}$ is given by (Bear, 1979),

$$\overrightarrow{\overrightarrow{K}}_{\kappa\ell} = \frac{D_{\kappa\ell}}{\tau}\delta_{ij} + \frac{\alpha_{T\ell}}{\phi S_\ell}\left|\overrightarrow{u_\ell}\right|\delta_{ij} + \frac{(\alpha_{L\ell}-\alpha_{T\ell})}{\phi S_\ell}\frac{u_{\ell i}u_{\ell j}}{\left|\overrightarrow{u_\ell}\right|} \quad\text{…………….. (6.6)}$$

where $\alpha_{L\ell}$ and $\alpha_{T\ell}$ are the longitudinal and transverse diffusivities of the phase ℓ, $u_{\ell i}$ and $u_{\ell j}$ are the components of the Darcy flux of phase ℓ in the i and j directions. and δ_{ij} is the Kronecker Delta function. The magnitude of the vector fluxes are calculated as

$$\overrightarrow{u}_\ell = \sqrt{(u_{x\ell})^2 + (u_{y\ell})^2 + (u_{z\ell})^2} \quad\text{……………………….………….. (6.7)}$$

6.3 RESERVOIR DESCRIPTION

This study was carried out on a sandstone reservoir 'M', having a moderate temperature of 62°C and a high average permeability of approximately 2 Darcy. The API gravity of the crude 'M' was 25° and it had a pour point of 42°F. The viscosity and acid number of crude M are 21 cp and 0.5 mg KOH/g oil respectively. The formation brine for the Reservoir 'M' has a salinity of 7452 ppm TDS, inclusive of a total divalent ion concentration of 313 ppm. The synthetic softened injection brine for the reservoir 'M' has

200

a salinity of 5425 ppm. Table 6.1 shows the ionic concentration of the formation brine and the injection brine for the reservoir 'M'.

6.4 SIMULATION OF THE CORE FLOOD M-9

Prior to doing the field scale simulations, the geochemical model was initially developed by considering the aqueous phase, dissolution/precipitation and ion exchange reactions of the formation fluids and the reservoir rock. A core flood experiment for the reservoir 'M' was performed on the reservoir core. This experiment was history matched using UTCHEM, taking into account all the geochemical reactions to study the scaling phenomenon for a 1-D case. This simulation also helped to determine the physical property data and other key simulation parameters which were used with the field scale simulations.

6.4.1 Brief Description of the Core Flood Experimental Results

The ASP formulation used for this experiment used a mixture of 0.15% TDA 18PO SO_4, 0.15% $C_{20\text{-}24}$ IOS, 0.3% Aerosol MA80I, 2.25% Na2CO3 and 3000 ppm FP3630S polymer in the synthetic injection brine. An ASP slug of 0.3 PV was injected into the core followed by 2.2 PV of a polymer drive consisting of a mixture of 2250 ppm FP3630S in the synthetic injection brine. Table 6.2 lists the composition of the ASP slug and the polymer drive for this experiment

The core used was a reservoir core. The core was initially saturated with the synthetic formation brine. This was followed by an oil flood where the filtered crude 'M' was injected up to the initial oil saturation (0.83). The core was subsequently water flooded with the synthetic formation brine to the residual oil saturation (0.35). Finally,

the chemical slug was injected at a frontal advance rate of 1.3 ft/day, followed by the polymer drive at the same rate. The oil recovery was 90% of the water flood residual oil with a final residual oil saturation after the chemical flood of 0.04. The rock properties and fluid properties for the core M-9 are summarized in Table 6.3.

6.4.2 Geochemical Reactions Modeled

EQBATCH, the pre-processor program for UTCHEM was used to set up the initial state with respect to the pH and the concentrations of the different geochemical species, including fluid species, solid species and sorbed species on both the clay as well as the surfactant micelles. Different types of geochemical reactions including aqueous phase reactions, dissolution/precipitation reactions and ion exchange reactions, both on the clay as well as on the micelles were modeled. Table 6.4 shows a list of reactive elements and species considered for this run. The list of reactions considered is as follows.

Aqueous Phase Reactions
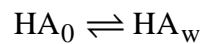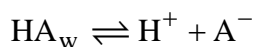
$$Ca^{2+} + OH^- \rightleftharpoons CaOH^+$$
$$Ca^{2+} + H^+ + CO_3^{2-} \rightleftharpoons CaHCO_3^+$$
$$H^+ + OH^- \rightleftharpoons H_2O$$
$$H^+ + CO_3^{2-} \rightleftharpoons HCO_3^-$$
$$2H^+ + CO_3^{2-} \rightleftharpoons H_2CO_3$$
$$Ca^{2+} + CO_3^{2-} \rightleftharpoons CaCO_3$$

Oil Alkali Reactions

$$HA_0 \rightleftharpoons HA_w$$

$$HA_w \rightleftharpoons H^+ + A^-$$

Dissolution/Precipitation Reactions

$$Calcite(CaCO_3) \rightleftharpoons Ca^{2+} + CO_3^{2-}$$

Cation Exchange Reactions on the matrix

$$2\overline{Na}^+ + Ca^{2+} \rightleftharpoons \overline{Ca}^{2+} + 2Na^+$$

$$\overline{H}^+ + Na^+ + OH^- \rightleftharpoons \overline{Na}^+ + H_2O$$
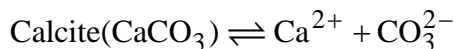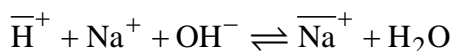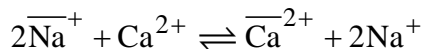
Cation Exchange Reactions on the Micelles

$$2\overline{\overline{Na}}^+ + Ca^{2+} \rightleftharpoons \overline{\overline{Ca}}^{2+} + 2Na^+$$
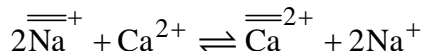
In addition to the reactions mentioned above, two other reactions occur, which were not modeled in this study. These are the reactions of the calcium ions with the sulfate and the sulfonate groups of the surfactant molecules forming calcium sulfate and sulfonate respectively.

Table 6.5 and 6.6 show the thermodynamic equilibrium data for the different aqueous and solid species considered for these simulations. These values were taken from the Geochemists' Workbench Release 6.0 database. Table 6.7 shows the mineralogy of the reservoir rock. The total clay content of the rock was 4.7% and the cation exchange capacity of the reservoir rock was calculated to be 0.03364 meq/ml PV (0.538 meq/100gm rock).

6.4.3 Phase Behavior Modeling

The phase behavior experiment M-325 was modeled using UTCHEM. The phase behavior screening was performed over a sodium carbonate concentration range of 0 to

3.5%. The oil concentration was varied from 10 to 50 volume %. Figures 6.1 to 6.5 show the solubilization ratio plots, along with the corresponding UTCHEM matches as functions of the sodium carbonate concentrations at different oil concentrations. The matching phase behavior input parameters are shown in Table 6.8, along with the other input parameters for the core flood.

6.4.4 Simulation of the Core Flood M-9

The 1-D simulation model was set up for the foot long core with diameter 3.63 cm. The one foot long core was simulated with 100 grid blocks of equal size. To reduce numerical dispersion, the total variation diminishing third order method finite-difference method in UTCHEM was used. The core flood simulations were history matched with the experimental results to determine the matching parameters. The simulation input parameters used for simulating this core flood have been summarized in Table 6.8.

Results of the Core Flood Simulations

Figures 6.6, 6.7 and 6.8 show the match of the oil recovery, pH and the pressure drops across the core respectively for the core flooding experiment M-9. The oil recovery showed an excellent match between the simulation and the experimental results. The simulated oil cut and the oil breakthrough time also showed an excellent agreement with the experimentally observed trends. The pressure drop and the pH histories were also successfully matched with the experimental data.

6.5 FIELD SCALE SIMULATIONS

This section discusses a pilot scale mechanistic simulation study of geochemical scaling. The rock and fluid properties, phase behavior and polymer modeling parameters used for this simulation are the same as those used for simulating the core flood described in section 6.3 and are listed in Table 6.8. The geochemical reactions modeled were also the same as those described for simulating the core flooding experiment. The list of geochemical species considered is listed in Table 6.4, while the corresponding equilibrium data are listed in Tables 6.5 and 6.6. The EQBATCH file used for the field scale runs is given in the Appendix.

The simulation model used for the field scale simulations was a 3 acre regular five spot pattern. A top view of the reservoir model which includes the pilot area along with the well locations is shown in Figure 6.9. The model used 15, 15 and 36 grid blocks in the X, Y and Z directions. Variable grid block sizes were used in the model. The grid blocks in the X and Y directions in the middle section of the reservoir (inside the five spot pattern area) were smaller than the grid blocks along the sides and corners. This reduces the numerical dispersion and improves the accuracy of the simulation results. The grid block sizes ranged from 32.8 ft to 131.2 ft in the X and Y directions. In the Z direction, they ranged from 2.23 ft to 5.68 ft. Table 6.9 lists the model specifications. Figures 6.10 and 6.11 show the porosity and permeability distributions respectively of the reservoir.

A total of four injection wells and one production well were modeled. All wells were rate constrained with the injection wells maintaining an injection rate (2105.5 ft^3/day), which was a fourth of the production rate of the lone production well (8422 ft^3/day), thereby maintaining a balanced injection and production from the reservoir.

205

6.5.1 Base Case Simulation

The base case simulation used the core flood history match data for simulating the field scale case. The simulation input parameters used are listed in Table 6.8. The UTCHEM input file used for the base case simulation is shown in the Appendix. The base case simulations used a longitudinal dispersivity of 0.2 ft (with a transverse dispersivity of 0.001 ft). A sensitivity study of the effect of dispersivity on the extent of scaling was done as a part of this research and is described in the next section.

The injection pattern followed is listed in Table 6.10. The ASP slug was initially injected for 151 days (0.44 Pilot PV). This was followed by the Polymer drive for a period of 289 days (0.85 Pilot PV). Finally, the chase water was injected for a period of 310 days (0.91 Pilot PV). The simulation was thus run for a total of 750 days (2.20 Pilot PV). The composition of the ASP slug and the polymer drive for the base case simulations was the same as that used in the core flooding experiment described in section 6.3 and is tabulated in Table 6.2. The chase water consisted of the injection brine for the Reservoir 'M' whose composition is listed in Table 6.1.

Figures 6.12 and 6.13 show the calcium ion concentrations at the end of 91 days (0.27 PV) and 750 days (2.20 PV) respectively for the base case. These show that a significant amount of calcium ions were consumed by the carbonate ions in the injected ASP slug. The concentration profile of the carbonate ions in the reservoir at the end of 91 days is shown in figure 6.14. Figure 6.15 shows the profile of the calcium and the carbonate ions, as well as the pH as a function of the dimensionless distance between an injector and producer in Layer 3 after 91 days.

The distribution of the calcium carbonate precipitate in the reservoir at the end of the injection period (750 days) is shown in Figure 6.16. Figure 6.17 shows the profile of the solid calcium carbonate in Layer 29 after 750 days. High concentrations of solid

calcium carbonate were observed, especially near the injection wells. Table 6.11 lists the mass of solid calcium carbonate in the reservoir and in each of gridblocks with a well at the end of the chemical injection (750 days). The UTCHEM units are gmoles per liter of pore volume. These values were converted to kg units.

6.5.2 Sensitivity Studies

This section analyzes the effect of two reservoir and process parameters, namely the physical dispersion and the alkali concentration on the extent of scaling, both in the formation as well as the wells.

Physical Dispersion

The effect of physical dispersion on scaling was studied by varying the dispersivity parameters. For the base case, the values of transverse and longitudinal dispersivities used were 0.2 ft and 0.001 ft respectively. To determine the effect of dispersivity on scaling, further runs were made using higher dispersivity values. The results of these runs are summarized in Table 6.12 which lists the mass of precipitates in the injection and production wells at the end of the chemicals injection (750 days). Figure 6.18 shows a plot of the mass of calcium carbonate precipitate in the formation at different times and using different values of longitudinal dispersivities.

These results show that as the dispersivity increased, the total mass of precipitates in the formation increased as shown in figure 6.18. This is on account of the greater mixing between the injection and the formation brines in the reservoir at higher dispersivities. However, the precipitations in the injection and production wells were not very sensitive to the change in dispersivity of the formation.

Alkali concentration

The effect of alkali concentration on the extent of scaling was studied by modifying the injected alkali concentration with the ASP slug. The base case considered the injection of 2.25 wt % sodium carbonate. To determine the effect of sodium carbonate concentration on the extent of scaling, runs were made with lower sodium carbonate concentrations. In each case, the reduction in the sodium carbonate concentration in the ASP slug was compensated by a corresponding increase in the sodium chloride concentration so as to maintain a constant total salinity. These runs were carried out at two different dispersivities, namely 0.2 ft and 5 ft. The results of these runs are summarized in Table 6.13, which lists the total mass of precipitates in the injection and production wells at different alkali concentrations and different dispersivities. Figure 6.19 shows a plot of the mass of calcium carbonate precipitate in the formation at different times and at different alkali concentrations; using a longitudinal dispersivity of 0.2 ft. Figure 6.20 does the same for the cases where a longitudinal dispersivity of 5 ft was used.

The results show that as the alkali concentration decreased, the mass of precipitates in the formation decreased, irrespective of the dispersivity, as shown in figures 6.19 and 6.20. The extent of decrease was greater at higher dispersivities. However, the quantity of precipitates in the injection and production wells was not very sensitive to the alkali concentration, irrespective of the extent of dispersion.

6.6 SUMMARY AND CONCLUSIONS

A mechanistic simulation study was done to predict the quantity and composition of the scale formed in the reservoir as well as in the injection and production wells. This study took into consideration the reactions occurring between the injected fluids, the in

situ fluids and the reservoir rock for the specific case where calcium carbonate was the precipitating species. Sensitivity studies were done to analyze the effect of key reservoir and process parameters like the physical dispersion and the alkali concentration to determine their effect on scaling in the reservoir as well as the injection and production wells. The following conclusions can be drawn from this study.

- A large quantity of calcium carbonate precipitation was predicted to occur at the injected sodium carbonate concentration (2.25 wt. %), both in the formation as well as the injection and production wells. For instance, in the base case where a dispersivity of 0.2 ft was used, a total of 14077 kg of scale was predicted to occur in the formation. Of this, 8905 kg was predicted to occur in the injection and production wells.

- An increase in the dispersivity increased the total quantity of precipitates in the formation. However, the quantity of precipitates in the injection and production wells was not very sensitive to the change in dispersivity.

- Reducing the alkali concentration resulted in a decrease in the total quantity of precipitates in the formation. This sensitivity was found to be more at higher dispersivities. However, the quantity of precipitates in the injection and production wells was not very sensitive to the change in the alkali concentration, irrespective of the physical dispersivity.

One important limitation of this study is that the geochemical model does not take into account the reaction occurring between the calcium ions, and the sulfate and sulfonate groups present in the surfactant molecules to form calcium sulfate and sulfonate respectively. This reaction competes with the precipitation reaction between the calcium and carbonate ions. Laboratory experiments have shown in many cases that no precipitation is seen indicating that the reaction between the calcium and the

sulfate/sulfonate reaction dominates over the precipitation reaction. The extent of the precipitation reaction is dependent on the whether an excess of sulfate/sulfonate groups or the calcium ions are present in the solution. Precipitation occurs only when an excess of calcium ions are present in the solution.

Table 6.1: Ionic concentration of the Formation Brine and the Injection Brine for the Reservoir 'M'

Ion	Conc. (ppm)	
	Formation Brine	Injection Brine
Na	2572	2046
Mg	86	0
Ca	227	0
Cl	4567	2680
HCO3	0	253
CO3	0	0
SO42-	0	447
TDS	7452	5425

Table 6.2: Composition of the ASP slug and the Polymer Drive for the Core Flood M-9

Alkali/Surfactant/Polymer Slug (0.3PV)
0.15% TDA-13PO-SO4
0.15% C_{20-24} IOS
0.3% Aerosol MA80I
2.25% Na_2CO_3
3000 ppm FP3630S
500 ppm dithionite
In Synthetic Injection Brine
Viscosity: 40 cp @ $10s^{-1}$, 62 °C
Frontal velocity: 1.3 ft/day
Polymer Drive: (2.2 PV)
2250 ppm FP3630S
500 ppm dithionite
In Synthetic Injection Brine
Viscosity: 40 cp @ $10s^{-1}$, 62 °C
Frontal velocity: 1.3 ft/day

Table 6.3: Rock and Fluid properties for the core M-9 and the Core Flooding
Experimental Results

Porosity	0.32
Permeability, md	4000
Initial Oil Saturation	0.83
Residual Oil Saturation	0.35
End Point Oil Relative Permeability	0.88
End Point Water Relative Permeability	0.11
Water Viscosity (62^0C), cp	0.52
Oil Viscosity (62^0C), cp	14
Cumulative Oil Recovery (%)	91.5
Residual Oil Saturation after the Chemical Flood	0.03

Table 6.4: List of elements and reactive species considered for simulating the core flood
experiment M-9

Elements or pseudo-elements	Calcium, Carbonate, Sodium, Hydrogen (Reactive),Oleic acid, chlorine
Independent Aqueous Species	H^+, Na^+, Ca^{2+}, CO_3^{2-}, HA_0, H_2O
Dependant Aqueous Species	$Ca(OH)^+$, $Ca(HCO3)^+$, A^-, OH^-, HCO_3^-, H_2CO_3, $CaCO_3$, HA_w,
Solid Species	$CaCO_3$ (Calcite)
Adsorbed Cations	H+, Na+, Ca2+
Adsorbed Cations on Micelles	Na+, Ca2+

Table 6.5: Equilibrium Constants for the modeled Fluid Species

Fluid Species	Equilibrium Constant
H^+	1
Na^+	1
Ca^{2+}	1
$CO3^{2-}$	1
HA_o	1
H_2O	1
$Ca(OH)^+$	3.4906E-12
$Ca(HCO3)^+$	2.3259E+11
A^-	9.59E-13
OH^-	1.2086E-13
HCO_3^-	1.3791E+10
H_2CO_3	2.7089E+16
$CaCO_3$	8.3100E+02
HA_w	9.59E-05

Table 6.6: Solubility products for the modeled Solid Species

Solid Species	Solubility Product
Calcite ($CaCO_3$)	1.66112E-09

Table 6.7: Mineralogy of Reservoir 'M'

Mineral	Wt%
Quartz	94.0
Siderite	1.6
K Feldspar	0.1
Dolomite	0.1
Kaolinite/ Dickite	3.2
Illite/ Mica	0.6
Chlorite	0.4
Total Clay Content	4.2

Table 6.8: Summary of UTCHEM Input Parameters for the simulation of the core flood M-9

Number of grids in x, y, z directions	1, 1, 100
Gridblock sizes in x, y, z directions, ft	0.1191, 0.1191, 0.009974
Components simulated	water, oil, surfactant, polymer, anion, calcium, carbonate, sodium, hydrogen, petroleum acid
Average porosity	0.32
Permeability, md	4000
Initial water saturation, fraction (After Water Flood)	0.65
Salinity slope parameter for Calcium (Beta 6)	0.8
Capillary desaturation parameter for water, oil, ME	1865 100000 364.2
Residual water saturation, fraction	0.17
Residual oil saturation, fraction	0.35
Endpoint relative permeability of water	0.11
Endpoint relative permeability of oil	0.88
Relative permeability exponent of water	4
Relative permeability exponent of oil	2.4
Water viscosity, cp (at 62^0C)	0.5

Table 6.8: Summary of UTCHEM Input Parameters for the simulation of the core flood M-9 (cont'd)

Oil viscosity, cp (at 62^{0}C)	19
Intercept of binodal curve at zero, OPT., and 2xOPT salinity (HBNC70, HBNC71, HBNC72)	0.065, 0.03, 0.055
Lower and Upper Effective salinity for the surfactant (CSEL7, CSEU7), meq/ml	0.33, 1.1
Lower and Upper Effective salinity for the generated soap (CSEL8, CSEU8), meq/ml	0.20, 0.45
Critcal micelle conc., volume fraction	0.001
Interfacial Tension Parameters for Huh's model, CHUH,AHUH	0.3 , 10
Log10 of oil/water interfacial tension , XIFTW	1.3
CMC, volume fraction	0.001
Compositional phase viscosity parameters for microemulsion (ALPHAV1-ALPHAV5)	0.5, 0.5, 0.1, 0.1, 0.1
Parameters to calculate polymer viscosity at zero shear rate (AP1, AP2 , AP3), wt%$^{-1}$	142, 265, 350
Parameter for salinity dependence of polymer viscosity (SSLOPE), dimensionless	-0.4922
Parameter for shear rate dependence of polymer viscosity (POWN)	1.67
Permeability reduction factors, (BRK , CRK)	100. , 0.05
Surfactant adsorption parameters, (AD31, dimensionless) (AD32, ml/meq) (B3D,volume of water/volume of surfactant)	1.5, 0.1, 1000.
Polymer adsorption parameters, (AD41, dimensionless) (AD42, ml/meq) (B4D,volume of water/volume of surfactant)	2, 0.1, 100
Longitudinal Dispersivity (ft)	0.03
Transverse dispersivity (ft)	0.003

Table 6.9: Reservoir Size and Dimensions for the Field Scale Simulations

Length, L ft	754.4
Width, W ft	754.4
Height, H ft	156.49
Number of grids in x, y, z directions	15 x 15 x 36 (8100)
Cell dimensions in x direction, ft	131.2, 65.6, 11*32.8, 65.6, 131.2
Cell dimension in y direction, ft	131.2, 65.6, 11*32.8, 65.6, 131.2
Cell dimension in z direction, ft	Variable , Max 5.68, Min 2.23

Table 6.10: Chemicals Injection Scheme for the Field Scale Simulations

ASP Slug	151 days (~0.44 PV) 0.15% TDA-13PO-SO4, 0.15% C20-24 IOS, 2.25% Na2CO3, 3000 ppm FP3630S in Synthetic Injection Brine
Polymer Drive:	289 days (~0.85 PV) 2250 ppm FP3630S in Synthetic Injection Brine
Chase Water	310 days (0.91 PV) Synthetic Injection Brine

Table 6.11: Mass of calcium carbonate precipitate (in kg) in the reservoir and in the well gridblocks after 750 days of chemicals injection for the Base Case

Location	Amt of ppt. (kg)
Injection Well IL-1 Gridblock	2205.273
Injection Well IL-2 Gridblock	2207.763
Injection Well IL-3 Gridblock	2194.178
Injection Well IL-4 Gridblock	2205.469
Production Well PL-1 Gridblock	92.005
Entire Formation	14077.87

Table 6.12: Mass of calcium carbonate precipitate (in kg) in the injection and production wells after 750 days of chemicals injection at different dispersivities

Longitudinal Dispersivity (ft)	Transverse Dispersivity (ft)	Mass of Precipitates (kg)				
		Injection Well IL-1	Injection Well IL-2	Injection Well IL-3	Injection Well IL-4	Production Well PL-1
0.2	0.001	2205.27	2207.76	2194.17	2205.47	92.01
1	0.1	2216.26	2219.06	2212.54	2222.54	78.7
5	0.2	2213.45	2128.15	2158.41	2237.61	52.63

Table 6.13: Mass of calcium carbonate precipitate (in kg) in the Injection and Production wells after 750 days of chemicals injection at different alkali concentrations in the ASP slug

Longitudinal Dispersivity (ft)	Alkali Concentration (wt %)	Mass of Precipitates (kg)				
		Injection Well IL-1	Injection Well IL-2	Injection Well IL-3	Injection Well IL-4	Production Well PL-1
0.2	2.25	2205.27	2207.76	2194.17	2205.47	92.01
0.2	1.75	2191.27	2180.16	2176.35	2199.8	112.75
0.2	1.5	2193.64	2191.09	2194.62	2202.38	140.3
0.2	1.25	2106.63	2208.33	2200.05	2212.25	171.76
5.0	2.25	2213.45	2128.15	2158.41	2237.61	52.63
5.0	1.75	2186.12	2133.31	2181.66	2223.8	66.71
5.0	1.5	2181.47	2170.19	2182.73	2223.19	62.57
5.0	1.25	2217.52	2222.96	2210.59	2250.91	109.05
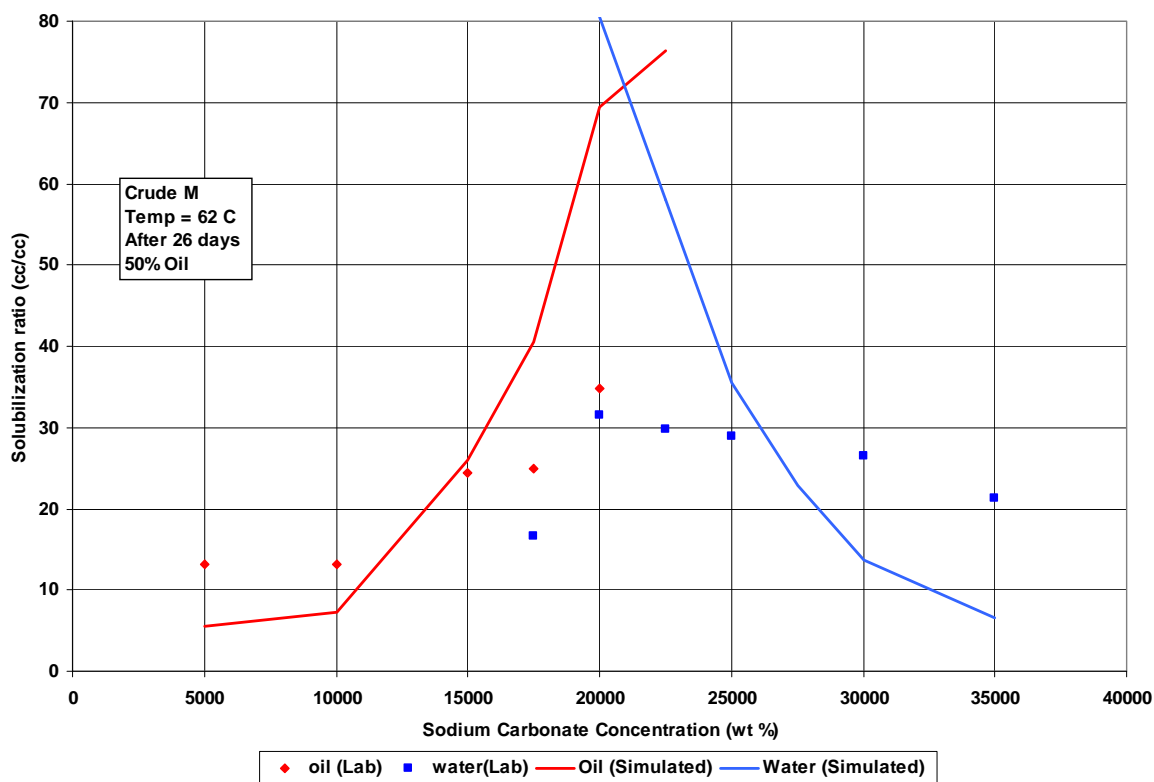
Figure 6.1: Solubilization ratio plot of the Phase Behavior Experiment M-325 using 50%
Crude 'M' at 62 C. The formulation contained 0.15% TDA-13PO-SO4,
0.15% C20-24 IOS in the Synthetic Mixing Brine. Data Points:
Experimental data, Curves: UTCHEM simulations
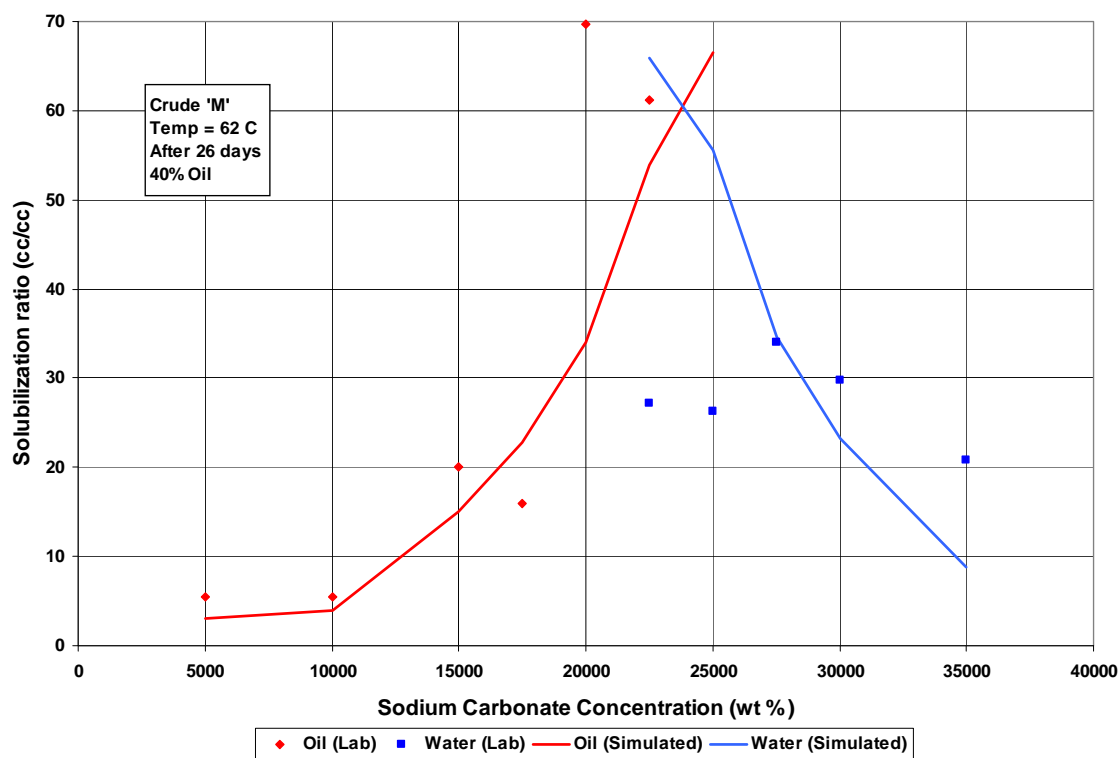
Figure 6.2: Solubilization ratio plot of the Phase Behavior Experiment M-325 using 40%
Crude 'M' at 62 C. The formulation contained 0.15% TDA-13PO-SO4, 0.15%
C20-24 IOS in the Synthetic Mixing Brine. Data Points: Experimental data,
Curves: UTCHEM simulations
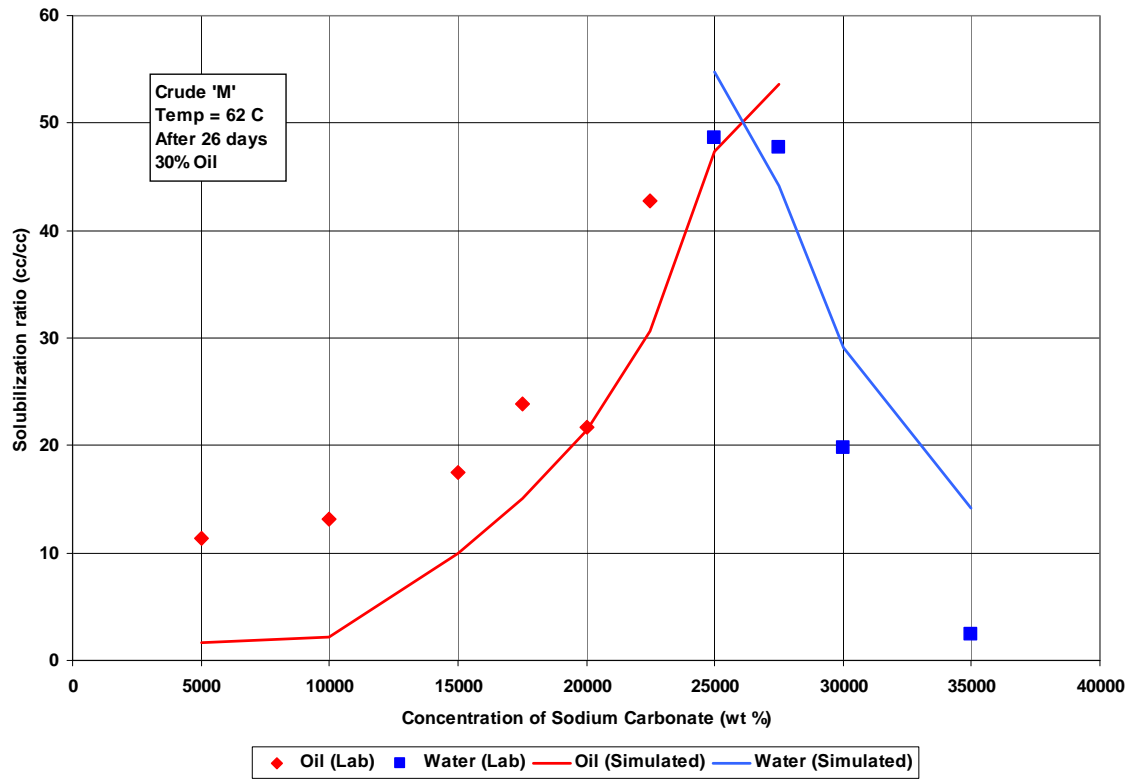
Figure 6.3: Solubilization ratio plot of the Phase Behavior Experiment M-325 using 30% Crude 'M' at 62 C. The formulation contained 0.15% TDA-13PO-SO4, 0.15% C20-24 IOS in the Synthetic Mixing Brine. Data Points: Experimental data, Curves: UTCHEM simulations.
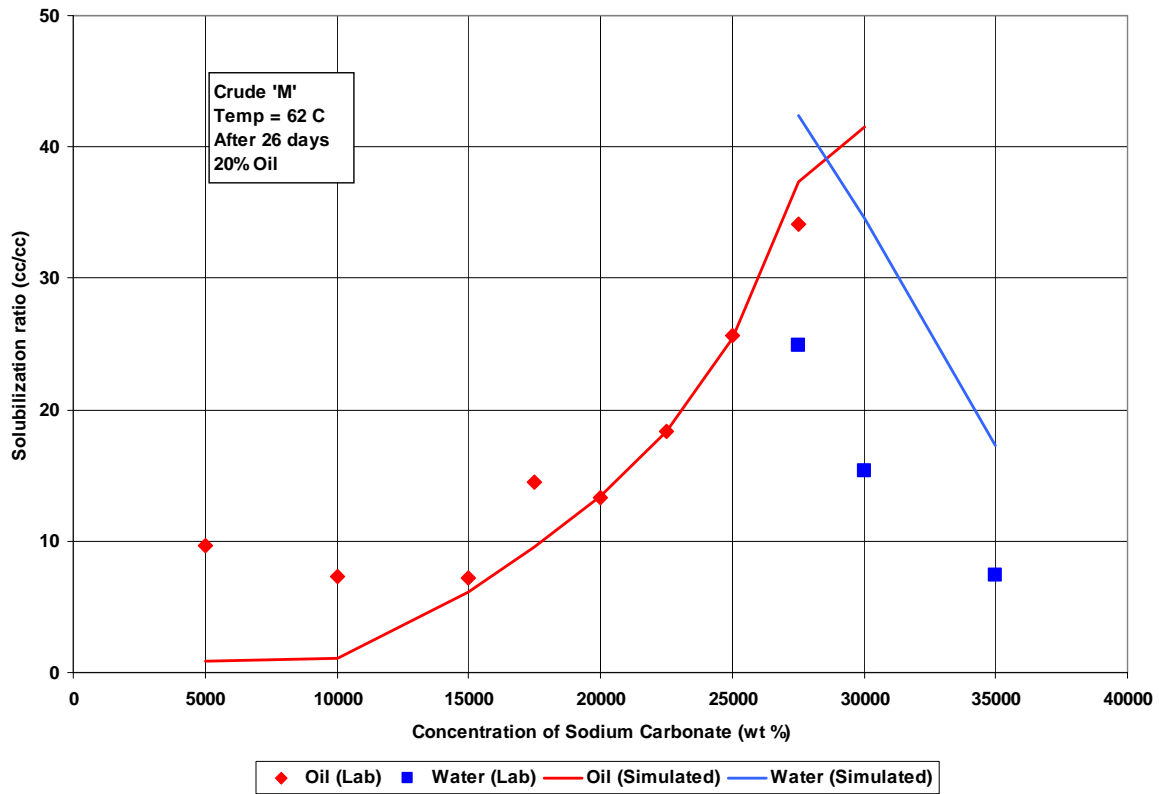
Figure 6.4: Solubilization ratio plot of the Phase Behavior Experiment M-325 using 20% Crude 'M' at 62 C. The formulation contained 0.15% TDA-13PO-SO4, 0.15% C20-24 IOS in the Synthetic Mixing Brine. Data Points: Experimental data, Curves: UTCHEM simulations.
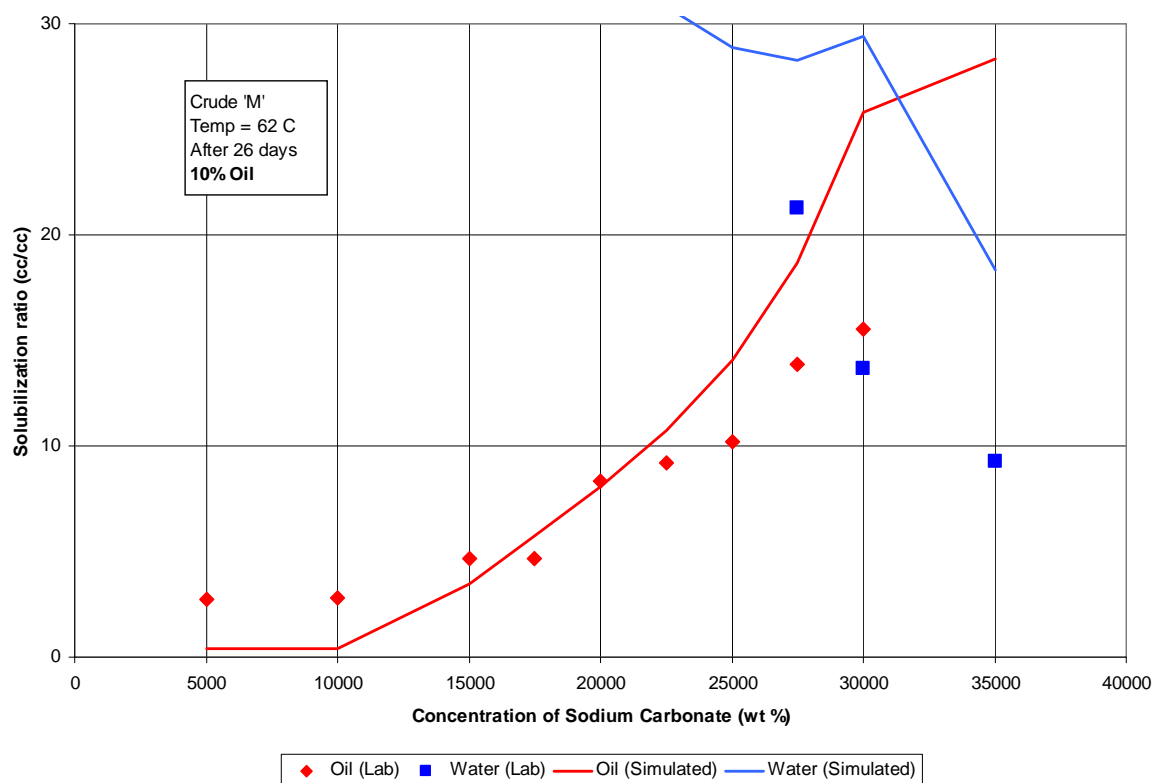
Figure 6.5: Solubilization ratio plot of the Phase Behavior Experiment M-325 using 10% Crude 'M' at 62 C. The formulation contained 0.15% TDA-13PO-SO4, 0.15% C20-24 IOS in the Synthetic Mixing Brine. Data Points: Experimental data, Curves: UTCHEM simulations.
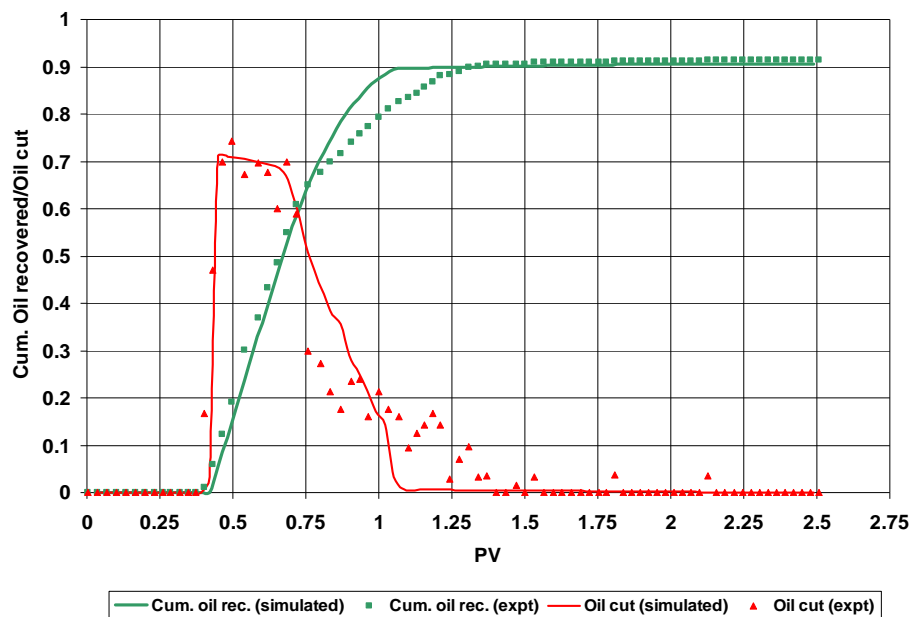
Figure 6.6: Cumulative Oil Recovery and Oil Cut for the Core Flooding Experiment M-9. Data Points: Experimental Data, Curves: UTCHEM Simulations.
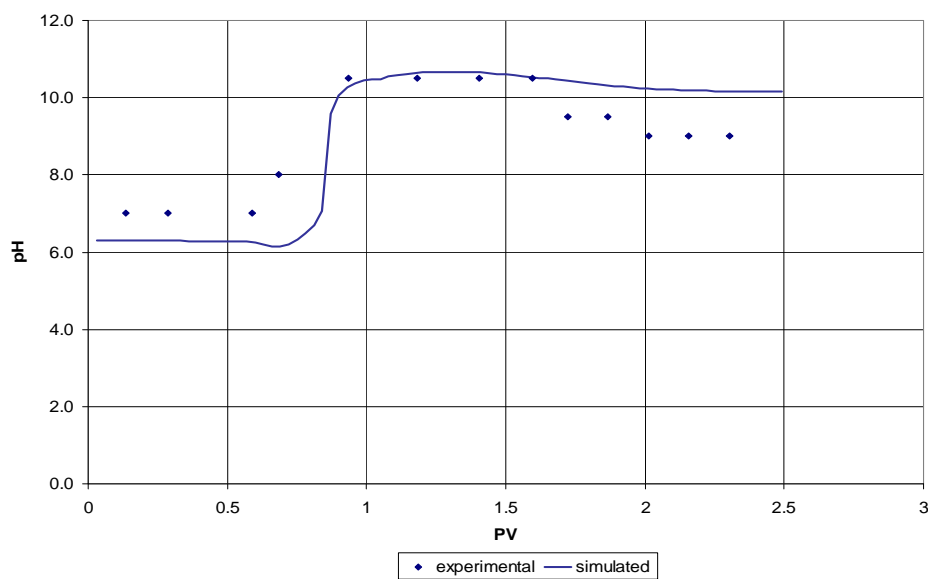
Figure 6.7: Effluent pH for the Core Flooding Experiment M-9. Data Points: Experimental Data, Curves: UTCHEM Simulations.
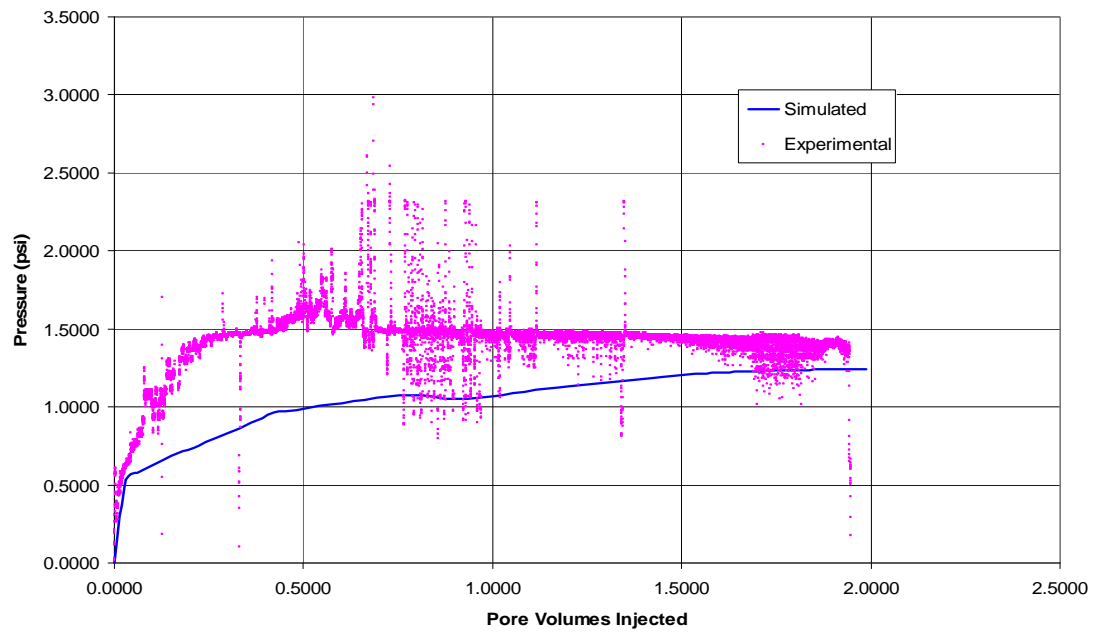
Figure 6.8: Pressure drop across the core during the Core Flood Experiment M-9. Data
Points: Experimental Data, Curves: UTCHEM simulations
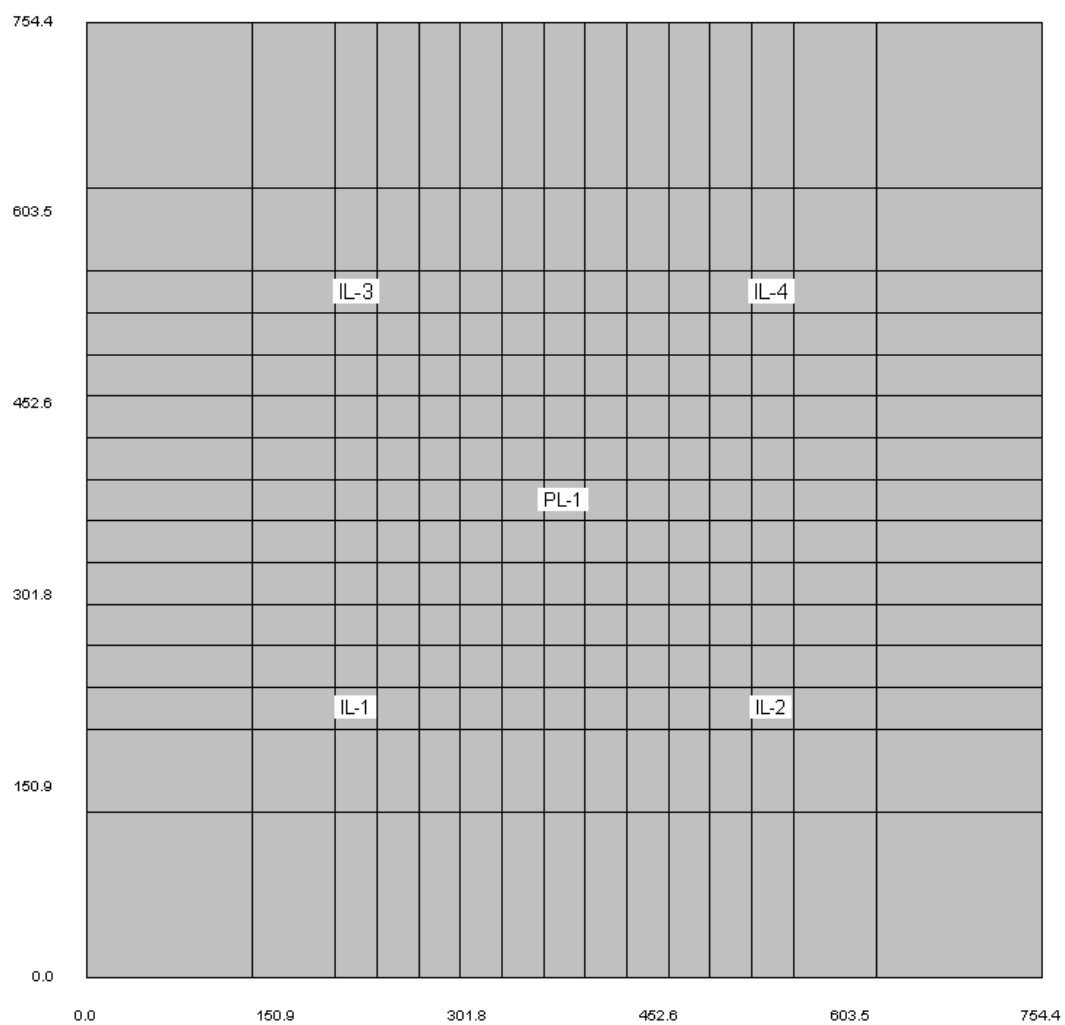
Figure 6.9: Top view of the Reservoir Model used for the Field Scale Simulations

225
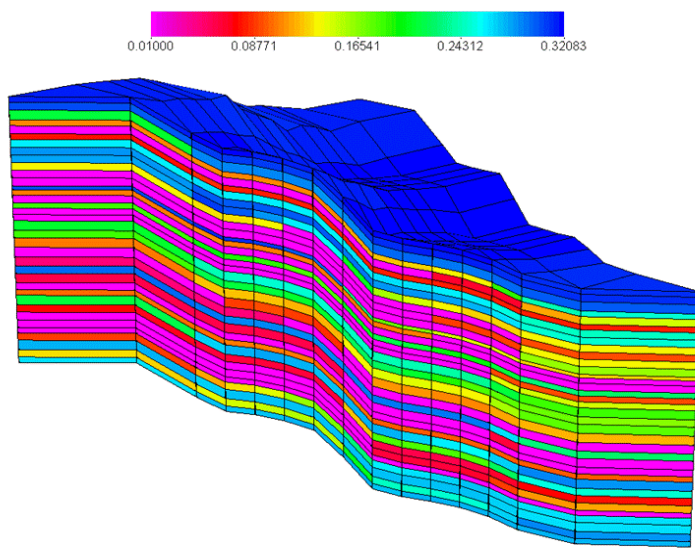
Figure 6.10: Diagonal Cross Section of the Porosity distribution in the Reservoir Model used for the Field Scale Simulations
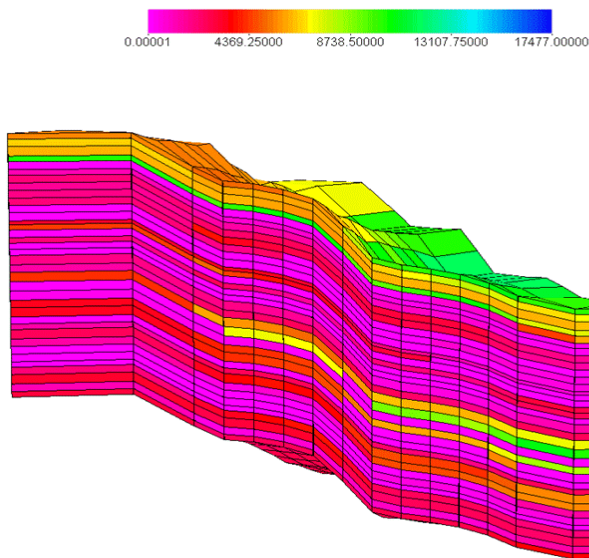
Figure 6.11: Diagonal Cross Section of the Permeability Distribution in the Reservoir Model used for the Field Scale Simulations
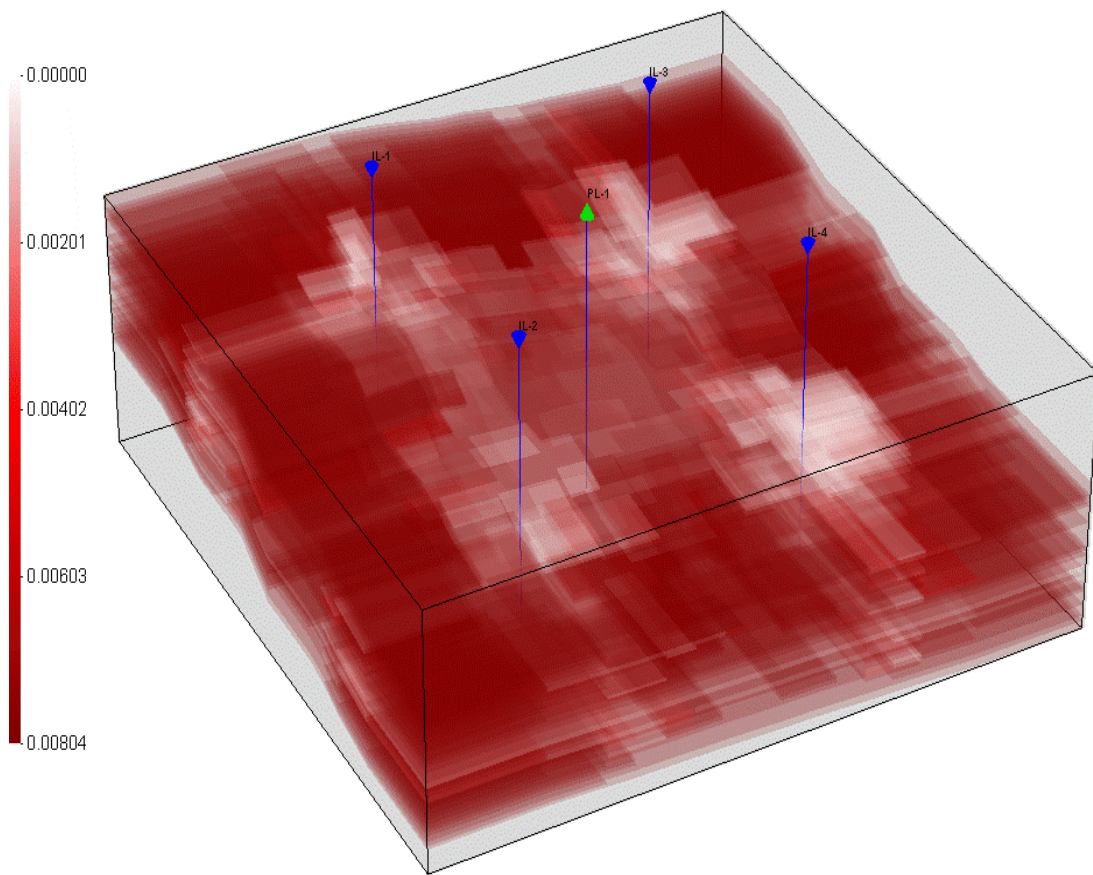
Figure 6.12: Concentration Profile of the Calcium ion (in moles/L) in the reservoir after 91 days (0.27 PV) of the ASP slug injection
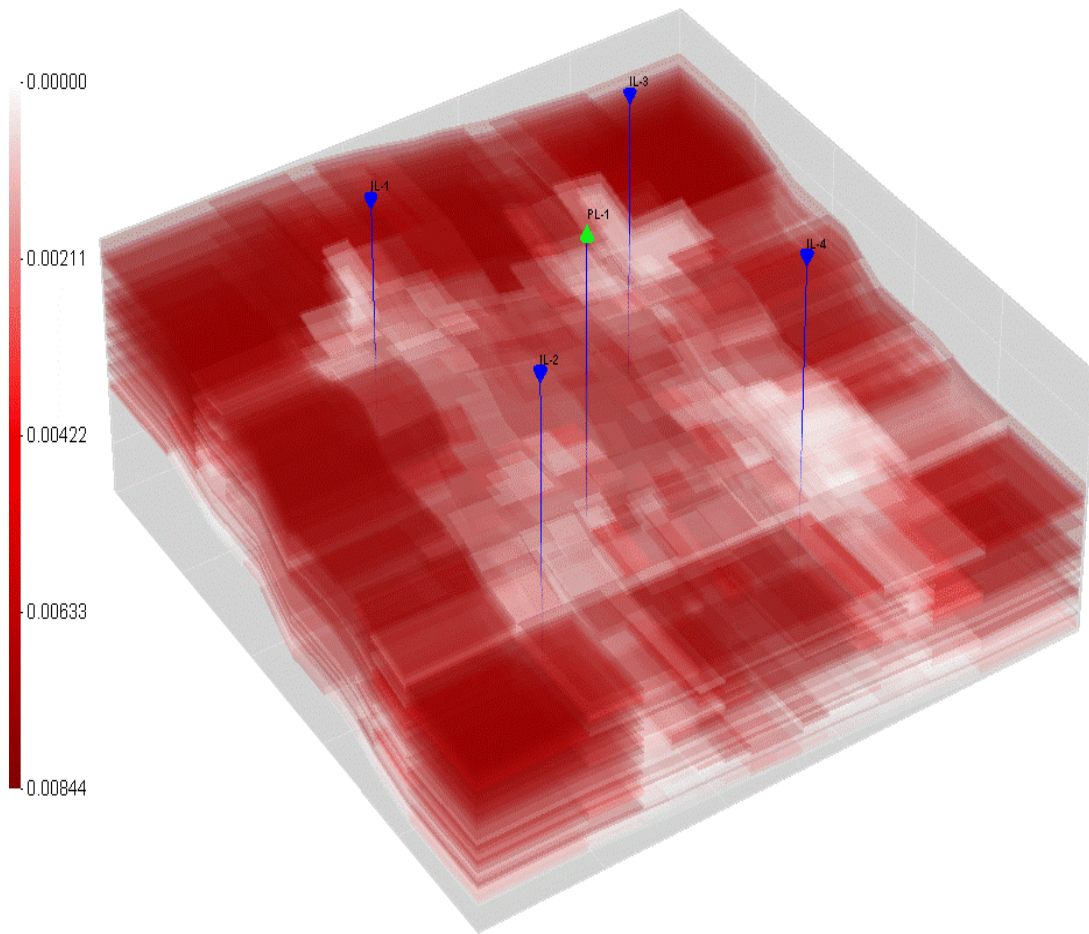
Figure 6.13: Concentration Profile of the Calcium ion (in moles/L) in the reservoir after 750 days (2.2 PV) chemicals injection
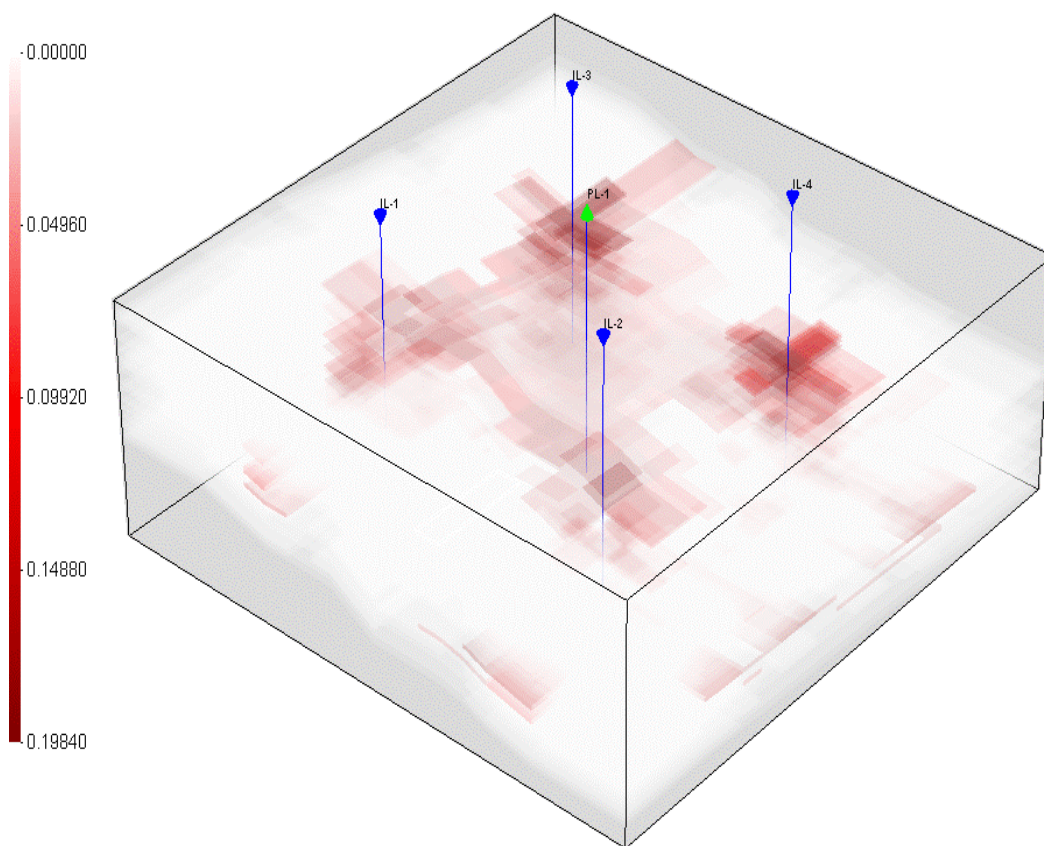
Figure 6.14: Concentration profile of the Carbonate ion (in mol/L) in the reservoir after
91 days (0.27 PV) of the ASP Slug injection
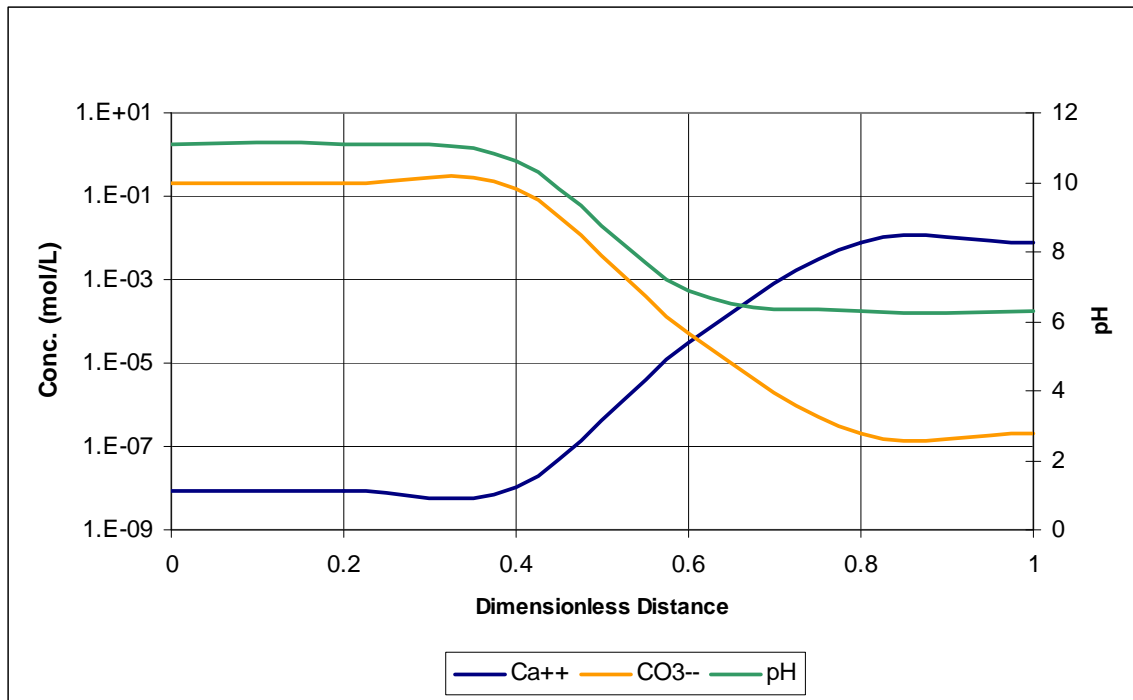
Figure 6.15: Calcium and Carbonate ion concentrations (in mol/L) and the pH between an injector and a producer in Layer 3 after 91 days (0.27 PV) of the ASP slug injection
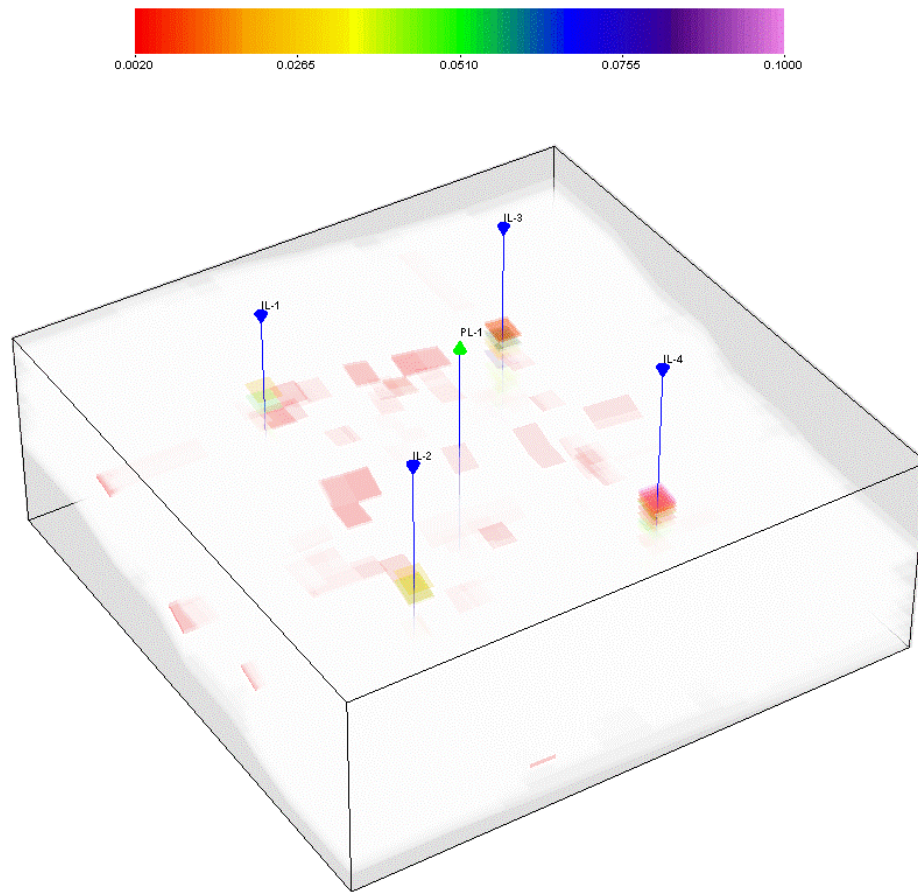
Figure 6.16: Concentration profile of the solid Calcium Carbonate (in mol/L PV) in the reservoir after 750 days (2.20 PV) of the Chemicals Injection
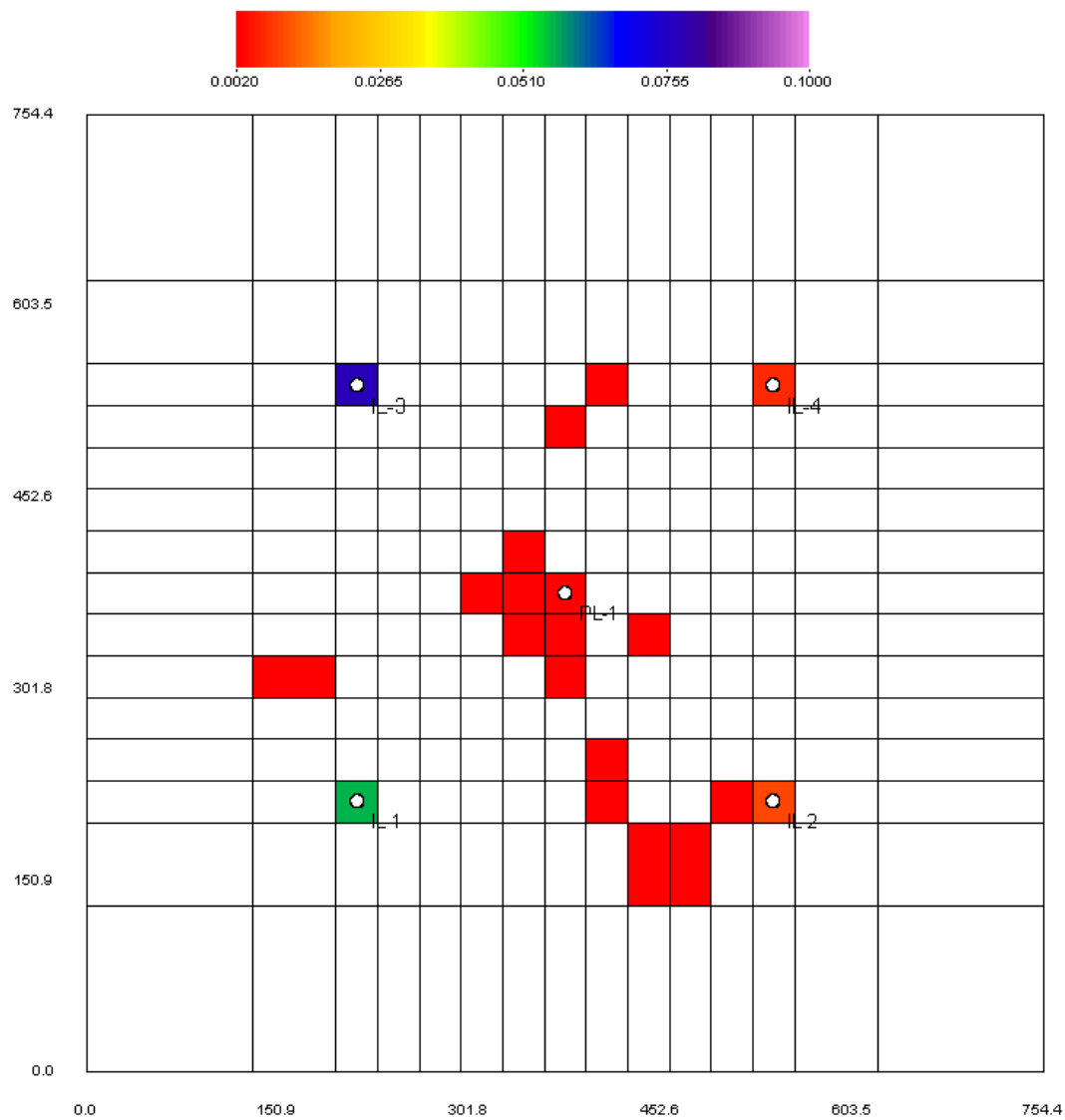
Figure 6.17: Concentration profile of the solid Calcium Carbonate (in mol/L PV) in Layer 29 after 750 days (2.20 PV) of the Chemicals Injection
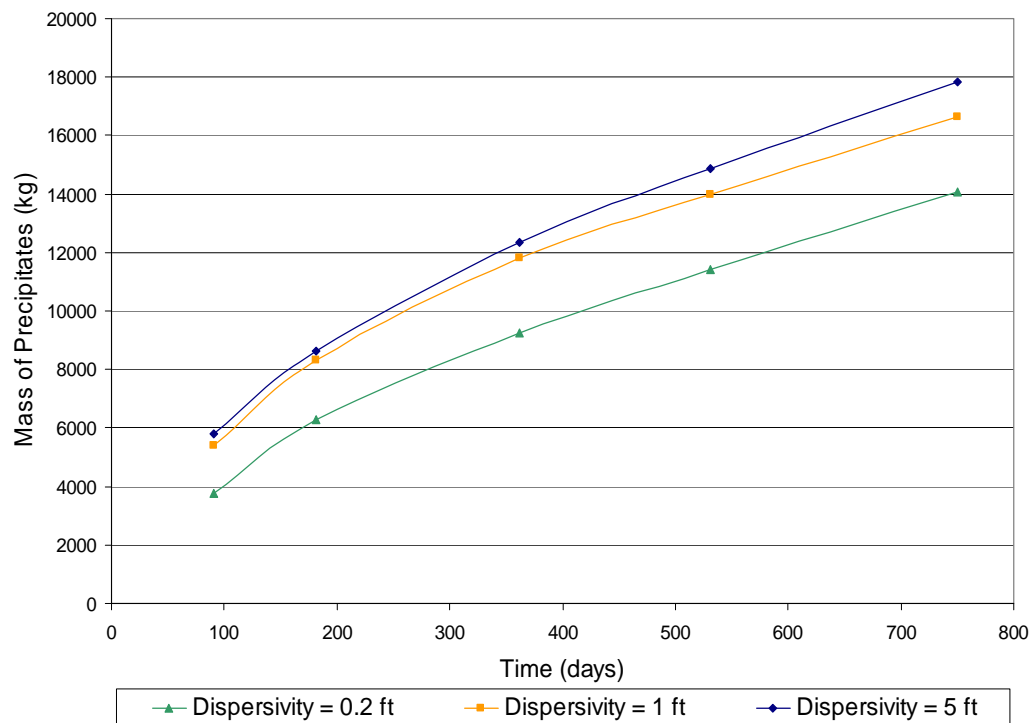
Figure 6.18: Mass of Calcium Carbonate precipitate in the formation at different
dispersivities at the end of the chemicals injection
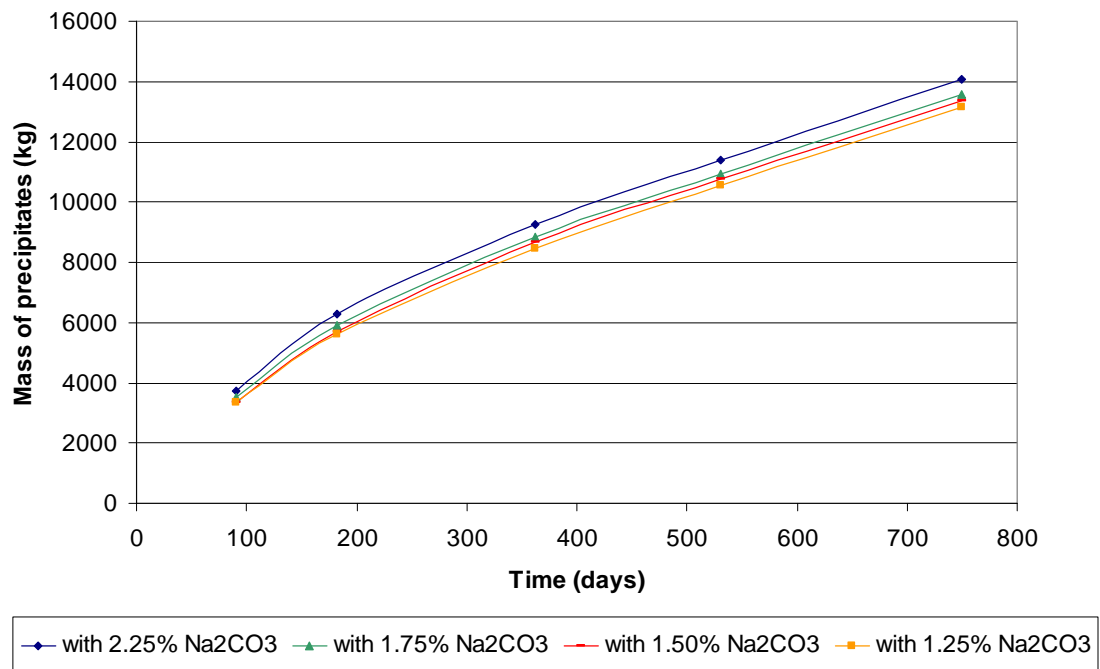
Figure 6.19: Mass of Calcium Carbonate precipitate in the formation at different alkali concentrations at the end of the chemicals injection using a dispersivity of 0.2 ft
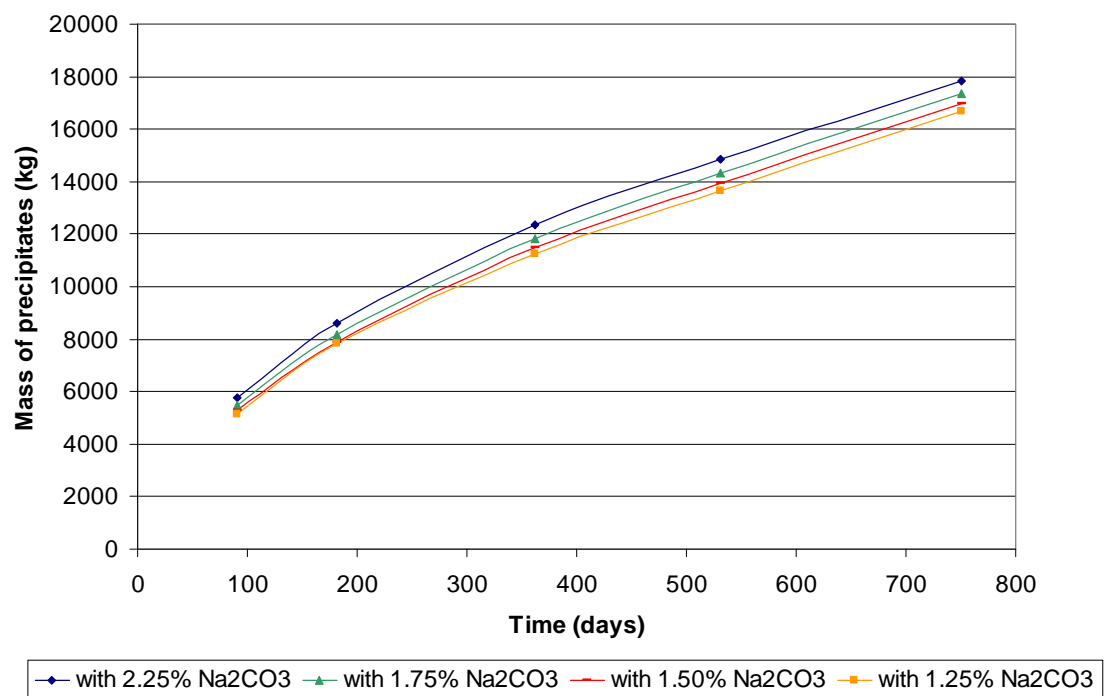
Figure 6.20: Mass of Calcium Carbonate precipitate in the formation at different alkali concentrations at the end of the chemicals injection using a dispersivity of 5.0 ft

Chapter 7: Summary and Conclusions

This chapter presents a brief summary of this research as well as discusses some of the main conclusions drawn and knowledge gained from this study.

7.1 SUMMARY

This overall objective of this research was to gain an insight into the challenges faced during chemical flooding under high hardness conditions. Such conditions are usually encountered when the formation brine and/or the injection brine contain high concentrations of calcium and magnesium ions. Different aspects of this problem were studied through a combination of laboratory experiments as well as simulation studies.

The first part of this research was aimed at designing an optimal chemical EOR formulation for a reservoir whose formation brine had high hardness content. An initial surfactant polymer formulation was designed through phase behavior experiments using surfactants which have been proven to perform well with brines of high salinity and hardness (Flaaten et al., 2008). This formulation was tested through core flooding experiments and was found to recover nearly 98% of the residual oil in the core. However, the surfactant adsorption was found to be on the higher side (0.294 mg/gm rock). In an effort to reduce this, an alkali surfactant polymer formulation was designed using the novel, hardness tolerant alkali, sodium metaborate. This formulation was tested in a core flooding experiment. Precipitation was encountered in the ASP slug. Experiments performed to determine the cause of the precipitation identified the precipitating species was identified as calcium sulfate, formed due to the incompatibility between the co-surfactant, which had an excess sulfate ion concentration, and the hard

formation brine. Reduction in the calcium content of the synthetic formation brine resulted in a clear ASP slug which was used for chemical flooding the core.

The second part of this research sought to understand the factors affecting the performance of novel alkali and chelating agents like sodium metaborate and tetrasodium EDTA with respect to their ability to sequester divalent ions in the form of soluble complexes. The computer program, PHREEQC was used to simulate the geochemical species in solution. Two aspects of this problem were studied, namely the extent of divalent ion sequestration under different conditions and the tolerance limits to calcium and magnesium ions in the presence of these chemicals. The effect of the presence of different solution species on the performance of these alkalis was also studied.

The last part of this research focused on field scale mechanistic simulation studies of geochemical scaling during ASP flooding in the presence of hard formation brines. The principal aim of this study was to determine the quantity and composition of the scales formed in the reservoir as well as the injection and production wells, where the scaling phenomenon has the potential to cause formation damage. This study took into consideration the reactions occurring between the in situ brine, injected fluids and the reservoir rock. A 1-D core flooding experiment was history matched to determine the key simulation parameters which were subsequently used for the field scale simulations. The effect of key reservoir and process parameters like the physical dispersion and the alkali concentration on the extent of scaling in the reservoir and the wells were studied.

7.2 CONCLUSIONS

Several general conclusions can be drawn based on the results discussed in the preceding chapters. These are summarized under the different sub headings below.

7.2.1 Design and Optimization of EOR formulation under high hardness conditions

The combination of the surfactants C_{16-17} 7PO SO_4 and C_{15-18} IOS showed good performance under high hardness conditions of up to 2800 ppm calcium and salinity of up to 65000 ppm TDS. A Surfactant Polymer formulation using these surfactants gave a core flood oil recovery of 98%.

The presence of sulfate ions was shown to be a major limitation of using sodium metaborate as an alkali under high hardness conditions, in spite of its good tolerance for calcium carbonate. The presence of small concentrations (50 ppm) of sulfate ions showed precipitation in the presence of 1500 ppm calcium at a salinity of 35000 ppm TDS. Reducing the calcium concentration to 750 ppm gave a clear solution without precipitation showing that the calcium tolerance in the presence of 50 ppm sulfate ions is at least 750 ppm calcium at a total salinity of about 35000 ppm TDS.

7.2.2 Simulation of Geochemical Species in Aqueous Solutions

Sodium metaborate formed soluble complexes with the calcium and magnesium ions under alkaline pH conditions. No complexes were formed under acidic or neutral pH conditions. Calcium ions formed soluble complexes with sodium metaborate more easily as compared to magnesium ions. The proportion of calcium/magnesium ions that was present in the chelated form was found to be a strong function of the concentrations of the calcium/magnesium ions, sodium metaborate, sulfate ions and the solution pH. This proportion increased with an increase in the sodium metaborate concentration and the solution pH and decreased with an increase in the concentration of the sulfate, calcium and magnesium ions. The major precipitating species in the presence of sodium metaborate when the calcium/ magnesium ion concentrations exceeded the corresponding tolerance limits were the respective carbonates and sulfates, along with magnesium

238

hydroxide. The predicted tolerance limits showed good matches with the corresponding experimental observations under different conditions at room temperature. However, at higher temperatures, significant deviations were observed from the experimental results.

Tetrasodium EDTA (Na_4EDTA) formed soluble complexes more easily with calcium ions as compared to that with magnesium ions. The fraction of calcium/ magnesium ions chelated was found to be a strong function of the solution temperature. Moreover, this fraction increased with an increase in the Na_4EDTA concentration and decreased with an increase in the calcium/ magnesium ion concentration. The major precipitating species in the presence of Na_4EDTA when the calcium/ magnesium ion concentrations exceeded the corresponding tolerance limits were the respective carbonates, along with magnesium hydroxide.

7.2.3 Mechanistic Simulations of Scaling during ASP flooding

A large quantity of calcium carbonate precipitates were found to be deposited as scale for the reservoir studied, both in the formation and in the injection and production wells. An increase in the physical dispersivity resulted in higher precipitation in the formation. However, the quantity of precipitates in the injection and production wells was not very sensitive to the change in dispersivity. Reduction in the alkali concentration resulted in a decrease in the total quantity of precipitates in the formation. The sensitivity to the alkali concentration was found to be more when higher dispersivity values were used. However, the quantity of precipitates in the injection and production wells was not very sensitive to the change in the alkali concentration, irrespective of the dispersivity values used.

An important limitation of this study was that the geochemical model used for the simulations did not take into account the reactions occurring between the calcium ions,

and the sulfate and sulfonate ions present in the surfactant molecules to form calcium sulfate and calcium sulfonate respectively. These reactions compete with the precipitation reaction between the calcium and the carbonate ions to form calcium carbonate. Laboratory experiments have shown in many cases that no precipitation is seen indicating that the reaction between the calcium and the sulfate/sulfonate reaction dominates over the precipitation reaction. The extent of the precipitation reaction is dependent on the whether an excess of sulfate/sulfonate groups or the calcium ions are present in the solution. Precipitation occurs only when an excess of calcium ions are present. Further research to determine the effect of these reactions on the precipitation of calcium carbonate scale in the reservoir and the wells is recommended.

Appendix: UTCHEM and EQBATCH Input Files

1. EQBATCH Input file for the base case field scale run in Chapter 6

```
Field 'M' (* TITLE *)
3 1 1  (* IREACT ICHARGE IMG *)
6 14 1 3 2 (* NNELET NFLD NSLD NSORB NACAT *)
6 1 2 9 (* NIAQ NEX NSLWL NSURF1 *)
4 3 1 0 2 (* NH NNA NCA NMG NCARB *)
0 0 0 (* NALU NSILI NOXYG *)
5  (* NACD *)
CALCIUM
CARBON (AS CARBOBATES)
SODIUM
HYDROGEN (REACTIVE)
Oleic acid
clorine  (* ELEMNT *)
2  -2  1  1 -1 -1 (* ELCRG *)
HYDROGEN ION
SODIUM ION
CALCIUM ION
CARBONATE ION
HAo
WATER
Ca(OH)+
Ca(HCO3)+
A-
OH-
HCO3-
H2CO3
CaCO3
HAw  (* FLDSPS *)
Calcium Carbonate (solid) (* SLDSPS *)
SORBED HYDROGEN ION
SORBED SODIUM ION
SORBED CALCIUM ION  (* SORBSPS *)
SURF ASSO SODIUM ION
SURF ASSO CALCIUM ION  (* ACATSPS *)
3 (* NSORBX *)
0   0   1   0   0   0   1   1   0   0   0   0   1   0
0   0   0   1   0   0   0   1   0   0   1   1   1   0
0   1   0   0   0   0   0   0   0   0   0   0   0   0
1   0   0   0   1   2   1   1   0   1   1   2   0   1
0   0   0   0   1   0   0   0   1   0   0   0   0   1    (* AR *)
1
1
0
0
0 (* BR *)
0   0   1
0   0   0
```

```
0   1   0
1   0   0
0   0   0   (* DR *)
0   1
0   0
1   0
0   0
0   0 (* ER *)
1   0   0   0   0   0   0   0   0   0   0
0   1   0   0   0   0   0   0   0   0   0
0   0   1   0   0   0   0   0   0   0   0
0   0   0   1   0   0   0   0   0   0   0
0   0   0   0   1   0   0   0   0   0   0
0   0   0   0   0   1   0   0   0   0   0
-1  0   1   0   0   0   0   0   0   0   0
1   0   1   1   0   0   0   0   0   0   0
-1  0   0   0   1   0   0   0   0   0   0
-1  0   0   0   0   0   0   0   0   0   0
1   0   0   1   0   0   0   0   0   0   0
2   0   0   1   0   0   0   0   0   0   0
0   0   1   1   0   0   0   0   0   0   0
0   0   0   0   1   0   0   0   0   0   0
0   0   0   0   0   0   1   0   0   0   0
0   0   0   0   0   0   0   1   0   0   0
0   0   0   0   0   0   0   0   1   0   0
0   0   0   0   0   0   0   0   0   1   0
0   0   0   0   0   0   0   0   0   0   1   (* BB *)
0   0   1   1   0   0   (* EXSLD *)
1
1
2
-2
0
0
1
1
-1
-1
-1
0
0
0   (* CHARGE *)
1
1
1
1
1
1
3.4906E-12
2.3259E+11
9.59E-13
1.2086E-13
1.3791E+10
```

```
2.7089E+16
8.3100E+02
9.59E-05     (* KEQ *)
1. 1. 2. (* SCHARGE *)
7.93  2.7+06  (* KEX *)
0      2      -1     0      0      0      0      -2     1      0      0
-1     1      0      0      0      0      1      -1     0      0      0    (* EXEX *)
-1.  0.  0.(* REDUC *)
0.033  (* EXCAI *)
1.661e-9  (* SPK *)
1      2       (* CHACAT *)
0.4   (* ACATK *)
0      2       -1     0      0    0    0    0    0    -2   1      (* EXACAT *)
0.128636  0.0 (*C50, Csurf*)
0.005676  0.001 0.111835  111.11 0.005581 (*CELFLT 1,NELEMENT-1*)
0.001  (*CSLD(I), I=1,NSLD*)
0.020  0.005  0.00015   (* CSORBI *)
0.1200077231590e-07  0.01  0.1e-04
0.3092684582095e-03  1.13e-3
55.49999314650  1.0e-06  1.0e-04  1.0e-04   1.0e-04  1.0e-04   (*CIND*)
0.65 (*S1*)
500
```

2. UTCHEM Input file for the base case field scale run in Chapter 6

```
CC*********************************************************************
CC                                                                   *
CC    BRIEF DESCRIPTION OF DATA SET: UTCHEM (VERSION 9.97)           *
CC                                                                   *
CC*********************************************************************
CC                                                                   *
CC  PILOT SCALE ALKALI SURFACTANT POLYMER FLOODING                   *
CC                                                                   *
CC  LENGTH (FT) :   754.4 feet        PROCESS : A/S/P FLOODING       *
CC  THICKNESS (FT) :  156.49 feet     INJ. PRESSURE (PSI) :          *
CC  WIDTH (FT) : 754.4 feet           COORDINATES : CARTESIAN        *
CC  POROSITY :                                                       *
CC  GRID BLOCKS : 15 X 15 X 36                                       *
CC                                                                   *
CC*********************************************************************
CC
CC*********************************************************************
CC                                                                   *
CC    RESERVOIR DESCRIPTION                                          *
CC                                                                   *
CC*********************************************************************
CC
CC
*----RUNNO
m11a
CC
CC
*----HEADER
```

```
Reservoir M field scale Alkali Surfactant Polymer flooding
CC  IMODE=1 for initial, 2 for restart  IREACT=3 for ASP, =0 for WF or
PF
CC SIMULATION FLAGS
*--- IMODE IMES IDISPC ICWM ICAP IREACT IBIO ICOORD ITREAC ITC IGAS
IENG
        1    4    3    0    0    3    0    1    0    0    0
0
CC
CC NUMBER OF GRID BLOCKS AND FLAG SPECIFIES CONSTANT OR VARIABLE GRID
SIZE
*--- NX   NY  NZ   IDXYZ   IUNIT
    15   15  36    2        0
CC
CC  CONSTANT GRID BLOCK SIZE IN X, Y, AND Z
*----DX
  131.2 65.6  11*32.8 65.6 131.2
cc
cc
*--- dy
  131.2 65.6  11*32.8 65.6 131.2
cc
cc
*--- dz
 3.34 4.46 5.57 3.36 4.69
 3.34 4.48 4.46 4.50 4.41
 4.39 4.80 2.23 3.24 4.40
 3.36 3.65 3.66 5.61 4.51
 5.61 5.68 5.39 4.49 5.54
 4.2 3.38 5.63 4.50 4.66
 4.66 3.2 4.52 5.65 4.53
 3.39
CC
CC TOTAL NO. OF COMPONENTS, NO. OF TRACERS, NO. OF GEL COMPONENTS
*----n    no    ntw    nta    ngc    ng    noth
    12    0     0      0      4      0     0
CC
CC
*---- SPNAME(I),I=1,N
WATER
OIL
SURFACTANT
POLYMER
ANION
CALCIUM
alc1
alc2
CARBONATE
SODIUM
HYDROGEN
pet acid
CC
CC FLAG INDICATING IF THE COMPONENT IS INCLUDED IN CALCULATIONS OR NOT
```

```
*----ICF(KC) FOR KC=1,N
     1  1  0  0  1  1   0  0  1  1   1 1
CC
CC*********************************************************************
CC                                                                   *
CC    OUTPUT OPTIONS                                                  *
CC                                                                   *
CC*********************************************************************
CC  ICUM=0 for output in days, =1 for PV
CC  ISTOP=0 for TMAX & TINJ in days, =1 for PV
CC 3.2.1 FLAG TO WRITE TO UNIT 3,FLAG FOR PV OR DAYS TO PRINT OR TO
STOP THE RUN
*---- ICUMTM  ISTOP  IOUTGMS
        0       0       0
CC
CC 3.2.2 FLAG INDICATING IF THE PROFILE OF KCTH COMPONENT SHOULD BE
WRITTEN
*---- IPRFLG(KC),KC=1,N
     1  1  1  1  1  1  0  0  1  1  1  1  1
CC
CC 3.2.3 FLAG FOR PRES.,SAT.,TOTAL CONC.,TRACER CONC.,CAP.,GEL,
ALKALINE PROFILES
*---- IPPRES IPSAT IPCTOT IPBIO IPCAP IPGEL IPALK IPTEMP IPOBS
        1      1      1      0     0     0     1      0      0
CC
CC 3.2.4 FLAG FOR WRITING SEVERAL PROPERTIES TO UNIT 4 (Prof)
*---- ICKL IVIS IPER ICNM ICSE IHYSTP IFOAMP INONEQ
        1    1    1    1    1     0     0     0
CC
CC 3.2.5 FLAG  for variables to PROF output file
*---- IADS IVEL IRKF IPHSE
        1    0    1    0
CC
CC*********************************************************************
CC                                                                   *
CC    RESERVOIR PROPERTIES                                           *
CC                                                                   *
CC*********************************************************************
CC
CC
CC MAX. SIMULATION TIME ( days)
*---- TMAX
     1000
CC
CC ROCK COMPRESSIBILITY (1/PSI), STAND. PRESSURE(PSIA)
*----COMPR   PSTAND
     3.6e-6     1620
CC
CC FLAGS INDICATING CONSTANT OR VARIABLE POROSITY, X,Y,AND Z
PERMEABILITY
*----IPOR1 IPERMX IPERMY IPERMZ  IMOD   ITRANZ  INTG
       4      4      3      3      1       0      1
CC
```

245

```
CC Y DIRECTION PERMEABILITY IS DEPENDENT ON X DIRECTION PERMEABILITY
*---- CONSTANT PERMEABILITY MULTIPLIER FOR Y DIRECTION PERMEABILITY
         1
CC
CC Z DIRECTION PERMEABILITY IS DEPENDENT ON X DIRECTION PERMEABILITY
*---- CONSTANT PERMEABILITY MULTIPLIER FOR Z DIRECTION PERMEABILITY
         0.3
CC
CC FLAG FOR CONSTANT OR VARIABLE DEPTH, PRESSURE, WATER SATURATION
*----IDEPTH  IPRESS  ISWI  ICWI
       4        1       4    -1
CC
CC INITIAL PRESSURE (PSIA)
*----PINIT    DEPTH
      1436    2632
cc
cc
*--- IMpor  IMkx  IMky  IMkz  IMsw
     1     0     0     0  0
cc
cc
*--- nmod
    4
cc
cc
*--- i1    i2   j1  j2  k1 k2  ifact   factX
     1     15   1   1   1  36    2        1
     1     1    2   14  1  36    2        1
     15    15   2   14  1  36    2        1
     2     14   14  15  1  36    2        1
CC
CC CONSTANT CHLORIDE AND CALCIUM CONCENTRATIONS (MEQ/ML)
*----C50       C60
    0.1286    0.01844
CC
CC******************************************************************
CC                                                                *
CC    PHYSICAL PROPERTY DATA                                      *
CC                                                                *
CC******************************************************************
CC
CC 3.4.1 OIL CONC. AT PLAIT POINT FOR TYPE II(+)AND TYPE II(-), CMC
CC                      CMC
*---- c2plc  c2prc   epsme   ihand
        0      1     0.001      0
CC
CC 3.4.2 flag indicating type of phase behavior parameters
*---- ifghbn=0 for input height of binodal curve; =1 for input sol.
ratio
        0
CC 3.4.3 SLOPE AND INTERCEPT OF BINODAL CURVE AT ZERO, OPT., AND 2XOPT
SALINITY
CC FOR ALCOHOL 1
```
246

```
*---- hbns70   hbnc70   hbns71   hbnc71   hbns72   hbnc72
        0    0.065      0     0.030     0     0.055
CC 3.4.5 SLOPE AND INTERCEPT OF BINODAL CURVE AT ZERO, OPT., AND 2XOPT
SALINITY
CC FOR ALCOHOL 2
*---- hbns80   hbnc80   hbns81   hbnc81   hbns82   hbnc82
        0    0.012      0     0.003     0     0.012
CC
CC 3.4.6 LOWER AND UPPER EFFECTIVE SALINITY FOR ALCOHOL 1 AND ALCOHOL 2
*---- csel7   cseu7   csel8   cseu8
      0.33    1.1     0.20     0.45
CC 3.4.7 THE CSE SLOPE PARAMETER FOR CALCIUM AND ALCOHOL 1 AND ALCOHOL
2
CC    Ca      Alcohol#1  Alcohol#2
*---- beta6     beta7     beta8
CC
CC 3.4.8 FLAG FOR ALCOHOL PART. MODEL AND PARTITION COEFFICIENTS
*---- ialc   opsk7o   opsk7s   opsk8o   opsk8s
        0       0        0        0        0
CC  these are used only for alcohol partitioning in a two alcohol
system:
CC 3.4.9 NO. OF ITERATIONS, AND TOLERANCE
*---- nalmax     epsalc
        20       0.0001
CC 3.4.10 ALCOHOL 1 PARTITIONING PARAMETERS IF IALC=1
CC   aq-oleic   aq-oleic   surf-oleic
*---- akwc7     akws7     akm7      ak7      pt7
       4.671    1.79       48      35.31    0.222
CC
CC 3.4.11 ALCOHOL 2 PARTITIONING PARAMETERS IF IALC=1
*---- akwc8     akws8     akm8     ak8      pt8
        0         0        0        0        0
CC
CC 3.4.22 ift model flag
*----  ift=0 for Healy&Reed; =1 for Chun Huh correl.
        1
CC 3.4.24 INTERFACIAL TENSION PARAMETERS
CC   typ=.1-.35   typ=5-20
*---- chuh         ahuh
      0.3           10
CC
CC     units of log 10 dynes/cm = mN/m
*---- xiftw
       1.146
CC 3.4.26 ORGANIC MASS TRANSFER FLAG
CC   imass=0 for no oil sol. in water.  icorr=0 for constant MTC
*---- imass   icor
        0       0
cc
cc
*--- IWALT    IWALF
       0        0
CC 3.4.31 CAPILLARY DESATURATION PARAMETERS FOR PHASE 1, 2, AND 3
                          247
```

```
CC                    AQ      OLEIC     ME
*---- itrap       t11      t22       t33
        1        1865     70000     364.2
CC
CC  3.4.32 FLAG FOR RELATIVE PERMEABILITY AND CAPILLARY PRESSURE MODEL
*---- iperm=0    irtype
      0          0
CC
CC 3.4.35 FLAG FOR CONSTANT OR VARIABLE REL. PERM. PARAMETERS
*---- isrw     iprw     iew
       0        0        0
CC
CC CONSTANT RES. SATURATION OF PHASES 1,2,AND 3 AT LOW CAPILLARY NO.
*----S1RWC   S2RWC   S3RWC
     0.028   0.2     0.028
CC
CC CONSTANT ENDPOINT REL. PERM. OF PHASES 1,2,AND 3 AT LOW CAPILLARY
NO.
*----P1RW  P2RW  P3RW
     0.6  0.93   0.6
CC
CC CONSTANT REL. PERM. EXPONENT OF PHASES 1,2,AND 3 AT LOW CAPILLARY
NO.
*----E1W     E2W  E3W
     2.5     4.0 2.5
CC
CC  RES. SATURATION OF PHASES 1,2,AND 3 AT HIGH CAPILLARY NO.
*----S1RC   S2RC   S3RC
     .0     .0     .0
CC
CC ENDPOINT REL. PERM. OF PHASES 1,2,AND 3 AT HIGH CAPILLARY NO.
*----P1RC    P2RC  P3RC
     1.0     1.0   1.0
CC
CC REL. PERM. EXPONENT OF PHASES 1,2,AND 3 AT HIGH CAPILLARY NO.
*----E13CW  E23C  E31C
     1.0     1.0   1.0
CC Stars  19 cp
CC   water    oil      =0 for isothermal modeling
*---- VIS1     VIS2    TSTAND
      0.5      19       0
CC
CC 3.4.80 COMPOSITIONAL PHASE VISCOSITY PARAMETERS for microemulsion
*----   ALPHAV1   ALPHAV2   ALPHAV3   ALPHAV4   ALPHAV5
          0.5       0.5       0.1       0.1       0.1
CC
CC 3.4.81 PARAMETERS TO CALCULATE POLYMER VISCOSITY AT ZERO SHEAR RATE
*---- AP1      AP2       AP3
     142      265       350
CC
CC 3.4.82 PARAMETER TO COMPUTE CSEP,MIN. CSEP, AND SLOPE OF LOG VIS.
VS. LOG CSEP
*---- BETAP    CSE1     SSLOPE
```

```
        10        0.01      -0.4922
CC
CC 3.4.83 PARAMETER FOR SHEAR RATE DEPENDENCE OF POLYMER VISCOSITY
*---- GAMMAC   GAMHF   POWN   ipmod   ISHEAR   RWEFF   GAMHF2
       16.0     3.275   1.67     0        1       0.3     0.0
CC
CC 3.4.84  FLAG FOR POLYMER PARTITIONING, PERM. REDUCTION PARAMETERS
*---- IPOLYM    EPHI3    EPHI4    BRK     CRK       rkcut
        1        1.0      0.9     100     0.05       10
CC
CC   if IDEN=1 ignore gravity effect; =2 then include gravity effect
*---- DEN1     DEN2     DEN23    DEN3     DEN7     DEN8     IDEN
      0.44    0.4065   0.4065   0.42     0.346      0        2
CC   ISTB=0:BOTTOMHOLE CONDITION , 1: STOCK TANK
CC 3.4.93 FLAG FOR CHOICE OF UNITS when printing
*----- ISTB
         1
CC  3.4.94 FORMATION VOLUME FACTOR - may set all these to 1.0 and just
factor in post-proc
CC        water   oil         me
*----- FVF(I), I=1 TO MXP (IGAS=0 MXP=3,IGAS=1 MXP=4)
       1.00265         1.057        1
CC
CC 3.4.95 COMPRESSIBILITY FOR VOL. OCCUPYING COMPONENTS 1,2,3,7,AND 8
*----   COMPC(1)         COMPC(2)    COMPC(3)  COMPC(7)  COMPC(8)
       2.7e-6          4.96e-5        0         0         0
CC  IOW=0 water wet, =1 oil wet, =2 mixed wet
CC 3.4.99 CONSTANT OR VARIABLE PC PARAM., WATER-WET OR OIL-WET PC CURVE
FLAG
*---- ICPC     IEPC     IOW
       0        0        0
CC    CPC = 0 for no capillary pressure
CC 3.4.100 CAPILLARY PRESSURE PARAMETER, CPC0
*---- CPC0
       0
CC
*---- EPC0
      2.0
cc
CC 3.4.117 MOLECULAR DIFFUSION COEF. KCTH COMPONENT IN PHASE 1
*---- D(KC,1),KC=1,N
        0   0   0   0   0   0   0   0   0   0   0   0
CC
CC 3.4.118 MOLECULAR DIFFUSION COEF. KCTH COMPONENT IN PHASE 2
*---- D(KC,2),KC=1,N
        0   0   0   0   0   0   0   0   0   0   0   0
CC
CC 3.4.119 MOLECULAR DIFFUSION COEF. KCTH COMPONENT IN PHASE 3
*---- D(KC,3),KC=1,N
        0   0   0   0   0   0   0   0   0   0   0   0
CC
CC 3.4.121 LONGITUDINAL AND TRANSVERSE DISPERSIVITY OF PHASE 1
*---- ALPHAL(1)     ALPHAT(1)
```

249

```
          0.2             0.001
CC
CC 3.4.122 LONGITUDINAL AND TRANSVERSE DISPERSIVITY OF PHASE 2
*---- ALPHAL(2)     ALPHAT(2)
          0.2             0.001
CC
CC 3.4.124 LONGITUDINAL AND TRANSVERSE DISPERSIVITY OF PHASE 3
*---- ALPHAL(3)     ALPHAT(3)
          0.2             0.001
CC
CC 3.4.125 flag to specify organic adsorption calculation
*---- iadso=0 if organic adsorption is not considered
           0
CC
CC 3.4.130 SURFACTANT AND POLYMER ADSORPTION PARAMETERS
*---- AD31   AD32  B3D  AD41   AD42  B4D  IADK  IADS1   FADS   REFK
      1.5    0.1  1000  2.0    0.1  100    0      0      0     50
CC
CC 3.4.131 PARAMETERS FOR CATION EXCHANGE OF CLAY AND SURFACTANT
*---- QV       XKC     XKS      EQW
      0         0       0         804
 2  1
   7   13   13  0.1
  0.2    0.45
   6 14  1  3  2  1
  6  1  2  9
  4  3  1  0  2
  0  0  0
  5
CALCIUM                             2.00
CARBON (AS CARBOBATES)             -2.00
SODIUM                              1.00
HYDROGEN (REACTIVE)                 1.00
Oleic acid                         -1.00
clorine  (* ELEMNT *)              -1.00
 HYDROGEN ION
 SODIUM ION
 CALCIUM ION
 CARBONATE ION
 HAo
 WATER
 Ca(OH)+
 Ca(HCO3)+
 A-
 OH-
 HCO3-
 H2CO3
 CaCO3
 HAw  (* FLDSPS *)
 Calcium Carbonate (solid) (* SLD *)
 SORBED HYDROGEN ION
 SORBED SODIUM ION
 SORBED CALCIUM ION  (* SORBSPS *)
```

```
 SURF ASSO SODIUM ION
 SURF ASSO CALCIUM ION  (* ACATSP *)
 3
 0.  0.  1.  0.  0.  0.  1.  1.  0.  0.  0.  0.  1.  0.
 0.  0.  0.  1.  0.  0.  0.  1.  0.  0.  1.  1.  1.  0.
 0.  1.  0.  0.  0.  0.  0.  0.  0.  0.  0.  0.  0.  0.
 1.  0.  0.  0.  1.  2.  1.  1.  0.  1.  1.  2.  0.  1.
 0.  0.  0.  0.  1.  0.  0.  0.  1.  0.  0.  0.  0.  1.
 1.
 1.
 0.
 0.
 0.
 0.  0.  1.
 0.  0.  0.
 0.  1.  0.
 1.  0.  0.
 0.  0.  0.
 0.  1.
 0.  0.
 1.  0.
 0.  0.
 0.  0.
 1.0  0.0  0.0  0.0  0.0  0.0  0.0  0.0  0.0  0.0  0.0
 0.0  1.0  0.0  0.0  0.0  0.0  0.0  0.0  0.0  0.0  0.0
 0.0  0.0  1.0  0.0  0.0  0.0  0.0  0.0  0.0  0.0  0.0
 0.0  0.0  0.0  1.0  0.0  0.0  0.0  0.0  0.0  0.0  0.0
 0.0  0.0  0.0  0.0  1.0  0.0  0.0  0.0  0.0  0.0  0.0
 0.0  0.0  0.0  0.0  0.0  1.0  0.0  0.0  0.0  0.0  0.0
-1.0  0.0  1.0  0.0  0.0  0.0  0.0  0.0  0.0  0.0  0.0
 1.0  0.0  1.0  1.0  0.0  0.0  0.0  0.0  0.0  0.0  0.0
-1.0  0.0  0.0  0.0  1.0  0.0  0.0  0.0  0.0  0.0  0.0
-1.0  0.0  0.0  0.0  0.0  0.0  0.0  0.0  0.0  0.0  0.0
 1.0  0.0  0.0  1.0  0.0  0.0  0.0  0.0  0.0  0.0  0.0
 2.0  0.0  0.0  1.0  0.0  0.0  0.0  0.0  0.0  0.0  0.0
 0.0  0.0  1.0  1.0  0.0  0.0  0.0  0.0  0.0  0.0  0.0
 0.0  0.0  0.0  0.0  1.0  0.0  0.0  0.0  0.0  0.0  0.0
 0.0  0.0  0.0  0.0  0.0  0.0  1.0  0.0  0.0  0.0  0.0
 0.0  0.0  0.0  0.0  0.0  0.0  0.0  1.0  0.0  0.0  0.0
 0.0  0.0  0.0  0.0  0.0  0.0  0.0  0.0  1.0  0.0  0.0
 0.0  0.0  0.0  0.0  0.0  0.0  0.0  0.0  0.0  1.0  0.0
 0.0  0.0  0.0  0.0  0.0  0.0  0.0  0.0  0.0  0.0  1.0
 0.0  0.0  1.0  1.0  0.0  0.0
 1.0  1.0  2.0 -2.0  0.0  0.0  1.0  1.0 -1.0 -1.0 -1.0  0.0
 0.0  0.0
 1.0  1.0  2.0
0.1000000000000E+01 0.1000000000000E+01 0.1000000000000E+01
0.1000000000000E+01 0.1000000000000E+01 0.1000000000000E+01
0.3490600000000E-11 0.2325900000000E+12 0.5137089283792E-12
0.1208600000000E-12 0.1379100000000E+11 0.2708900000000E+17
0.8310000000000E+03 0.5137089283792E-04
0.7930000000000E+01 0.2700000000000E+07
 0.0  2.0 -1.0  0.0  0.0  0.0  0.0 -2.0  1.0  0.0  0.0
```

```
-1.0  1.0  0.0  0.0  0.0  0.0  1.0 -1.0  0.0  0.0  0.0
-1.0  0.0
0.2144999414830E-01
0.1661000000000E-08
 1.0  2.0
0.4000000000000E+00
 0.0  2.0 -1.0  0.0  0.0  0.0  0.0  0.0  0.0 -2.0  1.0
0.1044745513306E-07 0.2728223436662E-24
0.1286360000000E+00 0.1601911305646E-01
0.6427057728920E-02
0.1143201355420E+00
0.1110995748091E+03
0.5456130308434E-06
0.1041768102803E-01
0.5122449140909E-06 0.1143201250946E+00 0.7810226418833E-02
0.2126698908491E-06 0.5580454386969E-02 0.5554463471084E+02
0.0000000000000E+00
0.1977636867009E-01 0.1634661451748E-02 0.1948201323362E-04
0.9999997271936E+00 0.9948181509115E+00
0.1000000000000E-07 0.5000000000000E+03
CC
CC********************************************************************

CC                                                                  *
CC     WELL DATA                                                    *
CC                                                                  *
CC********************************************************************
CC
CC
CC FLAG FOR PRESSURE CONST. BOUNDARIES
*---- IBOUND  IZONE
        0      0
CC
CC TOTAL NUMBER OF WELLS, WELL RADIUS FLAG, FLAG FOR TIME OR COURANT
NO.
*----NWELL    IRO    ITIME   NWREL
      5        2      1       5
CC
CC WELL ID,LOCATIONS,AND FLAG FOR SPECIFYING WELL TYPE, WELL RADIUS,
SKIN
*----IDW   IW   JW   IFLAG  RW   SWELL   IDIR   IFIRST   ILAST   IPRF
      1    8    8    4     0.26  0.      3      1        36      1
cc
cc
*--- kprf
     1 1 1 1 0 1 1 1 1 0 0 0 1 1 0 1 0 0 1 1 1 0 0 1 0 0 1 1 1 0 0 0 1 1 1 1
CC
CC WELL NAME
*---- WELNAM
PL-1
CC
CC ICHEK MAX. AND MIN. ALLOWABLE BOTTOMHOLE PRESSURE AND RATE
*----ICHEK   PWFMIN   PWFMAX  QTMIN   QTMAX
```

```
       0          950         5000     -0.0     -8425.
CC
CC WELL ID, LOCATION, AND FLAG FOR SPECIFYING WELL TYPE, WELL RADIUS,
SKIN
*----IDW  IW   JW   IFLAG    RW      SWELL  IDIR  IFIRST   ILAST    IPRF
     2   3    3     1       0.26    0.      3      1       36       1
cc
cc
*--- kprf
    1 1 1 1 0 1 1 1 1 0 0 1 1 0 1 0 0 1 1 1 0 1 1 1 0 1 1 1 0 0 0 1 1 1 1
CC
CC WELL NAME
*---- WELNAM
IL-1
CC
CC MAX. AND MIN. ALLOWABLE BOTTOMHOLE PRESSURE AND RATE
*----ICHEK  PWFMIN   PWFMAX   QTMIN   QTMAX
     0     0.0      2500     0.0     4211.
CC
CC WELL ID, LOCATION, AND FLAG FOR SPECIFYING WELL TYPE, WELL RADIUS,
SKIN
*----IDW   IW   JW   IFLAG    RW      SWELL  IDIR  IFIRST   ILAST    IPRF
     3   13    3     1       0.26    0.      3      1       36       1
cc
cc
*--- kprf
   1 1 1 1 0 1 1 1 1 0 0 0 1 0 0 1 0 0 1 1 1 1 0 1 1 0 1 1 1 0 0 0 1 1
1 1
CC
CC WELL NAME
*---- WELNAM
IL-2
CC
CC MAX. AND MIN. ALLOWABLE BOTTOMHOLE PRESSURE AND RATE
*----ICHEK   PWFMIN   PWFMAX   QTMIN   QTMAX
      0     0.0      2500.    0.0     4211.
CC
CC WELL ID, LOCATION, AND FLAG FOR SPECIFYING WELL TYPE, WELL RADIUS,
SKIN
*----IDW   IW   JW  IFLAG    RW     SWELL   IDIR  IFIRST   ILAST    IPRF
     4    3   13    1       0.26   0.       3      1       36       1
cc
cc
*--- kprf
   1 1 1 1 0 1 1 1 1 0 1 0 0 0 1 1 0 0 1 1 1 0 1 1 1 0 1 1 1 0 0 0 1 1 1 1
CC
CC WELL NAME
*---- WELNAM
IL-3
CC
CC MAX. AND MIN. ALLOWABLE BOTTOMHOLE PRESSURE AND RATE
*----ICHEK   PWFMIN   PWFMAX   QTMIN   QTMAX
      0     0.0      2500.    0.0      4211.
```

```
CC
CC WELL ID, LOCATION, AND FLAG FOR SPECIFYING WELL TYPE, WELL RADIUS,
SKIN
*----IDW  IW   JW   IFLAG    RW     SWELL  IDIR  IFIRST   ILAST    IPRF
     5   13   13     1      0.26    0.      3      1        36       1
cc
cc
*--- kprf
    1 1 1 1 1 1 1 1 0 1 0 1 0 0 1 1 1 1 1 1 1 1 0 1 1 0 1 1 1 1 1 0 1 1 1 1
CC
CC WELL NAME
*---- WELNAM
IL-4
CC
CC MAX. AND MIN. ALLOWABLE BOTTOMHOLE PRESSURE AND RATE
*----ICHEK  PWFMIN   PWFMAX  QTMIN   QTMAX
     0   0.0      2500    0.0     4211.
CC
CC ID,
*----ID   -q
    1   -8422
CC
CC ID,INJ. RATE AND INJ. COMP. FOR RATE CONS. WELLS FOR EACH PHASE
(L=1,3)
*---- ID   QI(M,L) water oil  surf polymer  anion    calcium    alc1
alc2 carbonat  sodium    hyd      petA
     2    2105.5 0.997 0.  0.003 0.3      0.08479  0.001     0.
0.   0.432814  0.513468  111.12 0.0
     2       0.   0.    0.  0.    0.       0.       0.        0.
0.      0.        0.    0.       0.
     2       0.   0.    0.  0.    0.       0.       0.        0.
0.      0.        0.    0.       0.
CC
CC ID,INJ. RATE AND INJ. COMP. FOR RATE CONS. WELLS FOR EACH PHASE
(L=1,3)
*---- ID   QI(M,L) water oil  surf polymer  anion    cation    alc1
alc2 carbonat sodium  hyd petA
     3    2105.5 0.997 0.  0.003 0.3      0.08479  0.001     0.
0.   0.432814  0.513468  111.12 0.0
     3       0.   0.    0.  0.    0.       0.       0.        0.
0.      0.        0.    0.       0.
     3       0.   0.    0.  0.    0.       0.       0.        0.
0.      0.        0.    0.       0.
CC
CC ID,INJ. RATE AND INJ. COMP. FOR RATE CONS. WELLS FOR EACH PHASE
(L=1,3)
*---- ID   QI(M,L) water oil  surf polymer  anion    cation    alc1
alc2 carbonat sodium  hyd petA
     4    2105.5 0.997 0.  0.003 0.3      0.08479  0.001     0.
0.   0.432814  0.513468  111.12 0.0
     4       0.   0.    0.  0.    0.       0.       0.        0.
0.   0.        0.    0.       0.
```

```
       4     0.    0.    0.    0.    0.       0.    0.       0.
0.       0.       0.    0.    0.
CC
CC ID,INJ. RATE AND INJ. COMP. FOR RATE CONS. WELLS FOR EACH PHASE
(L=1,3)
*---- ID   QI(M,L) water oil  surf polymer  anion    cation    alc1
alc2 carbonat sodium  hyd petA
       5    2105.5 0.997 0.  0.003 0.3      0.08479  0.001    0.
0.   0.432814   0.513468  111.12 0.0
       5     0.    0.    0.    0.    0.       0.    0.       0.
0.       0.       0.    0.    0.
       5     0.    0.    0.    0.    0.       0.    0.       0.
0.       0.       0.    0.    0.
CC 3.7.8 CUM. INJ. TIME , AND INTERVALS (PV) FOR WRITING TO O/P FILES
           profilesPROF     prodPROF    prodHIST   maps      recovery
*---- TINJ     CUMPR1           CUMHI1      WRHPV      WRPRF      RSTC
     151       30              60         1         30        274
CC
CC 3.7.11 FOR IMES=2 ,THE INI. TIME STEP,CONC. TOLERANCE,MAX.,MIN.
courant numbers
*---- DT       1 2 3 4 5 6 7 8 9 10 11 12 CNMAX   CNMIN
      0.000001  0.01 0.01  8*0.01            0.01 0.01 0.10    0.01
CC
CC FLAG FOR INDICATING BOUNDARY CHANGE
*---- IBMOD
       0
CC
CC  IRO, ITIME, NEW FLAGS FOR ALL THE WELLS
*---- IRO    ITIME      IFLAG
      2      1        4  1  1  1  1
CC
CC  NUMBER OF WELLS CHANGES IN LOCATION OR SKIN OR PWF
*---- NWEL1
         0
CC
CC  NUMBER OF WELLS WITH RATE CHANGES, ID
*---- NWEL2     ID     *10*
      4       2 3 4 5
CC
CC  ID,INJ. RATE AND INJ. COMP. FOR RATE CONS. WELLS FOR EACH PHASE
(L=1,3)
*---- ID   QI(M,L) water oil  surf  polymer  anion    cation    alc1
alc2 carbonat  sodium  hyd    petA
       2    2105.5 1.0   0.  0.0  0.225    0.08479  0.001    0.
0.   0.004143   0.08894  111.12 0.001
       2     0.    0.    0.    0.    0.       0.    0.       0.
0.   0.         0.    0.    0.
       2     0.    0.    0.    0.    0.       0.    0.       0.
0.   0.         0.    0.    0.
CC
CC ID,INJ. RATE AND INJ. COMP. FOR RATE CONS. WELLS FOR EACH PHASE
(L=1,3)
```

255

```
*---- ID   QI(M,L) water oil  surf  polymer  anion    cation    alc1
alc2  carbonat sodium  hyd  petA
     3    2105.5  1.0   0.   0.0   0.225   0.08479   0.001    0.
0.    0.004143   0.08894  111.12  0.001
     3       0.   0.   0.   0.    0.       0.       0.        0.
0.    0.         0.       0.       0.
     3       0.   0.   0.   0.    0.       0.       0.        0.
0.    0.         0.       0.       0.
CC
CC ID,INJ. RATE AND INJ. COMP. FOR RATE CONS. WELLS FOR EACH PHASE
(L=1,3)
*---- ID   QI(M,L) water oil  surf  polymer  anion    cation    alc1
alc2  carbonat sodium  hyd  petA
     4    2105.5  1.0   0.   0.0   0.225   0.08479   0.001    0.
0.    0.004143   0.08894  111.12  0.001
     4       0.   0.   0.   0.    0.       0.       0.        0.
0.    0.         0.       0.       0.
     4       0.   0.   0.   0.    0.       0.       0.        0.
0.    0.         0.       0.       0.
CC
CC ID,INJ. RATE AND INJ. COMP. FOR RATE CONS. WELLS FOR EACH PHASE
(L=1,3)
*---- ID   QI(M,L) water oil  surf  polymer  anion    cation    alc1
alc2  carbonat sodium  hyd  petA
     5    2105.5  1.0   0.   0.0   0.225   0.08479   0.001    0.
0.    0.004143   0.08894  111.12  0.001
     5       0.   0.   0.   0.    0.       0.       0.        0.
0.    0.         0.       0.       0.
     5       0.   0.   0.   0.    0.       0.       0.        0.
0.    0.         0.       0.       0.
CC 3.7.8 CUM. INJ. TIME , AND INTERVALS (PV) FOR WRITING TO OUTPUT
FILES
           profilesPROF     prodPROF     prodHIST    maps      recovery
*---- TINJ   CUMPR1          CUMHI1       WRHPV       WRPRF       RSTC
    440      30               60            1          30        274
CC
CC 3.7.11 FOR IMES=2 ,THE INI. TIME STEP,CONC. TOLERANCE,MAX.,MIN.
courant numbers
*---- DT       1 2 3 4 5 6 7 8 9 10 11  12   CNMAX    CNMIN
     0.000001  0.01 0.01  8*0.01             0.01 0.01  0.10     0.01
CC
CC FLAG FOR INDICATING BOUNDARY CHANGE
*---- IBMOD
      0
CC
CC  IRO, ITIME, NEW FLAGS FOR ALL THE WELLS
*---- IRO    ITIME     IFLAG
      2       1        4  1  1  1  1
CC
CC  NUMBER OF WELLS CHANGES IN LOCATION OR SKIN OR PWF
*---- NWEL1
       0
CC
```

```
CC  NUMBER OF WELLS WITH RATE CHANGES, ID
*---- NWEL2      ID      *10*
        4           2 3 4 5
CC
CC  ID,INJ. RATE AND INJ. COMP. FOR RATE CONS. WELLS FOR EACH PHASE
(L=1,3)
*----  ID   QI(M,L) water oil  surf  polymer  anion    cation    alc1
alc2 carbonat   sodium   hyd     petA
       2   2105.5 1.0   0.   0.0   0.0    0.08479  0.001     0.
0.   0.004143   0.08894  111.12  0.001
       2      0.   0.   0.   0.    0.       0.      0.        0.
0.   0.   0.   0.       0.       0.
       2      0.   0.   0.   0.    0.       0.      0.        0.
0.   0.   0.   0.       0.       0.
CC
CC ID,INJ. RATE AND INJ. COMP. FOR RATE CONS. WELLS FOR EACH PHASE
(L=1,3)
*----  ID   QI(M,L) water oil  surf  polymer  anion    cation    alc1
alc2 carbonat sodium  hyd  petA
       3   2105.5 1.0   0.   0.0   0.0    0.08479  0.001     0.
0.   0.004143   0.08894  111.12  0.001
       3      0.   0.   0.   0.    0.       0.      0.        0.
0.   0.   0.   0.       0.       0.
       3      0.   0.   0.   0.    0.       0.      0.        0.
0.   0.   0.   0.       0.       0.
CC
CC ID,INJ. RATE AND INJ. COMP. FOR RATE CONS. WELLS FOR EACH PHASE
(L=1,3)
*----  ID   QI(M,L) water oil  surf  polymer  anion    cation    alc1
alc2 carbonat sodium  hyd  petA
       4   2105.5 1.0   0.   0.0   0.0    0.08479  0.001     0.
0.   0.004143   0.08894  111.12  0.001
       4      0.   0.   0.   0.    0.       0.      0.        0.
0.   0.   0.   0.       0.       0.
       4      0.   0.   0.   0.    0.       0.      0.        0.
0.   0.   0.   0.       0.       0.
CC
CC ID,INJ. RATE AND INJ. COMP. FOR RATE CONS. WELLS FOR EACH PHASE
(L=1,3)
*----  ID   QI(M,L) water oil  surf  polymer  anion    cation    alc1
alc2 carbonat sodium  hyd  petA
       5   2105.5 1.0   0.   0.0   0.0    0.08479  0.001     0.
0.   0.004143   0.08894  111.12  0.001
       5      0.   0.   0.   0.    0.       0.      0.        0.
0.   0.   0.   0.   0.       0.       0.
       5      0.   0.   0.   0.    0.       0.      0.        0.
0.   0.   0.   0.   0.       0.       0.
CC 3.7.8 CUM. INJ. TIME , AND INTERVALS (PV) FOR WRITING TO OUTPUT
FILES
          profilesPROF    prodPROF    prodHIST    maps      recovery
*---- TINJ    CUMPR1          CUMHI1      WRHPV      WRPRF      RSTC
    750      30              60          1          30        274
CC
```

```
CC 3.7.11 FOR IMES=2 ,THE INI. TIME STEP,CONC. TOLERANCE,MAX.,MIN.
courant numbers
*----  DT          1  2  3  4  5  6  7  8  9  10   11   12  CNMAX    CNMIN
       0.000001  0.01 0.01  8*0.01                 0.01  0.01  0.10    0.01
```

Bibliography

Aoudia, Mohammed, Wade, William H., Weerasooriya, Vinitha, "Optimized microemulsions formulated with propoxylated guerbet alcohol and propoxylated tridecyl alcohol sodium sulfates", Journal of dispersion science and technology, 16(2), (1995), 115.

Adkins, S, Liyanage, P J, Arachchilage, G W P P, Mudiyanselage T, Weerasooriya U, Pope G A; "A New Process for Manufacturing and Stabilizing High Performance EOR Surfactants at Low Cost for High Temperature, High Salinity Oil Reservoirs", SPE 129923, Presented at the 2010 Improved Oil Recovery Symposium, Tulsa, OK, USA, 24-28 April 2010.

Allison, J.D., Brown, D.S., Novo-Gradac, K.J., "MINTEQA2/PRODEFA2--A geochemical assessment model for environmental systems--version 3.0 user's manual": Environmental Research Laboratory, U.S. Environmental Protection Agency, Athens, Georgia (1990), p.106.

Araque-Martinez, A, Lake, LW, "A Simplified Approach to Geochemical Modeling and its Effect on Well Impairment", SPE 56678, Presented at the 1999 SPE Annual Technical Conference and Exhibition, Houston, TX, 3-6 Oct. 1999

Austad, Tor, Milter, Jess, "Surfactant Flooding in Enhanced Oil Recovery", Surfactants: Fundamentals and Applications in the Petroleum Industry", Cambridge University Press (1998).

Barnes, J R, Smit, Johan P., Smit Jasper P., Shpakoff, P G, Raney, K H, Puerto, M C, "Developments of Surfactants for Chemical Flooding at Difficult Reservoir Conditions", SPE 113313, Presented at the 2008 SPE/DOE Improved Oil Recovery Symposium, Tulsa, OK, USA, 19-23 April 2008.

Barnes, J. R., Dirkzwager, H, Smit Jasper P., Smit, Johan P., On, An, Navarrette, R. C., Ellison, B. H., Buijse, M. A., Rijswijk, B. V., "Application of Internal Olefin Sulfonates and other Surfactants to EOR. Part 1: Structure - Performance Relationships for Selection at Different Reservoir Conditions", SPE 129766, Presented at the 2010 SPE/DOE Improved Oil Recovery Symposium, Tulsa, OK, USA, 24-28 April 2010.

Bear, J, "Hydraulics of Ground Water", McGraw Hill, New York, 1979

Bhuyan, D, "Development of an Alkaline/Surfactant/Polymer Compositional Reservoir Simulator", Dissertation, The University of Texas at Austin, Dec. 1989.

Bhuyan, D, Lake, L W, Pope, G A, "Mathematical Modeling of High pH Chemical Flooding", SPE 17398, SPE Reservoir Engineering, May, 1990, p.213-220.

Bourrel, M, Schechter, R S; "Microemulsions and Related Systems", Marcel Dekker Inc., New York, 1989.

Delshad, M, Pope, G A, Sepehrnoori, K, "A compositional Simulator for Surfactant Enhanced Aquifer Remediation", Journal of Contaminant Hydrology, 23 (1996), p.303-327.

Delshad, M, Han, W, Pope, G A, Sepehrnoori, K, Wu, W, Yang, R, Zhao, R, "Alkaline/Surfactant/Polymer predictions for the Karamay Oil Field", SPE 39610, Presented at the 1998 SPE/DOE Improved Oil Recovery Symposium, Tulsa, OK, USA, April 19-22, 1998.

Delshad, M, Pope, G A, "Effect of Dispersion on Transport and Precipitation of Barium and Sulfate in Oil Reservoirs", SPE 80253, Presented at the SPE International Symposium on Oilfield Chemistry , Houston, TX, USA, 5-7 Feb 2003.

Falls, A H, Thigpen, D R, Nelson, R C, Ciaston, J W, Ueber, R C, Shahin, G T, "Field Test of Co-surfactant Enhanced Alkaline Flooding", SPE 24117, Presented at the SPE Symposium on Enhanced Oil Recovery, Tulsa, OK, USA, 1992.

Farmer J B, "Metal Borates", Advances in Inorganic Chemistry and Radiochemistry, Vol. 25 (1982), p. 187-237.

Flaaten, Adam K, Nguyen, Quoc P, Pope, Gary A, Zhang, Jieyuan, "A Systematic Laboratory Approach to Low-Cost, High-Performance Chemical Flooding", SPE 113469, Presented at the SPE/DOE Improved Oil Recovery Symposium, Tulsa, OK, USA, 19-23 April 2008.

Flaaten, Adam K., Nguyen, Quoc P., Zhang, Jieyuan, Mohammadi, Hourshad, Pope, Gary A, "ASP flooding without the need for soft water", SPE116754, Presented at the 2008 SPE Annual Technology Conference and Exhibition, Denver,CO, USA, Sept. 21-24, 2008.

Gang, C, Liu He, Shi, G, Wang, G, Xiu, Z, Ren, H, Zhang, Y; "Technical Breakthrough in PCPs' Scaling Issue of ASP Flooding in Daqing Oil Field", SPE 109165, Presented at the 2007 SPE Annual Technical Conference and Exhibition, Anaheim, CA, USA, 11-14 Nov., 2007.

Glover, C J, Puerto, M C, Maerker, J M, Sandvik, E L, "Surfactant Phase Behavior and Retention in Porous Media", SPE 7053, SPE Journal, June, 1979, p.183-193.

Gogarty, W B, Tosch W C, "Miscible-Type water flooding: Oil recovery with Miscellar Solutions", SPE 001847-1-PA, Presented at the SPE 42nd Annual Fall meeting, Houston , TX, USA, Oct. 1-7, 1967.

Green, Don W, Willhite, G Paul, "Enhanced Oil Recovery", SPE Textbook Series, Vol. 6, 1998.

Hayes, M E, Bourrell, M, El-Emary, M, Schechter, R S, Wade, W H, "Interfacial Tension and Behavior of Non-Ionic Surfactants", SPE 7581, SPE Journal, Dec. 1979, p.349-356.

Healy, R N, Reed, R L, "Physicochemical Aspects of Microemulsion Flooding", SPE 4583, SPE Journal, Oct. 1974, p. 491-501.

Hirasaki, G J, "Ion Exchange with Clays in the presence of Surfactant", SPE 9279, SPE Journal, April, 1982, p.181-192

Hirasaki, G J, van Domselaar, H R, Nelson, R C; "Evaluation of the Salinity Gradient Concept in Chemical Flooding", SPE 8825, SPE Journal, June 1983, p. 486-500.

Hirasaki, G J, Zhang, D L; "Surface Chemistry of Oil Recovery from Fractured, Oil Wet, Carbonate Formations", SPE 80988, SPE Journal, 9(2), (June 2004), p151-162.

Hirasaki, G J, Miller, C A, Puerto, M; "Recent Advances in Surfactant EOR"; SPE115386, Presented at the 2008 SPE Annual Technical Conference and Exhibition, Denver, CO, USA, Sept 21-24, 2008.

Hsieh, W C, Shah, D O; "The Effect of the Chain Length of Oil and Alcohol as well as Surfactant to Oil Ratio on Solubilization, Phase Behavior and Interfacial Tension of Oil/Brine/Surfactant/Alcohol Systems", Presented at the 1977 SPE-AIME International Symposium on Oilfield and Geothermal Chemistry, La Jolla, CA, USA, June 27-28, 1977.

Huh, Chun, "Interfacial Tensions and solubilizing Ability of a Microemulsion Phase that coexists with oil and brine", Journal of Colloid and Interfacial science, 71(2), (September 1979), 408.

Ingri, N; "Equilibrium Studies of Polyanions containing B(III), Si(IV), Ge(IV) and V(V); Svensk Kemisk Tidskrift (1963); 75(4), p.199-230.

Jackson, Adam Christopher, "Experimental Study of the Benefits of Sodium Carbonate on Surfactants for Enhanced Oil Recovery", Thesis, The University of Texas at Austin, December 2006.

Jayanti, S, Pope, G A, Weerasooriya, V, Zhong L, Dwarakanath, V, Malik, T, "Use of Surfactants to Recover Oils from Ground Water", SPE 66753, Presented at the SPA/EPA/DOE Exploration and Production Environmental Conference, San Antonio, TX, USA, 26-28 Feb, 2001.

Jin, M, "A Study of Non-Aqueous Phase Liquid Characterization and Surfactant Remediation", Ph.D Dissertation, The Univ. of Texas, Austin, TX, 1995.

Johnson, C E, "Status of Caustic and Emulsion Methods", SPE 5561, Journal of Petroleum Technology (Jan 1976), p. 85-92.

Jones, S C, Dreher, K D, "Co-surfactants in Micellar Systems used for Tertiary Recovery", SPE Journal (June 1976), p. 167-7

Krueger, R F; "An Overview of Formation Damage and Well Productivity in Oilfield Operations", SPE 10029, Journal of Petroleum Technology, Feb.1986, p.131-52.

Krumrine, P H, Mayer, E H, Brock, G F; "Scale Formation During Alkaline Flooding", SPE 12671, Journal of Petroleum Technology, Aug. 1985, p.1466-74.

Labrid, Jean, "The Use of Alkaline Agents in Enhanced Oil Recovery Processes", Critical Reports on Applied Chemistry, Volume 33, Basic Concepts in Enhanced Oil Recovery Processes, 1991.

Lake, L W, Helfferich, F G, "Cation Exchange in Chemical Flooding: Part 2 - The Effect of Dispersion, Cation Exchange and Polymer/Surfactant Adsorption on Chemical Flood Environment", SPE 6769, SPE Journal, Dec. 1978, p. 435-444.

Lake, L W; "Enhanced Oil Recovery", Prentice Hall, Upper Saddle River, NJ, 1989.

Levitt, David B, Jackson, Adam C., Heinson, Christopher, Britton, Larry N, Malik, Taimur, Dwarakanath, Varadarajan, Pope, Gary A, "Identification and Evaluation of high performance EOR surfactants", SPE 100089, Presented at the 2006 SPE/DOE Symposium on Improved Oil Recovery, Tulsa, OK, USA, April 22-26 2006.

Levitt, David B, Pope, G A; Selection and Screening of Polymers for Enhanced Oil Recovery", SPE 113845, Presented at the SPE/DOE Improved Oil Recovery Symposium, Tulsa, OK, USA, 19-23 April 2008.

Mackay, E J, Jordan M M; "Impact of Brine Flow and Mixing in the Reservoir on Scale Control Risk Assessment and Subsurface Treatment Options: Case Histories", Journal of Energy Resources Technology, 127 (Sept. 2005), p.201-13.

Moghadasi J, Jamialahmadi, M, Mueller-Steinhagen, H, Sharif, A; "Scale Formation in Oil Reservoir and Production Equipment during Water Injection", SPE 82233, Presented at the SPE European Formation Damage Conference, The Hague, Netherlands, 13-14 May, 2003.

Moghadasi J, Jamialahmadi, M, Mueller-Steinhagen, H, Sharif, A; "Formation Damage due to Scale Formation in Porous Media Resulting from Water Injection", SPE

86524, Presented at the SPE International Symposium and Exhibition on Formation Damage Control, Lafayette, LA, USA, 18-20 Feb, 2004.

Mohammedi, H, "Mechanistic Modeling, Design and Optimization of Alkali/Surfactant/Polymer Flooding", Dissertation, The University of Texas at Austin, August 2008.

Nelson, R C, Pope, GA; "Phase Relationships in Chemical Flooding", SPE 6773, SPE Journal, Oct. 1978, p. 325-338.

Nelson, R C; "The Salinity-Requirement Diagram - A Useful Tool in Chemical Flooding Research and Development", SPE 8825, SPE Journal, April 1982, p.259-270.

Nelson, R C, Lawson, J B, Thigpen, D R, Stegemeier, G L, "Co-surfactant Enhanced Alkaline Flooding", SPE/DOE 12672, Presented at the SPE/DOE Fourth Symposium on Enhanced Oil Recovery, Tulsa, OK, USA, April 15-18 1984.

Parkhurst, D L, Appelo, C A J, "Users Guide to PHREEQC - A Computer Program for speciation, reaction-path, advective transport and inverse Geochemical calculations", USGS Water Resources Investigation Report 95-4227, 1995, p.143.

Parkhurst, D L, Thorstenson, D C, Plummer, L N, "PHREEQE - A Computer program for geochemical calculations", USGS Water Resources Investigation Report 80-96, 1980, p.195.

Plummer, L.N., Parkhurst, D.L., Fleming, G.W., Dunkle, S.A., "A computer program incorporating Pitzer's equations for calculation of geochemical reactions in brines", USGS Water-Resources Investigations Report 88–4153 (1988), p.310

Pope, G A, Lake, L W, Helfferich, F G, "Cation Exchange in Chemical Flooding: Part 1- Basic Theory Without Dispersion", SPE 6771, SPE Journal, Dec. 1978, p.418-434.

Pope, G A, Wu, W, Narayanaswamy, G, Delshad, M, Sharma, M M, Wang, P, "Modeling Relative Permeability Effects in Gas Condensate Reservoirs with a new Trapping Model". SPE Reservoir Eval. and Eng., 3(2), April 2000, p. 171-8.

Raimondi, P, Gallagher, B J, Ehrlich, R, Messmer, J H, Bennett, G S; "Alkaline Waterflooding: Design and Implementation of a Field Pilot", SPE 5831, Journal of Petroleum Technology, Oct. 1977, p. 1359-68.

Reisberg, J, Doscher, T M; "Interfacial Phenomena in Crude Oil - Water systems"; Producers Monthly, 21(1) (Nov. 1956), p. 43-50.

Rocha, A A, Frydman, M, da Fontoura, S A B, Rosario, F F, Bezerra, M C M, "Numerical Modeling of Salt Precipitation during Produced Water Reinjection",

SPE 68336, Presented at the 2001 SPE Third International Symposium on Oilfield Scale, Aberdeen, UK, 30-31 Jan 2001.

Rosen, Milton J, Wang, Hongzhuang, Shen, Pingping, Zhu, Youyi, "Ultralow Interfacial Tension for Enhanced Oil Recovery at Very Low Surfactant Concentrations", Langmuir, Vol. 21 (2005), 3749-56

Sahni, V, Dean, R M, Britton, C, Kim, D H, Weerasooriya, U, Pope, G A, "The Role of Co-solvents and Co-Surfactants in making Chemical Floods Robust", SPE 130007, Presented at the 2010 Improved Oil Recovery Symposium, Tulsa, OK, USA, 24-28 April 2010.

Salagar, J L, Anton, R E, Sabatini, D A, Harwell, J H, Acosta, E J, Tolosa, L I, "Enhancing Solubilization of Microemulsions - State of the Art and Current Trends", Journal of Surfactants and Detergents, 8(1) (Jan 2005), p. 3-21.

Sanz, C A, Pope, G A, "Alcohol Free Chemical Flooding: From Surfactant Screening to Core Flood Design", SPE 28956, Presented at the SPE International Symposium on Oilfield Chemistry, San Antonio, TX, USA, Feb 14-17, 1995.

Sorbie, K S; "Polymer Improved Oil Recovery", CRC Press Inc., Boca Raton, FL, 1991.

Surkalo, Harry, "Enhanced Alkaline Flooding", SPE19896, Journal of Petroleum Technology, 42(1), Jan. 1990, p. 6-7.

Taylor, G. I., "Dispersion of Soluble matter in solvent flowing slowly through a Tube", Proceeding of the Royal Society (London), A-219, 186-203, 1953.

UTCHEM Vol. II, Technical Documentation for UTCHEM-9.0, Center for Petroleum and Geosystems Engineering, The University of Texas at Austin, 2000.

Wade W H, Morgan, J C, Schechter, R S, Jacobson, J K, Salager, J L; "Interfacial Tension and Phase Behavior of Surfactant Systems", SPE 6844, SPE Journal (Aug, 1978), p. 242-52

Walsh, M P, Bryant, S L, Schechter, R S, Lake, LW, "Precipitation and Dissolution of Solids Attending Flow through Porous Media", AIChE Journal, Vol. 30, No. 2, March, 1984, p.317-328.

Wang, Y, Liu, J, Liu, B, Liu, Y, Wang, H, Chen, G; "Why Does Scale Form in ASP Flood? How to Prevent from It? A Case Study of the Technology and Application of Scaling Mechanism and Inhibition in the ASP Flood Pilot Area of N-1DX Block in Daqing", SPE 87469. Presented at the 6th International Symposium on Oilfield Scale, Aberdeen, UK, 26-27 May, 2004.

Wellington S L, Richardson E A; "Low Surfactant Concentration Enhanced Waterflooding", SPE 30748, SPE Journal, 2(4) (Dec. 1997), p. 389-405

Winsor, P A; "Solvent Properties of Amphiphilic Compounds"; Butterworths, London, 1954

Yang, H, Britton, C, Liyanage, P J, Solairaj, S, Kim, D H, Nguyen, Q P, Weerasooriya, U, Pope, G A; "Low Cost High Performance Chemicals for Enhanced Oil Recovery", SPE 129978, Presented at the 2010 Improved Oil Recovery Symposium, Tulsa, OK, USA, 24-28 April 2010.

Yang, H; "Development of Improved ASP Formulations for Reactive and Non-Reactive Crude Oils", Thesis, The University of Texas at Austin, Dec. 2010.

Zhang, D L, Liu, S, Yan, W, Puerto, M, Hirasaki, G J, Miller, C A, "Favorable Attributes of Alkali Surfactant Polymer flooding", SPE 99744, Presented at the SPE/DOE symposium on Improved Oil Recovery, Tulsa, OK, USA, 22-26 April 2006.

Zhang, J, Nguyen, Q. P., Flatten, A. K, Pope, G. A, "Mechanisms of Enhanced Natural Imbition with Novel Chemicals", SPE 113453, Presented at the SPE/DOE Improved Oil Recovery Symposium, Tulsa, OK, USA, 19-23 April 2008.

Zhao, Ping, Jackson, Adam C, Britton, Chris, Kim, Do Hoon, Britton, Larry N., Levitt, David B, Pope, Gary A., "Development of High-Performance Surfactants for Difficult Oils", SPE 113432, Presented at the 2006 SPE/DOE Symposium on Improved Oil Recovery, Tulsa, OK, USA, April 19-23 2008.

Vita

Vikram Chandrasekar, the son of D. Chandrasekaran and Radhika Chandrasekar was born in Jamshedpur, India. After finishing his high school education at P.S Senior Secondary School, Chennai, India in May, 2001, he enrolled at Sri Venkateswara College of Engineering (SVCE), Anna University, Chennai, India. There, he earned his Bachelor of Technology degree in Chemical Engineering in May 2005. Starting November, 2005, he worked as a Production Manager at Reliance Industries Limited, Mumbai, India. In August, 2007, he entered the University of Texas as a graduate student in Petroleum Engineering.

Permanent address: B-11, No. 2, Ramachandra Road,

Luz Avenue, Mylapore,

Chennai - 600004, Tamil Nadu, India

This thesis was typed by the author.